

DISS. ETH NO. 22308

# **ENGINEERING PHENOTYPICALLY STABLE CARTILAGE**

A thesis submitted to attain the degree of  
DOCTOR OF SCIENCES of ETH ZURICH

(Dr. sc. ETH Zurich)

presented by

DEBORAH STUDER

MSc en Chimie moléculaire et biologique, EPFL

born on 20.11.1984

citizen of Oberhof, AG, Switzerland

accepted on the recommendation of

Prof. Dr. Marcy Zenobi-Wong, examiner

Dr. Katharina Maniura, co-examiner

Prof. Dr. Mauro Alini, co-examiner

2014



Bù dēng gāoshān, bù xiǎn píngdì.

Wer nicht auf die hohen Berge steigt, kennt die Ebene nicht.

*Chinesisches Sprichwort*



# Acknowledgements

After four intense years, it is a great pleasure to thank the many people who made this thesis possible.

To my two supervisors, Marcy Zenobi-Wong and Katharina Maniura. Thank you Marcy for receiving me with open arms in your group and supporting me with valuable input, ideas and constructive criticism. The group atmosphere, whether in or outside of the lab, on a group retreat, ski weekend, or barbecue and cocktail evening made my time in CERL unforgettable. Thank you Katharina for sharing your experience of the biomedical field and life with me, giving me the freedom and the trust to develop my project according to my own ideas. Your encouragement in the difficult moments of this work was greatly appreciated.

To Mauro Alini for accepting to be part of the committee and take the time to review this thesis.

To the whole CERL team: Anne, Chris, Ece, Emma, Florian, Gemma, Matti, Mischa, Nicolas, and Rami; you made the last few years an unforgettable time! Thank you for the great company during endless weeks in the lab, discussions over coffee breaks and lunch, dinners and concert nights. It has been great to work in your team, and this PhD would not have been possible without you.

To Timothée Esteva, my wonderfully eccentric Masters student. Not only were you a great help to my project, but your contagious enthusiasm for life made the summer 2013 be a special one for the whole lab.

To the team at the Laboratory for Materials-Biology Interactions, Empa: Ari, Angela, Brigitte, Cordula, Liliane, Magda, Peter, Pius, Stefanie, Tina, Ursina, Verena, and Xenia. With your great support and patience in answering the endless questions of a stem cell-biology novice, you helped immensely in laying the foundation for this work. The girl-nights, Manser dinners and Konstanz evenings are fond memories of my time in the far east.

To Janos Vörös, who warmly welcomed me in the Laboratory of Biosensors and Bioelectronics (LBB) and remained a source of wise words and inspiration, even after our move to the far away Höggerberg.

To the LBB team for adopting me into your group from the very beginning. It has always been a pleasure to come to your lab and enjoy Friday beers. A glass of Lagrein or a Granita will forever take me back to skiing in Taufers, or to the group retreat in Sicily!

To the Ehrbar Lab, University Hospital Zürich which was not only my home for the initial months of my PhD, but remained a source of motivation later on. Thank you Martin for sharing your thoughts on the academic world and showing me direction when it was most needed.

To the Akashi Lab, Osaka University, especially Manami Shudo, Takami Akagi, and Michiya Matsusaki and Mitsuru Akashi for my incredible time in Osaka and a great collaboration thereafter. Your lessons on the secrets of eating Sushi, the art of enjoying meter-long Udon noodles with chopsticks and powernaps have fostered my love of the Japanese culture.

To Christina Mäusli (former Empa), Kyrena Schäpper (Empa), Silvia Pfister (CERL, ETH), Esther Singer (LBB, ETH) for taking care of many administrative issues.

To Lee Ann Laurent-Applegate and her team at the University Hospital Lausanne (CHUV) for sharing their epiphyseal chondroprogenitor cells and offering advice throughout my project.

To Matthias Steinwachs (Sport Clinic, Zürich), Gian Salzmann (Schulthess Clinic, Zürich), and Marcus Mumme (University Hospital, Basel) for a fruitful collaboration and valuable input on my work.

To Wolfram Jochum at the Kantonsspital St.Gallen for his help with histology.

To the Swiss National Science Foundation and the AO Foundation for financial support, which made this work possible

# Abstract

Although cell-based cartilage repair techniques date back to the 1990's, when the first autologous chondrocyte implantation (ACI) was performed, a predictable, and phenotypically stable treatment of cartilage lesions, has remained elusive. Since its inception, ACI has undergone several generations of improvements, but still focuses on the application of autologous articular chondrocytes (ACs), which not only suffer from high donor variability, but also require a long expansion time and two surgical interventions. In order to simplify the treatment, a more readily available cell source with reproducible chondrogenic potential is required. The aim of this thesis is to establish an alternative cell source with the ability to form phenotypically stable cartilage.

The first part of this thesis focus on the application of mesenchymal stromal cells (MSCs) as an alternative to ACs. MSCs are present in many bodily tissues (e.g. bone marrow, adipose, and synovium), and can be isolated with high cell yields. Their high self-renewal potential together with the ability to differentiate into the three mesenchymal lineages (adipo, bone and cartilage) makes MSCs a promising cell source. Unfortunately, the chondrogenic induction of MSCs has not yet led to the formation of phenotypically stable cartilage but progresses towards endochondral ossification. We have investigated two approaches for hypertrophy inhibition: the application of parathyroid hormone-related protein (PTHrP), as well as the use of RNA interference (RNAi). Regulation of growth plate hypertrophy is under the tight control of PTHrP, which makes it an attractive cytokine for manipulating MSC chondrogenesis in vitro. We show that PTHrP efficiently inhibits hypertrophic genes such as collagen 10, but at the same time also downregulates the chondrogenic matrix production. This unspecific action led to the exploration of small interfering RNA (siRNA) with the potential to knock-down protein expression in a highly sequence-specific manner.  $\gamma$ -PGA-Phe nanoparticles (NPs) were used as a delivery vehicle to carry siRNA inside their core, or adsorbed on the surface-coated polycations (polyethyleneimine, DEAE-dextran and chitosan). While encapsulated

siRNA yielded unstable NPs, its absorption was highly efficient. Chitosan-coated NPs efficiently entered the cells and delivered the siRNA into the cytoplasm.

The developed NPs showed potential in future RNAi therapeutics for MSC-based cartilage treatments, but their high regulatory requirements led us to reconsider the cell choice. We shifted the focus from undifferentiated cells towards immature chondrocytes with a more defined character. In a comparison of fetal epiphyseal chondrocytes (ECPs) with MSCs and ACs, the high chondrogenic potential of ECPs was demonstrated along with a phenotypic stability outperforming MSCs. The application of an allogenic cell source additionally provided a more predictable and reproducible outcome compared to autologous ACs or MSCs. Cartilage is, due to its avascular nature, an immune-isolated tissue, and thus allogenic treatments have been used for several decades. The high capacity for stable cartilage matrix production of ECPs makes them a cell source with great promise for next generation one-step cartilage treatments.

This thesis demonstrates that MSCs, despite their potential, are still a long way from clinical application. Immature cartilage, on the other hand, combines the benefit of a stable phenotype with off-the-shelf availability, advancing cartilage tissue engineering towards a fast and reproducible single step procedure.



# Zusammenfassung

Obwohl zellbasierte Techniken zur Knorpelregeneration aus den Neunzigerjahren stammen, als die erste autologe Chondrozytenimplantation (ACI) durchgeführt wurde, erwies sich ein vorhersehbares und phänotypisch stabiles Verfahren zur Behandlung von Knorpelverletzungen schwer realisierbar. Seit seiner Erfindung durchlief ACI einige Verbesserungsstadien, aber der Fokus liegt nachwievor auf der Anwendung von autologen Gelenkchondrozyten (ACs), welche nicht nur von grossen Spenderunterschieden geprägt sind, sondern auch eine lange Proliferationsphase sowie zwei chirurgische Eingriffe bedingen. Zur Vereinfachung dieses Verfahrens wird leichter verfügbares zelluläres Ausgangsmaterial mit reproduzierbarem chondrogenem Potential benötigt. Das Ziel dieser Dissertation ist die Etablierung eines alternativen Zelltypen, welcher phänotypisch stabilen Knorpel zu bilden vermag.

Der erste Teil dieser Arbeit konzentriert sich auf die Anwendung von mesenchymalen Stromazellen (MSCs) als Alternative zu den ACs. MSCs sind in vielen Körpergeweben (beispielsweise Knochenmark, Fettgewebe und Synovium) vorhanden und können mit hohen Zellerträgen isoliert werden. Ihr grosses Potential zur Selbsterneuerung zusammen mit der Fähigkeit sich in die drei mesenchymalen Entwicklungslinien (Fettgewebe, Knochen und Knorpel) zu differenzieren, macht die MSCs zu einem vielversprechenden Zelltypen. Die Chondrogenese der MSCs führt jedoch nicht zur Bildung von stabilem, sondern transientem, kalzifiziertem Knorpelgewebe. Wir untersuchten daher zwei Ansätze zur Hemmung dieser sogenannten Hypertrophie: Die Anwendung von "parathyroid hormone-related protein" (PTHrP) sowie die Verwendung von RNA-Interferenz (RNAi). Die endochondrale Ossifikation wird in vivo streng kontrolliert durch PTHrP, was dieses zu einem attraktiven Cytokin für die Manipulation der in vitro Chondrogenese von MSCs macht. Wir zeigen, dass PTHrP die hypertrophischen Gene wie Kollagen 10 effizient hemmt, aber gleichzeitig die Produktion der Knorpelmatrix hindert. Diese unspezifische Wirkung führte uns zur Erkundung der siRNA (small interfering RNA), welche se-

---

quenzspezifisch die Protein-Expressionen blockiert.  $\gamma$ -PGA-Phe Nanopartikel (NPs) wurden als Träger für die siRNA benutzt, welche im Kern eingekapselt oder auf die mit Polikationen (Polyethylenimin, DEAE-Dextran und Chitosan) beschichteten NPs absorbiert wurde. Während die Einkapselung der siRNA die NPs destabilisierte, war ihre Absorption höchst effizient. Die Chitosan-Beschichtung der NPs führte zu einer effizienten Aufnahme in das Zellinnere, wo die siRNA erfolgreich ins Cytoplasma abgegeben wurde.

Die entwickelten NPs zeigten Potential als zukünftige RNAi-Therapeutika in der Anwendung von MSC-basierten Knorpelbehandlungen, aber ihre hohen regulatorischen Anforderungen brachten uns zu einem Überdenken der Wahl des Zelltypen. Wir verlagerten daher den Fokus von undifferenzierten Zellen auf nicht voll ausgebildete Chondrozyten mit einem vordefiniertem Charakter. Der Vergleich von Chondrozyten der fetaler Epiphysenfuge (fetal epiphyseal chondrocytes, ECPs) mit MSCs und ACs, zeigte das hohe chondrogene Potential der ECPs zusammen mit einer phänotypischen Stabilität auf, welche MSCs klar übertrifft. Zusätzlich bietet die Anwendung eines allogenen zellulären Ausgangsmaterials ein vorhersehbareres und reproduzierbareres Ergebnis verglichen mit autologen ACs oder MSCs. Knorpel ist aufgrund seiner avaskulären Beschaffenheit ein immun-isoliertes Gewebe was bereits seit einigen Jahrzehnten zur allogene Knorpelbehandlungen geführt hat. Aufgrund der hohen Fähigkeit der ECPs zur Produktion stabiler Knorpelmatrix erweisen sich diese als verheissungsvollen Zelltypen für Knorpelbehandlungen der nächsten Generation, welche nur eine einzige Operation bedingen.

Diese Dissertation zeigt, dass MSCs trotz ihrem grossen Potential noch weit von einer klinischen Anwendung entfernt sind. Ein noch nicht voll ausgebildeter Knorpel hingegen kombiniert den Vorteil eines stabilen chondrozytären Phänotyps mit der sofortigen Verfügbarkeit, wodurch die Bildung von Knorpelgewebe zu einem schnellen und reproduzierbaren, einstufigen Verfahren wird.

## Abbreviations

<i>α-MEM</i>	Minimal essential medium - alpha modification
<i>ACI</i>	Autologous chondrocyte implantation
<i>ACI – Cs</i>	Cell-seeded matrix-supported autologous chondrocyte transplantation
<i>ACs</i>	Articular chondrocytes
<i>ALP</i>	Alkaline phosphatase
<i>AMIC</i>	Autologous matrix-induced chondrogenesis
<i>bp</i>	Base pair
<i>BSA</i>	Bovine serum albumin
<i>C4S</i>	Chondroitin 4-sulfate
<i>CAIS</i>	Cartilage autograft implantation system
<i>Chol</i>	Cholesterol
<i>COL</i>	Collagen
<i>CS</i>	Chondroitin sulfate
<i>DAPI</i>	4',6-Diamidin-2-phenylindol
<i>DCs</i>	Dendritic cells
<i>DEAE – dextran</i>	Diethylaminoethyl-Dextran
<i>DMEM</i>	Dulbecco's modified eagle's medium
<i>DMMB</i>	1,9-Dimethyl-Methylene Blue
<i>ECM</i>	Extracellular matrix
<i>ECPs</i>	Epiphyseal chondroprogenitors
<i>EDTA</i>	Ethylenediaminetetraacetic acid

---

<i>FBS</i>	Fetal bovine serum
<i>FGF – 2</i>	Basic fibroblast growth factor
<i>g – PGA – Phe</i>	Poly(gamma-glutamic acid)-Phenylalanine
<i>GAGs</i>	Glycosaminoglycans
<i>GAPDH</i>	Glyceraldehyde 3-phosphate dehydrogenase
<i>HA</i>	Hyaluronic acid
<i>HAT</i>	Histone acetyl transferase
<i>HDAC</i>	Histone deacetylase
<i>Ihh</i>	Indian Hedgehog
<i>IKK<math>\beta</math></i>	Inhibitor of nuclear factor kappa-B kinase subunit beta
<i>KS</i>	Keratin sulfate
<i>LDH</i>	Lactate dehydrogenase
<i>LPS</i>	Lipopolysaccharides
<i>MACH</i>	Matrix-associated chondroplasty
<i>mACI</i>	Matrix-induced autologous chondrocyte implantation
<i>MF</i>	Microfracture
<i>MMP</i>	Matrix metalloprotease
<i>mRNA</i>	Messenger RNA
<i>MSCs</i>	Mesenchymal stromal cells
<i>MW</i>	Molecular weight
<i>NF – <math>\kappa</math>B</i>	Nuclear factor kappa-light-chain-enhancer of activated B cells
<i>NPs</i>	Nanoparticles
<i>OATS</i>	Osteochondral autograft transplantation surgery
<i>PBS</i>	Phosphate buffered saline
<i>PEI</i>	Polyethyleneimine
<i>PenStrep</i>	Penicillin streptomycin
<i>PRP</i>	Platelet Rich Plasma
<i>PTHrP</i>	Parathyroid hormone-related protein
<i>qPCR</i>	Real time quantitative reverse transcription polymerase chain reaction

---

<i>RG</i>	Reference gene
<i>RISC</i>	RNA-induced silencing complex
<i>RNAi</i>	RNA interference
<i>RPL13a</i>	Ribosomal protein L13a
<i>RT</i>	Room temperature
<i>Runx2</i>	Runt-related transcription factor 2
<i>siRNA</i>	Small interfering RNA
<i>Sox9</i>	SRY (sex determining region Y)-box 9
<i>TGF-β</i>	Transforming growth factor beta



# Contents

<b>1</b>	<b>Cartilage tissue engineering</b>	<b>1</b>
1.1	Structure and function of articular cartilage . . . . .	2
1.2	Current clinical treatments for cartilage repair . . . . .	5
1.2.1	Autologous chondrocyte implantation . . . . .	7
1.2.2	Matrices for cartilage tissue engineering . . . . .	9
1.2.3	Cell sources for cartilage tissue engineering . . . . .	13
1.3	Engineering phenotypically stable cartilage . . . . .	16
1.3.1	Hypertrophy in the growth plate and in vitro . . . . .	16
1.3.2	Characterization of chondrocyte hypertrophy . . . . .	18
1.3.3	Strategies for hypertrophy inhibition based on molecular pathways . . . . .	20
1.3.4	Hypertrophy inhibition using RNA interference . . . . .	22
1.3.5	Lessons learnt from epigenetics . . . . .	23
<b>2</b>	<b>Scope</b>	<b>25</b>
<b>3</b>	<b>Materials and methods</b>	<b>27</b>
3.1	Reagents and solutions . . . . .	28
3.2	Media compositions . . . . .	28
3.2.1	Proliferation media . . . . .	28
3.2.2	Chondrogenic differentiation . . . . .	29
3.3	Cell isolation and culture . . . . .	30
3.3.1	Mesenchymal stromal cells . . . . .	30
3.3.2	Articular chondrocytes . . . . .	30
3.3.3	Epiphyseal chondroprogenitors . . . . .	31
3.4	Chondrogenic differentiation assays . . . . .	31
3.4.1	Pellet culture . . . . .	31
3.4.2	Scaffold culture . . . . .	31
3.5	Real-time quantitative RT-PCR assay . . . . .	32
3.5.1	RNA isolation and quantification . . . . .	32

3.5.2	RT-PCR . . . . .	32
3.6	Biochemical analysis . . . . .	34
3.6.1	Sample preparation . . . . .	34
3.6.2	Dimethylmethylene blue assay (DMMB) . . . . .	34
3.6.3	Pico green assay (DNA) . . . . .	35
3.7	Histological and immunohistochemical analyses . . . . .	35
3.7.1	Cryosectioning . . . . .	35
3.7.2	Alcian blue staining . . . . .	36
3.7.3	Immunohistological staining . . . . .	36
3.7.4	EdU - proliferation labeling and staining . . . . .	37
3.7.5	Phalloidin/DAPI staining . . . . .	37
3.8	Image acquisition and analysis . . . . .	37
3.9	Statistical analysis . . . . .	37
<b>4</b>	<b>Characterization of MSC hypertrophy by gene and protein expression</b>	<b>39</b>
4.1	Gene expression analysis . . . . .	40
4.2	Protein expression analysis . . . . .	42
4.3	Chapter summary . . . . .	43
<b>5</b>	<b>Inhibitory function of parathyroid hormone-related protein on mesenchymal stromal cell chondrogenesis and hypertrophy</b>	<b>45</b>
5.1	Materials and methods . . . . .	48
5.1.1	PTHrP administration . . . . .	48
5.2	PTHrP application at different concentrations . . . . .	48
5.3	Time point of administration . . . . .	50
5.4	PTHrP application under hypoxia . . . . .	52
5.5	The effects of PTHrP 1-34 versus 1-86 on pellet and scaffold culture . . . . .	54
5.6	Chapter summary . . . . .	57
<b>6</b>	<b>Application of amphiphilic poly(<math>\gamma</math>-glutamic acid) nanoparticles as siRNA carriers</b>	<b>59</b>
6.1	Materials and methods . . . . .	62
6.1.1	Preparation of $\gamma$ -PGA-Phe nanoparticles . . . . .	62
6.1.2	Preparation of siRNA carriers through encapsulation . . . . .	63
6.1.3	Preparation of nanoparticles with siRNA adsorbed outside . . . . .	63
6.1.4	Characterization of nanoparticles . . . . .	64



6.1.5 Cellular transfection . . . . .	64
6.1.6 RT-PCR . . . . .	65
6.1.7 Hemolysis . . . . .	65
6.1.8 TNF $\alpha$ ELISA . . . . .	66
6.1.9 Cytotoxicity . . . . .	66
6.2 Encapsulation of siRNA . . . . .	66
6.2.1 Encapsulation of siRNA by polyplex formation with protamine . . . . .	66
6.2.2 Encapsulation of cholesterol-modified siRNA . . . . .	68
6.3 Adsorption of siRNA onto polycation-coated NPs . . . . .	69
6.3.1 DEAE-dextran and PEI-coated NPs . . . . .	71
6.3.2 Chitosan-coated NPs . . . . .	74
6.4 Chapter summary . . . . .	78
<b>7 Human epiphyseal chondroprogenitor cells produce phenotypically stable cartilage:</b>	
<b>A new cell source for one-step treatment of cartilage lesions?</b>	<b>81</b>
7.1 Materials and methods . . . . .	83
7.1.1 Cells . . . . .	83
7.1.2 Effect of alginate on scaffold seeding . . . . .	83
7.1.3 Mechanical testing . . . . .	83
7.1.4 Scanning electron microscopy . . . . .	83
7.1.5 Statistical analysis . . . . .	84
7.2 Scaffold comparison . . . . .	84
7.3 Evaluation of seeding density . . . . .	86
7.4 Effect of alginate on scaffold seeding . . . . .	89
7.5 Comparison of chondrogenic potential . . . . .	90
7.6 Phenotypic stability . . . . .	91
7.7 Mechanical properties . . . . .	95
7.8 Chapter summary . . . . .	95
<b>8 Conclusion and outlook</b>	<b>97</b>
<b>Curriculum vitae</b>	<b>101</b>
<b>Bibliography</b>	<b>105</b>
<b>Appendices</b>	<b>131</b>



## List of Figures

1.1	Representations of the diarthrodial knee joint . . . . .	2
1.2	Zonal structure of cartilage . . . . .	3
1.3	Cartilage extracellular matrix composition . . . . .	4
1.4	Osteochondral autograft transplantation and microfracture . . .	6
1.5	Autologous chondrocyte implantation . . . . .	8
1.6	The three main cell sources for cartilage regeneration . . . . .	13
1.7	In vivo and in vitro chondrogenesis and hypertrophy . . . . .	17
1.8	Hypertrophy and the main actors . . . . .	19
1.9	Molecular pathways of hypertrophy . . . . .	21
1.10	Epigenetic regulation of hypertrophy . . . . .	23
4.1	Chondrogenic and hypertrophic gene array . . . . .	41
4.2	Alcian blue, collagen 2, and collagen 10 staining in pellet culture over time . . . . .	42
5.1	PTHrP application at different concentrations . . . . .	49
5.2	PTHrP administration at different time points - short term analysis	50
5.3	PTHrP administration at different time points - long term analysis	51
5.4	PTHrP from different sources . . . . .	52
5.5	PTHrP and its effect under hypoxia . . . . .	53
5.6	PTHrP 1-34 or 1-86 fragment . . . . .	54
5.7	Alcian blue, collagen 2 and 10 staining of pellets treated with PTHrP 1-34 or 1-86 . . . . .	55
5.8	Linear correlation of collagen 2 and 10 in scaffolds . . . . .	56
6.1	Synthesis of $\gamma$ -PGA-Phe . . . . .	61
6.2	Size-distribution, zeta potential and siRNA loading capacity of polyplex NPs . . . . .	67
6.3	Effect of NaCl concentration on siRNA loading efficiency of poly- plex NPs . . . . .	68
6.4	siRNA release from cholesterol-siRNA NPs . . . . .	68
6.5	Polycations and their characteristics . . . . .	70

6.6	Size-distribution of PEI and DEAE dextran-coated NPs . . . . .	71
6.7	Cellular uptake of PEI and DEAE dextran-coated NPs . . . . .	73
6.8	Gene knock-down of PEI and DEAE dextran-coated NPs . . . . .	74
6.9	Size distribution of chitosan-coated NPs . . . . .	75
6.10	Loading efficiency and release profile of chitosan-coated NPs . .	76
6.11	Uptake and cytotoxicity chitosan-coated NPs compared to lipofectamine . . . . .	76
6.12	Hemolysis and suppression of TNF- $\alpha$ secretion of LPS-stimulated DCs siRNA-CT-NPs . . . . .	77
7.1	Scaffold comparison . . . . .	85
7.2	Effect of cell seeding density . . . . .	87
7.3	Effect of cell seeding density analyzed by qPCR . . . . .	88
7.4	Effect of alginate in cell seeded scaffolds . . . . .	89
7.5	Gross appearance, GAG/DNA and dry weight of MSC, AC, and ECP-seeded scaffolds . . . . .	90
7.6	Chondrogenic potential of MSCs, ACs, and ECPs . . . . .	92
7.7	Hypertrophic phenotype of MSCs, ACs, and ECPs - qPCR analysis	93
7.8	Hypertrophic phenotype of MSCs, ACs, and ECPs - immunostaining . . . . .	94
7.9	Compressive modulus of MSC, AC, and ECP-seeded scaffolds .	95
A.1	GAG/DNA , gross view, alcian blue and EdU staining of MSC pellets and scaffolds . . . . .	134
A.2	Gene expression analysis and immunohistology of pellets and scaffolds . . . . .	135
B.1	IGF-1 for chondrogenic differentiation . . . . .	137
C.1	Gene expression profile of key differentiation markers . . . . .	148
C.2	Multilineage differentiation potential of MSCs . . . . .	149
C.3	Distribution of Cq values . . . . .	151
C.4	Fold changes ( $2^{-\Delta Cq}$ ) in reference gene expression . . . . .	152
C.5	Effect of reference gene stability on marker gene expression . .	156

## List of Tables

1.1	Clinically applied matrices for cartilage regeneration . . . . .	12
3.1	Common reagents and solutions . . . . .	28
3.2	MSC proliferation medium . . . . .	28
3.3	AC proliferation medium . . . . .	29
3.4	ECP proliferation medium . . . . .	29
3.5	Chondrogenic differentiation medium . . . . .	29
3.6	Collagen scaffold specifications . . . . .	31
3.7	Primer specifications (Species: <i>Homo sapiens</i> ) . . . . .	33
5.1	Literature overview of PTHrP publications for MSC hypertrophy inhibition . . . . .	47
6.1	siRNA sequences . . . . .	62
6.2	Primer sequences . . . . .	65
6.3	Characteristics of polycations . . . . .	70
6.4	Characterization of PEI and DEAE dextran-coated NPs . . . . .	72
6.5	Adsorption efficiency of Cy3-siRNA by DEAE-dextran and PEI-coated NPs . . . . .	72
6.6	Characterization of Chitosan-coated NPs . . . . .	74
6.7	Key characteristics of $\gamma$ -PGA-Phe NPs for siRNA delivery . . . . .	79
C.1	Primer specifications . . . . .	144
C.2	qPCR gene expression analysis of key differentiation markers . . . . .	147
C.3	Summary of the stability parameters evaluated for all seven reference genes in chondro, adipo and osteogenic differentiation . . . . .	153
C.4	Reference gene ranking based on geNorm, NormFinder, Best-keeper algorithms and IQR rating . . . . .	154



# 1 Cartilage tissue engineering



*Note: Part of this chapter has been published in *Molecular and biophysical mechanisms regulating hypertrophic differentiation in chondrocytes and mesenchymal stem cells*, D. Studer et al., *European Cells and Materials* (2012), 24, 118-135.*

Knee cartilage is particularly susceptible to traumatic lesions and degenerative joint disease from the nature, quantity, and force of the impacts it is subjected to over the course of a human lifetime. Its regeneration of cartilage has proven to be an enduring challenge, as attested to by William Hunter in 1742 “From Hyppocrates to the present age, it is universally allowed that ulcerated cartilage is a troublesome thing and that, once destroyed, is never recovered” [120]. Cartilage, once destroyed, does not spontaneously heal due to its avascular nature. The lack of intrinsic healing necessitates tissue engineered substitutes, a well investigated field motivated by the high number of knee injuries and osteoarthritis patients [113] who still do not have a viable treatment to regenerate damaged cartilage. To engineer functional cartilage tissue, principles of cell biology, material science, and medicine are combined. The two fundamental building blocks of a viable cartilage replacement are a suitable cell type, and a biocompatible matrix, which together should allow for the production of cartilage with mechanical and histological properties of native tissue. This chapter gives an overview of the clinically applied materials as well as the possible cell sources studied over the last decade with a focus on phenotypically stable cartilage engineering.

### 1.1 Structure and function of articular cartilage

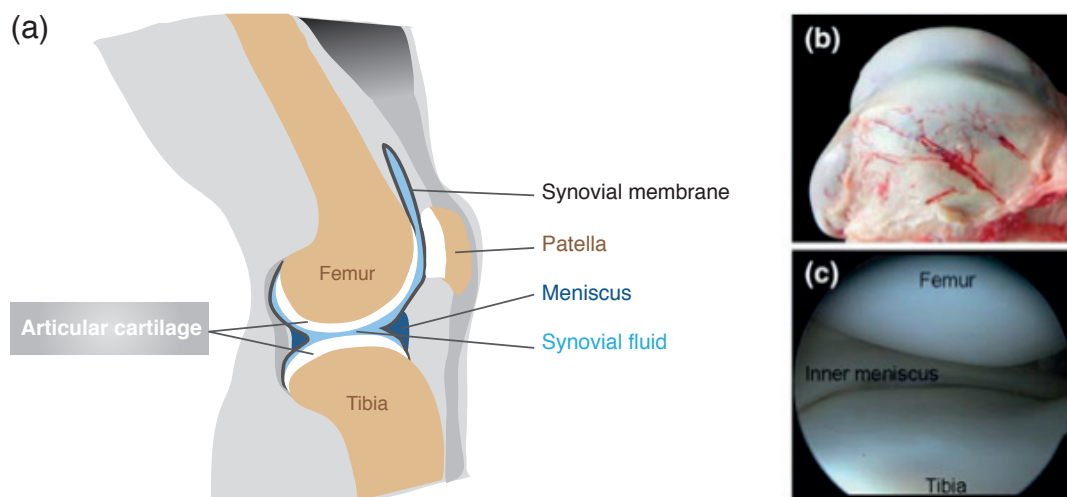


**Figure 1.1.:** Representations of the diarthrodial knee joint. (a) Side view of the knee joint composed of the distal end of the femur and the proximal end of the tibia, covered by articular cartilage. (b) Macroscopic and (c) Arthroscopic view of the hyaline cartilage in a healthy human knee joint. Image adapted from Schulz et al. [238].



Cartilage is present in three forms in the human body: elastic, fibrous, and hyaline. Elastic tissue can be found in the ear (external and auditory tubes) as well as in the epiglottis. Fibrocartilage, on the other hand, contains collagen 1 fibers and less elastin, giving intervertebral disks and the meniscus their strength. Lastly, hyaline cartilage consists of a cross-linked network of collagen fibrils and large aggregating proteoglycans and is present in the nose, trachea, larynx, bronchi as well as in most joints. Articular cartilage, which is a type of hyaline cartilage, is an avascular tissue that lines the end of articulating bones (see Figure 1.1) and functions as a friction reducing and shock absorbing material [238]. Synovial fluid, present in the joint capsule, transports nutrients into the otherwise secluded tissue.

Articular cartilage is a stratified tissue composed of a superficial, middle, deep and calcified layer. In the superficial zone, cells are flat and collagen fibrils are aligned in parallel. Going deeper, cells become rounder and increase in volume. In the deep zone, a columnar arrangement is observed. Once past the tidemark, the cell density, as well as their volume, is drastically decreased.

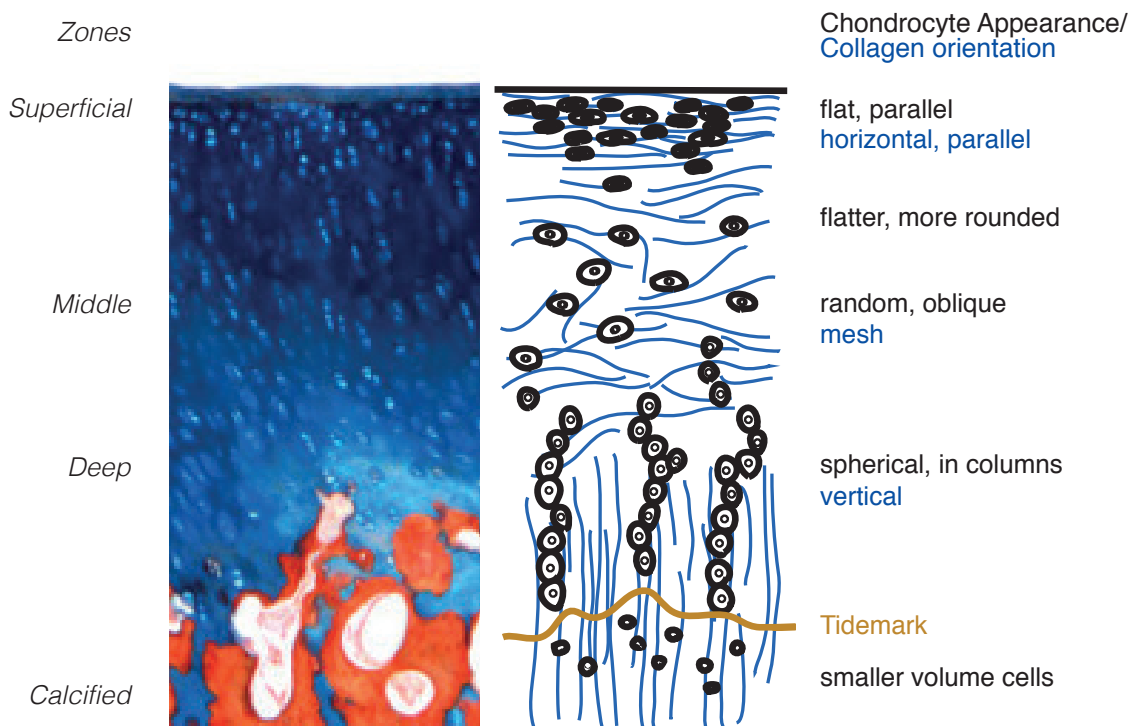


**Figure 1.2.:** Zonal structure of cartilage. In cartilage, both collagen and chondrocytes are organized within cartilage into superficial, middle, deep and calcified layers. Image adapted from Johnstone et al. [131] and Browne et al. [40].

Collagen fibrils in the middle zone arrange in a mesh, whereas the deep layer exhibits a dense vertical alignment extending into the calcified layer, acting as an anchor to the underlying bone. [238]

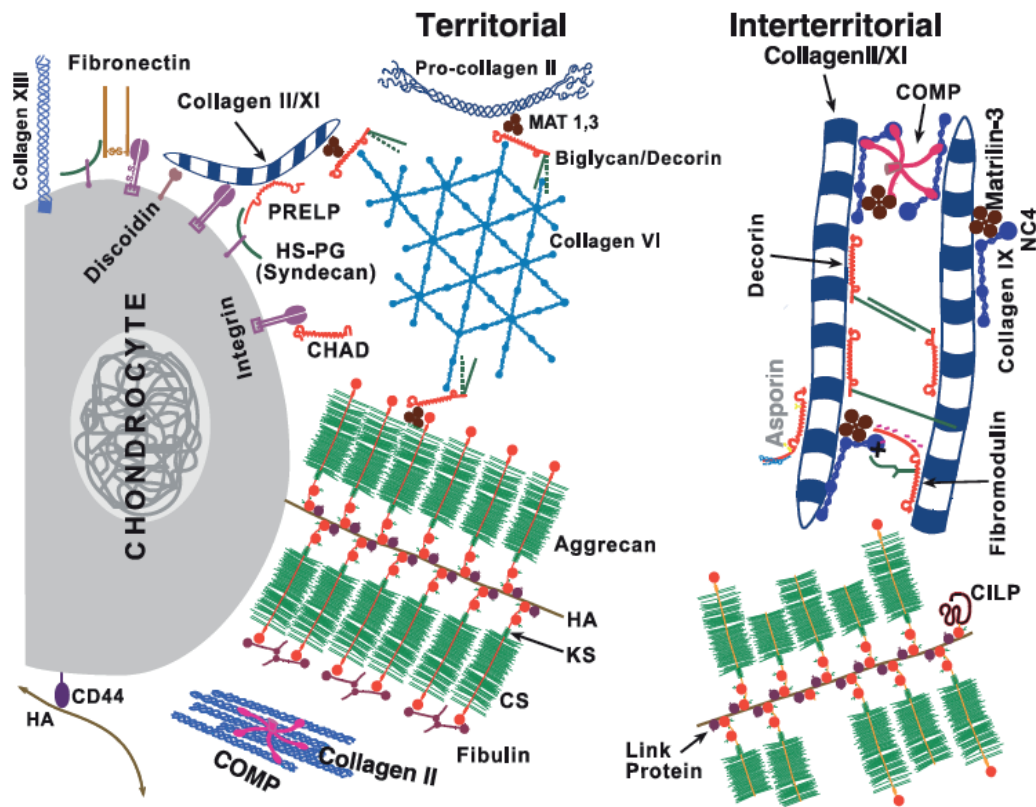


**Figure 1.3.:** Cartilage extracellular matrix composition. Image reproduced from Heinegård et al. [110].

Cartilage is produced and maintained by a single cell type, the chondrocytes, occupying only 1% of the tissue volume [261]. The dense extracellular matrix surrounding the cells inhibits cell-cell contact. Three matrix regions can be identified around the chondrocytes: the pericellular matrix (thin layer surrounding the cell), territorial matrix, and the interterritorial matrix (all three together forming the extracellular matrix (ECM)) [110]. The chondrocyte with its pericellular matrix (containing the ECM molecules closely associated with the plasma membrane) forms a chondron [218]. Besides the cells, articular cartilage is composed of ~ 65-75% w/w water and extracellular matrix [102]. Cartilage ECM consists of 60-86% w/w collagens, 15-40% w/w proteoglycans, fibronectin, integrins, cartilage oligomeric matrix protein (COMP) and other proteins involved in the maintenance of the complex structure [46] (see Figure 1.3). In proteoglycans the glycosaminoglycan (GAG)

side chains, present in the form of chondroitin sulfate (CS) and keratin sulfate (KS), are assembled on the core protein, which is attached via a link protein to hyaluronan (HA). HA forms the backbone of the brush-like aggrecans. The highly charged GAGs are a reservoir for water molecules and are responsible for the compressive strength of cartilage [102, 109]. The tensile strength is provided by collagen 2, the prevalent (90-95%) collagen type in cartilage [52, 106].

## 1.2 Current clinical treatments for cartilage repair

Damaged cartilage can cause severe joint pain, which can be controlled by several non-surgical methods. Regular physical exercises, weight loss, acupuncture or transcutaneous electrical nerve stimulations are treatments proposed by Osteoarthritis Research Society International (OARSI) [308]. These measures can be combined with pharmacological treatments such as the application of selective or non-selective cyclooxygenase-2 (COX-2) inhibitors (so called non-steroidal anti-inflammatory drugs, NSAIDs) as well as chondroprotective molecules (hyaluronates, glucosamine, and chondroitin sulphate) for further symptom relief [172]. Non-surgical approaches lead to short-term reduction in pain, but for a long term improvement, surgical intervention is required.

Surgical treatments range from palliative intervention, to biological repair or even total joint replacement with a metallic prosthesis [121]. Palliative treatment reduces pain and improves joint motion; during arthroscopic lavage or debridement, cartilage pieces and flaps that hinder joint motion are removed [78] whereas an osteotomy realigns the joint, moving the body weight from the injured area to healthy cartilage [292]. A total joint replacement is the last option, and is rarely done for young individuals, as the long term wear can lead to prosthesis failure and hence the need for future revision surgery. Biological repair aims to regenerate cartilage using one of two main techniques: chondrocyte implantation and bone marrow stimulation.

Osteochondral autograft transplantation surgery (OATS or mosaicplasty, see Figure 1.4) was introduced by several surgeons in the 1980/1990's [35, 298]. The transplantation of autologous osteochondral plugs from a non load-bearing region to the injury site has been associated with donor site morbidity and fibrocartilage formation at the graft interface [104, 121]. The stimulation of the subchondral bone by microfracture (see Figure 1.4) was first applied by Steadman in 1983 [256]. Bone marrow stimulation leads to the formation of a blood clot and the recruitment of

mesenchymal stromal cells (MSCs) which promote the resurfacing of the defect by fibrocartilage, a tissue with inferior mechanical properties compared to hyaline cartilage. A slight adaptation of the microfracture technique was introduced by Behrens in 2005 [27], which incorporates a collagen I/III matrix (termed AMIC) to retain the MSCs and protect the lesion [29].

In 1989, Grande et al. [96] proposed the first tissue engineering approach using in vitro expanded autologous chondrocytes implanted (ACI) in rabbit knees. By 1994, the first application of ACI in humans was reported in Sweden by Brittberg and Peterson [39] and has since undergone many modifications as described in the following section.

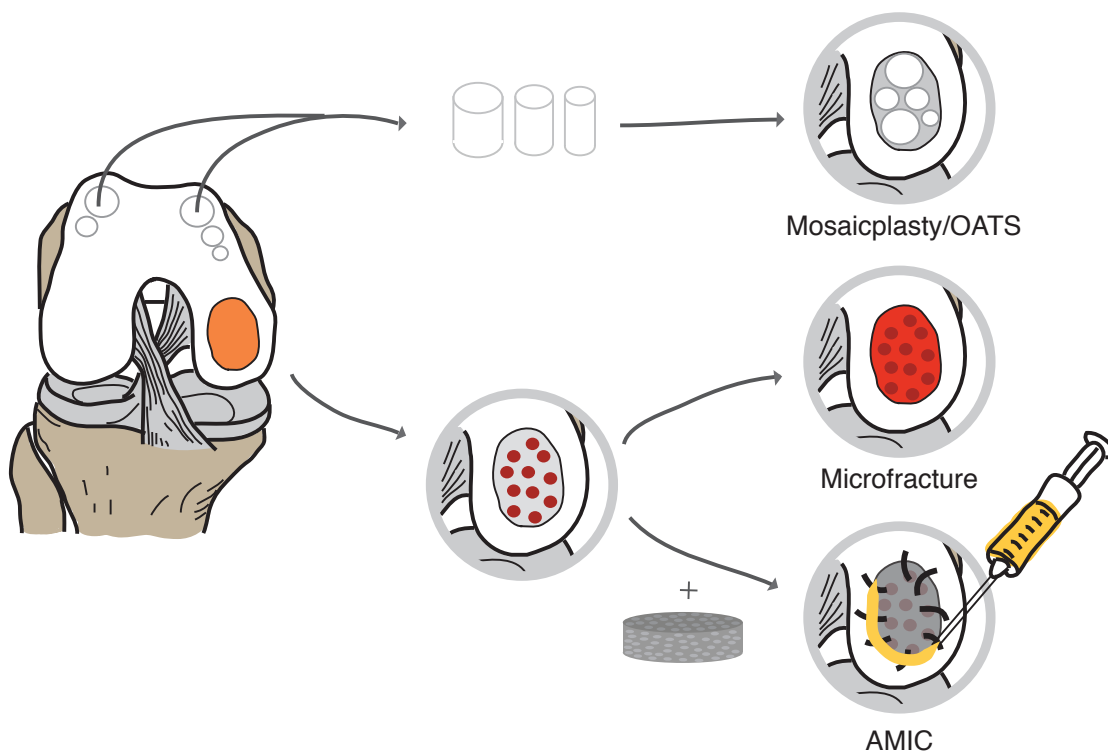


**Figure 1.4.:** Osteochondral autograft transplantation, microfracture. Osteochondral autograft transplantation surgery (OATS or mosaicplasty) implants osteochondral plugs from a non load-bearing region of the knee. The microfracture (MF) technique stimulates the release of mesenchymal stromal cells by drilling into the subchondral bone (fractures indicated by red dots). The formed blood clot initiates the formation of repair tissue. Autologous matrix-induced chondrogenesis (AMIC), an adaptation of the conventional MF, uses a matrix which is sutured onto the defect, and further secured with fibrin glue (yellow syringe). The matrix enables the retention of stimulated MSCs and growth factors in the defect.

### 1.2.1 Autologous chondrocyte implantation

ACI is based on a two-step procedure where a biopsy is removed arthroscopically from a non load-bearing area of the knee, the chondrocytes isolated and then expanded in vitro. Once the required cell number is obtained, the chondrocytes are implanted into the defect [179].

The implantation method has undergone several generations of refinement:

*First generation ACI:* proposed by Brittberg et al. [39] makes use of a periosteal flap sutured over the defect. Through additional application of fibrin glue, a water-tight seal is formed and the chondrocytes are injected into the cavity. The main drawbacks of this technique are the fragility of the periosteal flap which leads to leakage through tears and holes, the long operation time (performed in an open surgery), as well as the additional donor site morbidity caused by the flap removal [258].

*Second generation ACI:* the periosteal flap is replaced by a collagen I/III matrix which is sutured onto the defect. The use of a collagen membrane allows the ACI treatment to be simplified into a purely arthroscopic intervention. A randomised clinical trial of 68 patients showed no benefit of the use of periosteum over a collagen I/III membrane. [95]. In addition, McCarty et al. [186] reported a superior outcome of ACI using a collagen scaffold compared to periosteum. Together with the reduced occurrence of hypertrophy associated with periosteum [100], the collagen membrane is now accepted as the cover of choice for ACI. Steinwachs et al. [257] modified this procedure by incubating the collagen scaffold with the cell suspension directly before transplantation, thereby eliminated the requirement of a water tight seal. This cell-seeded matrix-supported autologous chondrocyte transplantation (ACI-Cs) allows for easier handling than classical ACI.

*Third generation ACI:* cells are not injected in suspension, but rather pre-cultured on a chondro-inductive or chondro-conductive matrix [190]. This method can be performed in a mini-arthrotomy as it only requires trimming of the defective area and fitting the scaffold to the defect without the need for sutures. The application of fibrin glue is sufficient to keep the scaffold in place.

## 1. Cartilage tissue engineering

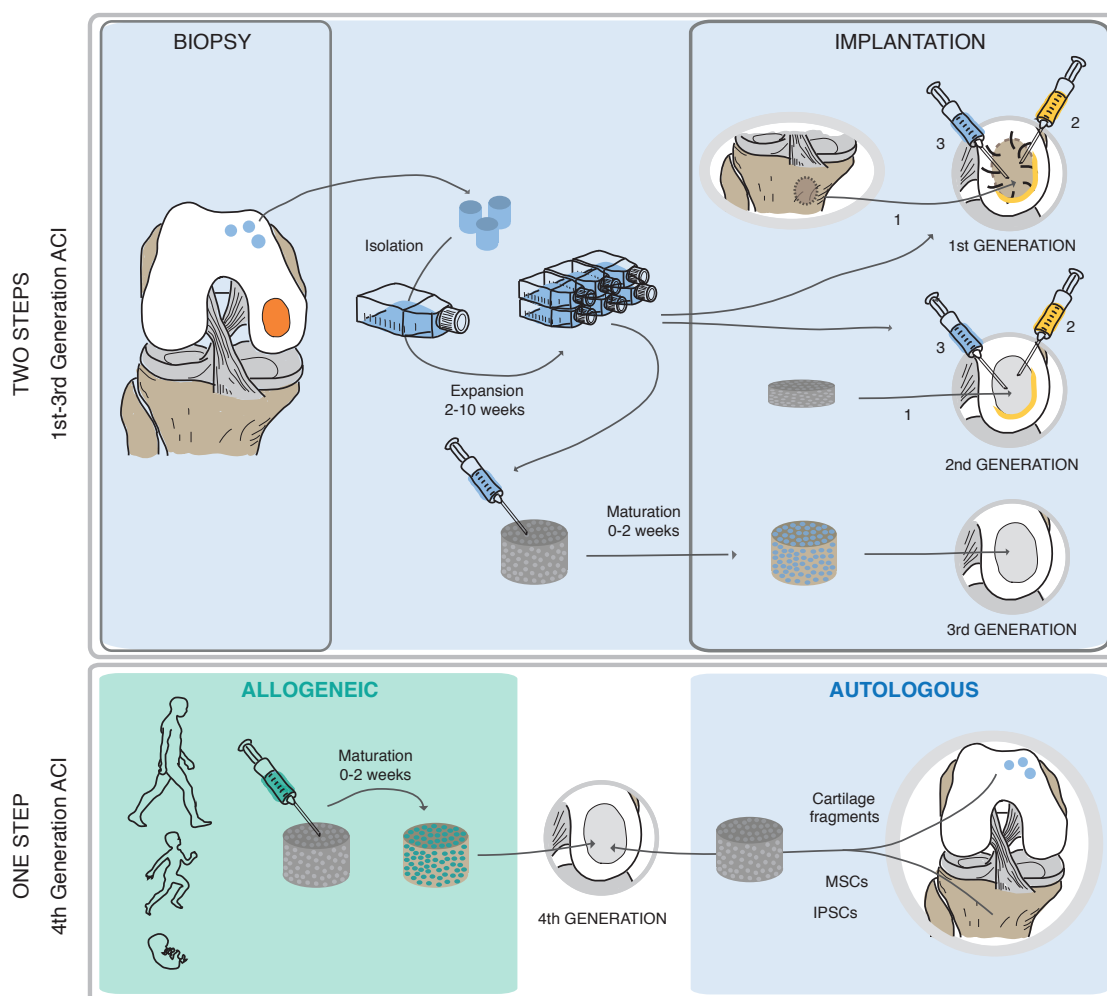


**Figure 1.5.:** Autologous chondrocyte implantation (ACI). 1st to 3rd generation ACI require two surgical interventions, with an initial biopsy removal from a non-load bearing area of the joint followed by the implantation of the isolated and expanded chondrocytes. The biopsy is processed in an external laboratory where the cells are isolated and expanded in tissue culture for 2-10 weeks. For 1st and 2nd generation ACI, the cells are injected beneath a periosteal flap secured by sutures and fibrin glue (1st generation) or a scaffold (2nd generation). For 3rd generation ACI, the expanded cells are seeded on a matrix and directly implanted or pre-cultured for 2-14 days before transplantation. 4th generation ACI uses a one-step surgical procedures applying off-the-shelf allogeneic cells (green shading) or autologous cells/tissue fragments (blue shading) prepared directly during surgery. Further 4th generation ACI might be augmented by gene modifications, siRNA silencing, or growth factor supplements. 3rd and 4th generation ACI require thick, defect-filling scaffolds whereas in 2nd generation ACI dense, tear-resistant scaffolds are applied.

*Fourth generation ACI:* in an attempt to reduce the surgical procedure to a single step, fourth generation ACI uses non-expanded autologous cells or allogeneic progenitor cells in combination with growth factors and gene therapy to produce a hyaline-like tissue. The potential cell sources are discussed in the following chapter. Gene therapy is an additional tool to improve the regeneration of cartilage via the overexpression of growth factors or the knock-down of undesired pathways via RNA interference. [201] A proposed one-step technique uses matrix-associated chondroplasty (MACH) which combines autologous platelet-rich plasma (PRP) with cells obtained from bone marrow aspirate of the distal femur. PRP is added onto of a collagen scaffold, sutured, and the bone marrow aspirate concentrate (obtained by centrifugation) injected together with fibrin. [260] Another MSC-based single step product is Cartistem<sup>®</sup>, a combination of microfracture and allogeneic umbilical cord blood-derived MSCs in a hyaluronic acid gel [207]. Two additional methods are currently in clinical phase III trial, DeNovo<sup>®</sup> natural tissue (NT), and engineered tissue (ET). Both procedures are based on the application of allogeneic juvenile cartilage which in the case of DeNovo<sup>®</sup> NT is implanted in fragments, whereas for DeNovo<sup>®</sup> ET, chondrocytes are isolated, expanded, and a scaffold-free construct produced. [77,268]

### 1.2.2 Matrices for cartilage tissue engineering

*Note:* Statements on clinical trials are based on <http://clinicaltrials.gov> and information concerning the legislation status in the European Union (EU) retrieved from <http://www.ema.europa.eu/ema/>.

Matrices in the form of scaffolds and gels have found widespread application in cartilage regeneration (see Table 1.1). Historically, collagen scaffolds were used to replace the periosteum, where their sole purpose was to seal the defect before the subsequent injection of chondrocytes. Since their initial use, scaffolds have evolved from a simple two-dimensional barrier to a three-dimensional cell carrier with a biological function such as the promotion of differentiation, proliferation, as well as a structural and mechanical support [127].

One of the most widely used scaffolds is Chondro-Gide<sup>®</sup> from Geistlich, Switzerland, a collagen I/III fleece initially developed for 2nd generation ACI (trademarked under CartiGro<sup>®</sup> [234]). The collagen fleece exhibits a bilayered structure with a dense, cell repellent sealing layer and a thin, slightly more open porous outer layer. Over time, the same matrix was applied together with microfracturing in the AMIC<sup>®</sup> procedure. Despite the low porosity of the scaffold, this method makes us

of the slightly open-porous defect-facing side to capture MSCs released into the defect by drilling into the subchondral bone. A controlled randomized trial performed at the University of North Norway, is currently underway to compare the use of Chondro-Gide<sup>®</sup> in AMIC and ACI. Following the development of the first commercial AMIC<sup>®</sup> product, several scaffolds such as Chondrotissue<sup>®</sup>, a non-woven polyglycolic acid scaffold treated with hyaluronic acid [210], Vericart<sup>™</sup>, as well as several gels entered the market for autologous matrix-induced chondrogenesis. Injectable gels have the advantage of being adaptable to the lesion, and to be stabilized in this form in situ through polymerisation. Such gels are composed of chitosan/ $\beta$ -glycerolphosphate (BST-CarGel<sup>®</sup> [253, 254, 259]), collagen I (Chondrofiller<sup>®liquid</sup>), as well as photocrosslinkable hyaluronic acid mixed with bioadhesive chondroitin sulphate (ChonDux<sup>™</sup> [273]) or polyethylene glycol diacrylate combined with denatured fibrinogen (Gelrin C<sup>™</sup> [51]).

The application of gels and scaffolds for the augmentation of microfracture is, from a regulatory point of view, much simpler than a cell-matrix composite. A cell-free product requires approval as a medicinal device III to receive the CE mark in the European Union (EU). Cell-based products, on the other hand, undergo an extensive process with three stage clinical trials. Furthermore, products that had been approved before 2008, are re-evaluated by the European Medicinal Agency (EMA) based on the implementation of new standards for advanced therapy medicinal products (ATMP). The new legislation further complicates the development of tissue engineering constructs. It is therefore not surprising that many commercial products are currently available for augmented microfracture (AMIC) but there is a limited number of m-ACI scaffolds.

The first 3rd generation ACI product, MACI<sup>®</sup>, has been available in Europe since 1998 and in 2013 received ATMP approval. MACI<sup>®</sup> uses a porcine collagen type I/III matrix (ACI-MAIX<sup>™</sup>, with structural similarity to Chondro-Gide<sup>®</sup>). Products that entered the market before 2008 were provided a transitional provision extending to 2012 when the newly required ATMP took effect, leading to the withdrawal of Fidia's Hyalograft<sup>®</sup> C from the market in 2013. The 2003 launched Novocart<sup>®</sup> 3D, a bi-layered collagen-chondroitin sulphate scaffold [305] and CaReS<sup>®</sup>, a collagen 1 gel used with unexpanded chondrocytes [236] still appear to be approved for use. After the strict regulations were put in place, the cartilage tissue engineering market experienced several years of cessation. Only recently, new clinical studies have evaluated the potential of novel m-ACI scaffolds such as bovine collagen 1-based Neocart<sup>®</sup> [53], freeze-dried fibrin-hyaluronan scaffold BioCart<sup>™</sup> II [126,200], and the agarose/alginate construct Cartipatch<sup>®</sup> [240]. Next to natural polymers, synthetic



constructs composed of polyglycolic acid, as in the case of BioSeed-C<sup>®</sup> [72], have also been tested in ongoing phase III clinical trials.

The long processing time of cartilage biopsies for ACI has prompted the development of single stage methods. The fragmentation and direct re-implantation of autologous cartilage constitutes the so called Cartilage Autograft Implantation System (CAIS<sup>®</sup>, phase III clinical trials) [77]. In 2007, Zimmer launched, together with ISTO, DeNovo NT, a product using allogeneic juvenile cartilage fragments. Due to its classification as "minimally manipulated tissue", DeNovo NT was allowed to be marketed without the complicated approval process. Next to DeNovo NT (natural tissue), ISTO also developed DeNovo ET (engineered tissue), a scaffold-free engineered tissue produced by juvenile chondrocytes. This product is in phase III clinical trials expected to be completed in late 2014. MSCs are an alternative cell source explored for one-step procedures. Clinical tests at Stanford University apply autologous adipose-derived MSCs whereas the use of allogeneic umbilical cord blood-derived MSCs together with an injectable hyaluronan gel is tested in Cartistem<sup>®</sup> [207].

Most studies on the aforementioned products report equivalent or superior outcomes compared to microfracture or classical ACI. There is a lack in studies comparing the effectiveness of different scaffolds, and therefore no conclusive statements can be made concerning the superiority of a certain matrix composition or structure over another for human applications. The group of Marlovits [10, 202] analysed the characteristics of MACI<sup>®</sup>, Hyalograft<sup>®</sup>, CaReS<sup>®</sup>, and Novocart<sup>®</sup> cell-seeded matrices at the pre-implantation stage. In Novocart<sup>®</sup>, cells were present in a spherical morphology, whereas more polygonal and elongated cells were observed in MACI<sup>®</sup>, Hyalograft<sup>®</sup>, and CaReS<sup>®</sup>. Whether this difference will affect the final m-ACI outcome is difficult to predict as there are already substantial differences in the formation of the construct before implantation. While ACs are used without expansion in CaReS<sup>®</sup>, Novocart<sup>®</sup> is composed of first passage cells while MACI<sup>®</sup> and Hyalograft<sup>®</sup> use chondrocytes passaged several times. Further, cell seeding densities in different m-ACI approaches (ranging from  $2 \times 10^3$  to  $20 \times 10^3$  cells/mm<sup>3</sup>) have been shown to affect cartilage regeneration [128,141,191,227,284,287]. Additionally, the in vitro pre-culture of cell-seeded constructs can influence the in vivo regeneration [191, 229]. Clinically, this parameter is highly inconsistent with Chondron<sup>®</sup> using no pre-culture, whereas Cartipatch<sup>®</sup>, CaReS<sup>®</sup> and Hyalograft<sup>®</sup> use constructs matured for up to 2 weeks. Overall, the high variance in culture protocols makes a direct comparison of the available matrices for cartilage regeneration difficult.

**Table 1.1.: Clinically applied matrices for cartilage regeneration (as of August 2014)**

Type	Product	Carrier name	Material	Technique	Stage	Cells	Cell density [cells/mm <sup>3</sup> ]	Passage	Pre-culture	Process time	Company
Scaffold	Chondroitin <sup>®</sup>		PGA/HA	AMIC	one						Biotissue
	VeriCart <sup>™</sup>		collagen	AMIC	one						Histogenics
	AMIC <sup>®</sup>	Chondro-Gide <sup>®</sup>	collagen I/III	AMIC	one						Geistlich
	CartiGro <sup>®</sup>	Chondro-Gide <sup>®</sup>	collagen I/III	2nd ACI	two	auto-AC	6-10×10 <sup>3</sup>	1	n/a	n/a	CellGenix/Stryker
	MACF <sup>®</sup>	ACI-MAIX <sup>™</sup>	collagen I/III	3rd ACI	two	auto-AC	10-20×10 <sup>3</sup>	n/a	7 days	4-6 weeks	Astrom
	Neocart <sup>®</sup>		collagen I	3rd ACI	two	auto-AC	n/a	n/a	n/a	6-12 weeks	Histogenics
	Novocart <sup>®</sup> 3D	Novocart <sup>®</sup> Basic	collagen I - CS	3rd ACI	two	auto-AC	2.5-15×10 <sup>3</sup>	1	2 days	3 weeks	Telec
	BioCart <sup>™</sup> II	CartiMate	fibrin/HA	3rd ACI	two	auto-AC	2-3×10 <sup>3</sup>	n/a	3-4 days	3-4 weeks	ProChon
	Hyalograft <sup>®</sup> C	HYAFF <sup>®</sup> 11	esterified HA	3rd ACI	two	auto-AC	3.3×10 <sup>3</sup>	n/a	> 2 weeks	6 weeks	Fidia
	Bioseed-C <sup>®</sup>		polymer scaffold*	3rd ACI	two	auto-AC	20×10 <sup>3</sup>	n/a	n/a	4-5 weeks	Biotissue
	CAIS <sup>®</sup>		polymer foam**	4th ACI	one	minced auto-Cart			none	n/a	DePuy/Mitek
	Gel	BST-CartGel <sup>®</sup>		chitosan	gel-AMIC	one					
Chondrofiller <sup>®</sup> liquid			collagen I	gel-AMIC	one						Amedix
Chondux <sup>™</sup>			HA/CS	gel-AMIC	one						CartiliX/Bionet
Gelrin C <sup>™</sup>			fibritogen/PEG-DA	gel-AMIC	one						Regentis
Cartistem <sup>®</sup>			HA	gel-AMIC	one	allo-UC-MSC					Dong-A Pharma
CAREs <sup>®</sup>			collagen I gel	3rd ACI	two	auto-AC	n/a	primary	10-14 days	2 weeks	Arthro Kinetics
Chondron <sup>®</sup>			fibritogen	3rd ACI	two	auto-AC	n/a	n/a	none	4-6 weeks	Sewon CellOnTech
Cartipatch <sup>®</sup>		GelForCel	agarose/alginate	3rd ACI	one	auto-AC	10-20×10 <sup>3</sup>	3	15 days	6 weeks	Tissue Bank of France
DeNovo <sup>®</sup> NT			fibrin	4th ACI	one	minced allo-Cart					Zimmer

\* scaffold of polyglycolic/polylactic acid and polydioxanone

\*\* copolymer foam of 35% polycaprolactone, 65% polyglycolic acid, and polydioxane mesh

Abbreviations: autologous articular chondrocytes (AC), cartilage (Cart), autologous chondrocyte implantation (ACI), microfracture (MF), autologous (auto), allogeneic (allo), hyaluronic acid (HA), chondroitin sulfate (CS), polyethylene glycol diacrylate (PEG-DA), polyglycolic acid (PGA), umbilical cord blood-derived MSCs (UC-MSC)

### 1.2.3 Cell sources for cartilage tissue engineering

Cartilage regeneration requires a cell type that produces abundant extracellular matrix closely resembling the matrix of native articular cartilage. The human body possesses a variety of cell sources with chondrogenic potential, from the chondrocytes found in native cartilage, to various progenitor cells derived from non-cartilaginous tissue sources shown in Figure 1.6. Chondrocytes can, based on the maturation stage of the tissue, be divided into immature (generally below 13 years old) and mature cells.

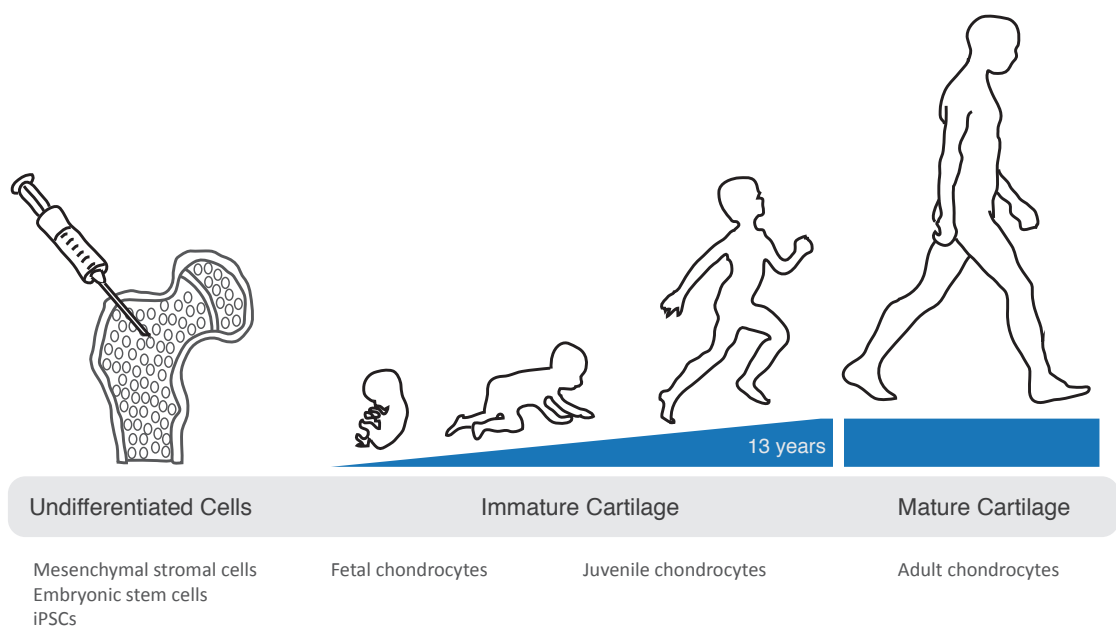


**Figure 1.6.:** The three main cell sources for cartilage regeneration: undifferentiated cells, immature and mature chondrocytes. Examples for undifferentiated cells are embryonic stem cells, adult mesenchymal stromal cells as well as induced pluripotent stem cells (iPSCs). Cartilage reaches maturity between the age of 13 to 20 and therefore allogeneic immature chondrocytes from fetal or juvenile tissue as well as autologous mature chondrocytes have been considered for treatment of cartilage lesions.

### *Mature chondrocytes*

The most obvious source of cells for cartilage regeneration are the only cells in cartilage, chondrocytes. Current clinical treatments use these cells for their inherent capacity to form cartilage ECM. Chondrocytes are isolated from a tissue biopsy removed in a non-weight bearing region of the knee. This process damages healthy cartilage and might be responsible for further degeneration of the joint [157]. Furthermore, the low cell yield from adult cartilage requires tissue culture expansion over several weeks. During this time, chondrocytes undergo de-differentiation characterized by the loss of collagen 2, increase in collagen 1, and the appearance of a fibroblastic phenotype [58,235]. Despite the possibility for re-differentiation [45,69,199], the two-step procedures, using passaged autologous chondrocytes, are time and cost intensive. In an attempt to reduce the necessary intra-articular procedures, minced cartilage pieces have been used in the cartilage autograft implantation system (CAIS), a technique in phase III clinical trials. Although CAIS eliminates the expansion phase, donor site morbidity due to cartilage harvest is still present.

Hyaline cartilage is not only found in the joints but also in the nose and in the rib bones (costal cartilage). To minimize damage to the articular joint, the exploitation of other hyaline sources as well as elastic cartilage, such as auricular cartilage, has become popular. Several studies show promise in de-novo cartilage formation [16,112,212,216], but the question remains whether these cells are able to produce the cartilage components specific to articular cartilage. Furthermore, autologous chondrocyte implantations suffers from a unpredictable patient variability which might be partially caused by age-related decline of proliferation and chondrogenic capacity [20].

The inherent difficulties with autologous cells has motivated the study of allogenic alternatives. Cartilage is, due to its avascular nature and the dense extracellular matrix, an immune-isolated tissue. Furthermore, chondrocytes themselves have been identified to be immunosuppressive [4]. Mature chondrocytes from allogenic sources have the advantage of being available as a potential off-the-shelf treatment, but the low cell density requires cell expansion, and de-differentiation occurs as in the case of autologous chondrocytes. The application of mature allogenic chondrocytes in alginate beads has nevertheless shown satisfactory results after 5-8 years [64].

*Immature chondrocytes*

Cartilage maturation is a process that takes between 15 to 20 years in humans [6], and is marked by a decrease in cell density, as well as chondrogenic potential [3, 268]. Thus the use of fetal or juvenile (younger than 13 year old) chondrocytes has attracted attention in recent years. Juvenile chondrocytes have shown promise compared to adult chondrocytes [165, 248] with increased matrix synthesis. These factors, taken together, have led to development of two new products applying juvenile cartilage allografts in the form of minced cartilage (deNovo NT [268]) and expanded chondrocytes (deNovo ET). Fetal cartilage is a more immature tissue compared to juvenile cartilage with an even higher cell density [73]. In a comparison of fetal and adult ovine chondrocytes, fetal cells showed higher proliferative potential as well as increased GAG and collagen 2 synthesis [87].

*Undifferentiated progenitors*

Progenitor cells are, for their high cell number and chondrogenic potential, an attractive alternative to chondrocytes. Adult mesenchymal stromal cells (MSCs) can be found in many tissues in the body such as bone marrow, synovium, fat pad, as well as in adipose tissue [22]. MSCs not only exhibit a high proliferation rate, but more importantly, are able to differentiate into the three mesenchymal lineages: bone, fat, cartilage and others [215]. The utility of undifferentiated MSCs is hampered by their tendency to differentiate into a tissue with an undefined character. MSCs induced towards chondrogenesis do not form stable cartilage, but immediately upon induction, initiate hypertrophic markers and eventually mineralize. The same endochondral ossification occurs during chondrogenic differentiation of embryonic stem cells (ESCs) [133] and iPSCs [66]. ESCs and iPSCs nevertheless present, with their unlimited self-renewal, great potential for future cartilage treatments using optimized culture protocols. Before ESCs or iPSCs can be used for clinical treatment, their tumorigenic safety would need to be established [204].

### 1.3 Engineering phenotypically stable cartilage

The low cell number obtained from autologous chondrocytes and the resulting long expansion phase leading to de-differentiation has motivated the quest for a more abundant source of cells. MSCs with their high chondrogenic potential (see Section 1.2.3) have been at the centre of attention, however, their tendency towards hypertrophy has so far hindered their clinical application. This section presents the characteristics of hypertrophy together with possible strategies to engineer phenotypically stable cartilage.

#### 1.3.1 Hypertrophy in the growth plate and in vitro

Many clues for controlling hypertrophy can be found following the process of skeletal development which begins in humans 4 - 5 weeks after fertilization [117, 224]. Chondroprogenitor cells of diverse embryonic origin [220] begin to upregulate expression of transforming growth factor beta (TGF- $\beta$ ), fibronectin, N-CAM, and N-Cadherin which initiates cell condensation and cartilage differentiation [101] (Figure 1.7). The differentiation phase of stem cells towards chondrogenesis can be divided into distinct stages including cell attachment, proliferation/differentiation and differentiation/hypertrophy [193].

#### *MSC chondrogenesis in vitro*

Chondrogenesis of MSCs is typically induced in vitro by incubating cells in defined media containing TGF- $\beta$ , ascorbic acid and dexamethasone in combination with a 3D culture system such as micromass pellets [132, 175, 187, 215], hanging drop culture [36, 71] or cellular encapsulation in hydrogels [31, 162, 166, 184, 184]. While upregulation of the chondrogenic genes Sox9 and collagen 2 can be observed during in vitro induction of chondrogenesis, the differentiating cells also exhibit markers of hypertrophy including collagen 10, MMP-13, and ALP [195, 213, 239] (see Figure 1.7b).

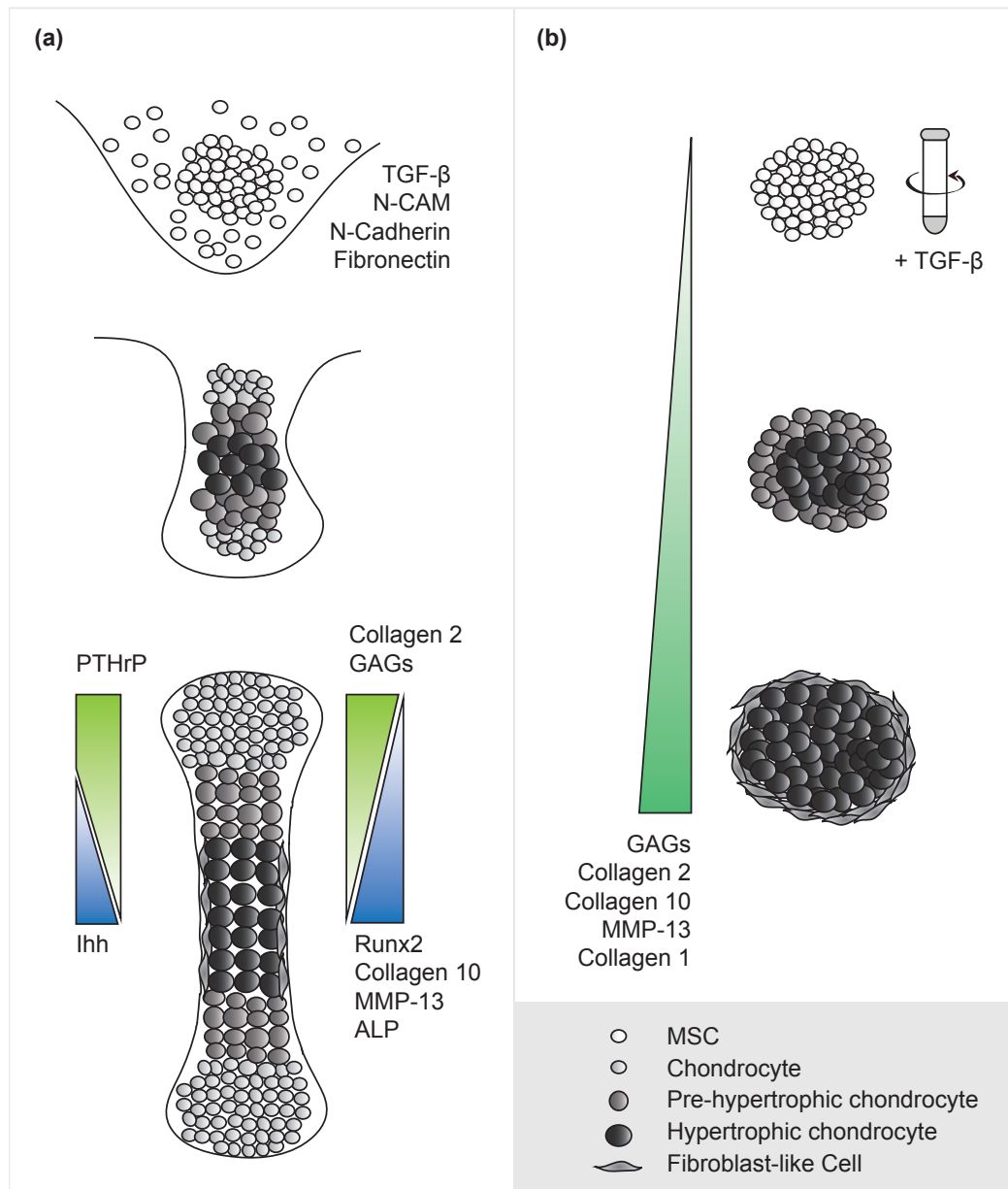


**Figure 1.7.:** In vivo and in vitro chondrogenesis and hypertrophy. (a) Chondrogenesis initiates in limb bud development when MSCs undergo condensation, a process facilitated by increased expression of cAMP, TGF- $\beta$ , fibronectin, N-CAM, and N-cadherin. Mature chondrocytes begin secreting cartilage matrix components primarily consisting of collagen 2 and glycosaminoglycans (GAGs). Chondrocytes outside the signaling range of PTHrP secreted by resting zone chondrocytes produce Ihh, a potent inducer of cell hypertrophy. Hypertrophic chondrocytes secrete collagen 10, which establishes the framework for subsequent calcification and endochondral ossification. Formation of the growth plate is accompanied by perichondrium development and vascular invasion, as well as an ossification centre containing fibroblast-like cells that express collagen 1. (b) During in vitro chondrogenesis, MSCs are centrifuged into a micromass pellet and cultured in medium containing TGF- $\beta$  to induce differentiation. The critical spatiotemporal cues are not present in this method, and the majority of the MSC population continues to express both collagen 2 and collagen 10 concomitantly.

### 1.3.2 Characterization of chondrocyte hypertrophy

Chondrocyte hypertrophy is marked by a 10-fold increase in cell volume [41], extracellular matrix remodelling (see Figure 1.8a) and expression of terminal differentiation markers including runt-related transcription factor 2 (Runx2), matrix metalloprotease 13 (MMP-13), collagen 10, alkaline phosphatase (ALP) and Indian Hedgehog (Ihh) [195] (see Figure 1.8b). The transcription factors Runx2 and myocyte enhancer factor-2C (MEF2C) drive the expression of the terminal differentiation markers including MMP-13 [246], collagen 10 [15, 255, 265], Ihh [303] and vascular endothelial growth factor (VEGF) [155], which all functionally contribute to endochondral ossification. Secreted MMP-13 degrades collagen 2 [124] and aggrecan [85], key ECM components of functional cartilage. Hypertrophic marker collagen 10 is deposited within the hypertrophic ECM and serves as a framework for subsequent calcification [244]. The large gradient in calcium concentration from a high extracellular to a lower intracellular concentration is most likely the major driving force behind mineralization, triggering the influx of calcium and subsequent volume increase [24, 97]. Calcification of the cartilage ECM originates at matrix vesicles (MVs) containing ALP, which are secreted from chondrocytes in response to increasing calcium concentrations [123] and are anchored to the collagen 10 matrix [244].

In the first step of mineralization, ALP hydrolyses pyrophosphate (PPi) into inorganic phosphate ( $\text{PO}_4^{3-}$ ) which, in the presence of calcium, forms hydroxyapatite inside the MVs [19]. Other sources of phosphate are the hydrolysis of phospholipids by PHOSPHO1 [177] as well as the influx through the type-III Na/Pi cotransporter. Calcium influx into matrix vesicles is regulated by annexin II, V and VI with annexin V activity simulated by binding to collagen 2 and 10 fibrils [146].

The second step of mineralization is initiated by the penetration of hydroxyapatite crystals into the extracellular space where their prolongation is regulated by the  $\text{PO}_4^{3-}$  production by tissue non-specific alkaline phosphatase (TNAP) as well as PC-1, a nucleoside triphosphate pyrophosphohydrolase, inhibiting mineralization through the production of PPi [205].

The final stages of endochondral ossification including degradation of the calcified matrix, VEGF-mediated vascular invasion of the calcified zone, and deposition of osteoid on the calcified trabecules by osteoblasts are under control of MMPs [206]. Post-mitotic hypertrophic chondrocytes pass through a transient autophagy stage to help meet the energy demands of cells [252] before undergoing apoptosis and being removed from the growth plate [242].



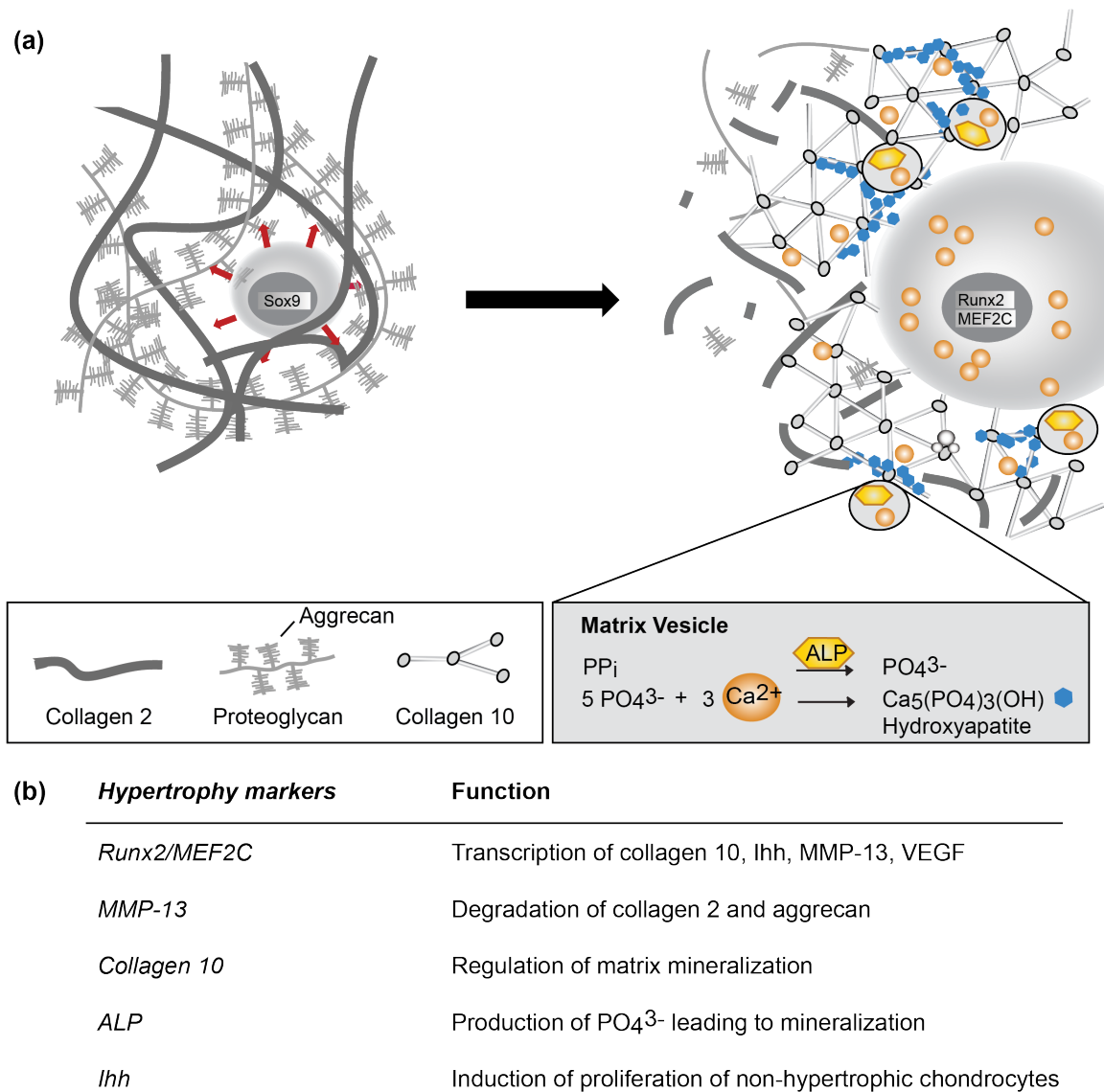


**Figure 1.8.:** Hypertrophy and the main actors. (a) Hypertrophy is marked by cell volume increase (red arrows) and ECM remodeling (b) These changes are regulated by the transcription factors Runx2/MEF2C, which regulate the transcription of collagen 10 [15,255,265], *Ihh* [303], MMP-13 [246] and VEGF [155]. MMP-13 degrades aggrecan and collagen 2 [124], *Ihh* increases non-hypertrophic chondrocyte proliferation [277], collagen 10 facilitates the mineralization process through association with matrix vesicles (MV) [244], and alkaline phosphatase (ALP) dephosphorylates pyrophosphate (PPi) to phosphate ( $PO_4^{3-}$ ), leading to hydroxyapatite formation [14].

### 1.3.3 Strategies for hypertrophy inhibition based on molecular pathways

A complex signaling network is involved in the hypertrophy regulation as outlined in Figure 1.9. This section focuses on TGF- $\beta$  and PTHrP as hypertrophy suppressive cytokines.

#### TGF- $\beta$

Transforming growth factor-beta (TGF- $\beta$ ) is a potent inducer of chondrogenesis in vitro [21, 289]. Signalling pathways of the TGF- $\beta$  superfamily have been reviewed [276] including its downstream phosphorylation of Sma and Mad Related Family (Smads), which exhibit both stimulatory and inhibitory effects on chondrocyte hypertrophy. The Smad1/5/8 route, through which BMPs signal and control FGF pathways [180, 302], induces hypertrophy by epigenetic changes and blocking phosphorylation of Smad1/5/8 inhibited expression of 3 terminal differentiation markers [111]. The Smad2/3 pathway is activated by TGF- $\beta$ , directly leading to inhibition of hypertrophy and the induction of chondrogenesis due to the stabilization of Sox9 transcription complex by Smad2/3 [90, 300]. TGF- $\beta$  activation of Smad3 also leads to Runx2 inhibition through epigenetic regulation [136]. Although TGF- $\beta$  is crucial in regulating chondrocyte hypertrophy, its addition to induction media during pellet culture of MSCs is not enough to suppress the onset of hypertrophy [195, 213, 239]. TGF- $\beta$ 1-supplemented expansion media has further shown to redirect chondrocytes towards hypertrophy [198].

**Figure 1.9** next page: Signaling pathways initiated by TGF- $\beta$  (grey shading), PTHrP/PTH (yellow shading), Wnt (orange shading), integrin- $\beta$ 1 interaction with collagen 10 [173] (green shading), and calcium ions (pink shading). The main transcription factors (rectangular boxes) regulating hypertrophy are Sox9, which is responsible for the expression of collagen 2 and aggrecan, and Runx2 which regulates transcription of collagen 10, MMP-13, VEGF and Ihh genes. Sox9 was shown to inhibit Runx2 [70] via Nkx3.2 [299, 311]. MEF2C is proposed to be the main regulator of Runx2 [15], which acts through Dlx5/Dlx6 [280]. SHOX/Shox2 is yet another upstream activator of Runx2. Nkx3.2 is induced by PTHrP [219] and acts synergistically with Sox9 [299] to inhibit Runx2 [160]. Ihh is triggering the protein degradation of Nkx3.2 [49]. Histone deacetylases (HDACs) participate in epigenetic regulation preventing transcription by stabilizing DNA packing around histones (grey cylinders), whereas histone acetylases (HATs) provide access to the DNA strands. HDACs are released via phosphorylation by kinases that provide a phosphate (P) which can then be bound by chaperones (14-3-3) and exported out of the nucleus. Green indicates a pathway involved in the suppression, and blue the promotion of hypertrophy. Dashed lines represent the expression of marker genes. <P> depicts phosphorylation/dephosphorylation and <Ub> ubiquitination.

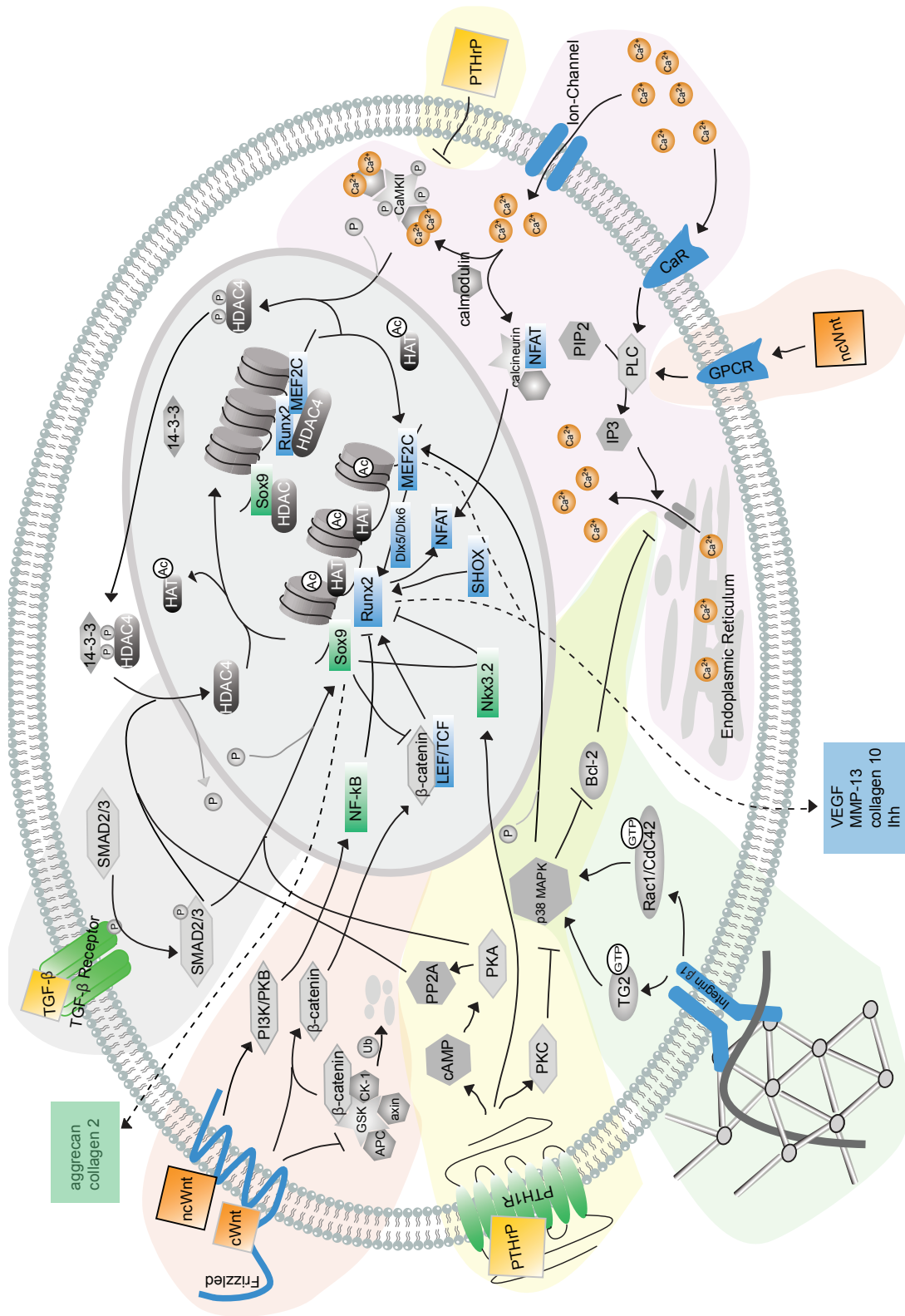


Figure 1.9.: Molecular pathways of hypertrophy.

### *PTHrP*

Parathyroid hormone-related protein (PTHrP) is emerging as one of the key anti-hypertrophy factors. The knockout of PTHrP [178, 283] or its receptor [99, 149, 156] leads to accelerated hypertrophy *in vivo*. PTHrP participates in a negative feedback loop with Indian Hedgehog (Ihh), a stimulatory factor of hypertrophy and chondrocyte proliferation [149, 153, 156]. Resting chondrocytes at the ends of long bones secrete PTHrP, subsequently suppressing Ihh production in the proliferating zone. Chondrocytes outside of this paracrine signalling range, however, do produce Ihh and undergo hypertrophy. Ihh also leads to hypertrophy independently of PTHrP [178].

PTHrP functions by activating protein kinase A and C (PKA and PKC) [161] and also interferes with the calcium pathway by dephosphorylation of calcium/calmodulin-dependent protein kinase (CaMKII) [163]. Cyclic adenosine monophosphate (cAMP)-dependent PKA phosphorylates Sox9 [118] and activates protein phosphatase II (PP2A), leading to the de-phosphorylation of histone deacetylase 4 (HDAC4) and the inactivation of MEF2C [152]. PKC inhibits the activity of the mitogen-activated protein kinase (MAPK) p38 [309] reducing MEF2C phosphorylation [255] and, ultimately, hypertrophic gene expression.

#### 1.3.4 Hypertrophy inhibition using RNA interference

Next to the application of hypertrophy-suppressive cytokines, the use of RNA interference (RNAi) presents a more directed approach [105]. The ancient defense mechanism of cells against parasitic nucleic acids has, since its discovery in 1998 [81], been explored for experimental cell research as well as RNAi therapeutics [61]. Double-stranded small interfering RNA (siRNA) assembles with the RNA-induced silencing complex (RISC) and after unwinding, gets bound with its antisense strand. Through binding to the complementary mRNA, its gene expression is suppressed. This post-transcriptional gene silencing method also been applied as a tool for hypertrophy inhibition. The knock-down of Runx2 and CCAAT/enhancer-binding protein- $\beta$ , both transcription factors involved in the regulation of endochondral ossification, led to decreased collagen 10, MMP-13 and VEGFA [116]. Wei et al. [288] further demonstrated the effectiveness of using siRNA to inhibit Ihh for decreased hypertrophy. Another target is the family of metalloproteinases involved in the degradation of the extracellular matrix. ADAMTS-4 siRNA could successfully reduce aggrecan degradation [250].

### 1.3.5 Lessons learnt from epigenetics

Histone (de)acetylation, DNA methylation, and microRNAs are epigenetic approaches strongly involved in chondro-specific differentiation [23, 89] (see Figure 1.10). When DNA is present in the nucleus in a highly packed form, wrapped around histones, access of transcription factors is restricted and transcription downregulated. Histone deacetylases (HDACs) keep the chromatin in this form, whereas histone acetyl transferases (HATs) decrease the association of the histone with the DNA strand allowing the access of transcription factors. The release of HDACs from the histone complex is performed through kinase-induced phosphorylation, which creates chaperone (such as 14-3-3) docking sites that, once bound, transport HDACs out of the nucleus. Phosphatases dephosphorylate HDACs to activate and relocate them into the nucleus. Another epigenetic control is the introduction of methylation sites on cytosine-guanine dinucleotides (CpG) by DNA methyltransferases [47]. CpG islands (areas with high concentration of CpGs) are mostly found in the promoter region of genes where methylation causes gene silencing. MicroRNAs are post-transcriptional regulators of messenger RNAs (mRNAs), that by binding to their complementary sequence, can repress translation or lead to the degradation of mRNAs [291].

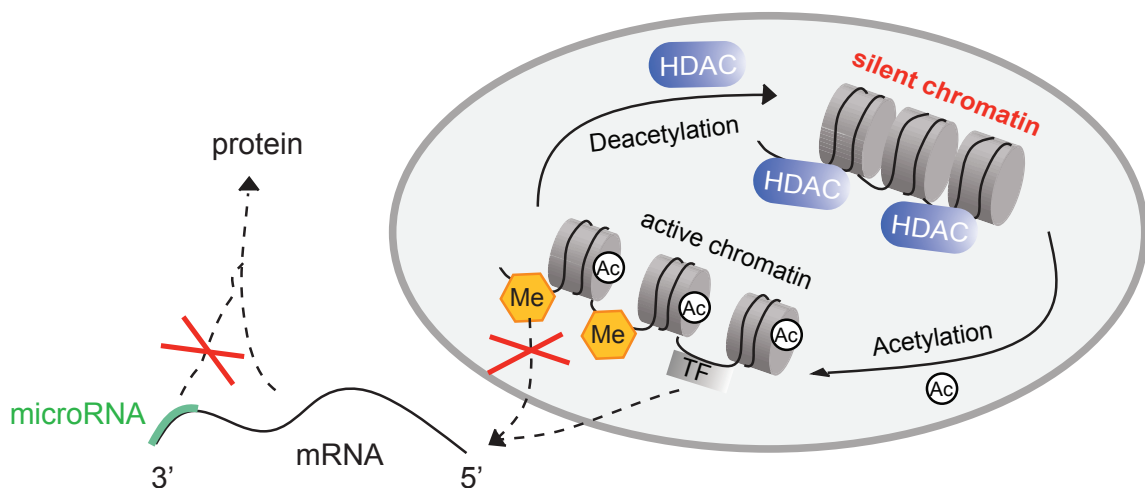


**Figure 1.10.:** The epigenetic regulation of hypertrophy involves histone deacetylases (HDACs), which act inside the nucleus to compact the chromatin into a silent structure. The acetylation (Ac) of histones opens up the chromatin for transcription of DNA by transcription factors (TF). Methylation (Me) of the DNA inhibits its transcription to messenger RNA (mRNA), whereas the post-transcriptional regulation of microRNAs inhibits the translation of mRNA by binding to its 3' untranslated region.

Many strategies have been proposed using histone (de)acetylation, (reviewed in [262]). The role of gene silencing through DNA methylation during chondrogenesis and hypertrophy is, in comparison, still in its infancy. Runx2 and Sox9 were shown to keep their methylation status during in vitro chondrogenesis of synovium-derived MSCs [76] whereas COL10A1, the gene encoding collagen 10 $\alpha$ 1, was found to be methylated in articular chondrocytes, in contrast to mesenchymal stem cells which were de-methylated during chondrogenesis [312]. This difference might explain why hypertrophy is less likely in chondrocyte pellet cultures compared to MSC pellets. The epigenetic regulation occurring during maturation of cartilage might be a benefit for using immature cartilage versus undifferentiated progenitor cells.

## 2 Scope

Cartilage regeneration has been an medical obstacle for decades. The developments in tissue engineering have allowed the progress from mainly pain-reducing interventions to treatments with the promise of regenerating cartilage in its native form. The current cell-based strategies focus on the expansion of chondrocytes obtained from the patient's own tissue. Autologous cartilage implantation (ACI) requires a two step procedure with the initial biopsy harvest, 2-12 weeks process time for isolation and expansion, and the final transplantation of cells. The need for two surgical interventions together with an external GMP-compliant laboratory for cell isolation and expansion makes ACI a time and cost intensive treatment, and low cell yields of autologous chondrocytes (ACs) hinder the development of a simpler and faster process. The establishment of abundant, chondrogenic cell sources is therefore one of the major challenges in cartilage research. This thesis focuses on possible alternative cell sources and their potential to produce phenotypically stable cartilage.

In the first part of this thesis, the potential of adult mesenchymal stromal cells (MSCs) for cartilage engineering was explored. MSCs are a promising candidate for treating cartilage lesions due to their presence in many tissues of the human body as well as their multipotent nature. In Chapter 4, the classical pellet culture system applied to induce MSCs towards chondrogenesis is presented. The stimulation of MSCs through cell condensation and the application of transforming growth factor beta (TGF- $\beta$ ) led to the expression of chondrogenic genes (collagen 2, aggrecan, Sox9) as well as markers associated with the progression of cartilage towards a calcified tissue (collagen 10, Ihh, MMP-13), so called hypertrophy. This process mimics the events naturally occurring during the formation of long bones. Articular cartilage, the tissue lining the surface of the bones, is developmentally different in that it does not progress towards endochondral ossification. The phenotypic instability of chondrogenically-induced MSCs is a major hurdle to their clinical application.

Chapter 5 presents the application of parathyroid hormone-related protein (PTHrP) as a possible drug to control the hypertrophy of MSCs. PTHrP is involved in the regulation of hypertrophy in the growth plate, where together with Ihh, it orchestrates the proliferation of chondrocytes and their progression towards calcification. Cells in close proximity to PTHrP secreting cells at the end of long bones, suppress

Ihh whereas further away, PTHrP levels drop and calcification starts. Its potent anti-hypertrophic action *in vivo* led to the assumption that its application during MSC chondro-differentiation would produce phenotypically stable cartilage. The effect of concentration and time point of application of PTHrP on MSC pellet culture was assessed by RT-PCR. The results clearly showed that PTHrP is not only a potent inhibitor of hypertrophic genes such as collagen 10 but also reduces collagen 2 expression. This adverse effect could not be reversed under hypoxia nor upon change from PTHrP fragment 1-86 to 1-34.

The unspecific effect of PTHrP prompted the focus to shift to the development of siRNA-based therapeutics which allowed the sequence-specific inhibition of target genes. The research group of Prof. Akashi at University Osaka has developed biodegradable  $\gamma$ -PGA-Phe nanoparticles (NPs) with broad applications in drug delivery. In a collaborative project described in Chapter 6, the use of these NPs for siRNA delivery was investigated. Incorporating the siRNA into the core of the particles resulted in a low loading efficiency. However, the use of polycation coatings on the surface of the negatively charged  $\gamma$ -PGA-Phe NPs produced siRNA carriers with efficient cell uptake. Chitosan-coated NPs showed superior biocompatibility to commercially available siRNA transfection reagents and could successfully inhibit the LPS-stimulated maturation of dendritic cells.

Despite the advances in MSC research, the undefined phenotype of their *de-novo* cartilage remains a hurdle to clinical application. Thus, research attention has recently shifted towards cell sources with a more defined composition, such as chondrocytes derived from immature cartilage. Chapter 7 presents the potential of fetal epiphyseal chondrocytes (ECPs) as an off-the-shelf solution for the future treatment of cartilage lesions. A comparison of fetal ECPs with adult MSCs and ACs in a collagen scaffold showed that ECPs are, in their genetic fingerprint, much closer to mature chondrocytes than MSCs. ECPs were able to produce an extracellular matrix rich in collagen 2 and proteoglycans with minor collagen 10 production. The absence of hypertrophy in ECP-derived tissues suggests that they have an epigenetic pre-programming similar to ACs which allows for the formation of phenotypically stable cartilage. Furthermore, ECPs used as an allogenic cell source allowed a more reproducible cartilage formation compared to ACs suffering from high donor-to-donor variability. This discovery is of great importance for future clinical applications aiming towards a one-step procedure.

Chapter 8 concludes this thesis by providing an overview of the most important findings, together with an outlook on future cartilage regeneration strategies.



### 3 Materials and methods



### 3. Materials and methods

---

This chapter describes the materials, protocols and experimental techniques used throughout this thesis. In addition, particular experimental techniques or alternative protocols are given in experimental (sub-)sections in Chapters 5 to 7

## 3.1 Reagents and solutions

**Table 3.1.:** Common reagents and solutions

Component	Storage	Supplier
Agarose	RT	Lonza #50004L
EDTA	RT	AppliChem #A2937
Formaldehyde	RT	Sigma #F15587
PBS	4 °C	Gibco® #10010-015
BSA	4 °C	Sigma #A7906
Trypsin-EDTA	-20 °C	Gibco® #25200-056
Recovery™ cell culture freezing media	-20 °C	Gibco® #12648-010

## 3.2 Media compositions

### 3.2.1 Proliferation media

*Mesenchymal stromal cell - proliferation medium*

**Table 3.2.:** MSC proliferation medium

Component	Volume	Stock conc	Final conc	Reconstitution	Storage	Supplier
alpha-MEM	445 ml				4 °C	Gibco® #22561
FBS	50 ml	100%	10% v/v		-20 °C	Gibco® #10270-106
Pen Strep	5 ml	100%	1% v/v		-20 °C	Gibco® #15140-122
FGF-2	10 µl	50 µg/ml	1 ng/ml	100 µl 5 mM Tris + 900 µl 0.1% BSA in PBS	-80 °C	Peptrotech #100-18B

*Articular chondrocytes - proliferation medium***Table 3.3.:** AC proliferation medium

Component	Volume	Stock conc	Final conc	Reconstitution	Storage	Supplier
DMEM	450 ml				4 °C	Gibco® #32430-027
FBS	50 ml	100%	10% v/v		-20 °C	Gibco® #10270-106
Gentamycin	500 µl	50 mg/ml	10 µg/ml		RT	Gibco® #15710-049
Ascorbic Acid	1 ml	25 mg/ml	50 µg/ml	DMEM	-80 °C	Sigma

*Epiphyseal chondroprogenitors - proliferation medium***Table 3.4.:** ECP proliferation medium

Component	Volume	Stock conc	Final conc	Reconstitution	Storage	Supplier
DMEM	500 ml				4 °C	Gibco® #41966-029
FBS	50 ml	100%			-20 °C	Gibco® #10270-106
L-Glutamine	5 ml				-20 °C	Gibco® #25030-024
Gentamycin	500 µl	50 mg/ml	10 µg/ml		RT	Gibco® #15710-049

**3.2.2 Chondrogenic differentiation****Table 3.5.:** Chondrogenic differentiation medium

Component	Volume	Stock conc	Final conc	Reconstitution	Storage	Supplier
DMEM	49 ml				4 °C	Gibco® #31966-021
ITS+	500 µl	100%	1% v/v		4 °C	Corning #354352
Pen Strep	250 µl	100%	0.5% v/v		-20 °C	Gibco® #15140-122
Sodium pyruvate	50 µl	100 mg/ml	100 µg/ml	water	-20 °C	Fluka #15990
L-proline	50 µl	40 mg/ml	40 µg/ml	water	-20 °C	Fluka #81709
L-ascorbate-2-phosphate	50 µl	50 mg/ml	50 µg/ml	water	-20 °C	Sigma #A8960
Dexamethasone	50 µl	100 µM	100 nM	96% ethanol	4 °C 2 weeks	Sigma #D4902
TGF-β3	500 µl	1 µg/ml	10 ng/ml	10 mM citric acid 0.1% BSA in PBS	-20 °C	Peptotech #100-36E

Media stable for 2 weeks at 4°C. Grey shading: only to be added immediately before use. For a control, TGF-β3 is omitted.

### 3.3 Cell isolation and culture

#### 3.3.1 Mesenchymal stromal cells

The mesenchymal stromal cells (MSCs) were isolated from femur-derived bone marrow samples that were obtained during surgical hip replacement of otherwise healthy patients after having received informed consent. The protocol was approved by the ethical board of the Kantonspital St.Gallen, Switzerland (ethical committee approval number EKSG08/014/1B). The bone marrow samples were incubated in 20 ml isolation medium (25 mM HEPES (Fluka, #54459), 128.5 mM NaCl (Fluka, 71380), 5.4 mM KCl (Fluka, #60130), 5.5 mM D(+)-glucose (Sigma, #G7528), 51.8 mM D(+)-saccharose (Sigma, 84097), 0.1% BSA (Sigma, #A6003)) overnight at 4°C. Afterwards, the sample was centrifuged at 110 g for 15 minutes at 4°C to remove fat tissue. The remaining pieces of trabecular bone were rinsed several times with isolation medium that was collected and filtered through a 200 µm filter. The filtered cell solution was centrifuged, the resulting cell pellet resuspended in MSC-proliferation medium (see Section 3.2.1) and seeded at a density of  $1 \times 10^7$  cells in a T75 culture flask containing proliferation medium.

#### 3.3.2 Articular chondrocytes

Human articular chondrocytes were isolated from cartilage pieces obtained during surgical knee operations performed at the Schulthess Clinic, Zürich, Switzerland (ethical committee approval number KEK-ZH 2013-0097). The pieces were minced into 1-3 mm<sup>3</sup> pieces using a scalpel and digested in 0.1% collagenase solution (DMEM Gibco® #32430-027, 1 mg/ml collagenase from Clostridium histolytic Sigma #C6885, 10% v/v FBS) overnight with gentle stirring at 30 °C. The resulting cell suspension was passed through a 100 µm and subsequently 40 µm strainer. By centrifugation at 500×g for 8 minutes, the cell pellet was collected and the supernatant aspirated. This step was repeated twice to remove the remaining collagenase. Further, the cell number was determined and the cells treated according to the experimental needs. For cryopreservation,  $0.5-1 \times 10^6$  cells/ml were suspended into recovery™ cell culture freezing media (Gibco® #12648-010) and placed in a Mr. Frosty™ Freezing Container (Thermo Scientific™ #5100-0001) at -80 °C. For tissue culture expansion, cells are resuspended in AC proliferation medium (see Section 3.2.1) and seeded at a density of 3'000 cells/cm<sup>2</sup>.

### 3.3.3 Epiphyseal chondroprogenitors

The biopsy was collected and processed as described by Darwiche et al. [59]. From one vial of the parental cell bank, a working cell bank was developed for the project. These cells were expanded to passage 5 in ECP proliferation medium (see Table 3.4).

## 3.4 Chondrogenic differentiation assays

### 3.4.1 Pellet culture

Chondrogenic differentiation of MSCs was induced by pellet culture for which 200'000 - 250'000 cells/well were placed in 96-well V-bottom plates (Thermo Scientific™, Nunc #249946) and centrifuged at 250×g for 5 minutes. The pellet was cultured at 37°C with 5% CO<sub>2</sub> in 250 µl of chondrogenic or control medium (see Section 3.2.2). The medium was replaced every 3-4 days for 21 days. As a control, pellets were cultivated in chondrogenic medium lacking TGF-β3.

**Note:** Plates for pellet culture are required to be made out of polypropylene as this material, compared to common polystyrene, does not lead to cell attachment.

### 3.4.2 Scaffold culture

Different collagen scaffolds were used in this thesis:

**Table 3.6.:** Collagen scaffold specifications

Name	Composition	Thickness	Clinically used	Supplier
Optimaix 3D	porcine collagen I/III	1.5 mm	no	Matricel, Germany
Novocart® Basic	porcine collagen, chondroitin-sulfate	2 mm	yes	TeTeC, Germany
Chondro-Gide®	porcine collagen I/III	1 mm	yes	Geistlich, Switzerland

With the help of a biopsy puncher with plunger (Polymed, #8511616), punches of 2 mm diameter were taken from the scaffolds and transferred into a 96-well plate pre-coated with agarose (40 µl per well, UV-sterilized for 30 minutes) to inhibit cell attachment to the well plate. Cells were seeded at the indicated density (between 10'000 to 50'000 cells/mm<sup>3</sup> in a total volume of 5 µl per punch and left at RT for 15 minutes before adding 250 µl of chondrogenic medium or the control medium (see Section 3.2.2). The medium was replaced every 3-4 days. After completion

of the experiment, scaffolds are washed once in PBS, transferred into eppendorf tubes, excess PBS removed and stored at  $-80^{\circ}\text{C}$  until the qPCR (see Section 3.5) or GAG/DNA (see Section 3.6) analysis. For cryosectioning, scaffolds are transferred with a spatula into cryomolds, covered with O.C.T., frozen on dry ice and stored at  $-80^{\circ}\text{C}$  until processing (subsequent steps described in Section 3.7)

## 3.5 Real-time quantitative RT-PCR assay

### 3.5.1 RNA isolation and quantification

The RNA isolation protocol was changed over the course of the PhD project. Data presented in Chapter 4 and Chapter 5 up to Section 5.4 are performed using a collagenase-based procedure: Chondrogenic pellets were digested in 3 mg/ml collagenase II (Sigma, #C6885) for 2 h to break down the abundant negatively charged extracellular matrix and thereby increasing the RNA yield using affinity column-based extraction. Afterwards, the pellet was washed in PBS, and total RNA prepared using the RNeasy<sup>®</sup> Micro Kit (Qiagen, Hombrechtikon, CH, #74004) according to the manufacturer's protocol.

All data presented in the above mentioned chapters was done with a new protocol using mechanical disruption of the tissue: Cartilage pellets and scaffolds were washed in PBS, shock-frozen in liquid nitrogen and crushed using Kimble-Chase Kontes<sup>™</sup> Pellet Pestle<sup>™</sup> (Thomas Scientific, United States, #3411D50). Total RNA was prepared using NucleoSpin<sup>®</sup> miRNA kit from Macherey Nagel #740971.

The RNA concentration was determined using Take3 Micro-Volume Plate on a Microplate reader Synergy H1<sup>™</sup> (BioTek, Instruments) or on a Nanodrop<sup>™</sup> ND-1000 Spectrophotometer (Nanodrop, Wilmington, DE). Only RNA with an OD 260/280 ratio between 1.9-2.1 was used for PCR analysis. RNA was stored at  $-80^{\circ}\text{C}$  until further use.

### 3.5.2 RT-PCR

RT-PCR was performed on the StepOnePlus<sup>™</sup> Real Time PCR system (Applied Biosystems<sup>®</sup>). Reverse transcription of 200 - 500 ng total RNA to cDNA was done with oligo(dT)<sub>20</sub> Primer (Invitrogen<sup>™</sup>, #18418-020) and 10mM dNTP Mix (Invitrogen<sup>™</sup>, #18427-013) using SuperScript<sup>®</sup> III Reverse Transcriptase (Invitrogen<sup>™</sup>, #18080-044)

in a total reaction volume of 20  $\mu$ l. A temperature program of 5 minutes priming at 65°C followed by the reverse transcription at 50°C for 30 minutes and the reverse transcription inactivation at 70°C for 15 minutes was run. After a final cool-down to 4°C, the cDNA was stored at -80°C for subsequent use. The oligonucleotides (purchased from Microsynth AG, Balgach, Switzerland) displayed in Table 3.7 were reconstituted at a concentration of 100  $\mu$ M and stored at -20°C for further use. All primers are designed over exon-exon junctions using the Real Time PCR Design Tool from Integrated DNA Technologies to avoid the amplification of genomic DNA. Only primer pairs with efficiency between 90-110% were used. A final concentration of 150 nM forward and reverse primer, respectively, was used for each qPCR reaction.

**Table 3.7.:** Primer specifications (Species: *Homo sapiens*)

Gene	Name	Accession n°	bp	Primer sequence (5'-3')
RPL13a	Ribosomal protein L13a	NM_012423	100	F - AAGTACCAGGCAGTGACAG R - CCTGTTCCGTAGCCTCATG
GAPDH	Glyceraldehyde-3-phosphate dehydrogenase	NM_002046.3	98	F - AGTCAGCCGCATCTCTTTT R - CCAATACGACCAAAATCCGTTG
Collagen 1	Collagen, type I, alpha 1	NM_000088	83	F - CAGCCGCTTCACCTACAGC R - TTTTGATTCAATCACTGTCCGC
Collagen 2	Collagen, type II, alpha 1	NM_001844	92	F - GGAATTCGGTGTGGACATAGG R - ACTTGGGTCCTTGGGTTTG
Collagen 10	collagen, type X, alpha 1	NM_000493	108	F - ATTCTAGTGGCTCCAATGTG R - GCCTACCTCCATATGCATTTT
AGG	Aggrecan	NM_001135	98	F - GAATGGGAACCGCCTATAACC R - TCTGTACTTCTCTGTGTCTG
Sox9	SRY (sex determining region Y)-box 9	NM_000346.3	93	F - TCTGGAGACTTCTGAACGAGAGC R - TGTAATCCGGGTGGTCCTTC
Runx2	Runt-related transcription factor 2	NM_001015051.3	100	F - CGCATTTCAGGTGCTTCAGA R - GCATTCGTGGGTTGGAGAA
MMP13	Matrix metalloproteinase 13	NM_002427.3	115	F - CCTTCAAAGTTTGGTCCGATG R - TCAAATGGGTAGAAGTCGCC
Ihh	Indian hedgehog	NM_002181.3	119	F - GGAGGGTGTGCATTGGTAC R - CAGCGGTGGAGTCCTTTC
PTH1R	Parathyroid hormone 1 receptor	NM_000316.2	119	F - ATGCTCTTCAACTCTTCCAG R - TTGAAGTCCAGTGCCAGTG
TGFBR1	Transforming growth factor, beta receptor 1	NM_004612.2	116	F - TGCTCCAAACCACAGAGTG R - AGCCCATTGCATAGATGTCAG
TGFBR3	Transforming growth factor, beta receptor 3	NM_003243.4	109	F - TGGTGTGGCATCTGAAGAC R - GCTGTCAAGGAGAAGTTTGC
AnnexinV	Annexin A5	NM_001154.3	108	F - CGAAGTATACCTGCCTACCTTG R - ATCAATCTCACTCTGGAAACC

The Fast SYBR<sup>®</sup> Green Master Mix (Applied Biosystems<sup>®</sup>, #4385614) was used to perform the qPCR amplification from the cDNA in a final volume of 20  $\mu$ l with 5  $\mu$ l of 1:5 diluted cDNA. The cycling conditions were as follows: an initial 95°C for 3

minutes, followed by 40 cycles of 95°C for 10 seconds, 60°C for 30 seconds. Then, a melting curve was constructed by heating from 65°C to 95°C in temperature steps of 0.5°C.

All RT-PCR data was analyzed using the  $2^{-\Delta\Delta Cq}$  method [167] (assuming that the amplification efficiency equals 100%) and normalized against the reference gene RPL13a (established as the most stable reference gene for MSC chondrogenesis, see Appendix Chapter C. Each gene was evaluated in independent PCR runs including the complete set of samples.

## 3.6 Biochemical analysis

### 3.6.1 Sample preparation

Pellets or scaffolds were weighed wet (using a microbalance), lyophilised and weighed dry (only possible for scaffolds as pellets are below the range of microbalance) and digested in 100 µl papain digestion buffer at 60°C with 1000 rpm shaking (and several vortexing steps) overnight. Papain digestion solution consisted of 25 µl/ml papain from papaya latex Sigma #P4762 in 5 mM L-cysteine HCl Sigma #C7477, 50 mM sodium phosphate Sigma #342483, 2 mM EDTA in water. pH was adjusted between 6.3-6.5 and the solution sterile filtered. The solution is stable at 4 °C for 10 days. The digested samples are used for the analysis of amount of glycosaminoglycans (GAGs) using the cationic dye 1,9-Dimethyl-Methylene Blue (see Section 3.6.2) that selectively binds to GAGs as well as for the amount of DNA determined by a Pico green assay (see Section 3.6.3).

### 3.6.2 Dimethylmethylene blue assay (DMMB)

The sGAG content was determined using the dimethylethylene blue (DMMB) assay. Chondroitin 4-sulfate sodium salt from bovine trachea (C4S, Fluka #27042) was used to create a standard curve (1-5 µg, above 5 µg assay isn't linear anymore). 25 µl of digested sample (if necessary diluted between 1:5 and 1:20 in papain solution to yield values within the linear range) was transferred into a 96-well plate and 100 µl of DMMB solution (preparation see below) added. The absorbance at 595 nm was measured on the plate reader and the corresponding amount calculated using a linear regression for the standard curve of C4S. The GAG contents were reported per sample or normalized to the DNA amount measured (see Section 3.6.3)



Preparation of DMMB solution:

- dissolve 21 mg of DMMB (1,9-Dimethyl-Methylene Blue zinc chloride double salt, Sigma #341088) in 5 ml absolute ethanol with 2 g of sodium formate (Sigma #71539)
- stir thoroughly in 800 ml double distilled water
- titrate concentrated formic acid (Fluka #06440) into the dye solution to adjust pH to 3
- add double distilled water to complete to 1 l of total volume

### 3.6.3 Pico green assay (DNA)

The Quant-iT™ PicoGreen® dsDNA Assay Kit (Invitrogen™, #P7589) was applied to quantify the DNA content of the constructs using Deoxyribonucleic acid sodium salt from calf thymus (Sigma #D3664, 1 ng/ml - 1 µg/ml) as standard. 2-5 µl of digested sample was diluted in 45-48 µl of TE-Buffer and transferred into a black 96-well plate (Sigma #CLS3603) and 50 µl of Pico green solution added. The samples were analyzed in a Microplate reader Synergy H1™ (BioTek, Instruments), with an excitation wavelength of 480 nm and the emission measured at 520 nm. The DNA content was reported as weight per sample or normalised to day 1.

## 3.7 Histological and immunohistochemical analyses

*Note:* All samples were processed without fixation (except for EdU-stained tissue pieces).

### 3.7.1 Cryosectioning

Samples were transferred directly from the culture plate into a cryomold (Cryomold® Intermediate 15×15×5 mm, Sysmex #4566), excess media was removed, samples covered with O.C.T (Tissue-Tek® O.C.T™ Compound Blue, Sysmex #4530) and frozen on dry ice. Samples were stored at -80 °C until processing employing the cryotome. Sections were cut 4 µm-thick using a CryoStar™ NX70 Cryostat (Thermo Scientific™) and microtome blades (ACCU-Edge® LOW CRYO SECT Sysmex #4810). The sections were collected on a Polysine™ Microscope Adhesion Slide (Menzel-Gläser, Thermo Scientific™ #P4981) or a Superfrost™ Plus Adhesion Slides (Menzel-Gläser,

Thermo Scientific™ #P10143352), left at room temperature to dry and stored at -20 °C until processed for stainings.

#### 3.7.2 Alcian blue staining

Cryosections were postfixed in 4% formaldehyde for 7 minutes, washed 3× in PBS and hydrated in double distilled water for 2 minutes (crucial to avoid unspecific staining). Further, alcian blue solution (Sigma #B8438) was added for 30 minutes and washed under running water. Nuclear fast red (Sigma #N3020) counterstain was incubated for 5 minutes. The slides were dehydrated sequentially in 95% ethanol and 100% ethanol, allowed to dry before mounting with Richard-Allan Scientific™ Mounting Medium (Thermo Scientific™ #4112).

#### 3.7.3 Immunohistological staining

Antibody stainings of collagen 1, 2 and 10 were performed on cryosections. First, O.C.T was removed in PBS for 5 minutes and sections were left to dry in order to outline the sections with a PAP pen (Sigma #Z672548). Further, 5% BSA in PBS was applied for 1 hour to block unspecific staining. For collagen 1 staining, no epitope retrieval was required and anti-collagen 1 antibody (Abcam #ab6308, clone COL-1) was applied at 1:200 dilution. Collagen 2 staining was performed after 30 minutes of 0.2% w/v hyaluronidase (Sigma #H3506) digestion at 37 °C, applying 1:20 diluted anti-collagen 2 antibody (Developmental Studies Hybridoma Band, clone II-II6B3). One hour of 0.2% w/v hyaluronidase digestion was required for collagen 10 staining before antibody (Abcam ab49945, clone COL-10, 1:50 dilution) incubation. All primary antibodies were diluted in 1% BSA in PBS and incubated overnight at 4 °C. After three washing steps with PBS, secondary antibody (Alexa Fluor® 594 Goat Anti-Mouse IgG (H+L) Antibody, Molecular Probes®, Invitrogen™, #A-11005) was applied at 1:200 dilution in 1% BSA in PBS for 1 hour at RT. Another three PBS washes were performed before incubation of nuclear stain DAPI (Molecular Probes®, Invitrogen™, #D1306) and the subsequent mounting with VectaMount™ AQ Mounting Medium (Vector Laboratories #H5501).

### 3.7.4 EdU - proliferation labeling and staining

A Click-iT<sup>®</sup> EdU (5-ethynyl-2'-deoxyuridine) Imaging Kit (Invitrogen<sup>™</sup> #C10086) was used to examine cell proliferation in pellets and scaffolds. Samples cultured in chondrogenic medium (see Section 3.2.2) were incubated with 10  $\mu$ M EdU for 24-48 hours prior to harvesting. Samples were processed as described in Section 3.7.1, with an additional step of fixation in 1% formaldehyde for 10 minutes prior to O.C.T embedding. Sections were permeabilized with 0.1% Triton for 10 minutes and stained for EdU with Alexa 488 according to the provider's protocol.

### 3.7.5 Phalloidin/DAPI staining

F-actin and cell nuclei were visualized on cryosections using rhodamine-labelled phalloidin and DAPI respectively. Sections were post-fixed with 4% formaldehyde for 10 minutes and permeabilized in 0.1% Triton X-100 for 10 minutes. F-actin fibers were stained for 30 minutes followed by 10 minutes of DAPI (Molecular Probes<sup>®</sup>, Invitrogen) incubation. After completion, slides were washed in PBS and mounted with VectaMount AQ Mounting Medium (Vector Laboratories).

## 3.8 Image acquisition and analysis

Histological images were acquired with a Axio Vert.A1 microscope (Zeiss). Fluorescent images were taken with a ApoTome.2 microscope (Zeiss).

## 3.9 Statistical analysis

All box plots used in this thesis have the following structure: The central line represents the median, the circle the mean, the box delimits the 25th and 75th percentiles and the whiskers extent to the minimum and maximum values (not considered outliers). Outliers were defined as an observation 1.5 times larger than the interquartile range.

Statistical evaluation was performed using Prism (Graphpad Software Inc., Version 6.0d) unless otherwise stated. P-values below 0.05 were considered statistically significant and if  $p < 0.001$  noted with an asterisk (\*) or otherwise with their exact number.



## 4 Characterization of MSC hypertrophy by gene and protein expression



Adult mesenchymal stromal cells (MSCs) are a promising cell source for cartilage regeneration due to their high proliferation potential and their capacity to undergo chondrogenic differentiation [21,215,239]. The chondrogenic induction of MSCs has been shown in many culture systems, pellet cultures being the oldest and most extensively studied. Yoo et al. [301] first introduced the pellet system as an *in vitro* tool to study MSC chondrogenesis. In this procedure, condensation occurring during *in vivo* mesenchymal chondrogenesis is mimicked by the centrifugation of MSCs which results in a dense cell aggregate. Thereby, N-cadherin is transiently unregulated, indicating the onset of cell-cell interaction and condensation [271]. Pellets cultured in a chemically defined TGF- $\beta$ -containing media upregulate cartilage-specific and hypertrophic genes in parallel [195,213]. To characterize the chondrogenic and hypertrophic induction in pellets a wide array of chondrogenic and hypertrophic markers was analyzed in MSC pellet culture in a 2-4 day interval, over a total of 22 days and stainings were performed for the key markers, collagen 2 and 10, as well as for proteoglycan production.

### 4.1 Gene expression analysis

During TGF-beta induced pellet culture, the multitude of genes affected can be classified into: 1) change from the early start of pellet culture (see light grey boxes in Figure 4.1), 2) from day 6 onwards (marked in light blue) and 3) starting in the second week of culture (dark blue boxes). The main extracellular components of cartilage, aggrecan, and collagen 2 are both strongly upregulated. Aggrecan is one of the early markers, whereas collagen 2 shows a steep increase in mRNA only after 9 days. This is interesting as the master chondrogenic transcription factor, Sox9, is correlated with collagen 2 appearance but aggrecan precedes it. It must therefore be concluded that aggrecan is also induced in a Sox9-independent manner, which is contrary to the findings of others [48,103]. In parallel to the induction of genes responsible for the cartilage matrix production, a whole array of hypertrophic genes are unregulated. Collagen 10 peaks at day 9, overlapping with an increase in collagen 2. *Ihh*, another inducer of endochondral ossification, exhibits an earlier increase, but an overall similar expression pattern to collagen 10.

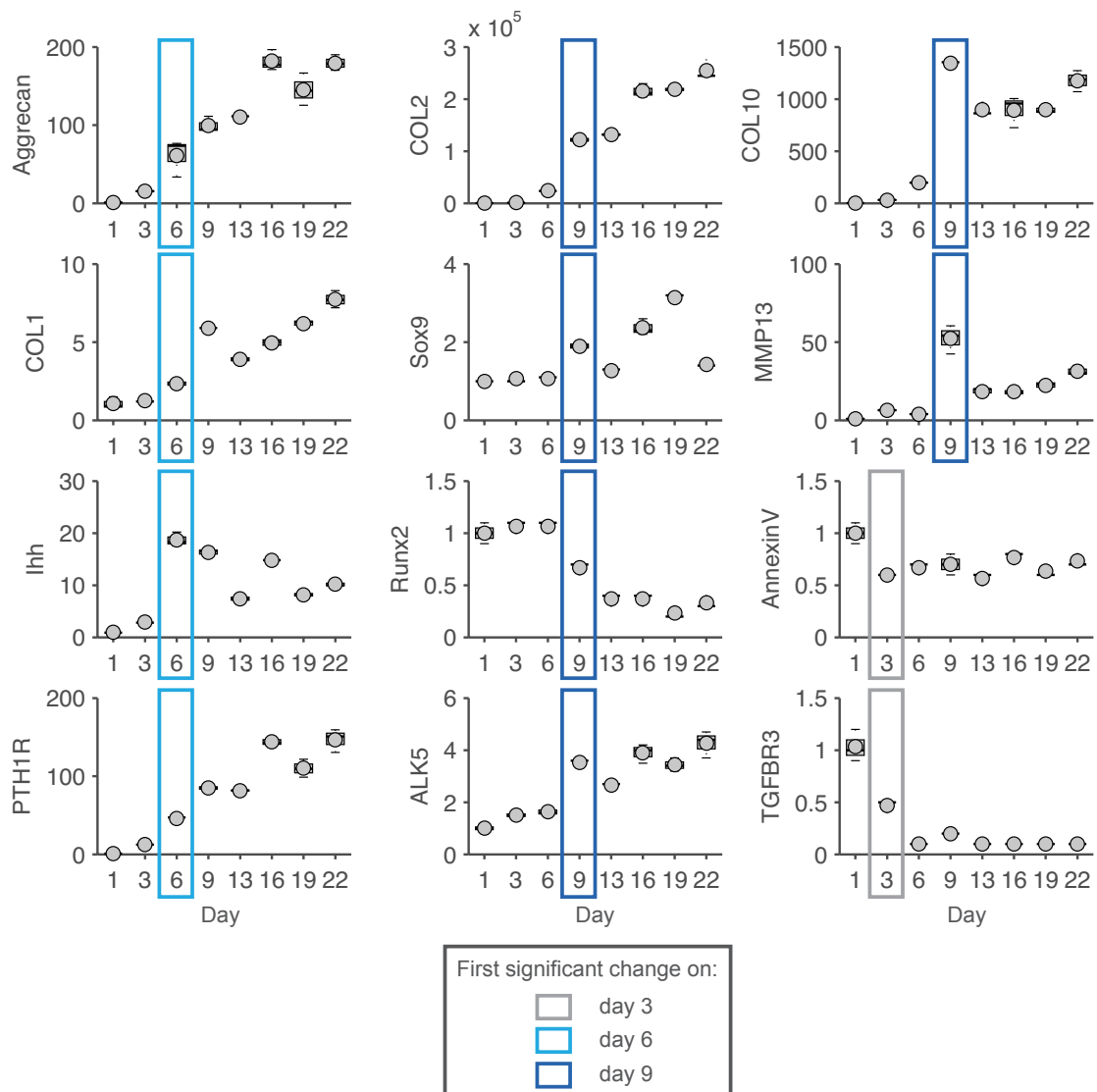


**Figure 4.1.:** Gene expression analysis of MSCs in Pellet culture on day 1, 3, 6, 9, 13, 16, 19 and 22 of Aggrecan, Collagen 2, Collagen 10, Collagen 1, Sox9, MMP-13, Ihh, Runx2, Annexin V, PTH1R, ALK-5 and TGFBR3. All data normalized to day 1. First significant gene expression change indicate by a grey box for day 3, light blue for day 6 and dark blue for day 9.

It seems clear that after one week of chondrogenic culture, a strong change occurs, initiated by a peak in MMP13, which indicates the catabolic break-down of collagen 2 [124] and the initiation of endochondral ossification [57]. The same trend is reported by Sekiya et al. [239] with a peak of MMP13 at day 7. In contrast to Sox9, Runx2 (the transcription factor involved in hypertrophy) slightly decreases during culture.

Annexin V, that had been shown to be involved in calcification by promoting  $\text{Ca}^{2+}$  influx into matrix vesicles [146] as well as to initiate apoptosis [286], only showed minor fluctuations over 22 days of chondrogenic differentiation. TGF- $\beta$ , the growth factor applied during MSC chondrogenesis, signals via its three receptors in an orchestrated sequence: TGF- $\beta$  gets activated by TGF type 3 receptor (TGFBR3), subsequently binding to, and activating TGFBR2 which then forms a complex with the type 1 receptor (TGFBR1) [122]. It has been shown that TGF- $\beta$  can signal through two subtypes of TGFBR1, known as activin receptor-like kinase type 1 (ALK1) and type 5 (ALK5) [276]. The activation of ALK5 results in Smad 2/3 phosphorylation, inhibiting chondrocyte hypertrophy [300]. Signalling through ALK1, on the other hand, leads to Smad 1/5/8 phosphorylation, a process involved in hypertrophy [34]. The analysis shows a steady up regulation of ALK5 over the 3 weeks of culture whereas TGFBR3 was subjected to downregulation. PTH1R expression level, the receptor for endocrine PTH and paracrine PTHrP signalling [233], also increased over time.

## 4.2 Protein expression analysis

The Alcian blue staining of pellets reveals, similar to the gene expression, the appearance of proteoglycans on day 5. Collagen 2 and 10 stainings, on the other hand, are only visible after 10 days and further increase up to 20 days of culture.

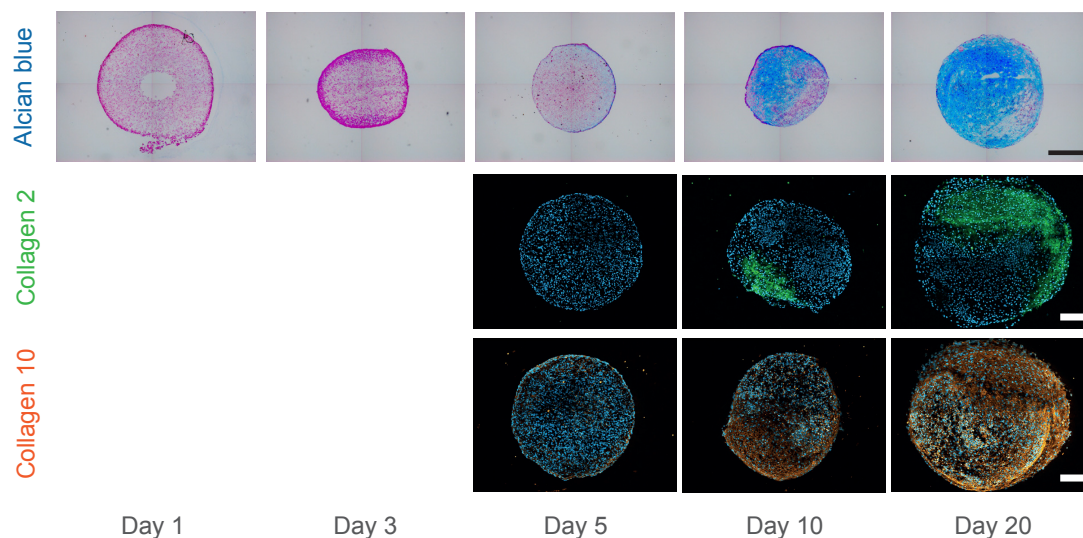


**Figure 4.2.:** Alcian blue and collagen 2 and 10 immunostaining on day 1, 3 (only for Alcian blue) as well as day 5, 10, 20 for all stainings. Scale bars 500  $\mu\text{m}$ .



Interestingly, collagen 2 staining is located in collagen 10 positive areas. This shows that the cells undergo chondrogenic induction differently than in the growth plate, where the chondrogenic phenotype is first induced and only afterwards progresses towards endochondral ossification. In pellets, MSCs from the beginning are steered towards hypertrophic phenotype. The size of the pellets decrease from day 1 to day 3. This contraction leads to condensation similar to the process observed in the earliest phase of embryonic limb development. The resulting high cell density favours the production of extracellular matrix with aggrecan being the earliest marker. Through the deposition of matrix, the cells are pushed further apart and the cell pellet increases in size.

### **4.3 Chapter summary**

Overall, a variety of chondrogenic, as well as hypertrophic genes are increased in MSC chondrogenic pellets. This confirms that the TGF-beta induction of stem cells does not lead to a phenotypically stable cartilage formation, but rather an ill-orchestrated, instable de-novo cartilage with a tendency towards endochondral ossification.



5 Inhibitory function of parathyroid hormone-related protein on mesenchymal stromal cell chondrogenesis and hypertrophy



As presented in Section 1.3.3, parathyroid hormone-related protein (PTHrP) is a main regulator of hypertrophy in the growth plate and has been studied by several groups as a hypertrophy-inhibiting drug for MSC chondrogenesis.

PTHrP is part of the parathyroid hormone family together with PTH and the more recently discovered tuberoinsfundibular peptide 39 (termed TIP39 or PTH2) [274]. PTHrP is involved in many physiological processes, ranging from skeletal development [153] to placental calcium transport [151].

Circulating PTHrP levels are elevated during fetal development and pregnancy, as well as during breast feeding. [150] Later in development as well as in adults, its levels become undetectable. PTHrP is then acting via paracrine and autocrine pathways. Alternative splicing of 9 exons leads to PTHrP translation into three initial products: PTHrP (1-139), PTHrP (1-141), and PTHrP (1-173) that are all homologues in their 1-139 sequence but differ in their carboxyl terminus. During the secretory trafficking, post-translational changes occur that account for the secretion of several mature peptides: 1) N-terminal, 2) mid-region, and 3) C-terminal fragments. [25, 295, 296]. The N-terminus (1-36) contains the PTH-homologous domain (1-13) which is involved in binding to the parathyroid hormone receptor 1 (PTH1R) [91]. The other secretory forms of PTHrP likely signal through their own receptor. The mid-region contains a nuclear localisation sequence (87-106) [181] responsible for the survival of chondrocytes in an apoptotic environment [114]. Further, the sequence 67-137 has been shown to affect Runx2 and Sox9 levels important during skeletal development [269]. C-terminal PTHrP (107-139), called osteostatin, is involved in bone resorption [79] and bone regeneration [171].

Based on the knowledge of the highly varying effects of the different PTHrP peptides, a distinct action is expected upon their exogenous application during MSC chondrogenesis. Lee et al. [159] has supplemented MSC pellets with 100 nM of PTHrP (1-34), (1-86), (7-34) and (107-139). Their results showed an inhibition of chondrogenesis in the presence of a C-terminal fragment (107-139) as well as with the peptide (7-34) missing part of the N-terminus. Isoforms (1-34) and (1-86) inhibited collagen 10 expression without affecting chondrogenesis. This suggests that the receptor binding domain needs to be present in order to selectively address hypertrophic genes. In all other studies presented in Table 5.1, PTHrP (1-34), (1-40) or (1-86) were used which all contain the full N-terminus. Despite this fact, the reported effect on chondrogenesis and hypertrophy are inconsistent.

The major question to address in PTHrP treatments is if it selectively down-regulates hypertrophy, or whether an overall chondrogenic inhibition occurs. The current literature is divided on this topic; several groups [17, 134, 145, 159] reported an increased collagen 2 expression, others observed a down regulation [83, 194, 289]. The reason behind this fundamental difference is difficult to establish, as all publications were performed under disparate conditions. One of the main differences might arise from the concentration range and the different time point of application. Further, MSCs induced in pellets might not react in the same way to PTHrP as cells in hydrogels and scaffolds.

**Table 5.1.:** Literature overview of PTHrP publications for MSC hypertrophy inhibition.

Citation	System	Type	Concentration	Treatment	Effect
[83]	Pellets	1-34 (Bachem)	2.5 nM	continuous 6h pulses day 21 (48 h)	decreased Col2 increased Col2, stable Col10 reduced ALP & Ihh decreased Col2 and Col10
[194]	Pellets	1-40 (Sigma)	10 and 100 pM 1 nM	day 0	stable Col2 and 10, ALP decrease decreased Col2, Col10 stable
[159]	Pellets	1-34 (Bachem) 1-86 (BioVision) 7-34 (Bachem) 107-139 (Bachem)	100 nM	day 14	increased Col2, decreased Col10 stable Col2, decreased Col10 Col2 decrease Col2 decrease
[31]	HA-H	1-86 (Peprotech)	50 ng/disc	day 0	decreased calcification
[17]	PEGDA-H	1-34 (Sigma)	300 nM	day 0	increased Col2, decreased Col10
[289]	Pellets	1-34 (Bachem)	2.5 nM 2.5 nM	day 0 day 21	decreased Col2 and 10 decreased Col2 and 10
[145]	Pellets	1-86 (Sigma)	1, 10 nM	day 14	Col2 increase, Col10 not significant
[135]	PEG-S	1-86 (Sigma)	1, 10 $\mu$ M	day 7	Col2 stable, Col10 decrease

Abbreviations: hydrogel (H), scaffold (S) hyaluronic acid (HA), polyglycolic acid (PEG), polyethylene glycol diacrylate (PEGDA)

The aim of this chapter was to address these differences by testing the effect of concentration, time point of administration, oxygen pressure, fragment type, as well as culture system, to determine the required conditions for a selective hypertrophy inhibition of PTHrP.

## 5.1 Materials and methods

### 5.1.1 PTHrP administration

The effect of PTHrP was studied using the fragment 1-34 (Hypercalcemia of malignancy factor fragment 1-34 amide human, Sigma #H9148) and 1-86 (Sigma #SRP4651 or Peptotech#100-09) at concentrations ranging from 1 nM to 1  $\mu$ M. PTHrP was added to the chondrogenic medium (see Section 3.2.2) at day 0 or after chondrogenic induction for 7, 14, or 21 days in 3% or 20% O<sub>2</sub> (Hypoxia or Normoxia).

### 5.2 PTHrP application at different concentrations

To start, we studied the effect of PTHrP 1-86 concentration on MSC chondrogenesis. PTHrP was applied on day 7 of pellet culture based on the previous established gene expression profile (see Chapter 4 on page 39) where collagen 10 upregulation started on day 9. The hypothesis was, that chondrogenesis had to be pre-induced before PTHrP was added. A later time point of application seemed counter-intuitive as hypertrophic genes were already high on day 9.

The analysis of the gene expression showed that PTHrP had a dose-dependent effect on all analysed genes with the strongest difference between 0 and 10 nM. At 1 nM a slight reduction in collagen 10 and *Ihh* was observed, accompanied by a decrease in collagen 2. 10 nM of PTHrP suppressed collagen 10, but also collagen 2. Interestingly, MMP-13, a gene induced during chondrocyte hypertrophy [57] and associated with collagen 2 degradation [267], was upregulated in a concentration-dependent manner. 10 and 100 nM showed the most effective hypertrophy inhibition and were therefore used in all subsequent experiments. These concentrations lie in the range applied by Weiss et al. [145] but 10 to 100-fold higher concentrations are reported by others [135, 159].

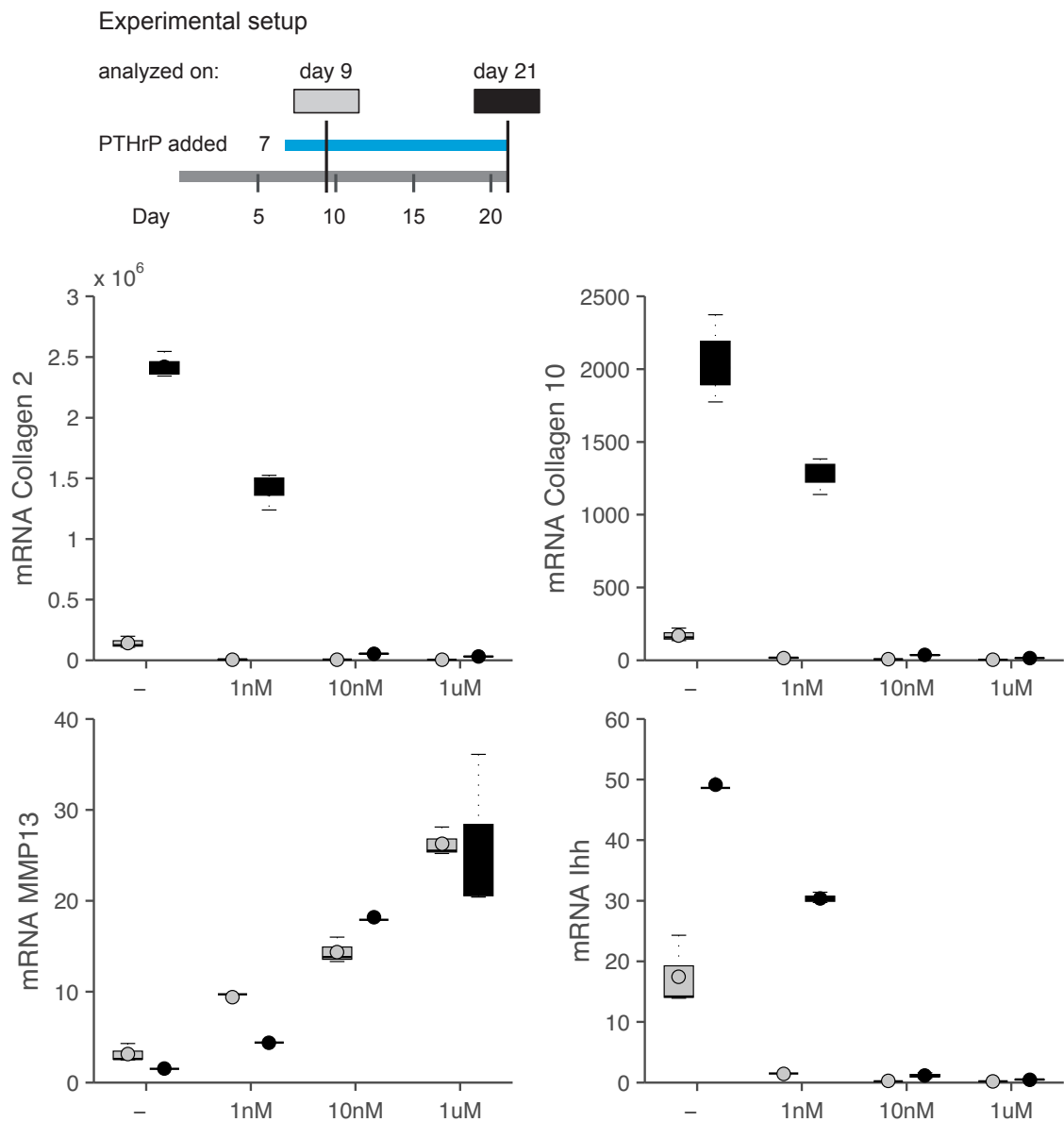


**Figure 5.1.:** PTHrP 1-86 (Peprotech) application of 1 nM, 10 nM, and 1  $\mu$ M on day 7, analyzed for gene expression after 2 and 14 days of treatment (total of 9 and 21 days of culture).

### 5.3 Time point of administration

Based on the negative influence of PTHrP on day 7, we tested whether the differentiation state of cells might influence the treatment (Figures 5.2 and 5.3). The more advanced pre-induction of MSCs previous to PTHrP administration might allow the stabilization of the chondrogenic gene expression as the work of Lee et al. [159] and Kim et al. [145] indicates.

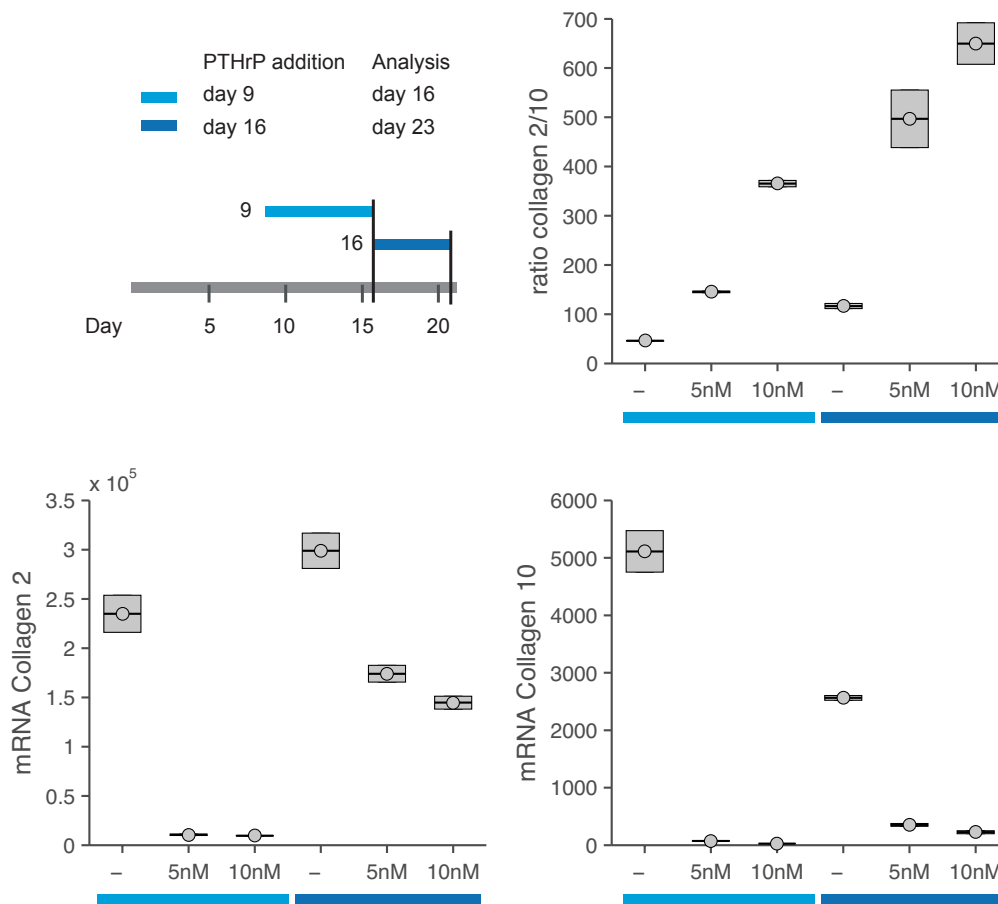


**Figure 5.2.:** PTHrP 1-86 (Peprotech) administration of 10 nm PTHrP on day 9, or 16; analysed for gene expression on day 16 or 23, respectively.

The assessment of PTHrP application over 7 days started on day 7 or 14 of pre-differentiation (Figure 5.2), revealed a beneficial collagen 2/10 ratio for late-stage administration. A decrease in collagen 2 was nevertheless observed in both situations with an unknown long term trend. We therefore further analysed how the gene expression evolves with PTHrP administration continued over 28 days (Figure 5.3).



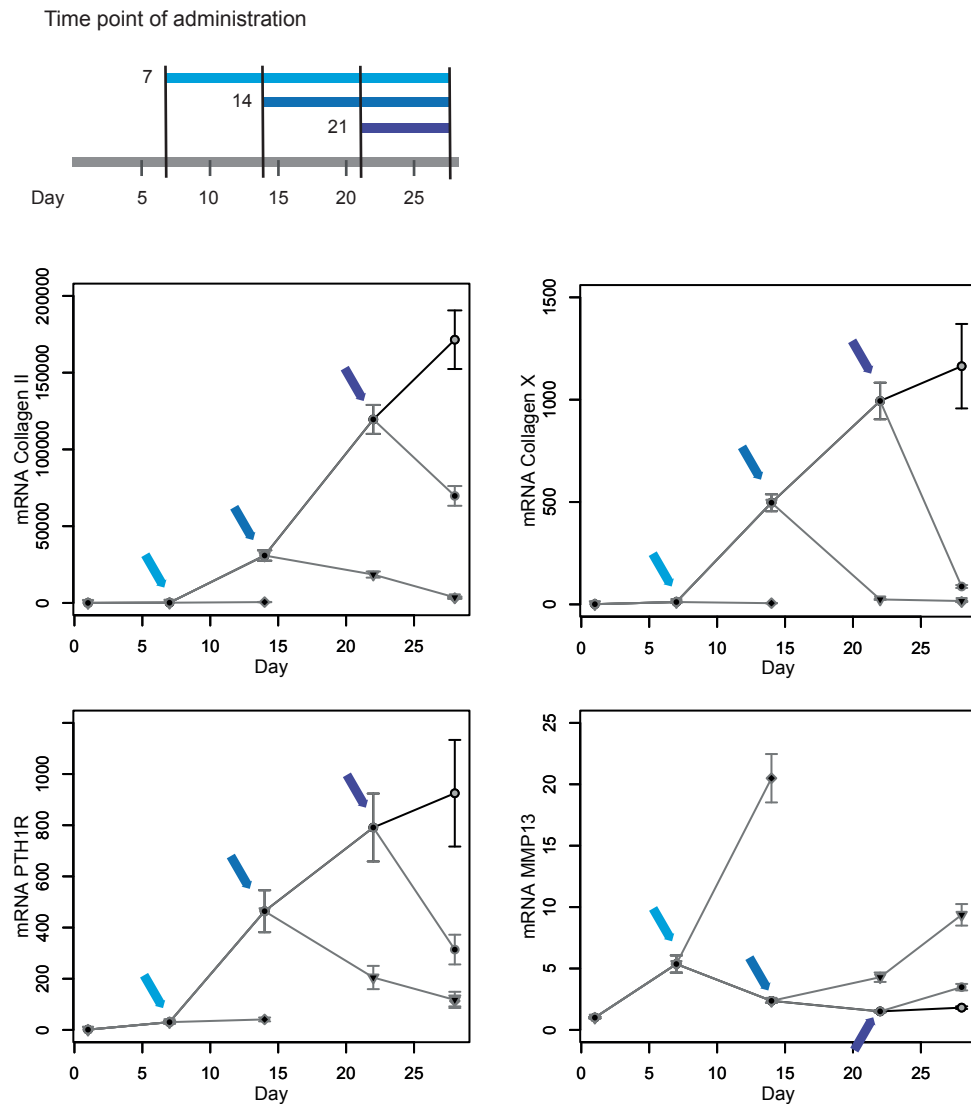


**Figure 5.3.:** PTHrP 1-86 (Peprotech) administration of 5 and 10 nM PTHrP on day 7, 14, or 21 analysed for gene expression on day 7, 14, 22, and 28. Note: samples with PTHrP application from day 7 onwards yielded too little RNA on day 22 and 28 for PCR analysis.

The decrease in collagen 2, observed above, further progressed with continued PTHrP application until a completely diminished level at day 28. The same tendency can be seen for PTHrP application starting on day 22, which showed a dramatic decline after 6 days. It appears that the collagen 10 decrease happens over a shorter time period than collagen 2. This difference might explain the observation by Fischer et al. [83] where a pulsed application reduced ALP and Ihh without loss of collagen 2.

An interesting observation was the decrease of parathyroid hormone receptor 1 (PTH1R), the receptor activated by the amino-terminal region of PTHrP [295]. The down regulation of PTH1R upon exogenous PTHrP application indicates a PTH1R-independent pathway which might be the source of adverse effects. Kim et al. [145] performed a similar experiment with 10 nM PTHrP 1-86 applied on day 14 of pellet culture, and reported an increase in collagen 2 as well as decreased Runx2 while collagen 10 remained stable. In an attempt to discern the origin of our fundamentally different results, we tested whether the source of PTHrP (Sigma versus Peprotech) could change the outcome. Both types of PTHrP were applied in 10 nM concentration on day 7 of chondrogenic culture, and analyzed after an additional 4 days. The analysis showed that collagen 2 gene expression was reduced upon PTHrP, independent of the source (Figure 5.4).

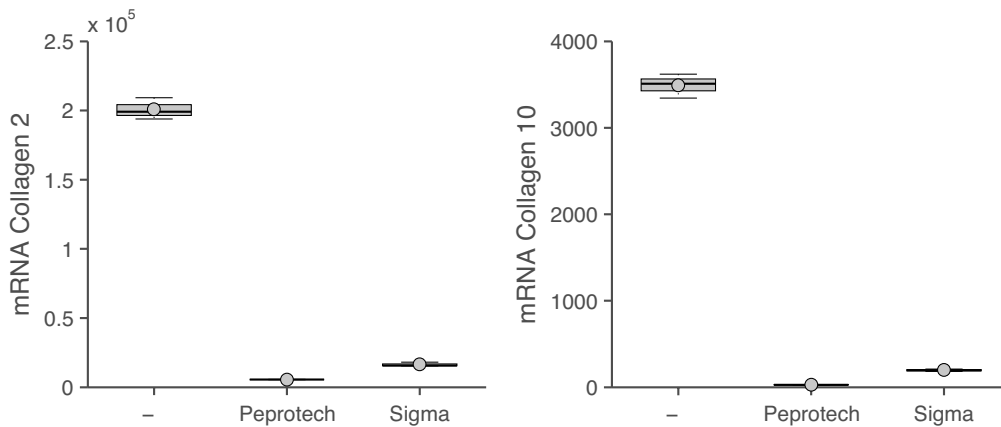


**Figure 5.4.:** Effect of 10 nM PTHrP 1-86 purchased from Peprotech or Sigma applied on day 7, analyzed on day 11.

## 5.4 PTHrP application under hypoxia

Based on the above described results it became apparent that hypertrophic and chondrogenic genes were equally inhibited by PTHrP. In an attempt to stabilize the chondrogenic phenotype, we analyzed the effect of hypoxia on the PTHrP treatment. Low oxygen pressure induces collagen 2 and aggrecan via the p38 MAPK pathway [115], as well as Sox9 via the hypoxia-inducible factor 1 alpha (HIF-1 $\alpha$ ) [137]. Hypoxia was further shown to increase MSC resistance to apoptosis, with a resulting decrease in endochondral ossification [158]. In contrast, Meretoja et al. [188] observed higher amounts of ALP and calcium after 42 days of culture in

electrospun nonwoven poly( $\epsilon$ -caprolactone) (PCL) scaffolds under hypoxia compared to normoxia. Pelosi et al. [211] could prove a direct relationship of PTHrP production in human articular chondrocytes under hypoxic culture (1% O<sub>2</sub>). PTHrP thereby acts through its receptor PTH1R and HIF-1 $\alpha$  as well as HIF-2 $\alpha$ .

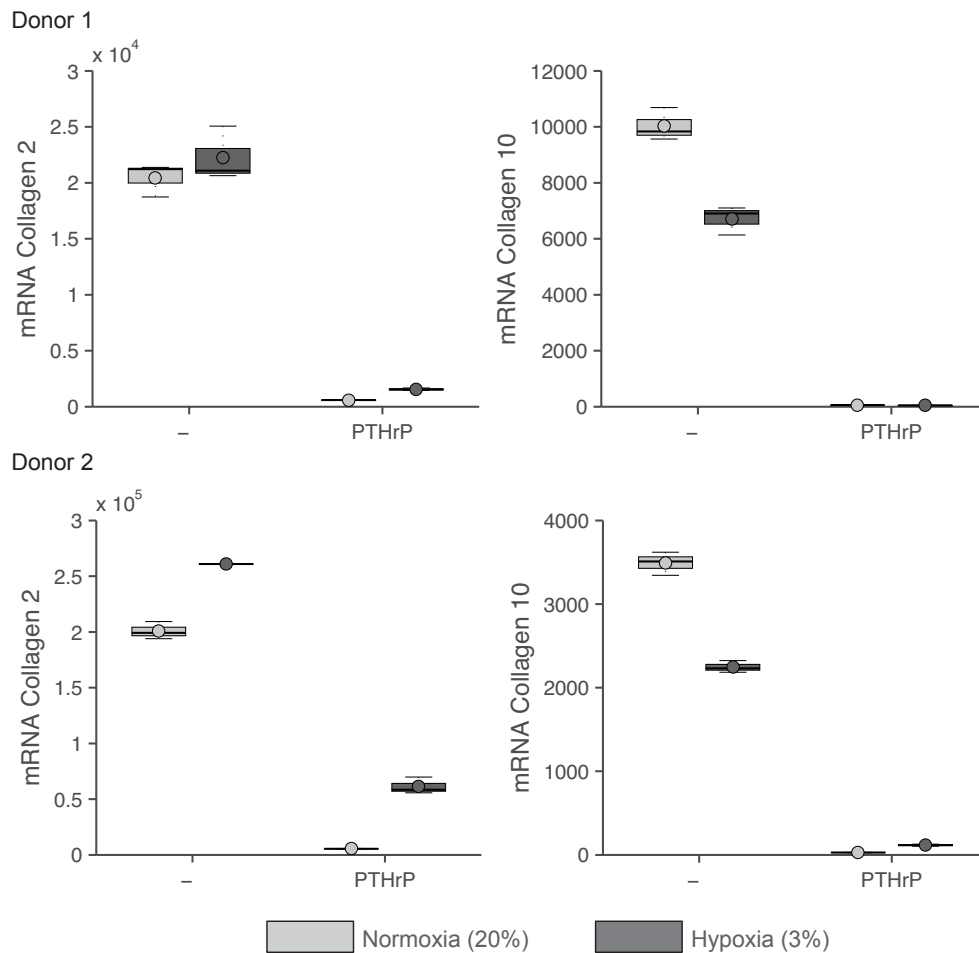


**Figure 5.5.:** Effect of 10 nM PTHrP 1-86 (Peprotech) under 3 or 20% O<sub>2</sub> (Hypoxia or Normoxia) on day 14 for two hBMC donors.

The assessment of the effects of 3% versus 20% O<sub>2</sub> revealed a donor-dependent collagen 2 increase along with a 30-35% reduction of collagen 10. In PTHrP treated pellets, collagen 2 was downregulated, regardless of the oxygen concentration. Hypoxia could only slightly recover its loss, however, with a high variance between donor 1 and 2. The inhibition of collagen 10 on the other hand was equally efficient for both oxygen concentrations. In conclusion, hypoxia shows a beneficial trend improving collagen 2 expression under PTHrP treatment, but its level nevertheless remains low.

### 5.5 The effects of PTHrP 1-34 versus 1-86 on pellet and scaffold culture

The combination of concentration, timing, or oxygen concentration did not yield the desired hypertrophy reduction with stable or induced chondrogenesis when using PTHrP 1-86. The question thus arose, whether the shorter amino-terminal fragment (1-34), which only contains the N-terminus without the mid-region, would be a better choice. PTHrP 1-34 and 1-86 were therefore applied at 10 and 100 nM starting at the first day of culture (Figure 5.6).

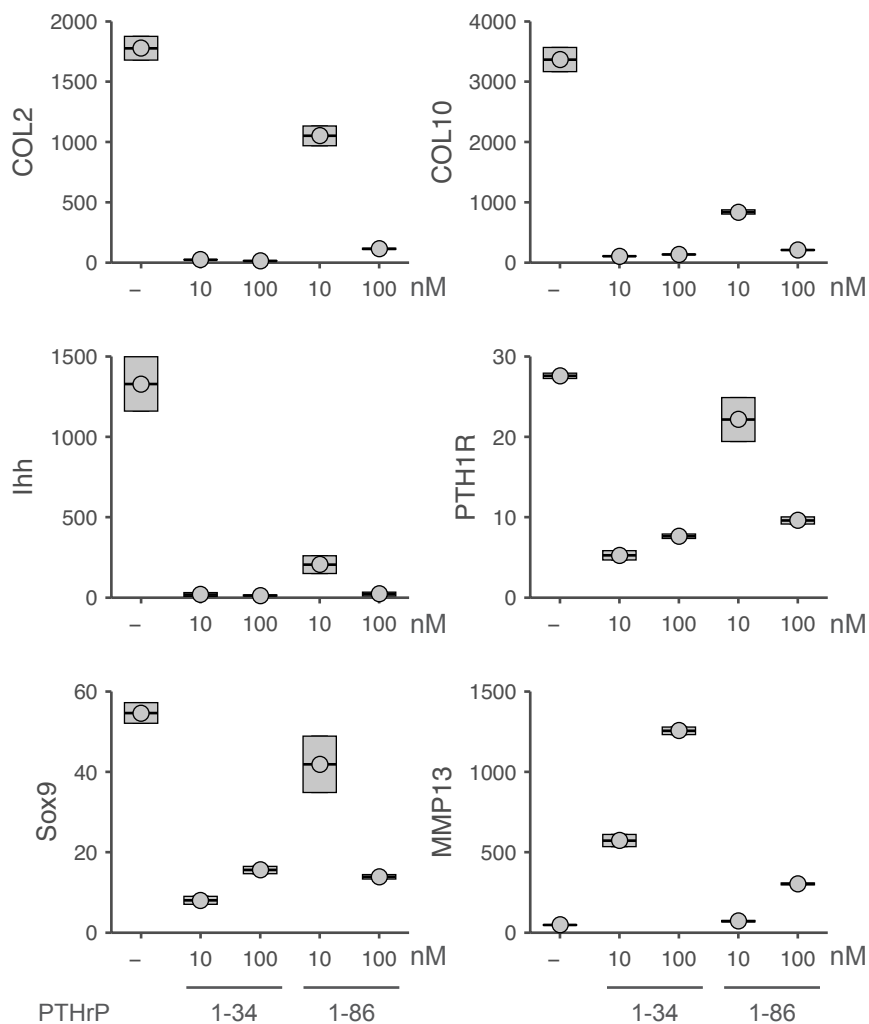


**Figure 5.6.:** The effect of 10 or 100 nM PTHrP (1-34 or 1-86 fragment, Sigma) on hBMC chondrogenesis in Pellets was analyzed on day 21 by gene expression of collagen 2, collagen 10, Ihh, PTH1R, Sox9, and MMP13.

Gene expression analysis confirms the trend observed in previous experiments with a general downregulation of chondrogenic genes (Collagen 2, Sox9), as well as genes related to endochondral ossification (Collagen 10, Ihh) notwithstanding the PTHrP isoform applied. The 1-34 fragment showed a stronger decrease than 1-86, with a total elimination of collagen 2 and 10 at just 10 nM. It remains to be tested whether a lower concentration range could be more beneficial as proposed by Mueller et al. [194]. We observed that both isoforms downregulate the PTHrP receptor along with increasing MMP-13, with an even stronger effect for PTHrP 1-34.

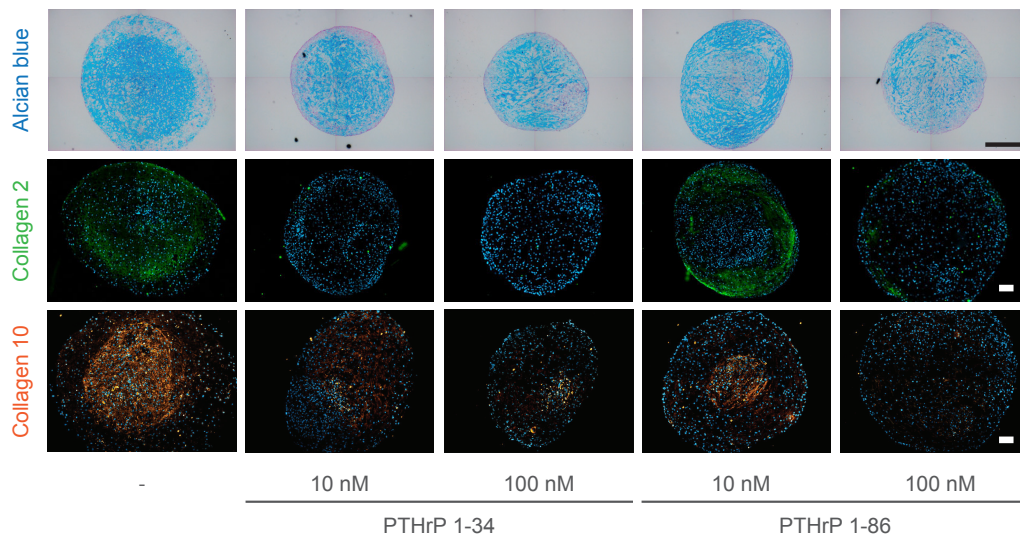


**Figure 5.7.:** Alcian blue, Collagen 2 and 10 staining of Pellets treated with PTHrP 1-34 or 1-86. Scale bars 500  $\mu\text{m}$ .

The trend of the mRNA expression profiles was confirmed with immunostaining (Figure 5.7). Except for 10 nM PTHrP 1-86, no pellet revealed a collagen 2 or 10 staining after 21 days of culture. Interestingly, in the 10 nM PTHrP 1-86 sample, collagen 2 is observed on the outer edge of the pellet whereas the remaining collagen 10 staining was in the centre. This inverse location might indicate to a diffusion dependent effect, where the concentration of PTHrP gradually decreases towards the centre and eventually drops below a certain threshold necessary to inhibit hypertrophy. On the edge of the pellet, no collagen 2 suppression is observed, contrary to all other tested conditions. The reason for this effect remains elusive. Another striking result is the unaffected alcian blue staining. There is a strong indication that PTHrP acts through a pathway that specifically targets collagen 2 without interfering with the proteoglycan synthesis. This is even more surprising as mRNA levels of Sox9, the master regulator of chondrogenesis, also dropped strongly with

PTHrP treatment. Aggrecan, the major proteoglycan in cartilage, was shown to be regulated by a Sox9-dependent pathway [48, 103]. Despite the evidence in literature, results presented in this thesis point towards a Sox9-independent regulation of proteoglycan production. This is not only supported by the unchanged alcian blue staining after PTHrP treatment, but also by the aggrecan induction in pellet culture prior to an increase in Sox9 (see Figure 4.1)

In a final experiment, PTHrP was added to MSCs cultured in Optimaix scaffolds (Figure 5.8) to test whether the culture system might influence the outcome. This test was motivated by the beneficial effect observed in hyaluronic acid [31] or PEGDA hydrogels [17] as well as PEG scaffolds [135] where PTHrP treatment led to a specific reduction of collagen 10.

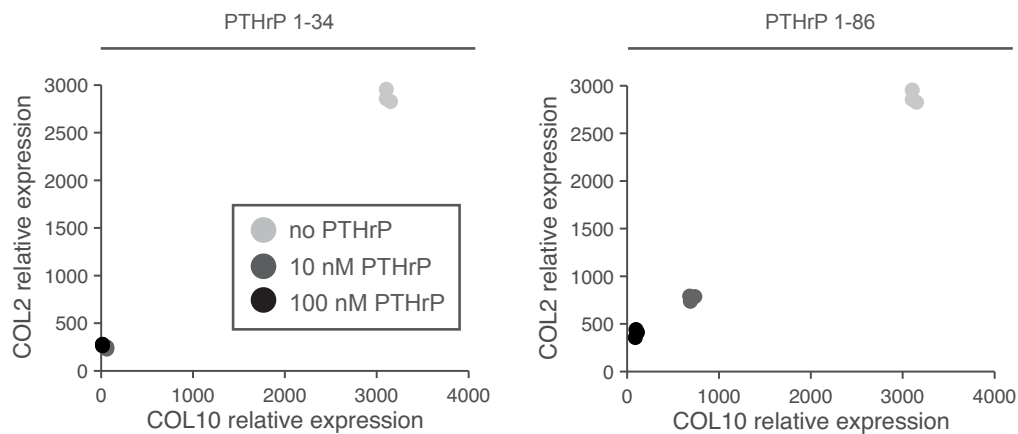


**Figure 5.8.:** Collagen 2 expression decrease is directly proportional to the collagen 10 in scaffolds cultured for 21 days in chondrogenic media supplemented with 10 nM or 100 nM PTHrP 1-34 (left) or 1-86 (right).

The analysis showed once again the trend of chondrogenic inhibition in parallel to the hypertrophic decrease. This is evident in the linear dependency of collagen 2 and 10 for both PTHrP 1-34 as well as 1-86.

## 5.6 Chapter summary

The premature induction of hypertrophy of chondrogenically induced MSCs is a major hurdle for their clinical application. PTHrP, with its reported anti-hypertrophic properties (see Table 5.1), is a key molecule to investigate for improved MSC chondrogenesis. However, our results showed that PTHrP, notwithstanding the application scheme (concentration, time point, oxygen concentration), leads to a general suppression of differentiation rather than a specific down regulation of hypertrophy. This result is in contrast with others [17,135,159] that report a decrease of collagen 10 as response to PTHrP without the adverse effect on collagen 2. The origin of this discrepancy is not possible to discern as our results under the same conditions led to an opposing outcome. A report by Weiss et al. [289], on the other hand supports the observation of a generally suppressed differentiation. In a follow-up work performed by the same group [83], the constant PTHrP application was identified as the source of the catabolic effect whereas an intermittent exposure allowed to switch to an anabolic action with increased collagen 2 production and reduced ALP activity. The same switch has been observed for PTH which under a constant application regime leads to bone loss whereas a short time exposure allows for bone formation [74]. The molecular regulation behind this fundamental change is unknown, the cAMP/PKA pathway has though been identified to take part in both anabolic as well as catabolic processes induced by PTHrP [83]. The intermittent application might well be the solution for a PTHrP-based treatment of chondrocyte hypertrophy, its clinical relevance is though questionable as it would require a cost-intensive multiple injection regime or a complex engineered construct that releases PTHrP by an external trigger (such as a magnetic field or heat). Another route to be taken for an improved effect of PTHrP is its endogenous application via overexpression, which would allow to study its nuclear targeting, a pathway totally ignored by exogenous supplementation.

The current literature does not only debate on the benefit of PTHrP for cartilage regeneration but also on the general definition of hypertrophy. While collagen 10 has been for a long time considered as a key marker for endochondral ossification, recent publications have shown that its upregulation does not necessarily lead to ossification and vascularization [65]. When evaluating the effect of PTHrP, an unaffected high collagen 10 but a decreased ALP level was therefore considered as a positive outcome [83,194]. Follow-up experiments will have to be performed to evaluate whether a reduction in ALP is enough for the suppression of endochondral ossification. Overall, a better understanding of the complex action of PTHrP

## *5. Inhibitory function of PTHrP on MSC chondrogenesis and hypertrophy*

---

on MSC differentiation will be required to make it a viable option for cartilage regeneration strategies.



## 6 Application of amphiphilic poly( $\gamma$ -glutamic acid) nanoparticles as siRNA carriers



*Note:* Part of this chapter is in preparation for submission to *Macromolecular Bioscience*

Small interfering RNA (siRNA) is a naturally occurring double stranded RNA molecule (19-23 base pairs) that can be used to reduce the expression of proteins through sequence-specific degradation of target mRNA [30]. Because of its ability to silence genes in a sequence-specific manner, RNA interference (RNAi)-based therapeutics carry great promise in treating many chronic diseases or cancers thereby presenting an attractive approach over traditional drugs (such as PTHrP) which suffer from unwanted side effects [37]. Despite its great therapeutic potential, clinical applications of siRNA-based treatments are limited by inefficient delivery to the extracellular and intracellular target sites. siRNA cannot diffuse efficiently across cellular membranes due to its water-soluble polyanionic nature and relatively large molecular weight. Furthermore, siRNA is unstable under in vivo conditions; if not broken down by serum nucleases [192, 313], it is degraded in the endocytotic pathway [68, 164]. Thus, safe and effective delivery systems capable of transporting siRNA through extracellular and intracellular barriers, to reach the target site in the cytosol, are required for further development of siRNA therapeutics.

Both viral and non-viral vectors have been developed for siRNA delivery. In particular, non-viral siRNA delivery systems such as cationic polymers and lipids have been intensively studied. The most common non-viral carriers involve complexes formed between polycations and siRNA via electrostatic interactions. The practical application of such polyplexes, however, suffers from several problems such as induced toxicity, low serum stability, and non-specific immune responses [230]. Many alternatives with respect to the safety of cationic polymers and lipids commonly used to form polyplexes/lipoplexes have been explored for in vivo gene delivery carriers. Polymeric micelles composed of poly(ethylene glycol) (PEG)-block-cationic poly(amino acid) derivatives have been widely investigated as carriers for DNA and oligonucleotides due to their small particle size and favorable safety profile [18]. Another system based on nanoparticles (NPs) composed of poly(lactide-co-glycolide) (PLGA) has also recently shown promise for the delivery of siRNA both in vitro and in vivo [54]. Even though significant advances have been made in the field, the development of carriers that can efficiently deliver RNAi therapeutics both in vitro and in vivo remains a major challenge.

In a previous study [7], the group of Prof. Akashi in Osaka has prepared biodegradable NPs composed of poly( $\gamma$ -glutamic acid) ( $\gamma$ -PGA) conjugated with L-phenylalanine (Phe) as the hydrophobic segment. The  $\gamma$ -PGA-graft-Phe copolymer ( $\gamma$ -PGA-Phe) self-assembles into monodispersed NPs in water due to their amphiphilic nature [7, 183]. The formed NPs exhibit a core-corona structure with a hydrophobic inner core and a hydrophilic outer shell (see Figure 6.1). The 200 nm-sized NPs

could stably encapsulate various types of proteins, and were efficiently taken up by antigen-presenting cells (APCs), such as dendritic cells (DCs) and macrophages [9, 275]. Interestingly, protein-encapsulated  $\gamma$ -PGA-Phe NPs efficiently delivered loaded proteins from the endosomes to the cytoplasm in DCs [8]. Both active cellular entry and endosomal escape are essential for siRNA delivery.

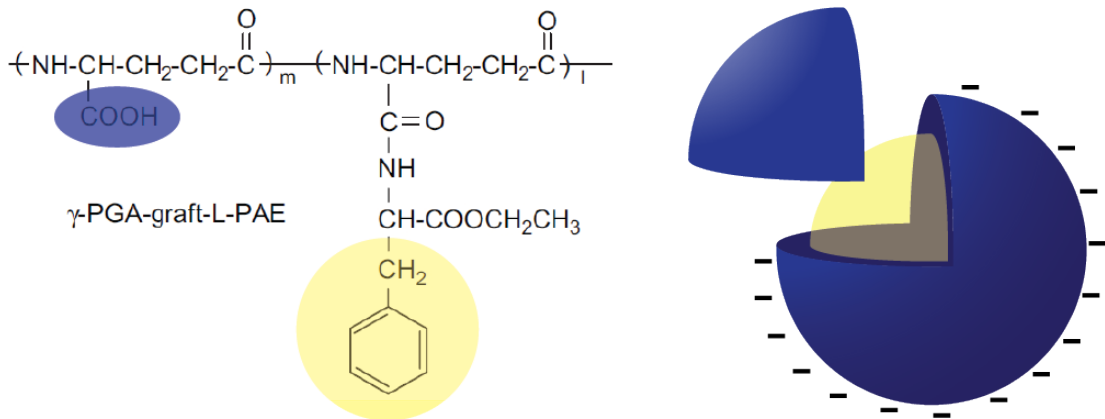


**Figure 6.1.:** Molecular structure of  $\gamma$ -PGA-Phe co-polymer composed of L-phenylalanine (Phe) grafted onto a poly( $\gamma$ -glutamic acid) backbone. Hydrophobic phenyl groups marked in yellow and hydrophilic carboxyl groups in blue. The amphiphilic co-polymer forms core-corona nanoparticles in water with an inner hydrophobic core and an outer hydrophilic shell. Image adapted from Akagi et al. [7].

In this chapter we present several strategies to develop  $\gamma$ -PGA-Phe siRNA nanoparticles with the following properties:

- colloidal stability
- effective loading of siRNA
- efficient cellular uptake
- intracellular release of siRNA resulting in subsequent gene knock-down

In the first half of this chapter, the potential of siRNA encapsulation into  $\gamma$ -PGA-Phe NPs was evaluated. The second part of the chapter is dedicated to polycation-coated NPs and their potential for siRNA delivery.

## 6.1 Materials and methods

*Note:* The work described in this chapter has been performed both in the Cartilage Engineering + Regeneration Laboratory in Zürich, Switzerland as well as in the laboratory of Professor Akashi at Department of Applied Chemistry, Graduate School of Engineering, Osaka University, Japan. This resulted in different protocols used for the siRNA-NP preparation as outlined in this section. The establishment of the chitosan-coated NPs as well as the polyplex approach was started during a research stay at Osaka University, Japan, and its development continued thereafter. DEAE-dextran and PEI-coated NPs were developed at the ETH, Zürich Switzerland. Cholesterol-modified siRNA NPs were tested in Osaka and Zürich.

**Table 6.1.:** siRNA sequences. GAPDH was used as a model siRNA and non-targeting (NT) sequence as a control. Cholesterol modifications indicated by 'Chol'

	Name	Sense sequence 5'-3'	Modification 3'	Modification 5'	Provider
Zürich	NT	GAACGACGCCGTACTCATT-dTdT	-	-	Microsynth
	NT-Cy3	GAACGACGCCGTACTCATT-dTdT		Cy3	Microsynth
	NT-Chol-Cy3	GAACGACGCCGTACTCATT-dTdT	Chol	Cy3	Microsynth
	GAPDH	GGUCAUCCAUGACAACUUU-dTdT	-	-	Microsynth
	GAPDH-Chol-Cy3	GGUCAUCCAUGACAACUUU-dTdT	Chol	Cy3	Microsynth
Osaka	NT	n/a	-	-	Sigma
	IKK $\beta$	n/a	-	-	Sigma
	IKK $\beta$ -FAM	n/a	-	FAM	Sigma

### 6.1.1 Preparation of $\gamma$ -PGA-Phe nanoparticles

$\gamma$ -PGA was hydrophobically modified by Phe in the presence of EDC, as previously described by Matsusaki et al. [183].  $\gamma$ -PGA-graft-Phe ( $\gamma$ -PGA-Phe) with a 55% Phe grafting degree was used in this study. Nanoparticles composed of  $\gamma$ -PGA-Phe ( $\gamma$ -PGA-Phe NPs) were prepared by a precipitation method.  $\gamma$ -PGA-Phe dissolved in DMSO (10 mg/ml) was added to 100-150 mM NaCl in a 1:1 volume ratio. The NaCl concentration allows the precise tuning of nanoparticle size [143]. Depending on the protocol, the NPs were directly used for siRNA loading experiments or freeze-dried (after dialysis).

### 6.1.2 Preparation of siRNA carriers through encapsulation

#### *Encapsulation of siRNA/protamine polyplex*

First, 25  $\mu$ l of 100  $\mu$ g/ml protamine (MW 4.3 kDa, in pure water) was mixed with 25  $\mu$ l NaCl (0.5 M) solution. Next, 50  $\mu$ l of 2  $\mu$ M siRNA (in 10 mM Tris-HCl buffer, pH 8) was added and a polyplex formed after vortexing. The siRNA/protamine polyplex was subsequently encapsulated in  $\gamma$ -PGA-Phe by the addition of 100  $\mu$ l polymer solution (10 mg/ml). The resulting siRNA-polyplex NPs (PP-NPs) were washed twice in pure water and finally resuspended in PBS (by first adding 90  $\mu$ l pure water and then 10  $\mu$ l of 10 $\times$  PBS to prevent aggregation).

#### *Preparation of NPs with encapsulated cholesterol-modified siRNA*

Cholesterol-siRNA (Chol-siRNA) was encapsulated in  $\gamma$ -PGA-Phe NPs by mixing Chol-siRNA (in pure water) with 10 mg/ml  $\gamma$ -PGA-Phe in DMSO. After two washes, the Chol-siRNA encapsulated NPs (Chol-enNPs) were resuspended at 10 mg/ml in PBS. To test the siRNA loading efficiency, the NPs were dissolved in a solution of 1% Triton-X100 and 0.4 M NaOH and analysed by a fluorometer.

### 6.1.3 Preparation of nanoparticles with siRNA adsorbed outside

#### *DEAE-dextran or PEI coated nanoparticles*

DEAE-dextran or PEI-coated NPs were produced using freshly prepared NPs washed by two centrifugation steps at 15'000 rpm for 15 minutes. NPs were then re-suspended at 10 mg/ml and subsequently coated with 10 mg/ml DEAE-dextran, or PEI (1:1 volume ratio). Finally, the coated NPs were washed in two subsequent centrifugation steps at 15'000 rpm for 15 minutes.

The adsorption of siRNA was performed by mixing 0.5, or 10 mg/ml coated NPs with 600 nM siRNA. The siRNA-NPs were incubated for one hour before transfection. The adsorption efficiency of Cy3-siRNA onto the coated NPs was determined by measuring the fluorescence remaining in the supernatant after adsorption.

#### *Chitosan-coated nanoparticles*

Chitosan-coated NPs (CT-NPs) were prepared using freeze-dried NPs. Chitosan (CT) was dissolved in a 10 mM acetate buffer (pH 5.5) (10 mg/ml) and added into the NP solution (1.25 - 10 mg/ml in PBS) at the same volume. After 2 hours of incubation at RT, the resulting solution was centrifuged at 15'000 rpm for 10 minutes, rinsed with PBS twice, and re-suspended in PBS at a concentration of 2 mg/ml.

To prepare the siRNA adsorbed CT-NPs (siRNA-CT-NPs), CT-NPs (2 mg/ml) were mixed with siRNA (both FAM and unlabelled) solution dissolved in 10 mM Tris-HCl (pH = 8.0) at various concentrations (125 - 1000 nM) in a 1:1 volume ratio. After incubating for 1 hour, the NPs were isolated by centrifugation, washed twice with water, and resuspended at 10 mg/ml in PBS. FAM-siRNA-CT-NPs were dissolved in 2% SDS and the fluorescence intensity of the lysates measured by a fluorescence microplate reader (Fluoroskan Ascent FL, Thermo Fisher Scientific Inc., USA). The adsorption efficiency of siRNA onto the CT-NPs was calculated as (adsorbed siRNA amount onto the NPs / initial amount of siRNA)  $\times$  100.

The release experiment was carried out in vitro as follows: FAM-siRNA-CT-NPs (100 nM FAM-siRNA, 1 mg/ml CT-NPs) were suspended in PBS, and placed in a microtube at 37°C. At different time intervals, 100  $\mu$ l of the sample was withdrawn and centrifuged at 15'000 rpm for 10 minutes. The amount of siRNA released into the supernatant was then determined by the fluorescence measurements.

#### **6.1.4 Characterization of nanoparticles**

The size distribution (dynamic light scattering (DLS) method) and zeta potential of the NPs were measured by a using a Zetasizer Nano ZS (Malvern Instruments, UK).

#### **6.1.5 Cellular transfection**

##### *Mesenchymal stromal cells (MSCs)*

Human MSCs were seeded 24 hours prior to transfection in 24-well plates at a density of 35'000 cells/well. Freshly prepared siRNA-NPs were added in 600  $\mu$ l of medium. 6 hours after transfection, cells were washed twice in PBS and 1 ml of culture medium added. As a positive control, INTERFERin (Polyplus) was used according to the manufacturer's instruction.

*Dendritic cells (DCs)*

$1 \times 10^6$  cells/ml of mouse bone marrow-derived dendritic cells (DCs) were incubated with 50 nM siRNA (FAM-siRNA alone, FAM-siRNA mixed with Lipofectamine (siRNA/LF), FAM-siRNA mixed with CT (siRNA/CT) or FAM-siRNA-CT-NPs) for 1 hour at 37°C. The cell uptake was determined by measuring the cell-associated siRNA fluorescence using flow cytometry (FCM) (Cytomics FC500, Beckman Coulter, US).

**6.1.6 RT-PCR**

After the indicated siRNA transfection time, cells were washed with PBS and lysed in RLT-buffer containing  $\beta$ -mercaptoethanol. Gene expression analysis was performed as previously described (see Section 3.5).

**Table 6.2.:** Primer sequences

Primer	Forward sequence 5'-3'	Reverse sequence 5'-3'	Product length
GAPDH	CAGCCCCAGCAAGAGCACAAG	TTCAAGGGGTCTACATGGCAACTG	121
RPL13a	AAGTACCAGGCAGTGACAG	CCTGTTTCCGTAGCCTCATG	100

**6.1.7 Hemolysis**

The pH effect on membrane-disruptive activity of CT-NPs and  $\gamma$ -PGA-Phe NPs was measured by a hemolysis assay. Sheep red blood cells (RBCs) were washed three times with PBS and resuspended at  $2 \times 10^8$  cells/ml. The CT-NPs were dispersed in a 50 mM MES buffer (pH 5 and 7) containing 0.15 M NaCl, at a concentration of 2 mg/ml. CT-NP were added in a 1:1 volume ratio to the RBC suspensions (final concentration: CT-NPs 1 mg/ml, RBC  $1 \times 10^8$  cells/ml in 25 mM MES, 0.15 M NaCl). The samples were incubated in an aluminum block bath at 37°C for 1 hour, and then centrifuged at  $5'000 \times g$  for 5 minutes. To determine the hemolytic activity of the CT-NPs, the hemoglobin absorbance in the supernatant was measured with a microplate reader at 570 nm. To obtain 100% hemolysis, the RBCs ( $1 \times 10^8$  cells/ml) were lysed by dispersion in water. In the controls, the RBCs were separately incubated in each buffer.

### 6.1.8 TNF $\alpha$ ELISA

To evaluate the RNAi of siRNA-CT-NPs for I $\kappa$ B kinase  $\beta$  (IKK $\beta$ ), DCs ( $5 \times 10^5$  cells/500 $\mu$ l/well) were incubated with IKK $\beta$ -siRNA (50 nM) with LF or CT-NPs for 4 hours at 37°C, before pulsing the DCs with 100 ng/ml LPS. After 24 hours of incubation, the culture supernatants were collected, and the concentrations of TNF- $\alpha$  measured by ELISA (Invitrogen Co., Carlsbad, CA).

### 6.1.9 Cytotoxicity

Cytotoxicity was determined by measuring lactate dehydrogenase (LDH) activity in the supernatant (obtained as described above) using a LDH kit (Cayman Chemical Co., Ann Arbor, MI).

## 6.2 Encapsulation of siRNA

The encapsulation of siRNA into the core-corona  $\gamma$ -PGA-Phe nanoparticles was attempted using two techniques:

1. siRNA pre-complexation with protamine prior to encapsulation
2. self-assembly through cholesterol-modification of siRNA

### 6.2.1 Encapsulation of siRNA by polyplex formation with protamine

Protamine is a highly positively charged peptide that stabilizes DNA through ionic and hydrogen bonds in sperm [33, 281]. Protamine has shown promising results in siRNA complexation for in vivo delivery [50, 108, 129]. In addition, previous work performed by Kim et al. [144] complexed CpG oligodeoxynucleotides (CpG ODN), immunostimulants composed of short (20 base pairs) single stranded DNA, with protamine and subsequently encapsulated in  $\gamma$ -PGA-Phe. Based on this knowledge, protamine was used to form a polyplex with siRNA which was further encapsulated in  $\gamma$ -PGA-Phe (PP-NPs). The siRNA/protamine polyplex was formed at increasing N/P ratios (the ratio of amino groups on protamine versus phosphate groups of siRNA) to analyze its effect on the NP characteristics as well as the siRNA loading capacity.



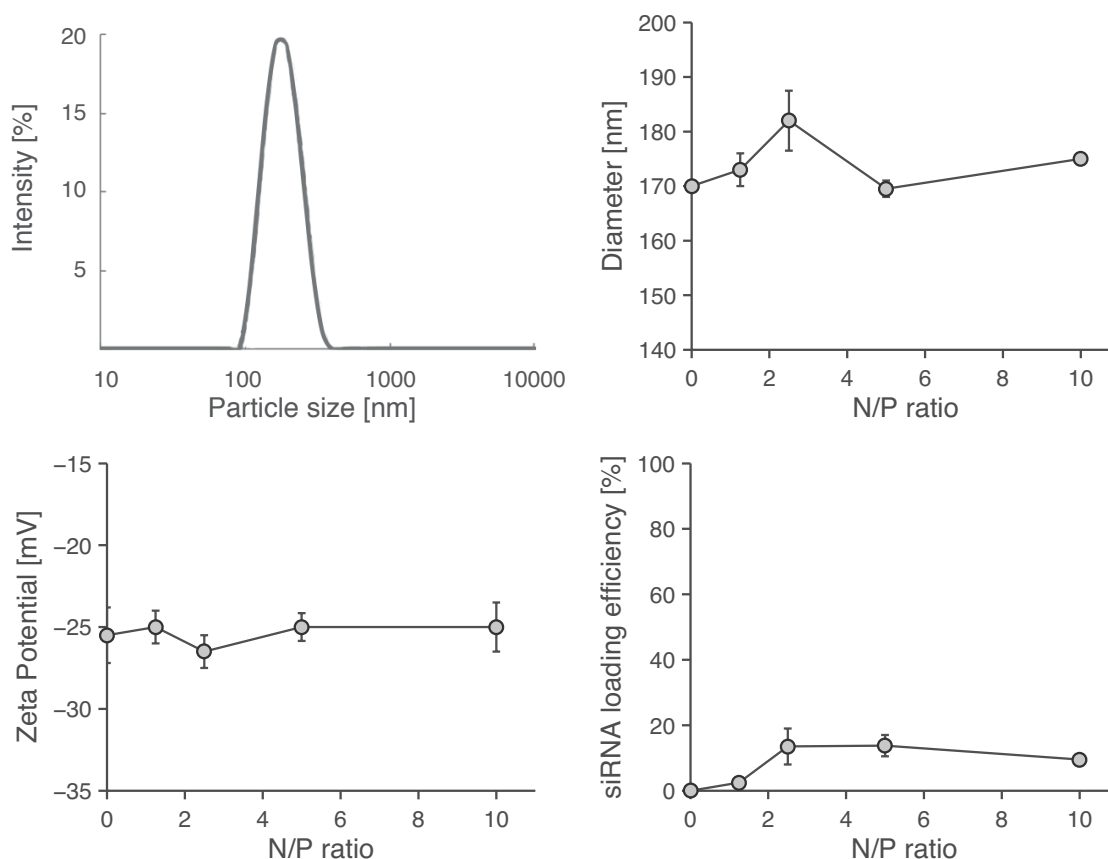


**Figure 6.2.:** Size-distribution, Zeta potential, and siRNA loading capacity analyzed at different N/P ratios of protamine/siRNA polyplexes encapsulated in  $\gamma$ -PGA-Phe nanoparticles in 125 mM NaCl. Size distribution represented for an N/P ratio of 2.5.

PP-NPs showed a narrow-width size-distribution with a mean diameter of 170-180 nm. The N/P ratio had little effect on the diameter and the zeta potential of the formed NPs. Generally, all PP-NPs exhibited a zeta potential of -25 mV indicative of a stable colloidal suspension with little aggregation. Despite the beneficial NP characteristics, siRNA loading was not efficient. Even though an increased N/P ratio led to higher loading, less than 20% of the applied siRNA could be encapsulated.

Further analysis revealed that the NaCl concentration used for the NP formation destabilized the polyplex. The addition of NaCl is required to form NPs of 55% grafting degree  $\gamma$ -PGA-Phe. A decrease in NaCl concentration is possible to a certain extent, but under total absence, NPs will no longer form. A titration of NaCl concentrations from 175 mM down to 100 mM showed an increase in loading efficiency. At the lowest NaCl concentration (100 mM), 25% of siRNA was loaded

which did not fulfill our requirement for efficient siRNA complexation.

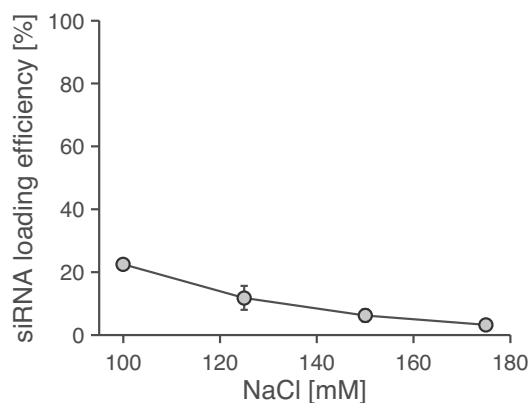


**Figure 6.3.:** Effect of NaCl concentration on siRNA loading efficiency of polyplex NPs (N/P = 5).

### 6.2.2 Encapsulation of cholesterol-modified siRNA

Cholesterol-modified siRNA (Chol-siRNA) showed higher nuclease resistance in rats compared to unmodified siRNA [251,313]. Further, the polyplex of Chol-siRNA and PLL-PEG allowed for efficient gene knock-down in primary breast tumours [12]. The hydrophobic cholesterol tag is additionally useful in core-corona nanoparticles with a hydrophobic core and hydrophilic shell. We hypothesized that Chol-siRNA could self-assemble during the nanoparticle formation of the amphiphilic  $\gamma$ -PGA-Phe.

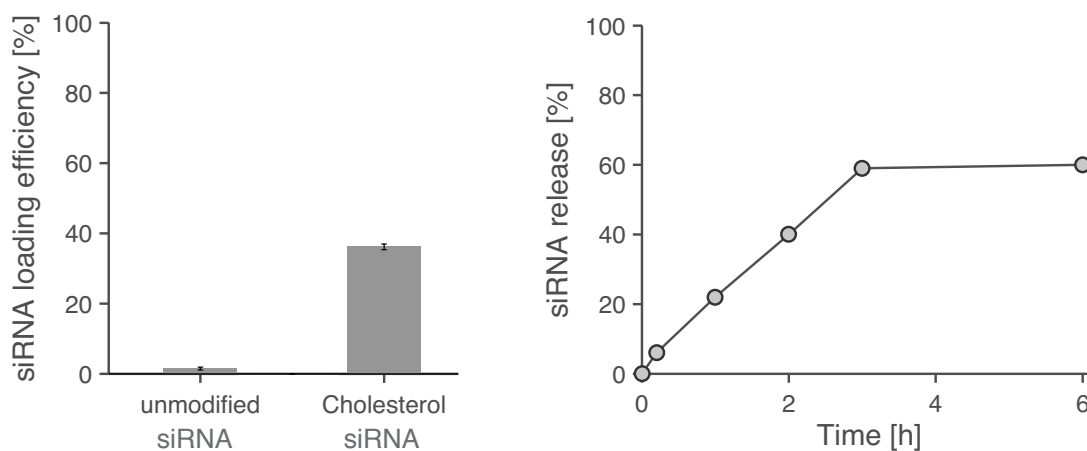


**Figure 6.4.:** siRNA release from cholesterol-siRNA NPs in PBS measured over 6 hours.

To form Chol-siRNA NPs, siRNA in water was mixed with the co-polymer in DMSO. A loading of 36% was observed for Chol-siRNA compared to a negligible encapsulation for unmodified siRNA. The analysis showed that the Chol-siRNA association with the NPs was highly unstable which led to a loss of 59% of its cargo after 3 hours. Considering that the NP uptake into the cell happens after 1-3 hours [8, 93], the release kinetics are unfavourable for successful siRNA delivery.

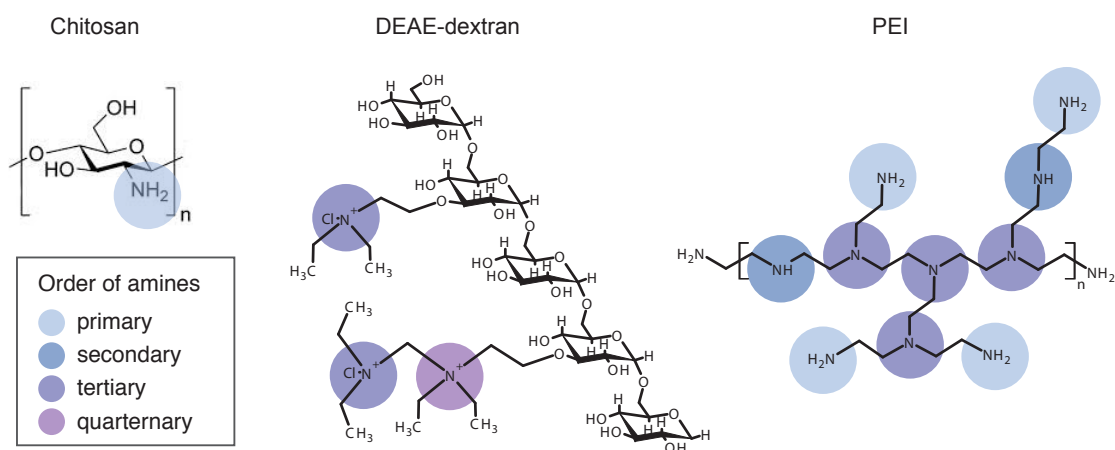
### 6.3 Adsorption of siRNA onto polycation-coated NPs

Following the unsuccessful encapsulation of siRNA into  $\gamma$ -PGA-Phe NPs, the strategy was changed to adsorption via electrostatic interaction of polycations. The highly negative zeta potential of  $\gamma$ -PGA-Phe allows for subsequent adherence of polycations which in turn are able to complex the negatively-charged phosphates on the backbone of siRNA. Besides their ability to bind oligonucleotides, polycations are known to favour cell uptake through charge interaction with the cell membrane [92] as well as to induce endosomal escape. In 1995, Behr proposed the so called "proton sponge" effect as the escape mechanism of polycations [26]. The effect is based on amines with a pKa below 7.4 which, once inside the endosome, get protonated and thereby promote a further influx of protons. The increase in osmotic pressure together with the incrementing charge repulsion of the protonated amines leads to the endosomal rupture and release into the cytoplasm. Ever since the description of this mechanism, doubts of its correctness arose. Recently, it has been shown [28] that the presence of strong polycations does not raise the endosomal pH, contrary to what is expected by increasing the proton influx. It was therefore proposed that polycations might escape due to their membrane-destablizing properties [28]. Although the escape mechanism of polycations is debated, they are accepted to be highly efficient delivery vehicles. Polyethyleneimine (PEI) with its high concentration of positively charged amines, is an attractive candidate for siRNA complexation. The high charge density allows for effective cell uptake [304] but also leads to in vitro toxicity as fast as 30 minutes after administration [82]. Godbye et al. [94] demonstrated that the immediate toxicity of PEI arises from the presence of free PEI, whereas bound PEI affects cells only after 7-9 hours. In addition, it has been demonstrated that PEI coated onto the surface of silica nanoparticles shows no apparent cytotoxicity [148, 297]. We therefore decided to use PEI adsorbed on  $\gamma$ -PGA-Phe nanoparticles as a delivery system for siRNA.

**Table 6.3.:** Characteristics of polycations

Polycation	Molecular weight	Order of amines (pKa)	Charge/monomer [82]
Chitosan	200 kDa	primary (6.5)	n/a
DEAE-dextran	20 kDa	tertiary (5.7 and 9.5) quaternary (14)	0.00278 (for 500 kDa)
PEI	10/25 kDa	primary (4.5) secondary (6.7) tertiary (11.6)	0.0233 (for 600-1000 kDa)

Diethylaminoethyl-dextran (DEAE-dextran) and chitosan were chosen as alternatives due to their reduced charge density and hence lower risk of toxicity [82, 174]. DEAE-dextran has found widespread use in DNA delivery for decades [209, 232], but its application for siRNA delivery has, surprisingly, never been explored. Chitosan, on the other hand, has already shown promise in siRNA delivery and is, due to its safety and transfection efficiency, considered one of the candidates for future in vivo applications [231, 279]. The high transfection efficiency has recently been associated with an even higher buffering capacity than PEI, based on its molar ratio [225].

**Figure 6.5.:** Polycations and their characteristics. Molecular structure of chitosan, DEAE-dextran, and PEI with indicated amines

### 6.3.1 DEAE-dextran and PEI-coated NPs

For the production of DEAE-dextran and PEI-coated NPs,  $\gamma$ -PGA-Phe (55% Phe grafting degree) was mixed with 100 mM NaCl to produce NPs of around 140 nm with a highly negative zeta potential (-56 mV). These particles were subsequently coated with an excess of polycations to avoid aggregation. For polycations, 20 kDa DEAE-dextran and branched PEI of 10 and 25 kDa were chosen. Low molecular weight PEI has been associated with decreased cytotoxicity and high transfection efficiency [32, 154, 290]. The addition of polycations reversed the surface charge and increased the nanoparticle size to 185 nm (10 kDa PEI), 191 nm (25 kDa PEI) and 197 nm (20 kDa DEAE-dextran). The formed positive layer was most charged and hence more compact for 10 kDa PEI. 25 kDa PEI formed a thicker layer likely due to an increased steric hinderance resulting from the higher molecular weight (MW). NPs coated with 20kDa DEAE-dextran yielded the biggest particles with the lowest zeta potential, a result of high MW and low charge density. Generally, the coated NPs were stable in solution and showed a narrow size distribution with low polydispersity index (PDI).

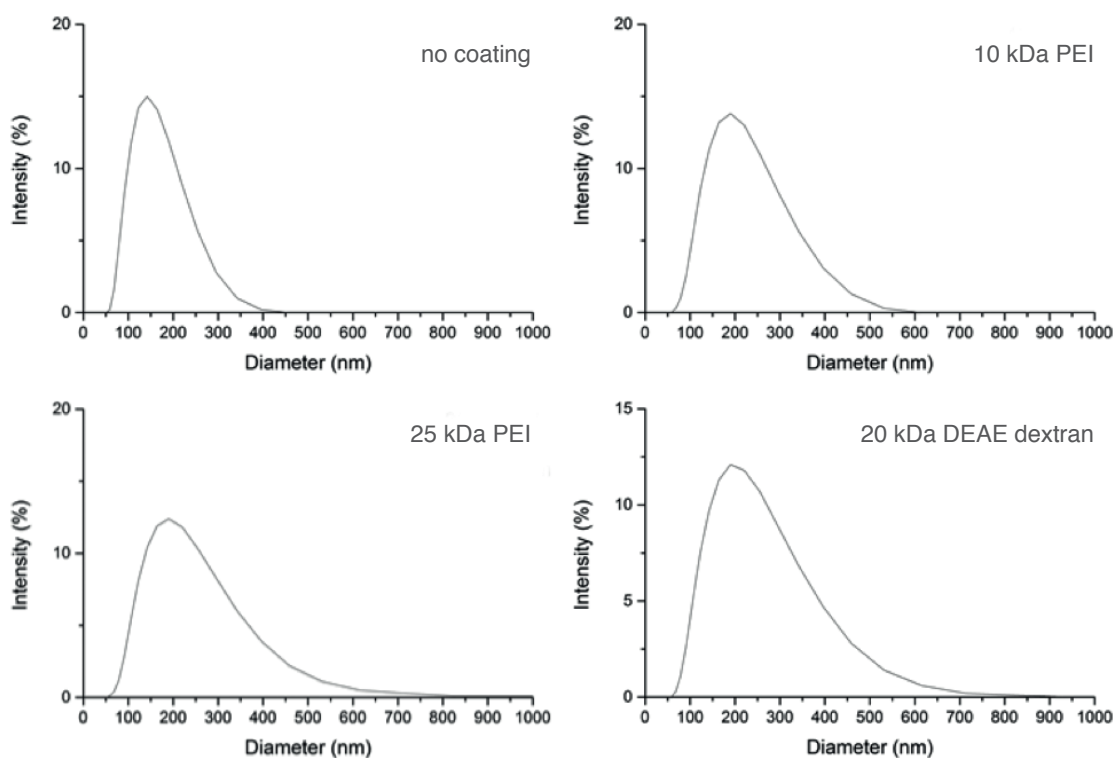


**Figure 6.6.:** Size-distribution of PEI and DEAE dextran-coated NPs.

**Table 6.4.:** Characterization of PEI and DEAE dextran-coated NPs

Coating material	Diameter [nm]	PDI	Zeta potential [mV]
-	137	0.119 2	-56 $\pm$ 0.3
10 kDa PEI	185	0.17	68 $\pm$ 0.3
25 kDa PEI	191	0.217	55 $\pm$ 0.3
20 kDa DEAE-dextran	197	0.206	44 $\pm$ 0.3

The strong positive charge of the polycations allowed for subsequent adsorption of siRNA. The adsorption efficiency could be calculated by measuring the non-adsorbed fraction of Cy3-labelled siRNA. Five mg/ml of NPs were able to complex more than 90% of siRNA whereas 0.25 mg/ml NPs only complexed a third of the siRNA. At 5 mg/ml, the NPs present an excess of amines which are necessary for the cell uptake and endosomal release. Based on the high adsorption efficiency, the following experiments were all performed with 5 mg/ml and the final siRNA concentration calculated assuming 100% efficient complexation.

**Table 6.5.:** Adsorption efficiency of Cy3-siRNA by DEAE-dextran and PEI-coated NPs

Coating material	NPs [mg/ml]	siRNA [nM]	Adsorption efficiency
10 kDa PEI	5	600	93.15 %
	0.25	600	31.33 %
25 kDa PEI	5	600	94.18 %
	0.25	600	27.86 %
20 kDa DEAE-dextran	5	600	91.3 %

For the transfection experiments, cells were seeded and left to adhere overnight before siRNA-NPs were added for 6 hours at an amount equivalent to 100 nM siRNA. The uptake could be observed 24 hours post transfection, with a strong perinuclear localization of the fluorescently-labelled Cy3-siRNA. INTERFERin, the commercially available transfection reagent, showed a lower transfection efficiency with less cells exhibiting a fluorescent signal. Cells treated with siRNA-NPs had a similar morphology compared to INTERFERin and showed no apparent signs of cell death. Interestingly, 48 hours after transfection, only INTERFERin exhibited a decrease in the target gene (GAPDH) whereas both PEI and DEAE-dextran coated NPs did not show any gene knock-down.

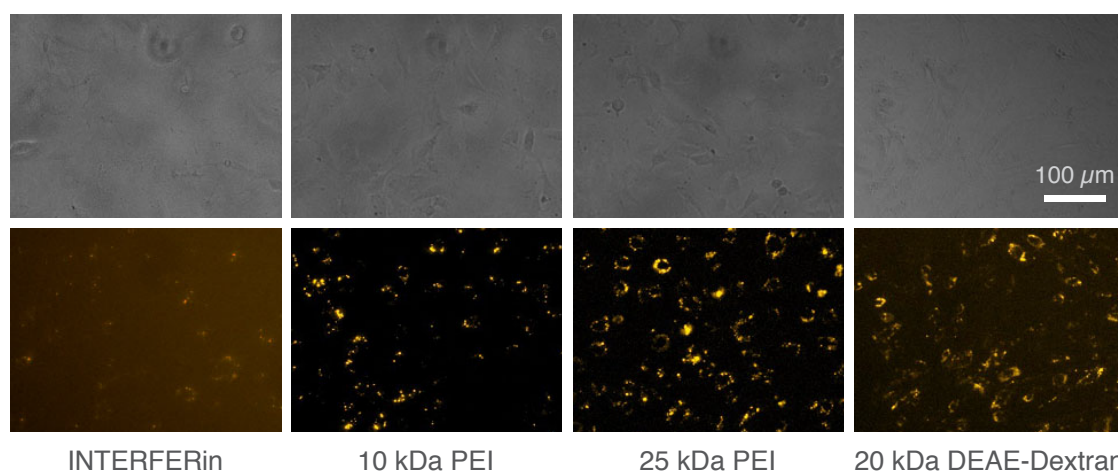


**Figure 6.7.:** Cellular uptake of DEAE-dextran and PEI coated NPs loaded with 100 nM Cy3-siRNA. Cells were incubated with siRNA-NPs for 6 hours and cells imaged after a total of 24 hours. Scale bar 100 μm.

One factor determining the knock-down efficiency is the N/P ratio of the amines in PEI and the phosphate groups of siRNA. In the work of Zheng et al. [310] 25 kDa PEI at an N/P ratio of 2 yielded the best transfection with the lowest cytotoxicity. Further, Richards Grayson et al. [226] determined an N/P ratio between 6-8 to be optimal. The N/P ratio in our system was unknown, as an excess of PEI was used to coat the NPs. A vague estimation based on 25% binding of PEI results in an approximate N/P ratio of 50. Compared to the literature, this N/P ratio is far too high. We therefore tested how the N/P ratio affects the RNAi interference of 10 kDa PEI-coated NPs and observed a good knock-down at an estimated ratio of 25. At higher molar ratios of PEI, an assay interference was observed which casts doubt on the results. Altogether, this preliminary data shows promise for PEI and DEAE-dextran-coated  $\gamma$ -PGA-Phe NPs as siRNA delivery system although further evaluation of their safety and efficiency would be required for successful in vitro and in vivo use.

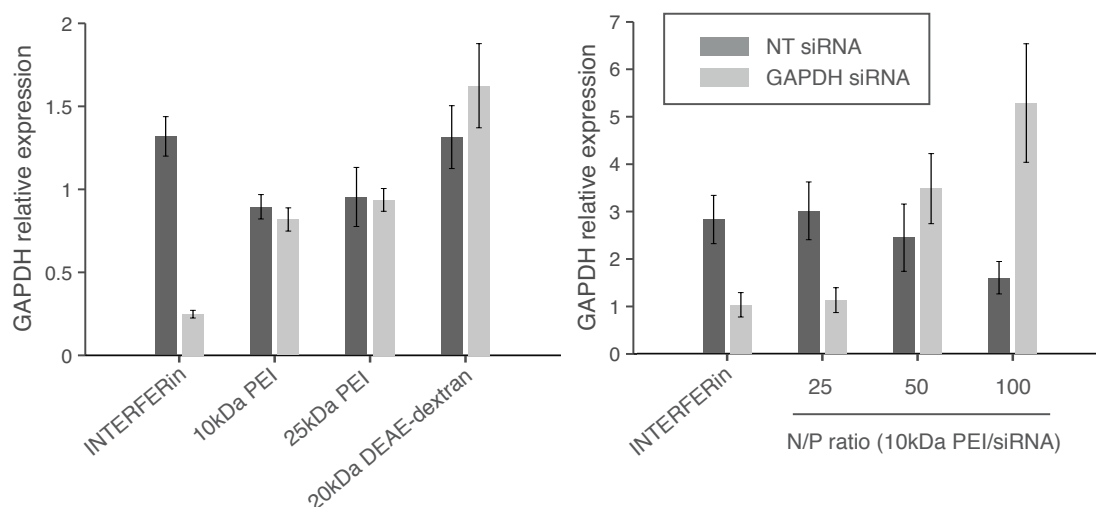


**Figure 6.8.:** Gene knockdown of DEAE-dextran and PEI coated NPs loaded with 100 nM GAPDH-siRNA. Cells were incubated with siRNA-NPs for 6 hours and RNA isolated after a total of 48 hours. GAPDH gene expression was normalized to RPL13a and a control sample without siRNA treatment used as normalizer. Commercially available INTERFERin was used as a positive control.

### 6.3.2 Chitosan-coated NPs

For the production of chitosan-coated NPs (CT-NPs), 200 nm-sized  $\gamma$ -PGA-Phe (55% Phe grafting degree) NPs were used. Table 6.6 summarizes the size and zeta potential of the CT-NPs. Untreated  $\gamma$ -PGA-Phe NPs showed a strongly negative zeta potential (- 44 mV), attributed to the presence of carboxyl groups located near the surface. In contrast, after CT coating, the zeta potential of the NPs changed from negative to positive (+ 25 mV), indicating that the surface of the NPs was successfully covered with CT. The size of the CT-NPs increased with decreasing CT/NP ratio (w/w), and showed a monodispersed size distribution (Figure 6.9). Upon mixture of  $\gamma$ -PGA-Phe NPs with a low concentration of CT (CT/NP ratio < 1), large-sized aggregations were detected.

**Table 6.6.:** Characterization of Chitosan-coated NPs

CT/NP [w/w]	Chitosan [mg/ml]	$\gamma$ -PGA-Phe NPs [mg/ml]	Diameter [nm]	Zeta potential [mV]
-	-	10	245 $\pm$ 2	-44.3 $\pm$ 0.3
1	10	10	310 $\pm$ 17	26.7 $\pm$ 0.3
2	10	5	283 $\pm$ 36	24.9 $\pm$ 0.3
4	10	2.5	251 $\pm$ 9	24.7 $\pm$ 0.3
8	10	1.25	230 $\pm$ 31	26.0 $\pm$ 0.3



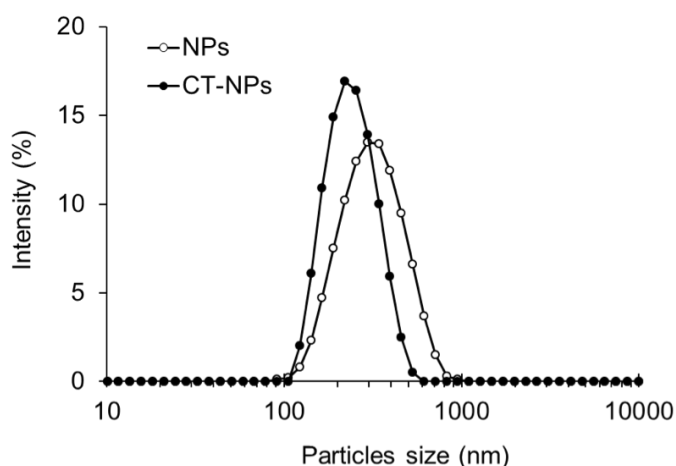


**Figure 6.9.:** Size distribution of  $\gamma$ -PGA-Phe NPs and CT-NPs (CT/NP=1). The size of the NPs was measured in PBS by DLS.

The molecular weight (MW) of the polyelectrolyte is another parameter affecting the formation of the polyion complex. CT with a MW of  $2 \times 10^5$  was suitable for preparing monodispersed cationic  $\gamma$ -PGA-Phe NPs. When low molecular weight CT (MW =  $2 \times 10^3$ ) was used, no charge reversal was observed. It is likely that the chain length of CT was not sufficient to cover the NP surface. In contrast, high molecular weight CT (MW =  $2 \times 10^6$ ) led to particle aggregation, indicating crosslinking of NPs by CT. For the subsequent experiments, 250 nm-sized CT-NPs produced with  $2 \times 10^5$  MW CT at a ratio of CT/NP = 4 were used.

siRNA loaded CT-NPs were prepared in order to study their potential application as siRNA carriers. siRNA was successfully adsorbed onto CT-NPs by electrostatic attraction (see Figure 6.10). A high adsorption efficiency of 80-90% was observed on CT-coated NPs compared to the uncoated control. The siRNA adsorption did not alter the size of siRNA-CT-NPs particles (250 nm), but the zeta potential decreased from 25 mV to 11 mV (data not shown).

To evaluate the stability of siRNA-CT-NPs, the siRNA release in PBS was measured over 24 hours (Figure 6.10). The loss of less than 5% of the adsorbed siRNA after one day indicates a highly stable complex formation.

## 6. $\gamma$ -PGA-Phe nanoparticles as siRNA carriers

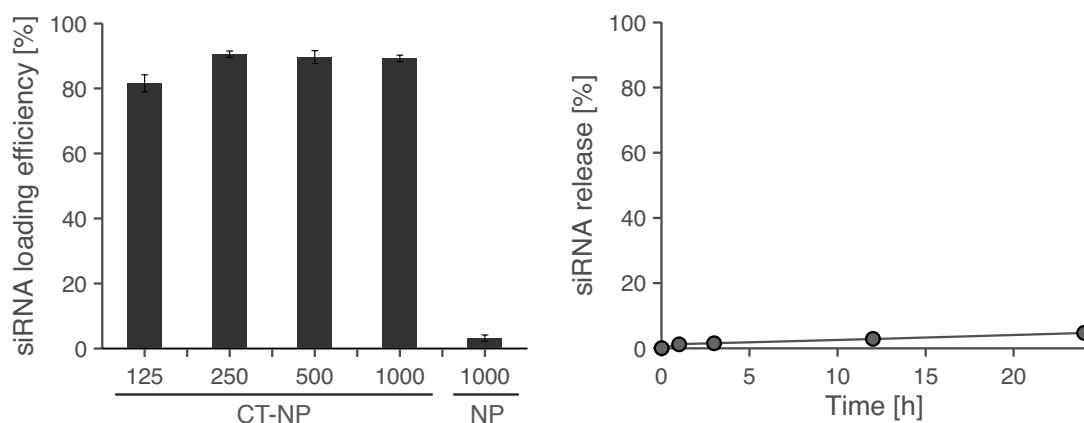


**Figure 6.10.:** Loading efficiency and release profile of chitosan-coated NPs. Adsorption efficiency of FAM-siRNA by CT-NPs compared to uncoated NPs at an siRNA concentration ranging from 125 to 1000 nM. Release profile of siRNA on chitosan-coated NPs analyzed over 24 hours in PBS at 37 °C.

To evaluate the uptake behaviour of siRNA-CT-NPs by DCs, the cells were incubated with FAM-tagged siRNA to monitor intracellular localization by FACS analysis.

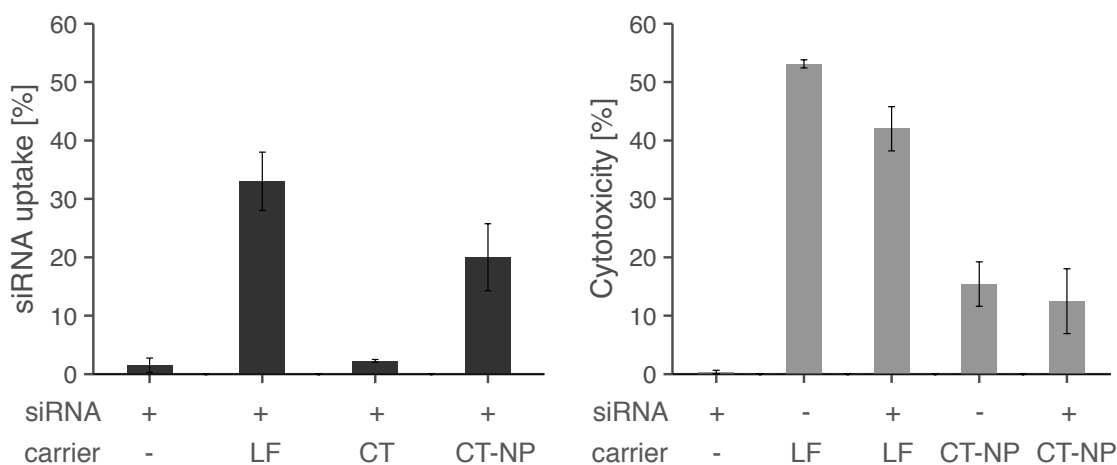


**Figure 6.11.:** Uptake and cytotoxicity of chitosan-coated NPs compared to lipofectamine. Uptake in DCs was analyzed using free siRNA or complexed with lipofectamine (LF), CT and CT-NPs. After 1 hour incubation, the cell-associated fluorescence was assessed by FACS. Cytotoxicity of siRNA-CT-NPs was compared to LF and CT-NPs with/without siRNA after 4 h and the subsequently administration of 100 ng/ml LPS. After 24 h incubation, the lactate dehydrogenase (LDH) activity in the supernatant was measured.

An uptake efficiency of 20% was measured for siRNA-CT-NPs, which was slightly lower than that achieved by siRNA/LF complexes (33%), but significantly higher than that of siRNA/CT polyplexes and siRNA alone (Figure 6.11) which do exhibit an overall negative surface charge leading to repulsion with the cell membrane. The positive zeta potential of the CT-NPs allows electrostatic interaction with the cell membrane and subsequent internalization. Despite the higher transfection efficiency of lipofectamine, it is a highly cytotoxic reagent as measured by lactate dehydrogenase (LDH) activity (Figure 6.11). CT-NPs, on the other hand, show remarkably low toxicity, most likely due to lower positive charge.

After the successful proof of the uptake of CT-NPs into the cell, the potential of their capacity to disrupt the endosomal membrane was evaluated. Red blood cells (RBCs) were used as a model for endosomal membranes. The hemolytic activity measured in the RBC model has been reported to correlate with the endosomal disruption capacity [75]. Figure 6.12 shows the hemolytic activity of the uncoated (NPs) and CT-coated NPs (CT-NPs) as a function of pH.

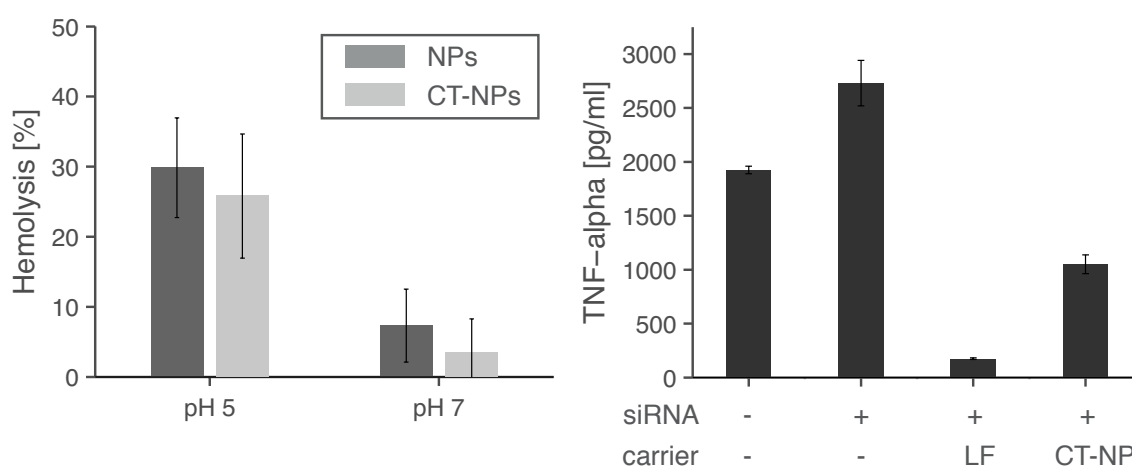


**Figure 6.12.:** Hemolysis and suppression of TNF- $\alpha$  secretion of LPS-stimulated DCs siRNA-CT-NPs. RBC hemolysis of CT-NPs compared to uncoated NPs at pH 5 and 7. Suppression of TNF- $\alpha$  secretion of LPS-stimulated DCs by IKKb-siRNA was compared for free siRNA or lipofectamine (LF) and CT-NPs complexed siRNA. After siRNA administration for 4 hours, 100 ng/ml LPS was added and the culture supernatants collected after 24 hours to analyze the TNF- $\alpha$  concentrations by ELISA. PBS treated samples served as a control.

No hemolytic activity was observed for NPs and CT-NPs at physiological pH. However, the hemolytic activity of the CT-NPs increased at pH 5, which resembles the endosomal condition. In a previous study, it was demonstrated that the hemolysis of  $\gamma$ -PGA-Phe NPs was dependent on the hydrophobicity of  $\gamma$ -PGA. It is therefore

assumed that due to a partial protonation of  $\gamma$ -PGA, chitosan coverage might be slightly decreased at the NP surface, allowing the interaction of the hydrophobic part of  $\gamma$ -PGA-Phe NPs to interact with the RBC membrane. The membrane-disruptive activity of CT-NPs at endosomal pH indicates their ability to escape the endocytotic degradation pathway and to deliver the siRNA into the cytoplasm.

It is well-known that DCs secrete a large amount of inflammatory cytokines, such as TNF- $\alpha$  and interleukins when stimulated and activated by lipopolysaccharide (LPS) [1]. NF- $\kappa$ B as transcriptional factors are rapidly activated in response to various stimuli, including cytokines and infectious agents. In non-stimulated cells, NF- $\kappa$ B is bound to inhibitory I $\kappa$ B proteins, which blocks the nuclear translocation signal of NF- $\kappa$ B. The NF- $\kappa$ B signaling pathway involves the enzymatic complex I $\kappa$ B kinase (IKK), which induces the phosphorylation of I $\kappa$ B. This event allows NF- $\kappa$ B to translocate to the nucleus and activate the transcription of several pro-inflammatory cytokines. [138] Therefore, inhibition of IKK by siRNA on DCs is expected to suppress TNF- $\alpha$  production in response to LPS stimulation.

To investigate the utility of siRNA-CT-NPs in the delivery of therapeutic siRNAs, we examined the suppression of TNF- $\alpha$  production in LPS-stimulated DCs by the knockdown of IKKb. DCs were incubated with IKKb-siRNA adsorbed onto CT-NPs for 4 h, prior to LPS stimulation. Figure 6.12 shows the suppression effect of TNF- $\alpha$  secretion by DCs treated with IKKb-siRNA with and without carriers. The siRNA/LF and siRNA-CT-NPs was able to suppress TNF- $\alpha$  secretion induced by LPS stimulation. A slight increase in TNF- $\alpha$  secretion by cells treated with siRNA alone was observed. This is probably due to non-specific stimulation of the siRNA. The suppression effect of siRNA/LF was higher than that of siRNA-CT-NPs, but considering the decreased cytotoxicity of CT-NPs compared to lipofectamine, they present a valuable alternative for siRNA delivery.

## 6.4 Chapter summary

In this chapter, several methods were presented for the production of siRNA carriers based on  $\gamma$ -PGA-Phe nanoparticles. Both encapsulation strategies were unsuccessful based on the instability of the formed NPs and hence low siRNA loading capacity. The complexation of siRNA on the outside of the NPs by electrostatic interaction with polycations showed promising results. Polycations with high, medium and low charge density (PEI, DEAE-dextran, and chitosan, respectively) all formed stable cationic layers on the negatively charged  $\gamma$ -PGA-Phe nanoparticles and al-

lowed the adsorption of siRNA with an efficiency of 80-95%. Further, all coated-NPs were efficiently taken up by the cells. Preliminary results of siRNA interference of PEI and DEAE-dextran modified NPs present a potential knock-down at lower N/P ratio, but further analysis is needed for complete evaluation of their efficiency and safety. Chitosan-coated NPs, on the other hand, have a proven low cytotoxicity and were successfully applied in the knock-down of TNF-alpha secretion of dendritic cells.

**Table 6.7.:** Key characteristics of  $\gamma$ -PGA-Phe NPs for siRNA delivery

Type	Material	Colloidal stability	siRNA loading	Cell uptake	Knock-down
Encaps	Protamine	✓	×	-	-
	Cholesterol-tagged	×	×	-	-
Coating	Chitosan low MW	×	-	-	-
	Chitosan high MW	✓	✓	✓	✓
	DEAE-dextran	✓	✓	✓	?
	PEI	✓	✓	✓	?

For clinical application of  $\gamma$ -PGA-Phe NPs, chitosan coating presents the most promising approach due to the high biocompatibility. PEI and DEAE-dextran, on the other hand, could both lead to cytotoxic effects once released from the NP surface. To pave the way for chitosan-coated  $\gamma$ -PGA-Phe NPs towards their use in disease treatment, specific tissue targeting is indispensable. Future work will therefore need to address how NPs can be directed to be taken up by chondrocytes. One strategy presents the immobilisation in a layer-by-layer coating on the cell surface which brings the NPs into the close proximity of the cells. This approach in addition circumvents the high diffusion barrier of the dense cartilaginous extracellular matrix which hinders the NP accumulation in cartilage.



7 Human epiphyseal chondroprogenitor cells produce phenotypically stable cartilage: A new cell source for one-step treatment of cartilage lesions?



*Note:* The work in this chapter is in preparation for submission to *Osteoarthritis and Cartilage*

Currently available cell-based treatments for cartilage regeneration are based on the use of autologous articular chondrocytes (ACs) or mesenchymal stromal cells (MSCs) recruited from the underlying bone through microfracture. Inter-patient variability of both cell types leads to an unpredictable tissue quality. MSCs, in addition, suffer from phenotypical instability, as presented in the previous chapters. In this part we therefore focus on the use of a novel allogeneic cells source derived from fetal epiphyseal cartilage.

As cartilage is avascular, and alymphatic and therefore immunoprivileged, allogenic adult chondrocytes can be considered and indeed have shown promising results in clinics [11, 64]. Allogenic cells derived from fetal or juvenile tissue have the additional benefit of a higher chondrogenic potential compared to adult chondrocytes [3] along with a potentially more stable phenotype than pluripotent MSCs [2, 221]. Further, due to the high cell number and proliferation potential, the cells from a single donor can be expanded to treat multiple patients with a homogeneous cell population [59]. The low immunogenicity [4] makes juvenile or fetal chondrocytes an allogeneic ready-to-use alternative to autologous MSCs.

This study compares the chondrogenic potential of fetal epiphyseal chondroprogenitor cells (ECPs) (from a 14-week gestation donor) with adult bone marrow-derived MSCs (MSCs), and adult articular chondrocytes (ACs) using Optimaix-3D, a collagen sponge with similar composition as m-ACI scaffolds. 2D expanded ACs are the cells used for the standard ACI procedure. MSCs from bone marrow were chosen since they are the most extensively-studied MSC source with superior potential for chondrogenesis using common culture methods [5, 67]. ECPs, on the other hand, are a newly proposed cell source [59] which we selected because of their potential off-the shelf availability and immature chondrodifferentiation which has shown to be beneficial for cartilage matrix production [3]. In the following study, ECPs, MSCs and ACs were evaluated on the basis of their chondrogenic potential (glycosaminoglycan content (GAG), collagen 2 to 1 mRNA ratio, mechanical properties) and phenotypic stability (collagen 10, indian hedgehog (Ihh) and parathyroid hormone receptor 1 (PTH1R) gene expression). Furthermore, we evaluated how scaffold structure influenced cellular distribution and how cell seeding density affected the balance between proliferation and matrix production in producing cartilaginous constructs.



## **7.1 Materials and methods**

### **7.1.1 Cells**

Human ECPs were isolated from the proximal ulnar epiphysis of a 14-week gestation donor were expanded to passage 5. Human chondrocytes (two female and one male, aged between 28 and 31) as well as human MSCs (two female and one male, aged between 34 and 50 years) were used at passage 3.

### **7.1.2 Effect of alginate on scaffold seeding**

To study the effect of alginate in combination with the scaffolds, 2.5  $\mu$ l of cell suspension was mixed 1:1 with 0.8% w/v sterile alginate (Novamatrix, Pronova, low viscosity (20-200 mPas) sodium alginate) solution, seeded into the scaffold and immediately placed into 102 mM CaCl<sub>2</sub> solution for 10 minutes. The medium was replaced every 3-4 days for 3 or 6 weeks.

### **7.1.3 Mechanical testing**

Pre-hydrated scaffolds were mechanically tested under unconfined compression using a standard mechanical testing machine with a 500 g load cell (TA.XTplus Texture Analyser, Stable Microsystems, UK). A preload of 0.4 g was applied to ensure that the surfaces of the scaffolds were in direct contact with the cylindrical 2 mm diameter stainless steel probe. Stress-strain testing was performed: the samples were compressed to a final strain of 10% at a loading rate of 0.01 mm/sec. The compressive modulus ( $E^*$ ) was calculated as the slope in the linear range of the stress-strain curve.

### **7.1.4 Scanning electron microscopy**

The morphology of the intact scaffolds was observed by scanning electron microscopy (SEM, Hitachi S-4800) after applying a 8 nm gold/palladium coating. All images were acquired at a voltage of 2.0 kV and a current of 10  $\mu$ A.

### 7.1.5 Statistical analysis

All experiments were performed with three biological replicates of MSCs and ACs (with the exception of Figure 7 which has only one donor/repetition). For ECPs, a single tissue donor was used and grown separately in three replicates. Differences between scaffolds can therefore be attributed to both technical and biologic variability. All numerical data is presented in boxplot diagrams. The central line represents the median, the circle the mean, the box delimits the 25th and 75th percentiles and the whiskers extent to the minimum and maximum values (not considered outliers). Outliers were defined as an observation  $1.5\times$  larger than the interquartile range. Statistical evaluation was performed using Prism (Graphpad Software Inc., Version 6.0d). The dispersion of data points around the mean is presented as coefficient of variance (%CV). Differences between cell types and seeding density were assessed by two-way ANOVA and the effect of culture time and cell type by repeated two-way ANOVA both with Tukey's post hoc. P-values below 0.05 were considered statistically significant and if  $p<0.001$  noted with an asterisk (\*) or otherwise with their exact number.

## 7.2 Scaffold comparison

In a first step, we compared two clinically-applied scaffolds, Chondro-Gide<sup>®</sup> and Novocart<sup>®</sup> Basic were compared with Optimaix-3D, a sponge developed for pre-clinical tissue engineering studies. Chondro-Gide<sup>®</sup> (thickness: 0.5 mm) is a low porosity, bi-layered porcine collagen I/III fleece with an open porous part facing the defect, and a dense sealing outer layer. The Novocart<sup>®</sup> Basic scaffold (2mm-thick porcine) is composed of collagen chondroitin-sulfate structured into an upper columnar and a lower sponge-like compartment. Optimaix-3D (1.5 mm in height) is an open-porous porcine collagen I/III sponge (containing <30% w/w elastin) produced by a zero-length cross-linking procedure using EDC/NHS chemistry.

The evaluation of the three scaffolds was focused on the homogeneity of cell seeding analyzed after 3 weeks of culture. DAPI staining of cryosections (Figure 7.1A) showed the distribution of nuclei primarily in the top third open-porous layer of Chondro-Gide<sup>®</sup> leaving 2/3 of the collagen fleece devoid of cells. In Novocart<sup>®</sup> Basic, cells were evenly distributed throughout the columnar part (defect facing side) with a slightly increased density in top/inner region. The Optimaix-3D scaffold showed the most even cell distribution and hence was used for the rest of the study.

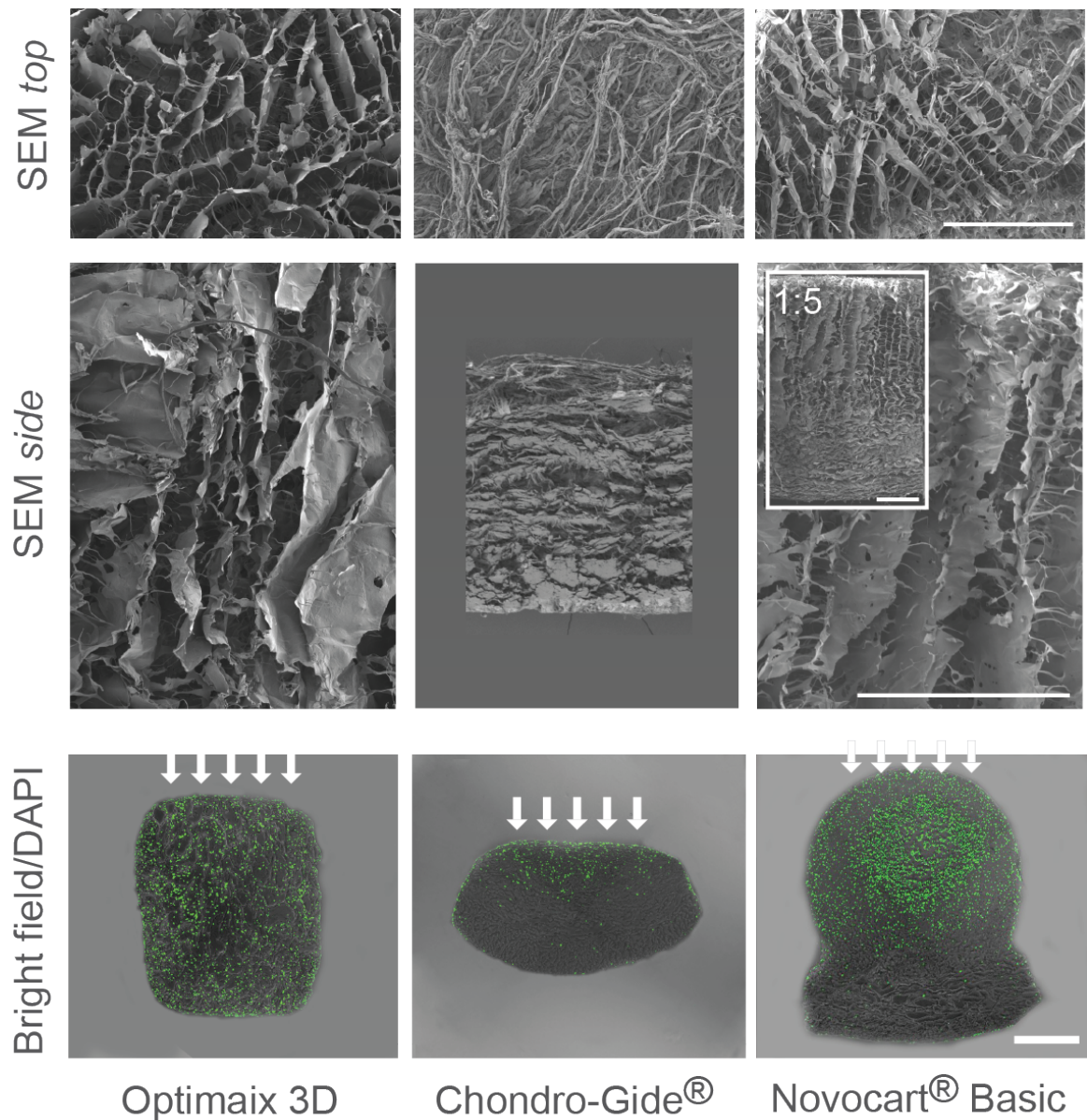


**Figure 7.1.:** Scaffold comparison. SEM top view images show the porosity of scaffolds. SEM side views show the bi-layered structure of Chondro-Gide® and the columnar structure of Novocart® Basic. Bright field images (background exposure adjusted for increased contrast to scaffold) merged with DAPI (coloured in green) show the localization of nuclei in Optimaix-3D, Chondro-Gide® and Novocart® Basic scaffolds at day 21 initially seeded with  $5 \times 10^4$  cells/mm<sup>3</sup>. Arrows indicate the seeding direction. Scale bars 500  $\mu$ m (SEM and bright field).

### 7.3 Evaluation of seeding density

In a second step, we established the relationship between seeding density and chondrogenic differentiation, with a clear trend of rounder morphology (closely resembling human cartilage (Figure 7.2D)) and increased GAG at high cell density ( $5 \times 10^4$  cells/mm<sup>3</sup> - Figure 7.2A: AC - 3.5 fold higher than  $1 \times 10^4$  cells/mm<sup>3</sup>,  $p < 0.001$ ; ECP - 4.7 fold higher,  $p < 0.001$ ). A low initial cell number ( $1 \times 10^4$  cells/mm<sup>3</sup>) resulted in increased proliferation (Figure 7.2C), a spreading phenotype (Figure 7.2D) and inferior matrix production for ACs and ECPs. This is in accordance with the observation of Vunjak-Novakovic et al. [284] that an initially higher seeding density ( $2.55 \times 10^4$  cells/mm<sup>3</sup>) of bovine chondrocytes surpasses the GAG production of the lower density ( $1 \times 10^4$  cells/mm<sup>3</sup>) even if they reach the same cell number after two weeks. A similar result is reported by Roche et al. [227] who used freshly isolated fetal bovine chondrocytes in collagen sponges that only proliferated at low density ( $2.1 \times 10^3$  cells/mm<sup>3</sup>) but showed higher abundance of collagen at high density ( $2.1 \times 10^4$  cells/mm<sup>3</sup>). A higher initial cell number further resulted in decreased collagen 1 expression of ACs and ECPs (also reported by Moretti et al. [191] for human chondrocytes in Hyalograft C), most probably due to the higher cell density where a single cell is in a local 3-dimensional environment rather than able to grow and elongate on 2D fibers. Interestingly, MSCs synthesized similar amounts of GAG for both initial cell densities, concomitantly with the most pronounced increase in cell proliferation (MSC: 5.4 fold increase from low to high density,  $p < 0.001$ ). Based on these results, all subsequent experiments were performed using the high cell density.

Altogether, phenotypic de-novo cartilage is produced at a cell density where proliferation is minimized. The current available clinical m-ACI treatments use low cell densities (Table 1.1) which is mainly due to the limited number of chondrocytes obtained from adult cartilage. Our results clearly show the importance of adequate cell seeding, a parameter also considered in the technique of ACI-Cs (cell-seeded collagen matrix-supported ACI) [257] and in the high density chondrospheres [237]. ECP isolation from fetal cartilage yields highly viable cells [268] which maintain their strong chondrogenic potential after 2D expansion, an advantage over the use of ACs that de-differentiate during 2D tissue culture.

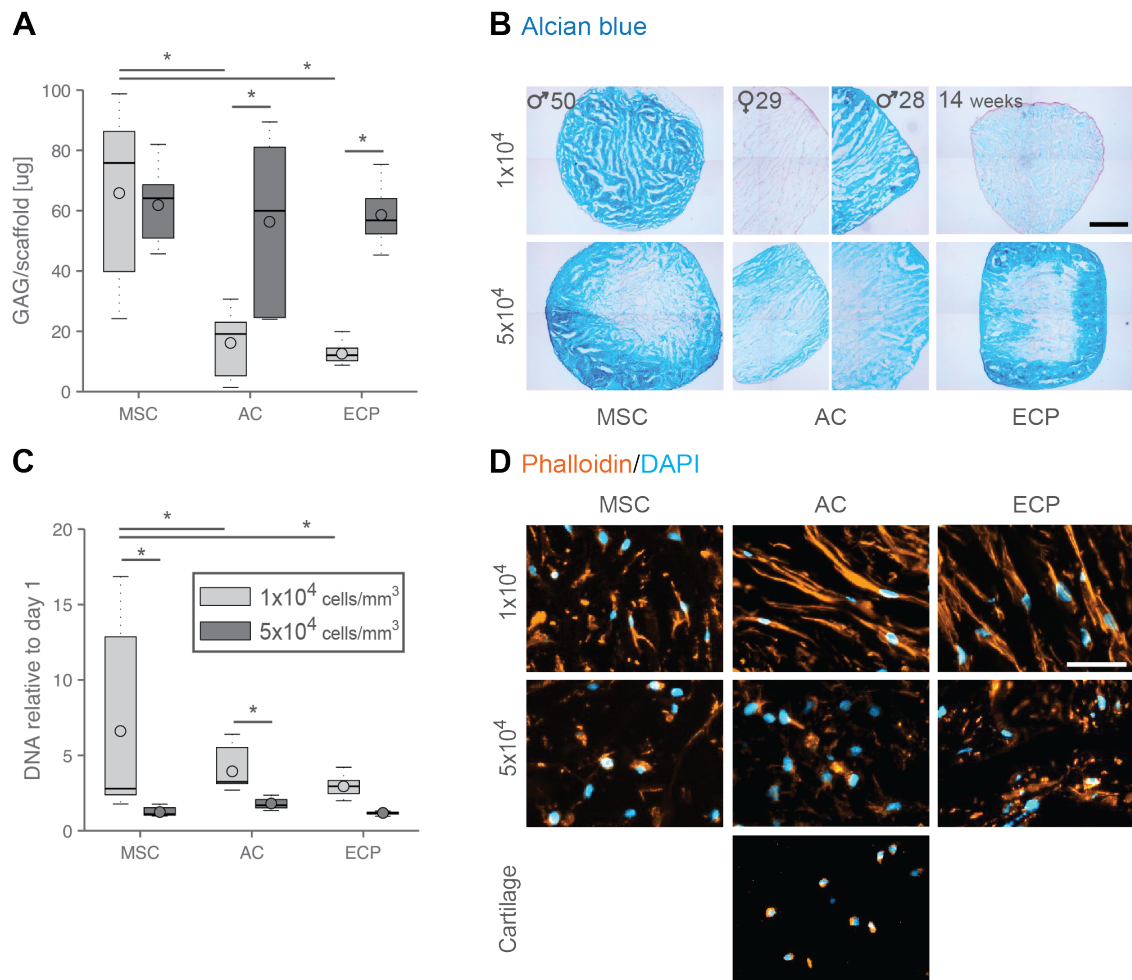


**Figure 7.2.:** Effect of cell seeding density. Initial cell seeding density of  $1 \times 10^4$  cells/mm<sup>3</sup> or  $5 \times 10^4$  cells/mm<sup>3</sup> compared at day 21 based on **A** GAG production, **B** representative alcian blue-stained sections (scale bar 500  $\mu$ m, donor demographics indicated by  $\sigma^7$  for male and  $\text{♀}$  for female followed by the age), **C** DNA content normalized to day 1, and **D** Phalloidin/DAPI staining (scale bar 50  $\mu$ m).

7. Epiphyseal chondroprogenitor cells produce phenotypically stable cartilage

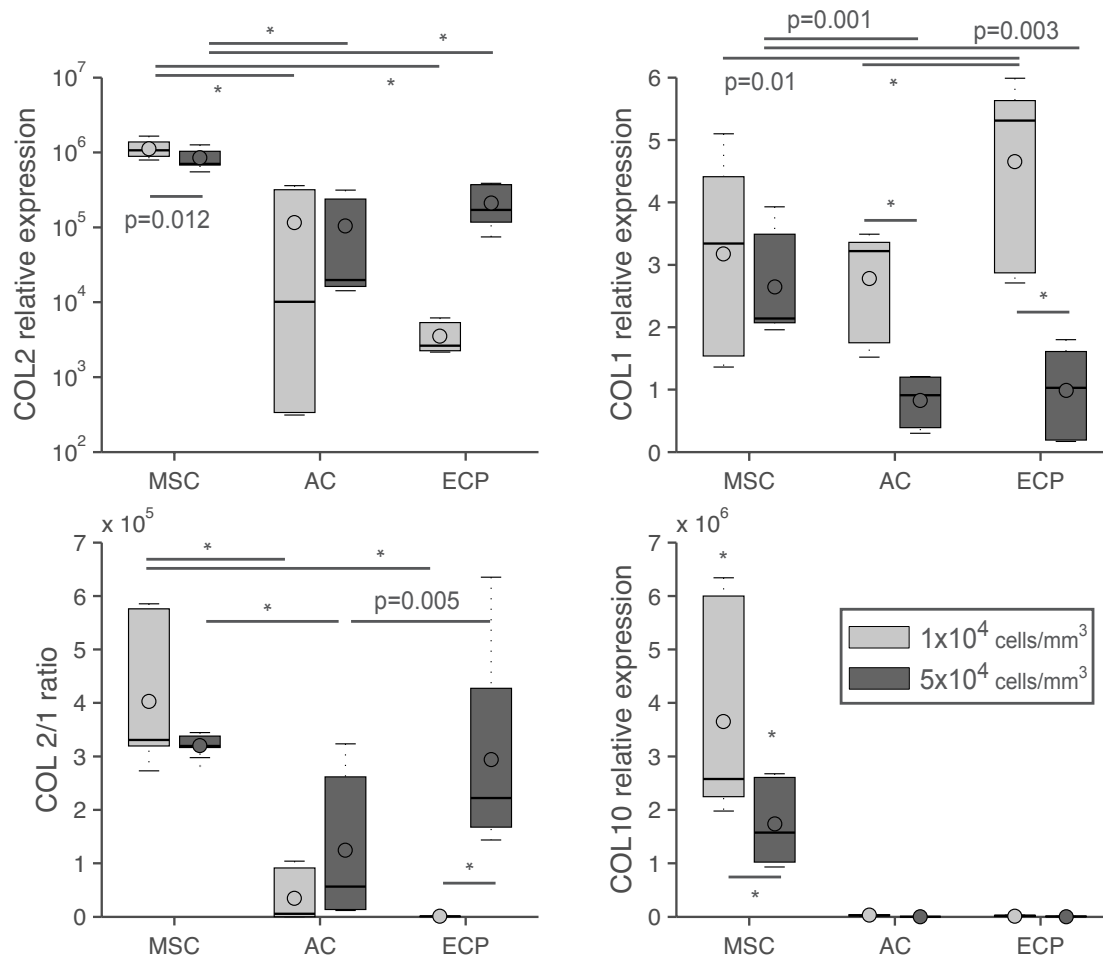


**Figure 7.3.:** Effect of cell seeding density analyzed by qPCR. Real time PCR analysis of  $1 \times 10^4$  or  $5 \times 10^4$  cells/mm<sup>3</sup> cell-laden scaffolds at day 21. Gene expression was analyzed for **A** collagen 2 (COL2), **B** collagen 1 (COL1), **C** collagen 2/1 ratio (COL2/1), and **D** collagen 10 (COL10). Gene expression was normalized to RPL13a and ECP 2D as calibrator sample.

## 7.4 Effect of alginate on scaffold seeding

To test whether the presence of a hydrogel could add a benefit to the scaffold culture system, we seeded cells pre-mixed in 0.4% w/v alginate. The addition of alginate resulted in increased collagen 2 expression for all cell types (Figure 7.4, MSC: 1.28 fold,  $p < 0.001$ , AC: 1.96 fold,  $p = 0.005$ , ECP: 1.62,  $p = 0.0946$ ). This effect might be even more pronounced at low cell density due to more unfilled space in the scaffold pores which by the addition of a hydrogel could be filled to reduce cell spreading and to create an immediate 3D environment. The combination of hydrogels and scaffolds presents a promising approach which should be further evaluated for its benefit in cartilage matrix production.

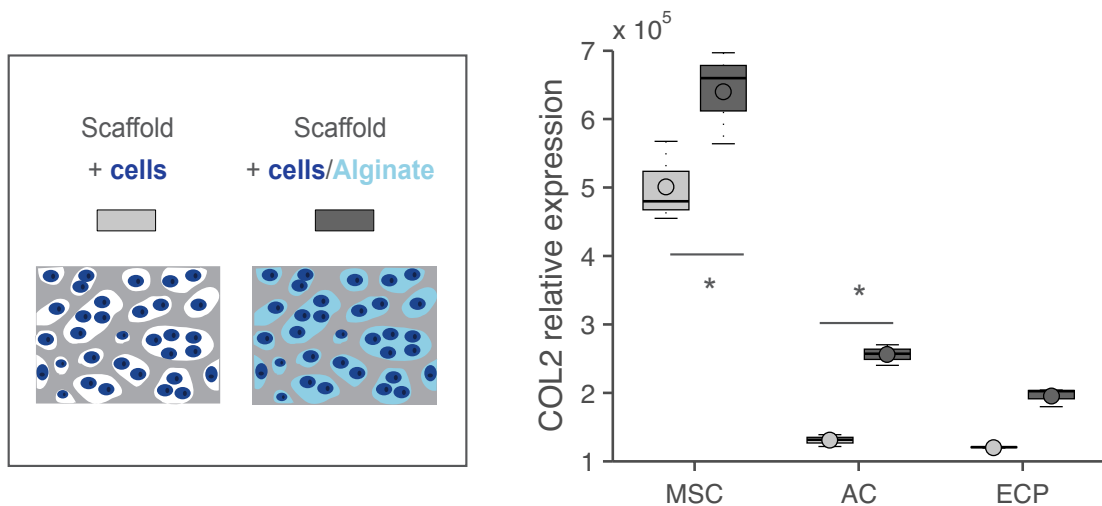


**Figure 7.4.:** Effect of alginate in cell seeded scaffolds. Optimaix-3D scaffolds were seeded in presence or absence of 0.4% w/v alginate and analyzed after 21 days by real time PCR for mRNA expression of collagen 2. Gene expression was normalized to RPL13a and ECP 2D as calibrator sample.

## 7.5 Comparison of chondrogenic potential

Overall, all cell types produced extracellular matrix, as evidenced by the opaque yellow colour of the constructs after 21 days of culture typical for cartilage (Figure 7.5A) and the increase in GAG/DNA (Figure 7.5B; increase between day 21 and 42 for MSC: 2.43-fold,  $p < 0.001$ , AC: 1.94-fold, and ECP: 1.93-fold, all  $p < 0.001$ ) over the culture period of 6 weeks. The accumulation of matrix further resulted in increased dry weight of the constructs (Figure 7.5C). The high matrix production of ECPs at higher passage number than MSCs and ACs (ECP: passage 5, MSC and AC: passage 3) is a demonstration of the superiority of young donors.

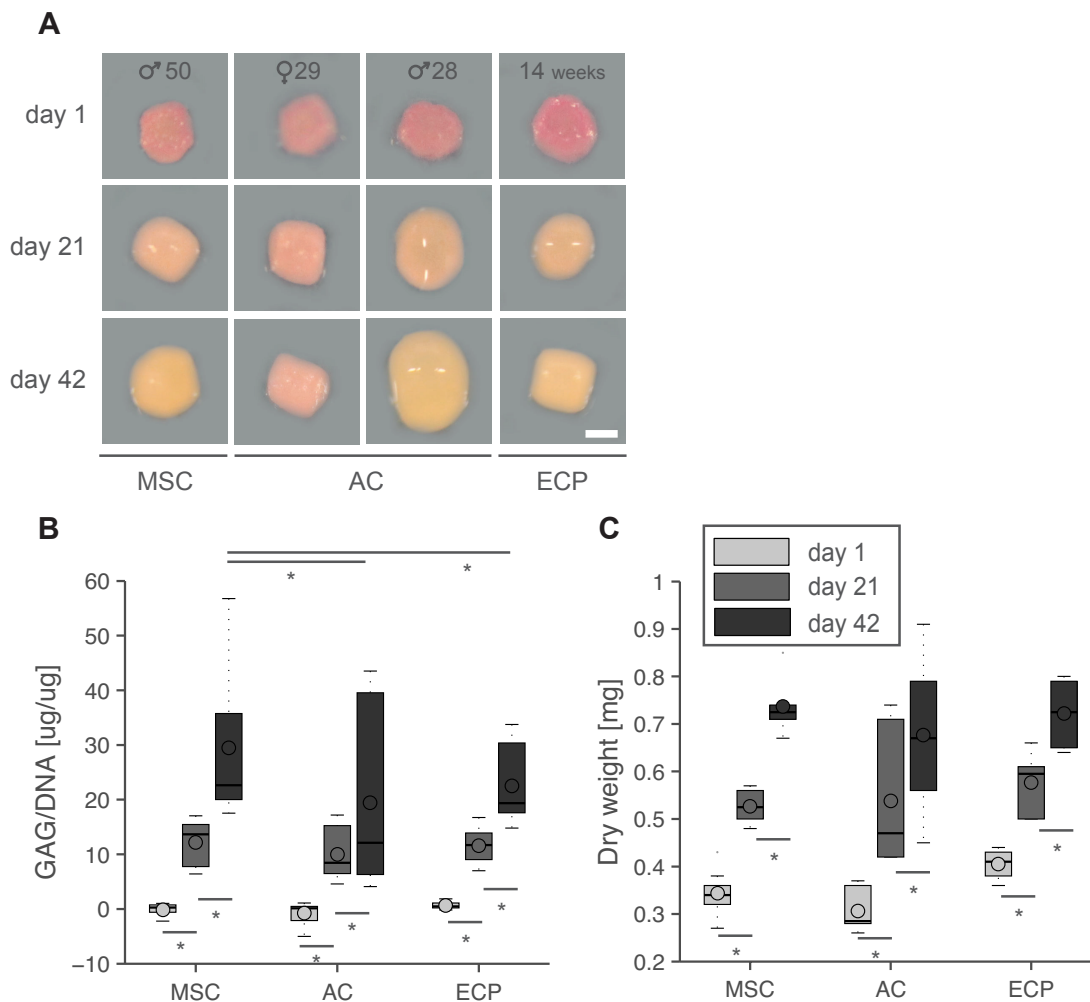


**Figure 7.5.:** Gross appearance, GAG/DNA and dry weight. Optimaix-3D scaffold at an initial cell density of  $5 \times 10^4$  cells/mm<sup>3</sup> were analyzed at day 1, 21, and 42 **A** Gross appearance (scale bar 1 mm, donor demographics indicated by ♂ for male and ♀ for female followed by the age) **B** GAG normalized by DNA content, and **C** dry weight.



ACs exhibited generally the highest variance in matrix production reflected in the gross appearance (Figure 7.5A), GAG/DNA (Figure 7.5B: 80.3 %CV in ACs compared to 47.1 in MSCs and 29.6 %CV in ECPs at day 42) as well as collagen 2 gene expression (Figure 7.6A: 121.5 %CV in ACs compared to 53.8 in MSCs and 68.1 %CV in ECPs at day 42) and collagen 2 staining (Figure 7.6D). Katopodi et al. [140] reported a 20-fold difference in GAG/DNA content between chondrocyte donors, which underlies the inherent variability of using adult articular chondrocytes as a cell source. Similar issues were reported with MSCs [84] as well as in our laboratory where MSCs, mainly from older donors, often do not undergo chondro-differentiation at all (data not shown).

Another drawback of MSCs is their tendency towards fibrocartilage as evidenced by a high collagen 1 expression. Fernandes et al. [80] presented the same trend in a comparison of MSCs and ACs in alginate hydrogels which might indicate that MSCs are prone to induce collagen 1 independently from the culture system. This is in contrast to the work by Zhang et al. [307], in which cells produced more collagen 1 in scaffolds than in hydrogels. This study, however, was conducted at a low cell density ( $4 \times 10^3$  cells/mm<sup>3</sup>) which in our comparison ( $1 \times 10^4$  versus  $5 \times 10^4$  cells/mm<sup>3</sup>) increased proliferation, cell spreading and collagen 1 compared to high initial cell numbers. An inverse correlation between collagen 1 and 2 protein synthesis was observed in AC donors where the lowest collagen 2 staining was accompanied by the highest collagen 1 staining and vice-versa (Figure 7.6D, orange and green box). MSCs, on the other hand, had high collagen 2 matrix production and also a higher collagen 1 mRNA expression compared to ACs (Figure 7.6B: MSCs 3.21 times higher than ACs,  $p < 0.001$ ) and ECPs (MSCs 2.69-fold higher,  $p < 0.001$ ) at day 21 evident also in a stronger collagen 1 staining (Figure 7.6D).

## 7.6 Phenotypic stability

The most striking result of our study was the absence of hypertrophy markers in differentiated ECPs (Figure 7.7) positioning this cell type clearly closer to adult chondrocytes than MSCs. MSCs were the only cell type to express collagen 10 (Figures 7.7 and 7.8), a key marker of hypertrophy. The endochondral phenotype was further confirmed by the gene expression of indian hedgehog (Ihh, Figure 7.7C) and parathyroid hormone 1 receptor (PTH1R, Figure 7.7D) [176] in MSCs compared to the complete absence of these markers in ECPs and ACs. Ihh has been shown to be an inducer of hypertrophy [178] triggering a signaling pathway that leads to the

7. Epiphyseal chondroprogenitor cells produce phenotypically stable cartilage

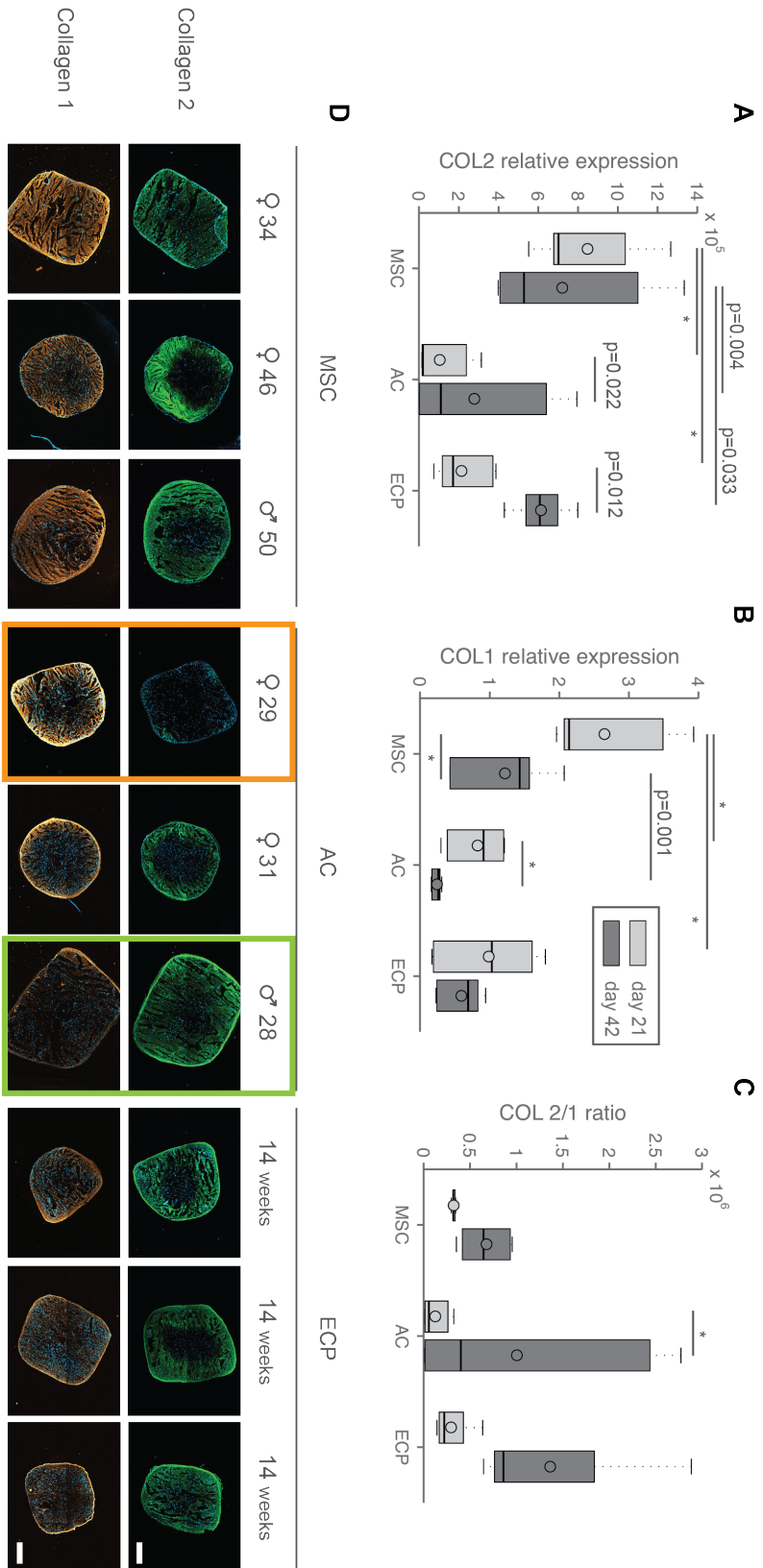


**Figure 7.6:** Chondrogenic potential. Optimaix-3D scaffolds were seeded at a density of  $5 \times 10^4$  cells/ $\text{mm}^3$  and analyzed based on gene expression at day 21 and 42 of **A** collagen 2, **B** collagen 1, **C** collagen 2/1 ratio. Gene expression was normalized to RPL13a and ECP 2D as calibrator sample. **D** shows the corresponding immunostaining at day 42 (scale bars 500  $\mu\text{m}$ , donor demographics indicated by ♂ for male and ♀ for female followed by the age).

activation of Runx2 (Runt-related transcription factor 2), a key transcription factor in chondrocyte hypertrophy and osteoblastic differentiation [142].

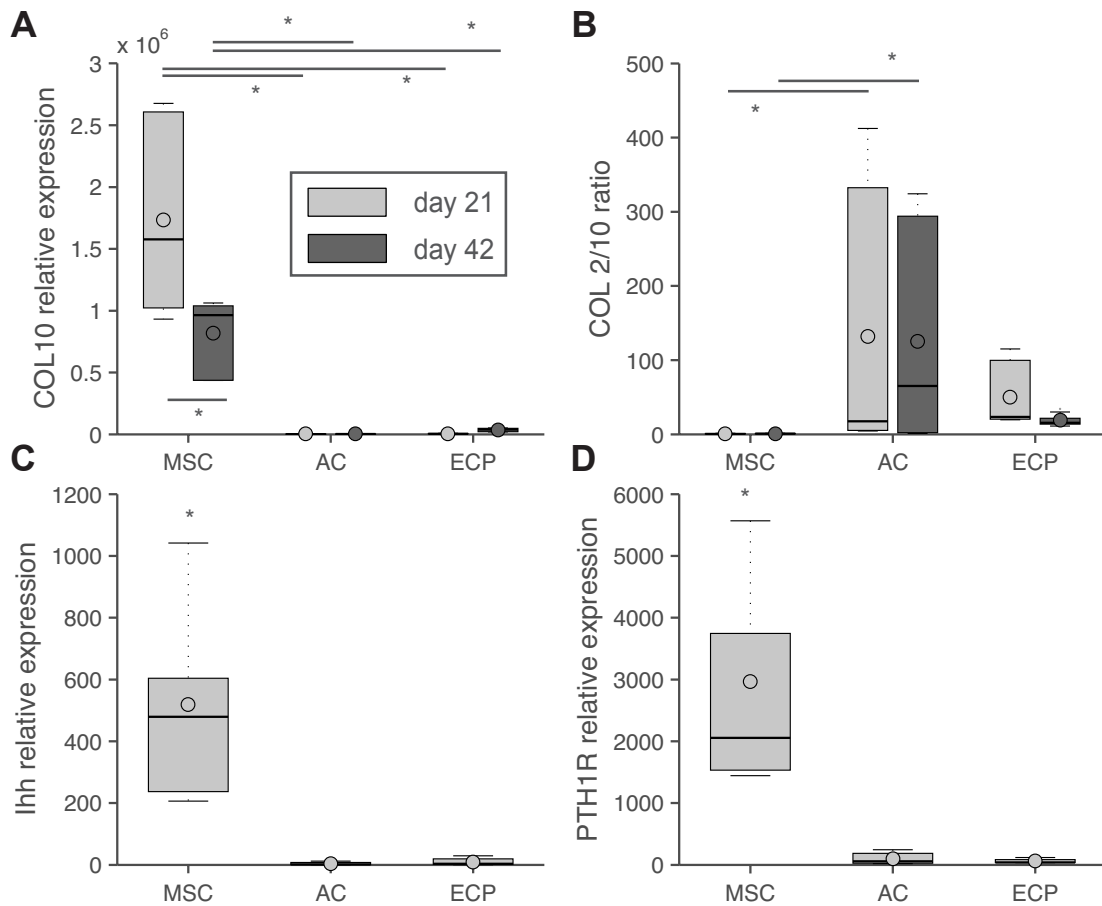


**Figure 7.7.:** Hypertrophic phenotype analyzed by qPCR. Optimaix-3D scaffolds seeded at a density of  $5 \times 10^4$  cells/mm<sup>3</sup> were cultured for 21 and 42 days and analyzed by real time PCR for **A** collagen 10 gene expression, **B** collagen 2/10 ratio, **C** Ihh, and **D** PTHrP receptor (PTH1R) expression normalized to RPL13a and ECP 2D as calibrator sample.

Based on the phenotypic instability, also shown *in vivo* [213,282], MSCs are a problematic cell choice for cartilage regeneration. ECPs, on the other hand, produce a phenotypically stable cartilage similar to the samples from the best AC donor. This suggests ECPs might have obtained an epigenetic stability without loss of collagen 10 methylation during their differentiation *in vivo* as observed for MSCs [312]. However, it needs to be noted that MSCs induced in an improved chondrogenic media containing growth factors such as leukemia inhibitory factor (LIF) [294] could potentially result in a stable cartilage phenotype.

7. Epiphyseal chondroprogenitor cells produce phenotypically stable cartilage

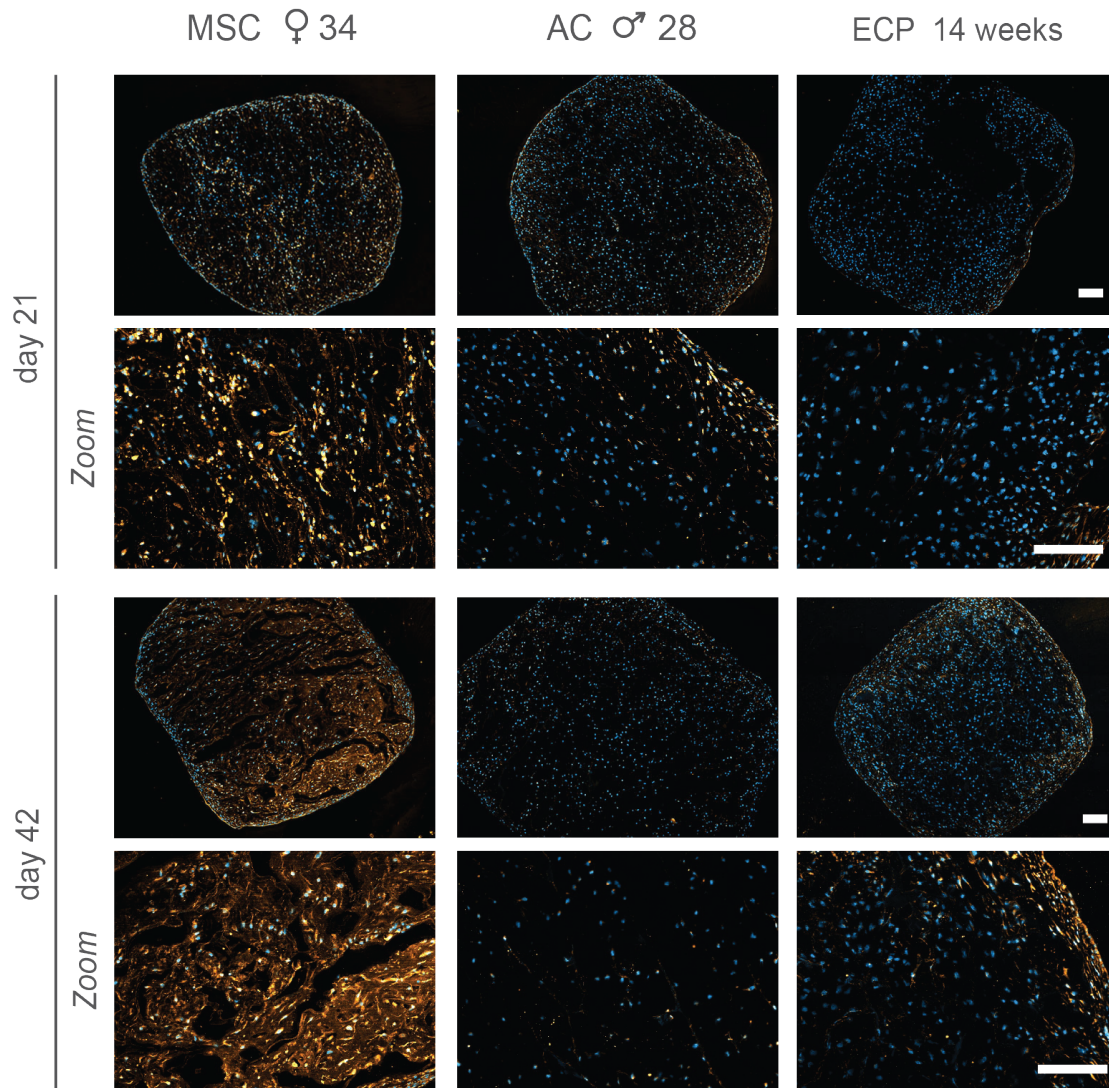


**Figure 7.8.:** Hypertrophic phenotype analyzed by immunostaining. Optimaix-3D scaffolds were seeded at a density of  $5 \times 10^4$  cells/mm<sup>3</sup> were cultured for 21 and 42 days and analyzed by immunohistological staining of collagen 10 of MSC (female, 34 years old), AC (male, 28 years old), and ECPs (14 weeks gestation). Scale bars 200  $\mu$ m.

## 7.7 Mechanical properties

In terms of compressive strength (Figure 7.9), a general increase is observed in all cell types over time, reaching a modulus of  $98.6 \pm 23.6$  kPa for ACs,  $81 \pm 18.6$  kPa for MSCs and  $78.8 \pm 6.7$  for ECPs at day 42 of chondrogenic cultivation. Their values were all less than that measured for native cartilage (ranging from 288 to 476 kPa, data not shown).

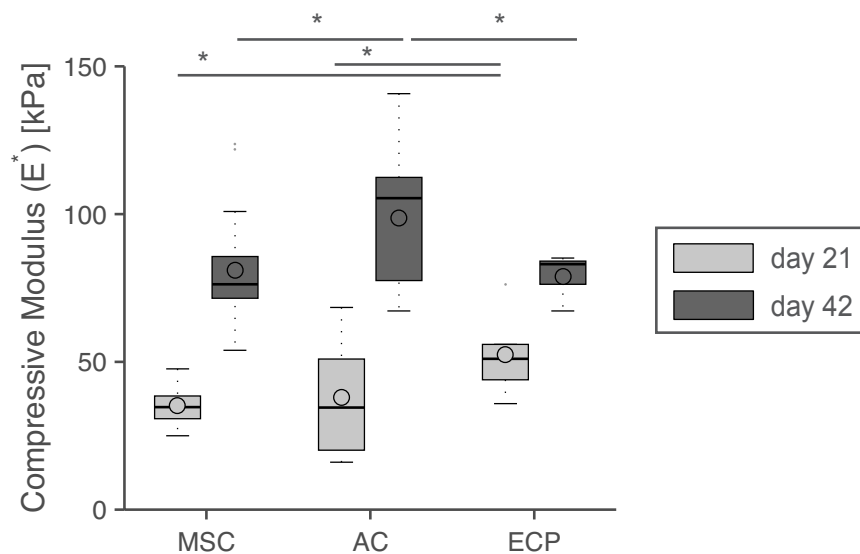


**Figure 7.9.:** Compressive modulus ( $E^*$ ) measured at day 21 and 42 of culture in Optimaix-3D scaffolds ( $5 \times 10^4$  cells/ $\text{mm}^3$ ). *Note:* day 1 and empty scaffolds were not possible to be measured with the chosen settings.

## 7.8 Chapter summary

Our data demonstrates that epiphyseal chondroprogenitor cells produce similar amounts of cartilage matrix proteins compared to articular chondrocytes, the current cell type used in clinics, which due to its low cell yield and high donor variability makes m-ACI an unpredictable, time and cost intensive procedure. The de-novo cartilage matrix from epiphyseal chondroprogenitor cells is in addition more resistant to hypertrophy compared to MSC-derived ECM, which stained strongly for collagen 10. Fetal ECPs also carry a higher potential for matrix production than adult cell types even after multiple passaging as shown in the comparison of ECPs at passage 5 compared to passage 3 ACs and MSCs. An important observation

was the superior matrix production at high cell seeding density ( $5 \times 10^4$  cells/mm<sup>3</sup>) compared to the clinically applied low cell number ( $1 \times 10^4$  cells/mm<sup>3</sup>). Collagen 2 expression further increased upon addition of alginate which shows the importance of a complete pore filling for successful chondrogenesis. Compared to ACs that require several weeks of expansion for the currently used low cell seeding density, ECPs, as an allogeneic cell source with high cell yield, allow for adequate seeding regime also for large defects.

It is possible that commercially-viable cell sources for cartilage repair will eventually be off-the-shelf allogeneic products with proven regeneration potential. Although the use of allogeneic tissues and cells is controversial, the use of immunoeengineering and type matching approaches have shown success [306]. Fortunately, cartilage has several passive and active mechanisms which support the use of allografts and allogeneic cells. Indeed, cartilage allografts have been used successfully in the clinics for decades [86,245] and recently there has been a strong academic and commercial interest in allogeneic tissue fragments and chondrocytes from juvenile donors due to their superior chondrogenic capacity compared to adult chondrocytes [3, 77]. Like other avascular sites in the body without lymphatic drainage (i.e. cornea, anterior part of the eye and vertebrae [55, 243]), cartilage exists in immune-isolation which precludes the trafficking of donor antigen presenting cells (APC) into host secondary lymphoid organs and/or entry of recipient APC into the graft, two of the pathways by which allografts are rejected. In addition to vascular isolation, however, chondrocytes are also surrounded by large tracks of extracellular matrix which prevent direct contact between chondrocytes and migratory macrophages and dendritic cells of the joint space. Additionally, the matrix itself contains glycoproteins, such as chondromodulin 1 [147, 189], which have been shown to be anti-angiogenic and therefore immunosuppressive. The chondrocytes themselves can display surface receptors with immunosuppressive functions. Fujihara found expression of Fas ligand (FasL) on chondrocytes initiated apoptosis of macrophages bearing the Fas death receptor [88]. The long-term fate of allogeneic cells in articular cartilage, also during inflammation and disease states, need to be addressed. However, considering the immune privileged situation of cartilage, the use of allogeneic epiphyseal chondroprogenitor cells would be a big step towards a future one-step procedure with a more predictable outcome than ACI.

## 8 Conclusion and outlook

Current cell-based approaches for cartilage regeneration suffer from a complicated, time-, and cost-intensive procedure due to low cell yields of the applied autologous articular chondrocytes (ACs). The replacement of ACs with a more abundant cell source would greatly improve the ACI technique. With this in mind, the aim of this thesis was to establish an alternative cell type with the potential to produce cartilage ECM with a special focus on its phenotypic stability.

The first part of this work was focused on MSCs which carry great potential in replacing ACs due to their occurrence in several body tissues and their ease of procurement. MSCs obtained from bone marrow aspirates or adipose tissue were isolated by adherence to tissue culture plastic, yielding a highly heterogeneous cell population. We showed that TGF- $\beta$ -supplemented MSC pellets express cartilage-specific genes, but at the same time hypertrophic markers. It is clear that the clinical application of MSCs would require the administration of a drug capable of inhibiting endochondral ossification.

We therefore focused on PTHrP, a potent hypertrophy-inhibiting drug, which unfortunately not only suppressed collagen 10 and *Ihh*, but also the production of collagen 2, most probably through induction of MMP-13. Contrary to the literature, neither the application at later time point (day 7, 14, 21), nor the switch from isoform 1-86 to 1-34 restored cartilage ECM production.

In the quest for a more targeted drug, the use of RNAi therapeutics was explored. Small interfering RNA (siRNA) sequences specifically bind to target mRNA, thereby inhibiting protein expression. This system allows to directly target the protein of interest, rather than broadly inhibit pathways as is the case for PTHrP. Together with the laboratory of Professor Akashi in Osaka, we were able to successfully produce  $\gamma$ -PGA-Phe siRNA carriers with high biocompatibility as well as transfection efficiency. The negatively charged  $\gamma$ -PGA-Phe NPs were coated with polycations such as DEAE-dextran, PEI, or chitosan to form a positive outer layer capable of

binding to siRNA. The overall positive charge allowed the NPs to enter the cell as well as escape the endosomal pathway through membrane destabilization.

While working with MSCs, it became apparent that their clinical use requires the addition of highly complex systems such as gene therapy, which, from a regulatory point of view, are a massive hurdle. Furthermore, strategies to inhibit hypertrophy (Section 1.3) so far show limited improvement compared to stable chondrocytes. It is clear that the generally accepted chondrogenic induction through TGF- $\beta$  does not provide the right trigger for MSCs to produce hyaline cartilage, but rather directs them towards endochondral ossification. An update of the pellet culture protocol from 1999 [215] towards a more directed induction would hold more promise than evaluating strategies to fix the ill-defined procedure. The analysis of the developmental cues involved in the distinction of growth plate and articular chondrocytes will be key in understanding the culture conditions required for the stable induction of MSCs. One such approach is presented by Wu et al. [294] who determined leukemia inhibitory factor (LIF) to be an indispensable growth factor for the formation of hyaline cartilage. Recent literature further focuses on the development of an early marker to sort cells according to their chondrogenic or osteogenic tendency such as the Runx2/Sox9 ratio presented by Loebel et al. [168].

Another strategy to produce phenotypically stable cartilage is to use immature chondrocytes, which are more abundant and exhibit a higher chondrogenic potential than ACs, but more importantly, carry a pre-determined genotype. Such chondroprogenitors can be isolated from fetal or juvenile tissue up to the age of thirteen when cartilage has attained its maturity. We compared fetal epiphyseal chondroprogenitors (ECPs) with adult ACs and MSCs in a collagen scaffold supplemented with TGF- $\beta$ . After 3-6 weeks of culture, passage 5 ECPs reached similar levels of collagen 2 production as passage 3 MSCs, but without the undesired induction of collagen 10. ECPs present an allogeneic off-the-shelf solution for cartilage regeneration with a more reproducible outcome than the current ACI procedure which suffers from high inter-patient variability. The in vitro experiments are very promising, and follow-up experiments will show if ECPs can withstand vascularization in vivo. Another interesting topic will be to evaluate the gene expression after in vitro differentiation (collagen 10, Ihh, MMP-13, ALP) with respect to in vivo mineralization. The definition of a distinct genotype necessary for the production of an avascular tissue would provide a future screening tool for vascularization-resistant tissue engineering.



---

Allogeneic cell therapies have been successfully applied for several decades [86,245] in the regeneration of the immune-privileged cartilage. The unpredictable outcome of autologous tissue engineered constructs due to inter-patient variability can be overcome with the use of allogeneic cells. Compared to adult cartilage, immature tissue offers a higher cell density and superior chondrogenic potential, making juvenile and fetal chondrocytes the most promising cell source for future one-step treatments of cartilage lesions. This is affirmed by two products, DeNovo NT and DeNovo ET, based on juvenile cartilage, that recently entered the market. Undifferentiated cells such as MSCs, as well as embryonic stem cells and induced pluripotent stem cells might eventually be viable cell sources, but more work is needed to assess their safety and determine a protocol to produce phenotypically stable cartilage.



# Curriculum vitae

## Personal

Name: Deborah Studer  
Date of Birth: November 20, 1984  
Nationality: Swiss, Citizen of Oberhof (AG)  
Address: Eugen-Huber-Strasse 58  
8048 Zürich, Switzerland

## Study

2010 – 2014: PhD in Cartilage Tissue Engineering, Empa St.Gallen and ETH Zürich, Switzerland  
2007 – 2009: MSc in Molecular and Biological Chemistry, EPFL, Lausanne, Switzerland  
2006 – 2007: Exchange year at Tecnológico de Monterrey, Mexico  
2004 – 2007: BSc in Chemistry at EPFL, Lausanne, Switzerland  
2000 – 2003: Maturity in modern languages (Italian), Kantonsschule Solothurn, Switzerland

## Project Experience

### Engineering Phenotypically Stable Cartilage

PROJECT	<i>PhD thesis</i>
PERIOD	July 2010 – Oct 2014
LABORATORY	Laboratory for Materials-Biology Interactions, Empa, St.Gallen, Switzerland Cartilage Engineering + Regeneration Laboratory, ETH Zürich, Switzerland Identification of cell-based strategies to inhibit endochondral ossification.

### Superparamagnetic Nanoparticles (NPs) for Drug Delivery

PROJECT	<i>Research assistant</i>
PERIOD	February 2010 – May 2010
LABORATORY	Laboratory for Surface Science and Technology, ETH Zürich, Switzerland Characterization of superparamagnetic NPs by AFM and QCM.

### **Polyelectrolyte Microcapsules; A new Tool for in vivo Reporting**

PROJECT *Masters Thesis*

PERIOD November 2008 – May 2009

LABORATORY Laboratory of Biophysics, Jacobs University, Bremen, Germany

Proof of principle of in vivo reporting using polyelectrolyte microcapsules.

### **Study of the Dynamics of Charge Recombination in the Photosensibilization of TiO<sub>2</sub> by Alizarin**

PROJECT *Semester Project*

PERIOD March 2008 – May 2008

LABORATORY Laboratory of Photonics and Interfaces, EPFL, Lausanne, Switzerland

Investigation of Alizarin/TiO<sub>2</sub>-film electron recombination dynamics using Flash Photolysis with Nanosecond Laser Spectrometer.

## **Stipends and Fellowships**

2009 WISH Community Career Investment

2009 EPFL Stipend for Master's thesis abroad

2006 – 2007 Erasmus Stipend for exchange year in Mexico

## **Publications**

**Studer, D.**, Formica, F., Mumme, M., Salzmann, G., Steinwachs, M.R., Laurent-Applegate, L.A., Maniura-Weber, K., Zenobi-Wong, M., Human epiphyseal chondroprogenitor cells produce phenotypically stable cartilage: A new cell source for one-step treatment of cartilage lesions?, Manuscript in preparation

Akagi, T., Shudo, M., **Studer, D.**, Matsusaki, M., Zenobi-Wong, M., Akashi, M., Suppression of dendritic cell activation by siRNA-adsorbed amphiphilic poly ( $\gamma$ -glutamic acid) nanoparticles, Manuscript in preparation

**Studer, D.**, Lischer, S., Jochum, W., Ehrbar, M., Zenobi-Wong, M., Maniura-Weber, K., RPL13a as a Reference Gene for Human Bone Marrow-derived Mesenchymal Stem Cells during Expansion, Adipo-, Chondro-, and Osteogenesis, (2012) *Tissue Engineering Part C*, 18(10) pp. 761-771

**Studer, D.**, Millan, C., Öztürk, E., Maniura-Weber, K., Zenobi-Wong, M., Molecular and biophysical mechanisms regulating hypertrophic differentiation in chondrocytes and mesenchymal stem cells, (2012) *European Cells and Materials*, 24 pp. 118-135

**Studer, D.**, Palankar, R., Bédard, M., Winterhalter, M., Springer, M., Retrieval of a Metabolite from Cells with Polyelectrolyte Microcapsules, (2010) *Small*, 6(21) pp. 2412-2419

## Oral and Poster presentations

Studer, D, Esteva, T, Shudo, M, Akagi, T, Matsusaki, M, Akashi, M, Maniura-Weber, K, Zenobi-Wong, M, Coated gamma-PGA-Phe nanoparticles for siRNA delivery, FEBS Workshop - Biological Surfaces and Interfaces, Sant Feliu de Guixols, Spain. June 30 - July 5, 2013. (poster)

Studer, D, Born, A-K, Müller, M, Maniura-Weber, K, Zenobi-Wong, M, Tools to study co-culture interactions in cartilage regeneration, SSB, Davos, Switzerland. June 25-26, 2013 (poster)

Studer, D, Zenobi-Wong, M, Maniura-Weber, K, , Empa PhD Symposium, St.Gallen, Switzerland. Nov 13, 2012 (talk)

Studer, D, Millan, C, Zenobi-Wong, M, Maniura-Weber K, Proliferation rate as an indicator for the chondrogenic potential of mesenchymal stromal cells in 3D pellet culture, SSB, Zürich, Switzerland. May 3, 2012. (talk)

Studer, D, Millan, C, Zenobi-Wong, M, Maniura-Weber K, Proliferation rate as an indicator for the chondrogenic potential of mesenchymal stromal cells in 3D pellet culture, 3D Cell Culture Conference, Zürich, Mar 14-16, 2012. (poster)

Studer, D, Zenobi-Wong, M, Maniura-Weber, K, Housekeeping Gene Stability in Human Bone Marrow-derived Mesenchymal Stromal Cells during Adipo-, Chondro- and Osteogenesis, Empa PhD Symposium, St.Gallen, Switzerland. Oct 18, 2011 (best poster price)

Studer, D, Zenobi-Wong, M, Maniura-Weber, K, Housekeeping Gene Stability in Human Bone Marrow-derived Mesenchymal Stromal Cells during Adipo-, Chondro- and Osteogenesis, World Conference on Regenerative Medicine, Leipzig, Germany. Nov 2-4, 2011. (poster)

Studer, D, Zenobi-Wong, M, Maniura-Weber, K, Joint Regeneration - Novel 2D Patterned Co-Culture System For Investigating Chondrogenesis, Graduate Courses Cellular Systems, Heidelberg, Germany. Aug 24-30 (talk)

Studer, D, Zenobi-Wong, M, Vörös, J, Maniura-Weber, K, Investigating Chondrogenesis of Bone Marrow-derived MSCs, ETH - Tokyo Tech Symposium, Lausanne, Switzerland. June 2011 (poster)

Studer, D, Zenobi-Wong, M, Maniura-Weber, K, Novel 2D Patterned Co-culture System for Investigating Chondrogenesis of Mesenchymal Stem Cells, Empa PhD Symposium, St.Gallen, Switzerland. Oct 7, 2010 (poster)

Studer, D, Zenobi-Wong, M, Maniura-Weber, K, Joint Regeneration - Novel 2D Patterned Co-Culture System For Investigating Chondrogenesis, CCMX Travelling Lab Workshop: Materials for Life Sciences, Switzerland. Nov 8 - 12, 2010 (talk)

## Student project supervision

Esteva, Timothée, Gene silencing in human chondrocytes by means of nanoparticle-mediated siRNA delivery, March-June 2012



## Bibliography

- [1] K. Abdi, N. J. Singh, and P. Matzinger. Lipopolysaccharide-Activated Dendritic Cells: "Exhausted" or Alert and Waiting? *The Journal of Immunology*, 188(12):5981–5989, June 2012.
- [2] F. L. Acosta, L. Metz, H. D. Adkisson, J. Liu, E. Carruthers-Liebenberg, C. Milliman, M. Maloney, and J. C. Lotz. Porcine intervertebral disc repair using allogeneic juvenile articular chondrocytes or mesenchymal stem cells. *Tissue engineering. Part A*, 17(23-24):3045–3055, Dec. 2011.
- [3] H. D. Adkisson, J. A. Martin, R. L. Amendola, C. Milliman, K. A. Mauch, A. B. Katwal, M. Seyedin, A. Amendola, P. R. Streeter, and J. A. Buckwalter. The Potential of Human Allogeneic Juvenile Chondrocytes for Restoration of Articular Cartilage. *The American journal of sports medicine*, 38(7):1324–1324, July 2010.
- [4] H. D. Adkisson, C. Milliman, X. Zhang, K. Mauch, R. T. Maziarz, and P. R. Streeter. Immune evasion by neocartilage-derived chondrocytes: Implications for biologic repair of joint articular cartilage. *Stem cell research*, 4(1):57–68, Jan. 2010.
- [5] H. Afizah, Z. Yang, J. H. P. Hui, H. W. Ouyang, and E.-H. Lee. A Comparison Between the Chondrogenic Potential of Human Bone Marrow Stem Cells (BMSCs) and Adipose-Derived Stem Cells (ADSCs) Taken from the Same Donors. *Tissue Engineering*, 13(4):659–666, Apr. 2007.
- [6] T. Aigner, J. L. Cook, N. Gerwin, S. S. Glasson, S. Lavery, C. B. Little, W. McIlwraith, and V. B. Kraus. Histopathology atlas of animal model systems – overview of guiding principles. *Osteoarthritis and Cartilage*, 18:S2–S6, Oct. 2010.
- [7] T. Akagi, M. Baba, and M. Akashi. Preparation of nanoparticles by the self-organization of polymers consisting of hydrophobic and hydrophilic segments: Potential applications. *Polymer*, 48(23):6729–6747, Nov. 2007.
- [8] T. Akagi, F. Shima, and M. Akashi. Intracellular degradation and distribution of protein-encapsulated amphiphilic poly(amino acid) nanoparticles. *Biomaterials*, 32(21):4959–4967, July 2011.
- [9] T. Akagi, X. Wang, T. Uto, M. Baba, and M. Akashi. Protein direct delivery to dendritic cells using nanoparticles based on amphiphilic poly(amino acid) derivatives. *Biomaterials*, 28(23):3427–3436, Aug. 2007.

- [10] C. Albrecht, B. Tichy, S. Nürnberger, S. Hosiner, L. Zak, S. Aldrian, and S. Marlovits. Gene expression and cell differentiation in matrix-associated chondrocyte transplantation grafts: a comparative study. *Osteoarthritis and Cartilage*, 19(10):1219–1227, Oct. 2011.
- [11] K. F. Almqvist, A. A. M. Dhollander, P. C. M. Verdonk, R. Forsyth, R. Verdonk, and G. Verbruggen. Treatment of Cartilage Defects in the Knee Using Alginate Beads Containing Human Mature Allogenic Chondrocytes. *The American journal of sports medicine*, 37(10):1920–1929, Oct. 2009.
- [12] V. V. Ambardekar, R. R. Wakaskar, B. Sharma, J. Bowman, W. Vayaboury, R. K. Singh, and J. A. Vetro. The efficacy of nuclease-resistant Chol-siRNA in primary breast tumors following complexation with PLL-PEG(5K). *Biomaterials*, 34(20):4839–4848, July 2013.
- [13] C. L. Andersen, J. L. Jensen, and T. F. Ørntoft. Normalization of real-time quantitative reverse transcription-PCR data: a model-based variance estimation approach to identify genes suited for normalization, applied to bladder and colon cancer data sets. *Cancer research*, 64(15):5245–5250, Aug. 2004.
- [14] H. C. Anderson. Matrix vesicles and calcification. *Current rheumatology reports*, 5(3):222–226, June 2003.
- [15] M. A. Arnold, Y. Kim, M. P. Czubryt, D. Phan, J. McAnally, X. Qi, J. M. Shelton, J. A. Richardson, R. Bassel-Duby, and E. N. Olson. MEF2C transcription factor controls chondrocyte hypertrophy and bone development. *Developmental Cell*, 12(3):377–389, Mar. 2007.
- [16] Y. Asawa, T. Ogasawara, and T. Takahashi. Aptitude of auricular and nasoseptal chondrocytes cultured under a monolayer or three-dimensional condition for cartilage tissue engineering. *Tissue engineering. Part A*, 15(5):1109–1118, 2009.
- [17] A. Aung, G. Gupta, G. Majid, and S. Varghese. Osteoarthritic chondrocyte-secreted morphogens induce chondrogenic differentiation of human mesenchymal stem cells. *Arthritis and rheumatism*, 63(1):148–158, Jan. 2011.
- [18] Y. Bae and K. Kataoka. Intelligent polymeric micelles from functional poly(ethylene glycol)-poly(amino acid) block copolymers. *Advanced Drug Delivery Reviews*, 61(10):768–784, Aug. 2009.
- [19] M. Balcerzak, E. Hamade, L. Zhang, S. Pikula, J. Radisson, J. Bandorowicz-Pikula, and R. Buchet. The roles of annexins and alkaline phosphatase in mineralization process. *Acta biochimica Polonica*, 50(4):1019–1038, 2003.
- [20] A. Barbero, S. Grogan, D. Schäfer, M. Heberer, P. Mainil-Varlet, and I. Martin. Age related changes in human articular chondrocyte yield, proliferation and post-expansion chondrogenic capacity. *Osteoarthritis and Cartilage*, 12(6):476–484, June 2004.
- [21] F. Barry, R. E. Boynton, B. Liu, and J. M. Murphy. Chondrogenic differentiation of mesenchymal stem cells from bone marrow: differentiation-dependent gene expression of matrix components. *Experimental Cell Research*, 268(2):189–200, 2001.



- [22] F. Barry and M. Murphy. Mesenchymal stem cells in joint disease and repair. *Nature Reviews Rheumatology*, pages 1–11, July 2013.
- [23] M. J. Barter, C. Bui, and D. A. Young. Epigenetic mechanisms in cartilage and osteoarthritis: DNA methylation, histone modifications and microRNAs. *Osteoarthritis and Cartilage*, 20(5):339–349, Jan. 2012.
- [24] J. W. Bawden. Calcium transport during mineralization. *The Anatomical record*, 224(2):226–233, June 1989.
- [25] K. L. Becker. Principles and practice of endocrinology and metabolism. Lippincott Williams & Wilkins, 2001.
- [26] J. P. Behr. The proton sponge: a trick to enter cells the viruses did not exploit. *CHIMIA International Journal for Chemistry*, 1997.
- [27] P. Behrens. Matrix-coupled microfracture. *Arthroscopie*, 18(3):193–197, Aug. 2005.
- [28] R. V. Benjaminsen, M. A. Matthebjerg, J. R. Henriksen, S. M. Moghimi, and T. L. Andresen. The Possible “Proton Sponge” Effect of Polyethylenimine (PEI) Does Not Include Change in Lysosomal pH. *Molecular Therapy*, 21(1):149–157, Oct. 2012.
- [29] J. P. Benthien and P. Behrens. Autologous Matrix-Induced Chondrogenesis (AMIC): Combining Microfracturing and a Collagen I/III Matrix for Articular Cartilage Resurfacing. *Cartilage*, 1(1):65–68, Feb. 2010.
- [30] E. Bernstein, A. A. Caudy, S. M. Hammond, and G. J. Hannon. Role for a bidentate ribonuclease in the initiation step of RNA interference. *Nature*, 409(6818):363–366, Jan. 2001.
- [31] L. Bian, D. Y. Zhai, E. Tous, R. Rai, R. L. Mauck, and J. A. Burdick. Enhanced MSC chondrogenesis following delivery of TGF- $\beta$ 3 from alginate microspheres within hyaluronic acid hydrogels in vitro and in vivo. *Biomaterials*, 32(27):6425–6434, Sept. 2011.
- [32] T. Bieber and H. P. Elsässer. Preparation of a low molecular weight polyethylenimine for efficient cell transfection. Technical report, University of Marburg, Marburg, Germany., Jan. 2001.
- [33] K. Biegeleisen. The probable structure of the protamine–DNA complex. *Journal of Theoretical Biology*, 241(3):533–540, Aug. 2006.
- [34] E. N. Blaney Davidson, D. F. G. Remst, E. L. Vitters, H. M. van Beuningen, A. B. Blom, M. J. Goumans, W. B. van den Berg, and P. M. van der Kraan. Correction: Increase in ALK1/ALK5 Ratio as a Cause for Elevated MMP-13 Expression in Osteoarthritis in Humans and Mice. *The Journal of Immunology*, 185(4):2629–2629, Aug. 2010.
- [35] V. Bobic, C. D. Morgan, and T. Carter. Osteochondral autologous graft transfer. *Operative Techniques in Sports Medicine*, 8(2):168–178, Apr. 2000.
- [36] F. Bohrsen, U. Lindner, M. Meier, A. Gadallah, P. Schlenke, H. Lehnert, J. Rohwedel, and J. Kramer. Murine mesenchymal progenitor cells from different tissues differentiated via

- mesenchymal microspheres into the mesodermal direction. *Bmc Cell Biology*, 10:92–107, Dec. 2009.
- [37] R. Bora. RNA interference therapeutics for cancer: Challenges and opportunities (Review). *Molecular Medicine Reports*, Apr. 2012.
- [38] A.-K. Born, M. Rottmar, S. Lischer, M. Pleskova, A. Bruinink, and K. Maniura-Weber. Correlating cell architecture with osteogenesis: first steps towards live single cell monitoring. *European cells & materials*, 18:49–60– 61–2– discussion 60, 2009.
- [39] M. Brittberg, A. Lindahl, A. Nilsson, C. Ohlsson, O. Isaksson, and L. Peterson. Treatment of Deep Cartilage Defects in the Knee with Autologous Chondrocyte Transplantation. *New England Journal of Medicine*, 331(14):889–895, Oct. 1994.
- [40] J. E. Browne and T. P. Branch. Surgical alternatives for treatment of articular cartilage lesions. *The Journal of the American Academy of Orthopaedic Surgeons*, 8:180–189, 2000.
- [41] P. G. Bush, C. A. Parisinos, and A. C. Hall. The osmotic sensitivity of rat growth plate chondrocytes in situ; Clarifying the mechanisms of hypertrophy. *Journal of cellular physiology*, 214(3):621–629, Mar. 2008.
- [42] S. Bustin. Quantification of mRNA using real-time reverse transcription PCR (RT-PCR): trends and problems. *Journal of Molecular Endocrinology*, 29(1):23–39, Aug. 2002.
- [43] S. A. Bustin, V. Benes, J. A. Garson, J. Hellems, J. Huggett, M. Kubista, R. Mueller, T. Nolan, M. W. Pfaffl, G. L. Shipley, J. Vandesompele, and C. T. Wittwer. The MIQE Guidelines: Minimum Information for Publication of Quantitative Real-Time PCR Experiments. *Clinical Chemistry*, 55(4):611–622, Mar. 2009.
- [44] A. I. Caplan. Adult mesenchymal stem cells for tissue engineering versus regenerative medicine. *Journal of cellular physiology*, 213(2):341–347, 2007.
- [45] M. M. J. Caron, P. J. Emans, M. M. E. Coolsen, L. Voss, D. A. M. Surtel, A. Cremers, L. W. van Rhijn, and T. J. M. Welting. Redifferentiation of dedifferentiated human articular chondrocytes: comparison of 2D and 3D cultures. *Osteoarthritis and Cartilage*, 20(10):1170–1178, Oct. 2012.
- [46] F. H. Chen, K. T. Rousche, and R. S. Tuan. Technology Insight: adult stem cells in cartilage regeneration and tissue engineering. *Nature Clinical Practice Rheumatology*, 2(7):373–382, July 2006.
- [47] Z. X. Chen and A. D. Riggs. DNA methylation and demethylation in mammals. *Journal of Biological Chemistry*, 286(21):18347–18353, May 2011.
- [48] C.-C. Cheng, Y. Uchiyama, A. Hiyama, S. Gajghate, I. M. Shapiro, and M. V. Risbud. PI3K/AKT regulates aggrecan gene expression by modulating Sox9 expression and activity in nucleus pulposus cells of the intervertebral disc. *Journal of cellular physiology*, 221(3):668–676, Aug. 2009.
- [49] S. W. Choi, D. U. Jeong, J. A. Kim, B. Lee, K. S. Joeng, F. Long, and D. W. Kim. Indian Hedgehog

- signalling triggers Nkx3.2 protein degradation during chondrocyte maturation. *Biochemical Journal*, 443(3):789–798, May 2012.
- [50] S. Chono, S.-D. Li, C. C. Conwell, and L. Huang. An efficient and low immunostimulatory nanoparticle formulation for systemic siRNA delivery to the tumor. *Journal of Controlled Release*, 131(1):64–69, Oct. 2008.
- [51] B. L. Clair, A. R. Johnson, and T. Howard. Cartilage repair: current and emerging options in treatment. *Foot & ankle specialist*, 2009.
- [52] N. P. Cohen, R. J. Foster, and V. C. Mow. Composition and Dynamics of Articular Cartilage: Structure, Function, and Maintaining Healthy State. *Journal of Orthopaedic & Sports Physical Therapy*, 28(4):203–215, Oct. 1998.
- [53] D. C. Crawford, C. M. Heveran, W. D. Cannon, L. F. Foo, and H. G. Potter. An Autologous Cartilage Tissue Implant NeoCart for Treatment of Grade III Chondral Injury to the Distal Femur: Prospective Clinical Safety Trial at 2 Years. *The American journal of sports medicine*, 37(7):1334–1343, June 2009.
- [54] D. Cun, C. Foged, M. Yang, S. Frøkjær, and H. M. Nielsen. Preparation and characterization of poly(dl-lactide-co-glycolide) nanoparticles for siRNA delivery. *International journal of pharmaceuticals*, 390(1):70–75, May 2010.
- [55] C. Cursiefen. Immune privilege and angiogenic privilege of the cornea. *Chemical immunology and allergy*, 92:50–57, 2007.
- [56] K. M. Curtis, L. A. Gomez, C. Rios, E. Garbayo, A. P. Raval, M. A. Perez-Pinzon, and P. C. Schiller. EF1alpha and RPL13a represent normalization genes suitable for RT-qPCR analysis of bone marrow derived mesenchymal stem cells. *BMC Molecular Biology*, 11(1):61, 2010.
- [57] M. D’Angelo, Z. Yan, M. Nooreyazdan, M. Pacifici, D. S. Sarment, P. C. Billings, and P. S. Leboy. MMP-13 is induced during chondrocyte hypertrophy. *J Cell Biochem*, 77(4):678–693, June 2000.
- [58] E. M. Darling and K. A. Athanasiou. Rapid phenotypic changes in passaged articular chondrocyte subpopulations. *J Orthop Res*, 23(2):425–432, 2006.
- [59] S. Darwiche, C. Scaletta, W. Raffoul, D. P. Pioletti, and L. A. Applegate. Epiphyseal Chondroprogenitors Provide a Stable Cell Source for Cartilage Cell Therapy. *Cell Medicine*, 4(1):23–32, 2012.
- [60] H. J. M. de Jonge, R. S. N. Fehrmann, E. S. J. M. de Bont, R. M. W. Hofstra, F. Gerbens, W. A. Kamps, E. G. E. de Vries, A. G. J. van der Zee, G. J. te Meerman, and A. ter Elst. Evidence based selection of housekeeping genes. *PloS one*, 2(9):e898, 2007.
- [61] Y. Deng, C. C. Wang, K. W. Choy, Q. Du, J. Chen, Q. Wang, L. Li, T. K. H. Chung, and T. Tang. Therapeutic potentials of gene silencing by RNA interference: principles, challenges, and new strategies. *Gene*, 538(2):217–227, Apr. 2014.
- [62] K. Dheda, J. F. Huggett, S. A. Bustin, M. A. Johnson, G. Rook, and A. Zumla. Validation

- of housekeeping genes for normalizing RNA expression in real-time PCR. *BioTechniques*, 37(1):112–119, July 2004.
- [63] K. Dheda, J. F. Huggett, J. S. Chang, L. U. Kim, S. A. Bustin, M. A. Johnson, G. A. W. Rook, and A. Zumla. The implications of using an inappropriate reference gene for real-time reverse transcription PCR data normalization. *Analytical Biochemistry*, 344(1):141–143, Sept. 2005.
- [64] A. A. M. Dhollander, P. C. M. Verdonk, S. Lambrecht, R. Verdonk, D. Elewaut, G. Verbruggen, and K. F. Almqvist. Midterm Results of the Treatment of Cartilage Defects in the Knee Using Alginate Beads Containing Human Mature Allogenic Chondrocytes. *The American journal of sports medicine*, 40(1):75–82, Jan. 2012.
- [65] A. Dickhut, K. Pelttari, P. Janicki, W. Wagner, V. Eckstein, M. Egermann, and W. Richter. Calcification or dedifferentiation: Requirement to lock mesenchymal stem cells in a desired differentiation stage. *Journal of cellular physiology*, 219(1):219–226, Apr. 2009.
- [66] B. O. Diekman, N. Christoforou, V. P. Willard, H. Sun, J. Sanchez-Adams, K. W. Leong, and F. Guilak. Cartilage tissue engineering using differentiated and purified induced pluripotent stem cells. *Proc Natl Acad Sci U S A*, 109(47):19172–19177, Nov. 2012.
- [67] B. O. Diekman, C. R. Rowland, D. P. Lennon, A. I. Caplan, and F. Guilak. Chondrogenesis of Adult Stem Cells from Adipose Tissue and Bone Marrow: Induction by Growth Factors and Cartilage-Derived Matrix. *Tissue engineering. Part A*, 18(9 and 10):1035–1044, Feb. 2010.
- [68] M. Dominska and D. M. Dykxhoorn. Breaking down the barriers: siRNA delivery and endosome escape. *Journal of Cell Science*, 123(8):1183–1189, Mar. 2010.
- [69] C. Domm. Redifferentiation of dedifferentiated bovine articular chondrocytes in alginate culture under low oxygen tension. *Osteoarthritis and Cartilage*, 10(1):13–22, Jan. 2002.
- [70] P. Dy, W. Wang, P. Bhattaram, Q. Wang, L. Wang, R. T. Ballock, and V. Lefebvre. Sox9 directs hypertrophic maturation and blocks osteoblast differentiation of growth plate chondrocytes. *Developmental Cell*, 22(3):597–609, Mar. 2012.
- [71] J. Elvenes, G. Knutsen, O. Johansen, B. T. Moe, and I. Martinez. Development of a new method to harvest chondroprogenitor cells from underneath cartilage defects in the knees. *Journal of orthopaedic science : official journal of the Japanese Orthopaedic Association*, 14(4):410–417, July 2009.
- [72] C. Erggelet, P. C. Kreuz, E. H. Mrosek, J. C. Schagemann, A. Lahm, P. P. Ducommun, and C. Ossendorf. Autologous chondrocyte implantation versus ACI using 3D-bioresorbable graft for the treatment of large full-thickness cartilage lesions of the knee. *Archives of Orthopaedic and Trauma Surgery*, 130(8):957–964, Aug. 2009.
- [73] I. E. Erickson, S. C. van Veen, S. Sengupta, S. R. Kestle, and R. L. Mauck. Cartilage Matrix Formation by Bovine Mesenchymal Stem Cells in Three-dimensional Culture Is Age-dependent. *Clinical orthopaedics and related research*, 469(10):2744–2753, Mar. 2011.
- [74] P. Esbrit and M. Jose Alcaraz. Current perspectives on parathyroid hormone (PTH) and PTH-

- related protein (PTHrP) as bone anabolic therapies. *Biochemical Pharmacology*, 85(10):1417–1423, 2013.
- [75] B. C. Evans, C. E. Nelson, S. S. Yu, K. R. Beavers, A. J. Kim, H. Li, H. M. Nelson, T. D. Giorgio, and C. L. Duvall. Ex Vivo Red Blood Cell Hemolysis Assay for the Evaluation of pH-responsive Endosomolytic Agents for Cytosolic Delivery of Biomacromolecular Drugs. *Journal of Visualized Experiments*, (73), 2013.
- [76] Y. Ezura, I. Sekiya, H. Koga, T. Muneta, and M. Noda. Methylation status of CpG islands in the promoter regions of signature genes during chondrogenesis of human synovium-derived mesenchymal stem cells. *Arthritis and rheumatism*, 60(5):1416–1426, May 2009.
- [77] J. Farr, B. J. Cole, S. Sherman, and V. Karas. Particulated articular cartilage: CAIS and DeNovo NT. *The journal of knee surgery*, 25(1):23–29, Mar. 2012.
- [78] D. T. Felson and J. Buckwalter. Débridement and Lavage for Osteoarthritis of the Knee. *New England Journal of Medicine*, 347(2):132–133, July 2002.
- [79] A. J. Fenton, T. J. Martin, and G. C. Nicholson. Long-term culture of disaggregated rat osteoclasts: Inhibition of bone resorption and reduction of osteoclast-like cell number by calcitonin and PTHrP[107-139]. *Journal of cellular physiology*, 155(1):1–7, Apr. 1993.
- [80] A. M. Fernandes, S. R. Herlofsen, T. A. Karlsen, A. M. Kuchler, Y. Fløisand, and J. E. Brinchmann. Similar Properties of Chondrocytes from Osteoarthritis Joints and Mesenchymal Stem Cells from Healthy Donors for Tissue Engineering of Articular Cartilage. *PloS one*, 8(5):e62994, May 2013.
- [81] A. Fire, S. Xu, M. K. Montgomery, S. A. Kostas, S. E. Driver, and C. C. Mello. Potent and specific genetic interference by double-stranded RNA in *Caenorhabditis elegans*. *Nature*, 391(6669):806–811, Feb. 1998.
- [82] D. Fischer, Y. Li, B. Ahlemeyer, J. Kriegelstein, and T. Kissel. In vitro cytotoxicity testing of polycations: influence of polymer structure on cell viability and hemolysis. *Biomaterials*, 24(7):1121–1131, Mar. 2003.
- [83] J. Fischer, A. Aulmann, V. Dexheimer, T. Grossner, and W. Richter. Intermittent PTHrP(1–34) Exposure Augments Chondrogenesis and Reduces Hypertrophy of Mesenchymal Stromal Cells. *Stem cells and development*, pages 1–11, July 2014.
- [84] J. Fischer, A. Dickhut, and M. Rickert. Human articular chondrocytes secrete parathyroid hormone-related protein and inhibit hypertrophy of mesenchymal stem cells in coculture during chondrogenesis. *Arthritis and rheumatism*, 62(9):2696–2706, 2010.
- [85] A. J. Fosang, K. Last, V. Knäuper, G. Murphy, and P. J. Neame. Degradation of cartilage aggrecan by collagenase-3 (MMP-13). *Febs Letters*, 380(1-2):17–20, 1996.
- [86] J. A. Fox, K. B. Freedman, S. J. Lee, and B. J. Cole. Fresh osteochondral allograft transplantation for articular cartilage defects. *Operative Techniques in Sports Medicine*, 10(3):168–173, July 2002.
- [87] J. R. Fuchs, S. Terada, D. Hannouche, E. R. Ochoa, J. P. Vacanti, and D. O. Fauza. Engi-

- neered fetal cartilage: Structural and functional analysis in vitro. *Journal of Pediatric Surgery*, 37(12):1720–1725, Dec. 2002.
- [88] Y. Fujihara, T. Takato, and K. Hoshi. Macrophage-inducing FasL on chondrocytes forms immune privilege in cartilage tissue engineering, enhancing in vivo regeneration. *Stem cells*, 32(5):1208–1219, May 2014.
- [89] T. Furumatsu and T. Ozaki. Epigenetic regulation in chondrogenesis. *Acta medica Okayama*, 64(3):155–161, June 2010.
- [90] T. Furumatsu, M. Tsuda, N. Taniguchi, Y. Tajima, and H. Asahara. Smad3 induces chondrogenesis through the activation of SOX9 via CREB-binding protein/p300 recruitment. *Journal of Biological Chemistry*, 280(9):8343–8350, Mar. 2005.
- [91] R. C. Gensure, T. J. Gardella, and H. Juppner. Parathyroid hormone and parathyroid hormone-related peptide, and their receptors. *Biochemical and Biophysical Research Communications*, 328(3):666–678, 2005.
- [92] W. T. Godbey, K. K. Wu, and A. G. Mikos. Size matters: molecular weight affects the efficiency of poly(ethylenimine) as a gene delivery vehicle. *Journal of Biomedical Materials Research Part A*, 45(3):268–275, June 1999.
- [93] W. T. Godbey, K. K. Wu, and A. G. Mikos. Tracking the intracellular path of poly(ethylenimine)/DNA complexes for gene delivery. *Proc Natl Acad Sci U S A*, 96(9):5177–5181, Apr. 1999.
- [94] W. T. Godbey, K. K. Wu, and A. G. Mikos. Poly(ethylenimine)-mediated gene delivery affects endothelial cell function and viability. *Biomaterials*, 22(5):471–480, Mar. 2001.
- [95] C. R. Gooding, W. Bartlett, G. Bentley, J. A. Skinner, R. Carrington, and A. Flanagan. A prospective, randomised study comparing two techniques of autologous chondrocyte implantation for osteochondral defects in the knee: Periosteum covered versus type I/III collagen covered. *The Knee*, 13(3):203–210, June 2006.
- [96] D. A. Grande, M. I. Pitman, L. Peterson, D. Menche, and M. Klein. The repair of experimentally produced defects in rabbit articular cartilage by autologous chondrocyte transplantation. *J Orthop Res*, 7(2):208–218, Mar. 1989.
- [97] M. Grandolfo, P. D’Andrea, M. Martina, F. Ruzzier, and F. Vittur. Calcium-activated potassium channels in chondrocytes. *Biochemical and Biophysical Research Communications*, 182(3):1429–1434, Feb. 1992.
- [98] I. Gum. *Guide to the expression of uncertainty in measurement*. BIPM, 1995.
- [99] J. Guo, U. I. Chung, H. Kondo, F. R. Bringhurst, and H. M. Kronenberg. The PTH/PTHrP receptor can delay chondrocyte hypertrophy in vivo without activating phospholipase C. *Developmental Cell*, 3(2):183–194, 2002.
- [100] O. Haddo, S. Mahroof, D. Higgs, L. David, J. Pringle, M. Bayliss, S. R. Cannon, and T. W. R. Briggs. The use of chondroglide membrane in autologous chondrocyte implantation. *The Knee*, 11(1):51–55, Feb. 2004.

- [101] B. K. Hall and T. Miyake. All for one and one for all: condensations and the initiation of skeletal development. *Bioessays*, 22(2):138–147, Jan. 2000.
- [102] L. Han, A. J. Grodzinsky, and C. Ortiz. Nanomechanics of the cartilage extracellular matrix. *Annual review of materials research*, 41:133–168, 2011.
- [103] Y. Han and V. Lefebvre. L-Sox5 and Sox6 Drive Expression of the Aggrecan Gene in Cartilage by Securing Binding of Sox9 to a Far-Upstream Enhancer. *Molecular and Cellular Biology*, 28(16):4999–5013, July 2008.
- [104] L. Hangody and P. Füles. Autologous osteochondral mosaicplasty for the treatment of full-thickness defects of weight-bearing joints: ten years of experimental and clinical experience. *The Journal of bone and joint surgery. American volume*, 85-A Suppl 2:25–32, 2003.
- [105] G. J. Hannon. RNA interference. *Nature*, 418(6894):244–251, July 2002.
- [106] T. Hardingham. Proteoglycans and Glycosaminoglycans. In *Dynamics of Bone and Cartilage Metabolism*, pages 85–98. Elsevier, 2006.
- [107] M. Hatori, K. J. Klatte, C. C. Teixeira, and I. M. Shapiro. End labeling studies of fragmented DNA in the Avian growth plate: Evidence of apoptosis in terminally differentiated chondrocytes. *Journal of Bone and Mineral Research*, 10(12):1960–1968, Dec. 2009.
- [108] P. V. Hauser, J. W. Pippin, C. Kaiser, R. D. Krofft, P. T. Brinkkoetter, K. L. Hudkins, D. Kerjaschki, J. Reiser, C. E. Alpers, and S. J. Shankland. Novel siRNA Delivery System to Target Podocytes In Vivo. *PloS one*, 5(3):e9463, Mar. 2010.
- [109] R. Hauser. The acceleration of articular cartilage degeneration in osteoarthritis by nonsteroidal anti-inflammatory drugs. *Journal of Prolotherapy*, 2(1):305–322, 2010.
- [110] D. Heinegård. Proteoglycans and more—from molecules to biology. *International journal of experimental pathology*, 90(6):575–586, Dec. 2009.
- [111] C. A. Hellingman, E. N. B. Davidson, W. Koevoet, E. L. Vitters, W. B. van den Berg, G. J. V. M. van Osch, and P. M. van der Kraan. Smad signaling determines chondrogenic differentiation of bone-marrow-derived mesenchymal stem cells: inhibition of Smad1/5/8P prevents terminal differentiation and calcification. *Tissue engineering. Part A*, 17(7-8):1157–1167, Apr. 2011.
- [112] C. A. Hellingman, E. T. P. Verwiel, I. Slagt, W. Koevoet, R. M. L. Poublon, G. J. Nolst-Trenité, R. J. Baatenburg de Jong, H. Jahr, and G. J. V. M. van Osch. Differences in Cartilage-Forming Capacity of Expanded Human Chondrocytes From Ear and Nose and Their Gene Expression Profiles. *Cell Transplantation*, 20(6):925–940, 2011.
- [113] C. G. Helmick, D. T. Felson, R. C. Lawrence, S. Gabriel, R. Hirsch, C. K. Kwok, M. H. Liang, H. M. Kremers, M. D. Mayes, P. A. Merkel, S. R. Pillemer, J. D. Reveille, J. H. Stone, and National Arthritis Data Workgroup. Estimates of the prevalence of arthritis and other rheumatic conditions in the United States: Part I. *Arthritis and rheumatism*, 58(1):15–25, 2007.
- [114] J. E. Henderson, N. Amizuka, and H. Warshawsky. Nucleolar localization of parathyroid hormone-related peptide enhances survival of chondrocytes under conditions that promote apoptotic cell death. *Molecular and Cellular Biology*, 1995.

- [115] M. Hirao, N. Tamai, N. Tsumaki, H. Yoshikawa, and A. Myoui. Oxygen tension regulates chondrocyte differentiation and function during endochondral ossification. *Journal of Biological Chemistry*, 281(41):31079–31092, Oct. 2006.
- [116] M. Hirata, F. Kugimiya, A. Fukai, T. Saito, F. Yano, T. Ikeda, A. Mabuchi, B. R. Sapkota, T. Akune, N. Nishida, N. Yoshimura, T. Nakagawa, K. Tokunaga, K. Nakamura, U. I. Chung, and H. Kawaguchi. C/EBP and RUNX2 cooperate to degrade cartilage with MMP-13 as the target and HIF-2 as the inducer in chondrocytes. *Human Molecular Genetics*, 21(5):1111–1123, Feb. 2012.
- [117] H. Holtzer. Control of Chondrogenesis in the Embryo. *Biophysical Journal*, 4(1):239–250, Jan. 1964.
- [118] W. D. Huang, X. Zhou, V. Lefebvre, and B. De Crombrughe. Phosphorylation of SOX9 by cyclic AMP-dependent protein kinase A enhances SOX9's ability to transactivate a Col2a1 chondrocyte-specific enhancer (vol 20, pg 4149, 2000). *Molecular and Cellular Biology*, 20(20):7838–7838, Oct. 2000.
- [119] J. Huggett, K. Dheda, S. Bustin, and A. Zumla. Real-time RT-PCR normalisation; strategies and considerations. *Genes and Immunity*, 6(4):279–284, Apr. 2005.
- [120] W. Hunter. Of the Structure and Diseases of Articulating Cartilages, by William Hunter, Surgeon. *Philosophical Transactions of the Royal Society of London*, 42(462-471):514–521, Jan. 1742.
- [121] E. Hunziker. Articular cartilage repair: basic science and clinical progress. A review of the current status and prospects. *Osteoarthritis and Cartilage*, 10(6):432–463, June 2002.
- [122] M. Hyytiäinen, C. Penttinen, and J. Keski-Oja. Latent TGF- $\beta$  Binding Proteins: Extracellular Matrix Association and Roles in TGF- $\beta$  Activation. *Critical Reviews in Clinical Laboratory Sciences*, 41(3):233–264, Jan. 2004.
- [123] J. P. Iannotti, S. Naidu, Y. Noguchi, R. M. Hunt, and C. T. Brighton. Growth plate matrix vesicle biogenesis. The role of intracellular calcium. *Clinical orthopaedics and related research*, 306:222–229, Sept. 1994.
- [124] M. Inada, Y. M. Wang, M. H. Byrne, M. U. Rahman, C. Miyaura, C. Lopez-Otin, and S. M. Krane. Critical roles for collagenase-3 (Mmp13) in development of growth and in endochondral plate cartilage ossification. *Proc Natl Acad Sci U S A*, 101(49):17192–17197, Dec. 2004.
- [125] N. Indrawattana, G. Chen, M. Tadokoro, L. H. Shann, H. Ohgushi, T. Tateishi, J. Tanaka, and A. Bunyaratvej. Growth factor combination for chondrogenic induction from human mesenchymal stem cell. *Biochemical and Biophysical Research Communications*, 320(3):914–919, July 2004.
- [126] V. H. Irion and D. C. Flanigan. New and Emerging Techniques in Cartilage Repair: Other Scaffold-Based Cartilage Treatment Options. *Operative Techniques in Sports Medicine*, 2013.
- [127] J. Iwasa, L. Engebretsen, Y. Shima, and M. Ochi. Clinical application of scaffolds for cartilage tissue engineering. *Knee surgery, sports traumatology, arthroscopy : official journal of the ESSKA*, 17(6):561–577, 2009.



- [128] J. Iwasa, M. Ochi, Y. Uchio, K. Katsube, N. Adachi, and K. Kawasaki. Effects of Cell Density on Proliferation and Matrix Synthesis of Chondrocytes Embedded in Atelocollagen Gel. *Artificial Organs*, 27(3):249–255, Mar. 2003.
- [129] N. Jiang, X. Zhang, X. Zheng, D. Chen, K. Siu, H. Wang, T. E. Ichim, D. Quan, V. McAlister, G. Chen, and W.-P. Min. A Novel In Vivo siRNA Delivery System Specifically Targeting Liver Cells for Protection of ConA-Induced Fulminant Hepatitis. *PLoS one*, 7(9):e44138, Sept. 2012.
- [130] Y. Jiang, B. N. Jahagirdar, R. L. Reinhardt, R. E. Schwartz, C. D. Keene, X. R. Ortiz-Gonzalez, M. Reyes, T. Lenvik, T. Lund, M. Blackstad, J. Du, S. Aldrich, A. Lisberg, W. C. Low, D. A. Largaespada, and C. M. Verfaillie. Pluripotency of mesenchymal stem cells derived from adult marrow. *Nature*, 418(6893):41–49, June 2002.
- [131] B. Johnstone, M. Alini, M. Cucchiari, G. R. Dodge, D. Eglin, F. Guilak, H. Madry, A. Mata, R. L. Mauck, C. E. Semino, and M. J. Stoddart. Tissue engineering for articular cartilage repair—the state of the art. *European cells & materials*, 25:248–267, 2013.
- [132] B. Johnstone, T. M. Hering, A. I. Caplan, V. M. Goldberg, and J. U. Yoo. In vitro chondrogenesis of bone marrow-derived mesenchymal progenitor cells. *Experimental Cell Research*, 238(1):265–272, 1998.
- [133] J. M. Jukes, S. K. Both, A. Leusink, L. M. T. Sterk, C. A. van Blitterswijk, and J. de Boer. Endochondral bone tissue engineering using embryonic stem cells. *Proc Natl Acad Sci U S A*, 105(19):6840–6845, May 2008.
- [134] W. Kafienah, M. Jakob, O. Démariseau, A. Frazer, M. D. Barker, I. Martin, and A. P. Hollander. Three-dimensional tissue engineering of hyaline cartilage: comparison of adult nasal and articular chondrocytes. *Tissue Engineering*, 8(5):817–826, Oct. 2002.
- [135] W. Kafienah, S. Mistry, S. C. Dickinson, T. J. Sims, I. Learmonth, and A. P. Hollander. Three-dimensional cartilage tissue engineering using adult stem cells from osteoarthritis patients. *Arthritis and rheumatism*, 56(1):177–187, 2007.
- [136] J. S. Kang, T. Alliston, R. Delston, and R. Derynck. Repression of Runx2 function by TGF- $\beta$  through recruitment of class II histone deacetylases by Smad3. *EMBO J*, 24(14):2543–2555, 2005.
- [137] M. Kanichai, D. Ferguson, P. J. Prendergast, and V. A. Campbell. Hypoxia promotes chondrogenesis in rat mesenchymal stem cells: a role for AKT and hypoxia-inducible factor (HIF)-1 $\alpha$ . *Journal of cellular physiology*, 216(3):708–715, Sept. 2008.
- [138] M. Karin and M. Delhase. The I $\kappa$ B kinase (IKK) and NF- $\kappa$ B: key elements of proinflammatory signalling. *Seminars in Immunology*, 12(1):85–98, Feb. 2000.
- [139] V. Kartsogiannis and K. W. Ng. Cell lines and primary cell cultures in the study of bone cell biology. *Molecular and cellular endocrinology*, 228(1-2):79–102, Dec. 2004.
- [140] T. Katopodi, S. R. Tew, P. D. Clegg, and T. E. Hardingham. The influence of donor and hypoxic conditions on the assembly of cartilage matrix by osteoarthritic human articular chondrocytes on Hyalograft matrices. *Biomaterials*, 30(4):535–540, Feb. 2009.

- [141] A. B. Khoshfetrat, M. Kino-Oka, Y. Takezawa, T. Yamamoto, K. Sugawara, and M. Taya. Seeding density modulates migration and morphology of rabbit chondrocytes cultured in collagen gels. *Biotechnology and bioengineering*, 102(1):294–302, Jan. 2009.
- [142] E.-J. Kim, S.-W. Cho, J.-O. Shin, M.-J. Lee, K.-S. Kim, and H.-S. Jung. Ihh and Runx2/Runx3 Signaling Interact to Coordinate Early Chondrogenesis: A Mouse Model. *PLoS one*, 8(2):e55296, Feb. 2013.
- [143] H. Kim, T. Akagi, and M. Akashi. Preparation of Size Tunable Amphiphilic Poly(amino acid) Nanoparticles. *Macromolecular Bioscience*, 9(9):842–848, Sept. 2009.
- [144] H. Kim, T. Akagi, and M. Akashi. Preparation of CpG ODN-encapsulated Anionic Poly(amino acid) Nanoparticles for Gene Delivery. *Chemistry Letters*, 39(3):278–279, 2010.
- [145] Y. J. Kim, H. J. Kim, and G. I. Im. PTHrP promotes chondrogenesis and suppresses hypertrophy from both bone marrow-derived and adipose tissue-derived MSCs (vol 373, pg 104, 2008). *Biochemical and Biophysical Research Communications*, 376(1):241–241, Nov. 2008.
- [146] T. Kirsch. Annexins and Tissue Mineralization: Matrix Vesicles, Ion Channel Activity of Annexins and Annexin V/Collagen Interactions. In *Annexins*, pages 172–181. Springer US, Boston, MA, 2003.
- [147] P. Klinger, C. Surmann-Schmitt, M. Brem, B. Swoboda, J. H. Distler, H.-D. Carl, K. von der Mark, F. F. Hennig, and K. Gelse. Chondromodulin 1 stabilizes the chondrocyte phenotype and inhibits endochondral ossification of porcine cartilage repair tissue. *Arthritis and rheumatism*, 63(9):2721–2731, Sept. 2011.
- [148] C. Kneuer, M. Sameti, U. Bakowsky, T. Schiestel, H. Schirra, H. Schmidt, and C.-M. Lehr. A Nonviral DNA Delivery System Based on Surface Modified Silica-Nanoparticles Can Efficiently Transfect Cells in Vitro. *Bioconjugate Chemistry*, 11(6):926–932, Nov. 2000.
- [149] T. Kobayashi, U. I. Chung, E. Schipani, M. Starbuck, G. Karsenty, T. Katagiri, D. L. Goad, B. Lanske, and H. M. Kronenberg. PTHrP and Indian hedgehog control differentiation of growth plate chondrocytes at multiple steps. *Development*, 129(12):2977–2986, June 2002.
- [150] C. S. Kovacs. The Role of PTHrP in Regulating Mineral Metabolism During Pregnancy, Lactation, and Fetal/Neonatal Development. *Clinical Reviews in Bone and Mineral Metabolism*, 12(3):142–164, Feb. 2014.
- [151] C. S. Kovacs, B. Lanske, J. L. Hunzelman, J. Guo, A. C. Karaplis, and H. M. Kronenberg. Parathyroid hormone-related peptide (PTHrP) regulates fetal-placental calcium transport through a receptor distinct from the PTH/PTHrP receptor. *Proc Natl Acad Sci U S A*, 93(26):15233–15238, Dec. 1996.
- [152] E. Kozhemyakina, T. Cohen, T.-P. Yao, and A. B. Lassar. Parathyroid hormone-related peptide represses chondrocyte hypertrophy through a protein phosphatase 2A/histone deacetylase 4/MEF2 pathway. *Molecular and Cellular Biology*, 29(21):5751–5762, Nov. 2009.
- [153] H. M. Kronenberg. PTHrP and skeletal development. *Annals of the New York Academy of Sciences*, 1068:1–13, Apr. 2006.

- [154] K. Kunath, A. von Harpe, D. Fischer, H. Petersen, U. Bickel, K. Voigt, and T. Kissel. Low-molecular-weight polyethylenimine as a non-viral vector for DNA delivery: comparison of physicochemical properties, transfection efficiency and in vivo distribution with high-molecular-weight polyethylenimine. *Journal of controlled release : official journal of the Controlled Release Society*, 89(1):113–125, Apr. 2003.
- [155] H. J. Kwon, K. Yasuda, Y. Ohmiya, K. Honma, Y. M. Chen, and J. P. Gong. In vitro differentiation of chondrogenic ATDC5 cells is enhanced by culturing on synthetic hydrogels with various charge densities. *Acta biomaterialia*, 6(2):494–501, 2010.
- [156] B. Lanske, A. C. Karaplis, K. Lee, A. Luz, A. Vortkamp, A. Pirro, M. Karperien, L. H. Defize, C. Ho, R. C. Mulligan, A. B. Abou-Samra, H. Juppner, G. V. Segre, and H. M. Kronenberg. PTH/PTHrP receptor in early development and Indian hedgehog-regulated bone growth. *Science*, 273(5275):663–666, Aug. 1996.
- [157] C. R. Lee, A. J. Grodzinsky, H. P. Hsu, S. D. Martin, and M. Spector. Effects of harvest and selected cartilage repair procedures on the physical and biochemical properties of articular cartilage in the canine knee. *J Orthop Res*, 18(5):790–799, Sept. 2000.
- [158] H.-H. Lee, C.-C. Chang, M.-J. Shieh, J.-P. Wang, Y.-T. Chen, T.-H. Young, and S.-C. Hung. Hypoxia Enhances Chondrogenesis and Prevents Terminal Differentiation through PI3K/Akt/FoxO Dependent Anti-Apoptotic Effect. *Scientific reports*, 3, Sept. 2013.
- [159] J.-M. Lee and G.-I. Im. PTHrP isoforms have differing effect on chondrogenic differentiation and hypertrophy of mesenchymal stem cells. *Biochemical and Biophysical Research Communications*, 421(4):819–824, 2012.
- [160] C. J. Lengner, M. Q. Hassan, R. W. Serra, C. Lepper, A. J. van Wijnen, J. L. Stein, J. B. Lian, and G. S. Stein. Nkx3.2-mediated repression of Runx2 promotes chondrogenic differentiation. *Journal of Biological Chemistry*, 280(16):15872–15879, Apr. 2005.
- [161] T. F. Li, Y. F. Dong, A. M. Ionescu, R. N. Rosier, M. J. Zuscik, E. M. Schwarz, R. J. O’Keefe, and H. Drissi. Parathyroid hormone-related peptide (PTHrP) inhibits Runx2 expression through the PKA signaling pathway. *Experimental Cell Research*, 299(1):128–136, Sept. 2004.
- [162] W. J. Li, R. Tuli, X. Huang, P. Laquerriere, and R. S. Tuan. Multilineage differentiation of human mesenchymal stem cells in a three-dimensional nanofibrous scaffold. *Biomaterials*, 26(25):5158–5166, Sept. 2005.
- [163] Y. Li, M. J. Ahrens, A. Wu, J. Liu, and A. T. Dudley. Calcium/calmodulin-dependent protein kinase II activity regulates the proliferative potential of growth plate chondrocytes. *Development*, 138(2):359–370, Jan. 2011.
- [164] P. Lingor, U. Michel, U. Schöll, M. Bähr, and S. Kügler. Transfection of “naked” siRNA results in endosomal uptake and metabolic impairment in cultured neurons. *Biochemical and Biophysical Research Communications*, 315(4):1126–1133, Mar. 2004.
- [165] H. Liu, Z. Zhao, R. B. Clarke, J. Gao, I. R. Garrett, and E. E. C. Margerrison. Enhanced Tissue Regeneration Potential of Juvenile Articular Cartilage. *The American journal of sports medicine*, 41(11):2658–2667, Nov. 2013.

- [166] S. Q. Liu, Q. Tian, J. L. Hedrick, J. H. Po Hui, P. L. Ee, and Y. Y. Yang. Biomimetic hydrogels for chondrogenic differentiation of human mesenchymal stem cells to neocartilage. *Biomaterials*, 31(28):7298–7307, Oct. 2010.
- [167] K. J. Livak and T. D. Schmittgen. Analysis of Relative Gene Expression Data Using Real-Time Quantitative PCR and the 2<sup>−(Delta Delta)</sup> CT Method. *Methods*, 25(4):402–408, Dec. 2001.
- [168] C. Loebel, E. M. Czekanska, M. Bruderer, G. Salzmann, M. Alini, and M. J. Stoddart. In Vitro Osteogenic Potential of Human Mesenchymal Stem Cells Is Predicted by Runx2/Sox9 Ratio. *Tissue engineering. Part A*, page 140804122539000, Aug. 2014.
- [169] L. Longobardi, F. Granero-Moltó, L. O’Rear, T. J. Myers, T. Li, P. J. Kregor, and A. Spagnoli. Subcellular localization of IRS-1 in IGF-I-mediated chondrogenic proliferation, differentiation and hypertrophy of bone marrow mesenchymal stem cells. *Growth Factors*, 27(5):309–320, Jan. 2009.
- [170] L. Longobardi, L. O’Rear, S. Aakula, B. Johnstone, K. Shimer, A. Chytil, W. A. Horton, H. L. Moses, and A. Spagnoli. Effect of IGF-I in the Chondrogenesis of Bone Marrow Mesenchymal Stem Cells in the Presence or Absence of TGF- $\beta$  Signaling. *Journal of Bone and Mineral Research*, 21(4):626–636, Dec. 2005.
- [171] D. Lozano, C. G. Trejo, E. Gómez-Barrena, M. Manzano, J. C. Doadrio, A. J. Salinas, M. Vallet-Regí, N. García-Honduvilla, P. Esbrit, and J. Buján. Osteostatin-loaded onto mesoporous ceramics improves the early phase of bone regeneration in a rabbit osteopenia model. *Acta biomaterialia*, 8(6):2317–2323, July 2012.
- [172] L. V. Luchikhina, O. I. Mendel, and D. A. Antonov. Knee osteoarthritis combination therapy with hyaluronic acid, chondroitine sulfate and glucosamine after arthroscopic lavage: long-term results. *Osteoarthritis and Cartilage*, 22:S480, Apr. 2014.
- [173] S. P. Luckman, E. Rees, and A. P. Kwan. Partial characterization of cell-type X collagen interactions. *Biochemical Journal*, 372(Pt 2):485–493, June 2003.
- [174] H. Lv, S. Zhang, B. Wang, S. Cui, and J. Yan. Toxicity of cationic lipids and cationic polymers in gene delivery. *Journal of Controlled Release*, 114(1):100–109, Aug. 2006.
- [175] A. M. Mackay, S. C. Beck, J. M. Murphy, F. P. Barry, C. O. Chichester, and M. F. Pittenger. Chondrogenic differentiation of cultured human mesenchymal stem cells from marrow. *Tissue Engineering*, 4(4):415–428, Jan. 1998.
- [176] H. E. MacLean and H. M. Kronenberg. Localization of Indian hedgehog and PTH/PTHrP receptor expression in relation to chondrocyte proliferation during mouse bone development. *Development, Growth and Differentiation*, 47:59–63, 2005.
- [177] V. E. Macrae, M. G. Davey, L. McTeir, S. Narisawa, M. C. Yadav, J. L. Millan, and C. Farquharson. Inhibition of PHOSPHO1 activity results in impaired skeletal mineralization during limb development of the chick. *Bone*, 46(4):1146–1155, Apr. 2010.
- [178] K. K. Mak, H. M. Kronenberg, P. T. Chuang, S. Mackem, and Y. Z. Yang. Indian hedge-

- hog signals independently of PTHrP to promote chondrocyte hypertrophy. *Development*, 135(11):1947–1956, June 2008.
- [179] S. Marlovits, P. Zeller, P. Singer, C. Resinger, and V. Vecsei. Cartilage repair: Generations of autologous chondrocyte transplantation. *European Journal of Radiology*, 57(1):24–31, Jan. 2006.
- [180] T. Maruyama, A. J. Mirando, C. X. Deng, and W. Hsu. The balance of WNT and FGF signaling influences mesenchymal stem cell fate during skeletal development. *Science signaling*, 3(123):ra40–ra40, 2010.
- [181] T. Massfelder, P. Dann, T. L. Wu, R. Vasavada, J. J. Helwig, and A. F. Stewart. Opposing mitogenic and anti-mitogenic actions of parathyroid hormone-related protein in vascular smooth muscle cells: A critical role for nuclear targeting. *Proc Natl Acad Sci U S A*, 94(25):13630–13635, 1997.
- [182] M. Mastrogiacomo, R. Cancedda, and R. Quarto. Effect of different growth factors on the chondrogenic potential of human bone marrow stromal cells. *Osteoarthritis and Cartilage*, 9:S36–S40, Aug. 2001.
- [183] M. Matsusaki, K. Hiwatari, M. Higashi, and T. Kaneko. Stably-dispersed and Surface-functional Bionanoparticles Prepared by Self-assembling Amphiphatic Polymers of Hydrophilic Poly (. GAMMA.-glutamic acid) Bearing .... *Chemistry Letters*, 2004.
- [184] R. L. Mauck, X. Yuan, and R. S. Tuan. Chondrogenic differentiation and functional maturation of bovine mesenchymal stem cells in long-term agarose culture. *Osteoarthritis and Cartilage*, 14(2):179–189, 2006.
- [185] R. McBeath, D. M. Pirone, C. M. Nelson, K. Bhadriraju, and C. S. Chen. Cell shape, cytoskeletal tension, and RhoA regulate stem cell lineage commitment. *Developmental Cell*, 6(4):483–495, Apr. 2004.
- [186] H. S. McCarthy and S. Roberts. A histological comparison of the repair tissue formed when using either Chondrogide® or periosteum during autologous chondrocyte implantation. *Osteoarthritis and Cartilage*, 21(12):2048–2057, Dec. 2013.
- [187] M. A. Mello and R. S. Tuan. High density micromass cultures of embryonic limb bud mesenchymal cells: an in vitro model of endochondral skeletal development. *In vitro cellular & developmental biology - Animal*, 35(5):262–269, May 1999.
- [188] V. V. Meretoja, R. L. Dahlin, S. Wright, F. K. Kasper, and A. G. Mikos. The effect of hypoxia on the chondrogenic differentiation of co-cultured articular chondrocytes and mesenchymal stem cells in scaffolds. *Biomaterials*, 34(17):4266–4273, June 2013.
- [189] S. Miura, J. Kondo, A. Takimoto, H. Sano-Takai, L. Guo, C. Shukunami, H. Tanaka, and Y. Hiraki. The N-terminal cleavage of chondromodulin-I in growth-plate cartilage at the hypertrophic and calcified zones during bone development. *PLoS one*, 9(4):e94239, 2014.
- [190] B. Mollon, R. Kandel, J. Chahal, and J. Theodoropoulos. The clinical status of cartilage tissue regeneration in humans. *Osteoarthritis and Cartilage*, 21(12):1824–1833, Dec. 2013.

- [191] M. Moretti, D. Wendt, S. C. Dickinson, T. J. Sims, A. P. Hollander, D. J. Kelly, P. J. Prendergast, M. Heberer, and I. Martin. Effects of in Vitro Preculture on in Vivo Development of Human Engineered Cartilage in an Ectopic Model. *Tissue Engineering*, 11(9/10):1421–1429, 2005.
- [192] D. V. Morrissey, K. Blanchard, L. Shaw, K. Jensen, J. A. Lockridge, B. Dickinson, J. A. McSwiggen, C. Vargeese, K. Bowman, C. S. Shaffer, B. A. Polisky, and S. Zinnen. Activity of stabilized short interfering RNA in a mouse model of hepatitis B virus replication. *Hepatology (Baltimore, Md.)*, 41(6):1349–1356, June 2005.
- [193] D. Mrugala, N. Dossat, J. Ringe, B. Delorme, A. Coffy, C. Bony, P. Charbord, T. Häupl, J.-P. Daures, D. Noël, and C. Jorgensen. Gene expression profile of multipotent mesenchymal stromal cells: Identification of pathways common to TGFbeta3/BMP2-induced chondrogenesis. *Cloning and stem cells*, 11(1):61–76, Mar. 2009.
- [194] M. B. Mueller, M. Fischer, J. Zellner, A. Berner, T. Dienstknecht, R. Kujat, L. Prantl, M. Nerlich, R. S. Tuan, and P. Angele. Effect of parathyroid hormone-related protein in an in vitro hypertrophy model for mesenchymal stem cell chondrogenesis. *International orthopaedics*, 37(5):945–951, May 2013.
- [195] M. B. Mueller and R. S. Tuan. Functional characterization of hypertrophy in chondrogenesis of human mesenchymal stem cells. *Arthritis and rheumatism*, 58(5):1377–1388, May 2008.
- [196] S. Munir, C. B. Foldager, M. Lind, V. Zachar, K. Søballe, and T. G. Koch. Hypoxia enhances chondrogenic differentiation of human adipose tissue-derived stromal cells in scaffold-free and scaffold systems. *Cell and tissue research*, 355(1):89–102, 2014.
- [197] F. Mwale, D. Stachura, P. Roughley, and J. Antoniou. Limitations of using aggrecan and type X collagen as markers of chondrogenesis in mesenchymal stem cell differentiation. *J Orthop Res*, 24(8):1791–1798, 2006.
- [198] R. Narcisi, R. Quarto, V. Ulivi, A. Muraglia, L. Molfetta, and P. Giannoni. TGF beta-1 administration during ex-vivo expansion of human articular chondrocytes in a serum-free medium redirects the cell phenotype toward hypertrophy. *Journal of cellular physiology*, 227(9):3282–3290, Nov. 2012.
- [199] R. Narcisi, L. Signorile, J. A. N. Verhaar, P. Giannoni, and G. J. V. M. van Osch. TGF $\beta$  inhibition during expansion phase increases the chondrogenic re-differentiation capacity of human articular chondrocytes. *Osteoarthritis and Cartilage*, 20(10):1152–1160, Oct. 2012.
- [200] S. Nehrer, C. Chiari, S. Domayer, H. Barkay, and A. Yayon. Results of Chondrocyte Implantation with a Fibrin-Hyaluronan Matrix: A Preliminary Study. *Clinical orthopaedics and related research*, 466(8):1849–1855, June 2008.
- [201] A. J. Nixon, L. R. Goodrich, and M. S. Scimeca. Gene therapy in musculoskeletal repair. *Annals of the New York Academy of Sciences*, 1117:310–327, 2007.
- [202] S. Nuernberger, N. Cyran, C. Albrecht, H. Redl, V. Vécsei, and S. Marlovits. The influence of scaffold architecture on chondrocyte distribution and behavior in matrix-associated chondrocyte transplantation grafts. *Biomaterials*, 32(4):1032–1040, Feb. 2011.

- [203] D. Nurminsky, C. Magee, L. Faverman, and M. Nurminskaya. Regulation of chondrocyte differentiation by actin-severing protein adseverin. *Developmental Biology*, 302(2):427–437, Feb. 2007.
- [204] H. Okano, M. Nakamura, K. Yoshida, Y. Okada, O. Tsuji, S. Nori, E. Ikeda, S. Yamanaka, and K. Miura. Steps Toward Safe Cell Therapy Using Induced Pluripotent Stem Cells. *Circulation Research*, 112(3):523–533, Jan. 2013.
- [205] H. Orimo. The mechanism of mineralization and the role of alkaline phosphatase in health and disease. *J Nihon Med Sch*, 77(1):4–12, Feb. 2010.
- [206] N. Ortega, D. J. Behonick, and Z. Werb. Matrix remodeling during endochondral ossification. *Trends in cell biology*, 14(2):86–93, Feb. 2004.
- [207] P. Orth, A. Rey-Rico, J. K. Venkatesan, H. Madry, and M. Cucchiari. Current perspectives in stem cell research for knee cartilage repair. *Stem cells and cloning : advances and applications*, 7:1–17, 2014.
- [208] C. Pan, C. Kumar, S. Bohl, U. Klingmueller, and M. Mann. Comparative proteomic phenotyping of cell lines and primary cells to assess preservation of cell type-specific functions. *Molecular & cellular proteomics : MCP*, 8(3):443–450, Mar. 2009.
- [209] G. S. Pari and Y. Xu. Gene Transfer into Mammalian Cells Using Calcium Phosphate and DEAE-Dextran. In *Gene Delivery to Mammalian Cells*, pages 25–32. Humana Press, New Jersey, Oct. 2003.
- [210] J. M. Patrascu, U. Freymann, C. Kaps, and D. V. Poenaru. Repair of a post-traumatic cartilage defect with a cell-free polymer-based cartilage implant: A FOLLOW-UP AT TWO YEARS BY MRI AND HISTOLOGICAL REVIEW. *Journal of Bone & Joint Surgery, British Volume*, 92-B(8):1160–1163, July 2010.
- [211] M. Pelosi, S. Lazzarano, B. L. Thoms, and C. L. Murphy. Parathyroid hormone-related protein is induced by hypoxia and promotes expression of the differentiated phenotype of human articular chondrocytes. *Clinical Science*, 125(10):461–470, July 2013.
- [212] K. Pelttari, B. Pippenger, M. Mumme, S. Feliciano, C. Scotti, P. Mainil-Varlet, A. Procino, B. von Rechenberg, T. Schwamborn, M. Jakob, C. Cillo, A. Barbero, and I. Martin. Adult human neural crest-derived cells for articular cartilage repair. *Science Translational Medicine*, 6(251):251ra119, Aug. 2014.
- [213] K. Pelttari, A. Winter, E. Steck, K. Goetzke, T. Hennig, B. G. Ochs, T. Aigner, and W. Richter. Premature induction of hypertrophy during in vitro chondrogenesis of human mesenchymal stem cells correlates with calcification and vascular invasion after ectopic transplantation in SCID mice. *Arthritis and rheumatism*, 54(10):3254–3266, Oct. 2006.
- [214] M. W. Pfaffl, A. Tichopad, C. Prgomet, and T. P. Neuvians. Determination of stable house-keeping genes, differentially regulated target genes and sample integrity: BestKeeper–Excel-based tool using pair-wise correlations. *Biotechnology letters*, 26(6):509–515, Mar. 2004.
- [215] M. F. Pittenger, A. M. Mackay, S. C. Beck, R. K. Jaiswal, R. Douglas, J. D. Mosca, M. A. Moor-

- man, D. W. Simonetti, S. Craig, and D. R. Marshak. Multilineage potential of adult human mesenchymal stem cells. *Science*, 284(5411):143–147, Apr. 1999.
- [216] M. M. Pleumeekers, L. Nimeskern, W. L. M. Koevoet, N. Kops, R. M. L. Poublon, K. S. Stok, and G. J. V. M. van Osch. The in vitro and in vivo capacity of culture-expanded human cells from several sources encapsulated in alginate to form cartilage. *European cells & materials*, 27:264–280, Apr. 2014.
- [217] M. Pombo-Suarez, M. Calaza, J. J. Gomez-Reino, and A. Gonzalez. Reference genes for normalization of gene expression studies in human osteoarthritic articular cartilage. *BMC Molecular Biology*, 9(1):17, 2008.
- [218] C. A. Poole, M. H. Flint, and B. W. Beaumont. Chondrons extracted from canine tibial cartilage: preliminary report on their isolation and structure. *J Orthop Res*, 6(3):408–419, 1988.
- [219] S. Provot, H. Kempf, L. C. Murtaugh, U.-i. Chung, D.-W. Kim, J. Chyung, H. M. Kronenberg, and A. B. Lassar. Nkx3.2/Bapx1 acts as a negative regulator of chondrocyte maturation. *Development*, 133(4):651–662, Feb. 2006.
- [220] L. Quintana, N. I. zur Nieden, and C. E. Semino. Morphogenetic and Regulatory Mechanisms During Developmental Chondrogenesis: New Paradigms for Cartilage Tissue Engineering. *Tissue engineering. Part B, Reviews*, 15(1):29–41, Mar. 2009.
- [221] A. Quintin, C. Schizas, C. Scaletta, S. Jaccoud, L. A. Applegate, and D. P. Pioletti. Plasticity of Fetal Cartilaginous Cells. *Cell Transplantation*, 19(10):1349–1357, 2010.
- [222] F. G. Quiroz, O. M. Posada, D. Gallego-Perez, N. Higuaita-Castro, C. Sarassa, D. J. Hansford, P. Agudelo-Florez, and L. E. López. Housekeeping gene stability influences the quantification of osteogenic markers during stem cell differentiation to the osteogenic lineage. *Cytotechnology*, 62(2):109–120, Apr. 2010.
- [223] A. Radonić, S. Thulke, I. M. Mackay, O. Landt, W. Siegert, and A. Nitsche. Guideline to reference gene selection for quantitative real-time PCR. *Biochemical and Biophysical Research Communications*, 313(4):856–862, Jan. 2004.
- [224] A. H. Reddi. Morphogenesis and Tissue Engineering of Bone and Cartilage: Inductive Signals, Stem Cells, and Biomimetic Biomaterials. *Tissue Engineering*, 6(4):351–359, Aug. 2000.
- [225] I. Richard, M. Thibault, G. De Crescenzo, M. D. Buschmann, and M. Lavertu. Ionization Behavior of Chitosan and Chitosan–DNA Polyplexes Indicate That Chitosan Has a Similar Capability to Induce a Proton-Sponge Effect as PEI. *Biomacromolecules*, 14(6):1732–1740, June 2013.
- [226] A. C. Richards Grayson, A. M. Doody, and D. Putnam. Biophysical and Structural Characterization of Polyethylenimine-Mediated siRNA Delivery in Vitro. *Pharmaceutical Research*, 23(8):1868–1876, July 2006.
- [227] S. Roche, M. C. Ronziere, D. Herbage, and A.-M. Freyria. Native and DPPA cross-linked collagen sponges seeded with fetal bovine epiphyseal chondrocytes used for cartilage tissue engineering. *Biomaterials*, 22:9–18, 2001.



- [228] J. P. Rodríguez, M. González, S. Ríos, and V. Cambiazo. Cytoskeletal organization of human mesenchymal stem cells (MSC) changes during their osteogenic differentiation. *J Cell Biochem*, 93(4):721–731, Nov. 2004.
- [229] G. M. Salzmänn, M. Sauerschnig, M. T. Berninger, T. Kaltenhauser, M. Schönfelder, S. Vogt, G. Wexel, T. Tischer, N. Sudkamp, P. Niemeyer, A. B. Imhoff, and P. B. Schöttle. The dependence of autologous chondrocyte transplantation on varying cellular passage, yield and culture duration. *Biomaterials*, 32(25):5810–5818, Sept. 2011.
- [230] S. K. Samal, M. Dash, S. Van Vlierberghe, D. L. Kaplan, E. Chiellini, C. van Blitterswijk, L. Moroni, and P. Dubruel. Cationic polymers and their therapeutic potential. *Chemical Society Reviews*, 41(21):7147, 2012.
- [231] J. Sarvaiya and Y. K. Agrawal. Chitosan as a suitable nanocarrier material for anti-Alzheimer drug delivery. *International journal of biological macromolecules*, 72C:454–465, Sept. 2014.
- [232] E. T. Schenborn and V. Goiffon. DEAE-Dextran Transfection of Mammalian Cultured Cells. In *Transcription Factor Protocols*, pages 147–154. Humana Press, New Jersey, Oct. 1999.
- [233] E. Schipani and S. Provot. PTHrP, PTH, and the PTH/PTHrP receptor in endochondral bone development. *Birth defects research. Part C, Embryo today : reviews*, 69(4):352–362, Dec. 2003.
- [234] H. Schmal, J. M. Pestka, G. Salzmänn, P. C. Strohm, N. P. Südkamp, and P. Niemeyer. Autologous chondrocyte implantation in children and adolescents. *Knee surgery, sports traumatology, arthroscopy : official journal of the ESSKA*, 21(3):671–677, May 2012.
- [235] M. Schnabel, S. Marlovits, G. Eckhoff, and I. Fichtel. Dedifferentiation-associated changes in morphology and gene expression in primary human articular chondrocytes in cell culture. *Osteoarthritis and Cartilage*, 2002.
- [236] U. Schneider, L. Rackwitz, S. Andereya, S. Siebenlist, F. Fensky, J. Reichert, I. Loer, T. Barthel, M. Rudert, and U. Noth. A Prospective Multicenter Study on the Outcome of Type I Collagen Hydrogel-Based Autologous Chondrocyte Implantation (CaReS) for the Repair of Articular Cartilage Defects in the Knee. *The American journal of sports medicine*, 39(12):2558–2565, Dec. 2011.
- [237] T. Schubert, S. Anders, E. Neumann, J. Schoelmerich, F. Hofstaedter, J. Grifka, U. Mueller-Ladner, J. Libera, and J. Schedel. Long-term effects of chondrospheres on cartilage lesions in an autologous chondrocyte implantation model as investigated in the SCID mouse model. *International journal of molecular medicine*, 23(4):455–460, Apr. 2009.
- [238] R. M. Schulz and A. Bader. Cartilage tissue engineering and bioreactor systems for the cultivation and stimulation of chondrocytes. *European Biophysics Journal*, 36(4-5):539–568, Feb. 2007.
- [239] I. Sekiya, J. T. Vuoristo, B. L. Larson, and D. J. Prockop. In vitro cartilage formation by human adult stem cells from bone marrow stroma defines the sequence of cellular and molecular events during chondrogenesis. *Proc Natl Acad Sci U S A*, 99(7):4397–4402, Apr. 2002.
- [240] T. A. S. Selmi, P. Verdonk, P. Chambat, F. Dubrana, J. F. Potel, L. Barnouin, and P. Neyret.

- Autologous chondrocyte implantation in a novel alginate-agarose hydrogel: OUTCOME AT TWO YEARS. *Journal of Bone & Joint Surgery, British Volume*, 90-B(5):597–604, May 2008.
- [241] O. V. Semenov, S. Koestenbauer, M. Riegel, N. Zech, R. Zimmermann, A. H. Zisch, and A. Malek. Multipotent mesenchymal stem cells from human placenta: critical parameters for isolation and maintenance of stemness after isolation. *American Journal of Obstetrics and Gynecology*, 202(2):193.e1–193.e13, Feb. 2010.
- [242] I. M. Shapiro, C. S. Adams, T. Freeman, and V. Srinivas. Fate of the hypertrophic chondrocyte: microenvironmental perspectives on apoptosis and survival in the epiphyseal growth plate. *Birth defects research. Part C, Embryo today : reviews*, 75(4):330–339, Dec. 2005.
- [243] H. Sheikh, K. Zakharian, R. P. De La Torre, C. Facek, A. Vasquez, G. R. Chaudhry, D. Svinarich, and M. J. Perez-Cruet. In vivo intervertebral disc regeneration using stem cell-derived chondroprogenitors. *Journal of neurosurgery. Spine*, 10(3):265–272, Mar. 2009.
- [244] G. Shen. The role of type X collagen in facilitating and regulating endochondral ossification of articular cartilage. *Orthodontics & craniofacial research*, 8(1):11–17, Feb. 2005.
- [245] S. L. Sherman, J. Garrity, K. Bauer, J. Cook, J. Stannard, and W. Bugbee. Fresh osteochondral allograft transplantation for the knee: current concepts. *The Journal of the American Academy of Orthopaedic Surgeons*, 22(2):121–133, Feb. 2014.
- [246] E. Shimizu, N. Selvamurugan, J. J. Westendorf, E. N. Olson, and N. C. Partridge. HDAC4 represses matrix metalloproteinase-13 transcription in osteoblastic cells, and parathyroid hormone controls this repression. *Journal of Biological Chemistry*, 285(13):9616–9626, Mar. 2010.
- [247] M. A. Sirover. New insights into an old protein: the functional diversity of mammalian glyceraldehyde-3-phosphate dehydrogenase. *Biochimica et biophysica acta*, 1432(2):159–184, July 1999.
- [248] P. Smeriglio, J. H. Lai, L. Dhulipala, A. W. Behn, S. B. Goodman, R. L. Smith, W. Maloney, F. Yang, and N. Bhutani. Comparative Potential of Juvenile and Adult Human Articular Chondrocytes for Cartilage Tissue Formation in 3D Biomimetic Hydrogels. *Tissue engineering. Part A*, page 140723072425006, July 2014.
- [249] M. Solanas, R. Moral, and E. Escrich. Unsuitability of using ribosomal RNA as loading control for Northern blot analyses related to the imbalance between messenger and ribosomal RNA content in rat mammary tumors. *Analytical Biochemistry*, 288(1):99–102, Jan. 2001.
- [250] R.-H. Song, M. D Tortorella, A.-M. Malfait, J. T. Alston, Z. Yang, E. C. Arner, and D. W. Griggs. Aggrecan degradation in human articular cartilage explants is mediated by both ADAMTS-4 and ADAMTS-5. *Arthritis and rheumatism*, 56(2):575–585, 2007.
- [251] J. Soutschek, A. Akinc, B. Bramlage, K. Charisse, R. Constien, M. Donoghue, S. Elbashir, A. Geick, P. Hadwiger, J. Harborth, M. John, V. Kesavan, G. Lavine, R. K. Pandey, T. Racie, K. G. Rajeev, I. Röhl, I. Toudjarska, G. Wang, S. Wuschko, D. Bumcrot, V. Kotliansky, S. Limmer, M. Manoharan, and H.-P. Vornlocher. Therapeutic silencing of an endogenous gene by systemic administration of modified siRNAs. *Nature*, 432(7014):173–178, Nov. 2004.

- [252] V. Srinivas, J. Bohensky, and I. M. Shapiro. Autophagy: A New Phase in the Maturation of Growth Plate Chondrocytes Is Regulated by HIF, mTOR and AMP Kinase. *Cells Tissues Organs*, 189(1-4):88–92, 2009.
- [253] W. D. Stanish, R. McCormack, F. Forriol, N. Mohtadi, S. Pelet, J. Desnoyers, A. Restrepo, and M. S. Shive. Novel Scaffold-Based BST-CarGel Treatment Results in Superior Cartilage Repair Compared with Microfracture in a Randomized Controlled Trial. *The Journal of bone and joint surgery. American volume*, 95(18):1640, Sept. 2013.
- [254] W. D. Stanish, A. Restrepo, R. G. McCormack, N. Mohtadi, S. Pelet, J. Desnoyers, F. Forriol, S. Méthot, and M. S. Shive. An International Randomized Clinical Trial Evaluating Bst-Cargel®, A Novel Scaffold For Cartilage Repair, Demonstrates Superiority of Repair When Compared with Microfracture Alone Treatment. *Arthroscopy-the Journal of Arthroscopic and Related Surgery*, 29(10):e137, Oct. 2013.
- [255] L. A. Stanton, S. Sabari, A. V. Sampaio, T. M. Underhill, and F. Beier. p38 MAP kinase signalling is required for hypertrophic chondrocyte differentiation. *Biochemical Journal*, 378:53–62, Feb. 2004.
- [256] J. R. Steadman, W. G. Rodkey, K. K. Briggs, and J. J. Rodrigo. Die Technik der Mikrofrakturierung zur Behandlung von kompletten Knorpeldefekten im Kniegelenk. *Der Orthopäde*, 28(1):26, 1999.
- [257] M. Steinwachs. New technique for cell-seeded collagen-matrix-supported autologous chondrocyte transplantation. *Arthroscopy*, 25(2):208–211, Feb. 2009.
- [258] M. Steinwachs, L. Peterson, V. Bobic, P. Verdonk, and P. Niemeyer. Cell-Seeded Collagen Matrix-Supported Autologous Chondrocyte Transplantation (ACT-CS): A Consensus Statement on Surgical Technique. *Cartilage*, 3(1):5–12, Feb. 2012.
- [259] M. R. Steinwachs, B. Waibl, and M. Mumme. Arthroscopic Treatment of Cartilage Lesions With Microfracture and BST-CarGel. *Arthroscopy Techniques*, 3(3):e399–e402, June 2014.
- [260] M. R. Steinwachs, B. Waibl, S. Wopperer, and M. Mumme. Matrix-Associated Chondroplasty: A Novel Platelet-Rich Plasma and Concentrated Nucleated Bone Marrow Cell-Enhanced Cartilage Restoration Technique. *Arthroscopy Techniques*, 3(2):e279–e282, Apr. 2014.
- [261] R. A. Stockwell. The cell density of human articular and costal cartilage. *Journal of anatomy*, 101(4):753–763, 1967.
- [262] D. Studer, C. Millan, E. Öztürk, K. Maniura-Weber, and M. Zenobi-Wong. Molecular and biophysical mechanisms regulating hypertrophic differentiation in chondrocytes and mesenchymal stem cells. *European cells & materials*, 24:118–135, 2012.
- [263] S. R. Stürzenbaum and P. Kille. Control genes in quantitative molecular biological techniques: the variability of invariance. *Comparative Biochemistry and Physiology Part B: Biochemistry and Molecular Biology*, 130(3):281–289, Oct. 2001.
- [264] T. Suzuki, P. J. Higgins, and D. R. Crawford. Control selection for RNA quantitation. *BioTechniques*, 29(2):332–337, Aug. 2000.

- [265] S. Takeda, J. P. Bonnamy, M. J. Owen, P. Ducy, and G. Karsenty. Continuous expression of *Cbfa1* in nonhypertrophic chondrocytes uncovers its ability to induce hypertrophic chondrocyte differentiation and partially rescues *Cbfa1*-deficient mice. *Genes & Development*, 15(4):467–481, Feb. 2001.
- [266] S. Tanaka, T. Furukawa, and S. A. Plotkin. Human cytomegalovirus stimulates host cell RNA synthesis. *Journal of virology*, 15(2):297–304, Feb. 1975.
- [267] E. V. Tchetina, M. Kobayashi, T. Yasuda, T. Meijers, I. Pidoux, and A. R. Poole. Chondrocyte hypertrophy can be induced by a cryptic sequence of type II collagen and is accompanied by the induction of MMP-13 and collagenase activity: Implications for development and arthritis. *Matrix Biology*, 26(4):247–258, May 2007.
- [268] M. Tompkins, H. D. Adkisson, and K. F. Bonner. DeNovo NT Allograft. *Operative Techniques in Sports Medicine*, 21(2):82–89, June 2013.
- [269] R. E. Toribio, H. A. Brown, C. M. Novince, B. Marlow, K. Hernon, L. G. Lanigan, B. E. I. Hildreth, J. L. Werbeck, S. T. Shu, G. Lorch, M. Carlton, J. Foley, P. Boyaka, L. K. McCauley, and T. J. Rosol. The midregion, nuclear localization sequence, and C terminus of PTHrP regulate skeletal development, hematopoiesis, and survival in mice. *Faseb Journal*, 24(6):1947–1957, June 2010.
- [270] R. S. Tuan, G. Boland, and R. Tuli. Adult mesenchymal stem cells and cell-based tissue engineering. *Arthritis research & therapy*, 2003.
- [271] R. Tuli. Transforming Growth Factor- $\beta$ -mediated Chondrogenesis of Human Mesenchymal Progenitor Cells Involves N-cadherin and Mitogen-activated Protein Kinase and Wnt Signaling Cross-talk. *Journal of Biological Chemistry*, 278(42):41227–41236, July 2003.
- [272] L. Uebersax, H. P. Merkle, and L. Meinel. Insulin-like growth factor I releasing silk fibroin scaffolds induce chondrogenic differentiation of human mesenchymal stem cells. *Journal of Controlled Release*, 127(1):12–21, Apr. 2008.
- [273] S. A. Unterman, N. A. Marcus, and J. H. Elisseeff. Injectable Polymers. In *Biodegradable Polymers in Clinical Use and Clinical Development*, pages 631–664. John Wiley & Sons, Inc., Hoboken, NJ, USA, May 2011.
- [274] T. B. Usdin, T. Wang, S. R. Hoare, E. Mezey, and M. Palkovits. New members of the parathyroid hormone/parathyroid hormone receptor family: the parathyroid hormone 2 receptor and tuberoinfundibular peptide of 39 residues. *Frontiers in neuroendocrinology*, 21(4):349–383, Oct. 2000.
- [275] T. Uto, X. Wang, K. Sato, M. Haraguchi, T. Akagi, M. Akashi, and M. Baba. Targeting of antigen to dendritic cells with poly( $\gamma$ -glutamic acid) nanoparticles induces antigen-specific humoral and cellular immunity. *The Journal of Immunology*, 178(5):2979–2986, Mar. 2007.
- [276] P. M. van der Kraan, E. N. B. Davidson, A. Blom, and W. B. van den Berg. TGF- $\beta$  signaling in chondrocyte terminal differentiation and osteoarthritis Modulation and integration of signaling pathways through receptor-Smads. *Osteoarthritis and Cartilage*, 17(12):1539–1545, Dec. 2009.

- [277] C. C. van Donkelaar and R. Huiskes. The PTHrP-Ihh feedback loop in the embryonic growth plate allows PTHrP to control hypertrophy and Ihh to regulate proliferation. *Biomechanics and Modeling in Mechanobiology*, 6(1-2):55–62, Jan. 2007.
- [278] J. Vandesompele, K. De Preter, F. Pattyn, B. Poppe, N. Van Roy, A. De Paepe, and F. Speleman. Accurate normalization of real-time quantitative RT-PCR data by geometric averaging of multiple internal control genes. *Genome biology*, 3(7):RESEARCH0034, June 2002.
- [279] C. Vauthier, C. Zandanel, and A. L. Ramon. Chitosan-based nanoparticles for in vivo delivery of interfering agents including siRNA. *Current Opinion in Colloid & Interface Science*, 18(5):406–418, Oct. 2013.
- [280] M. P. Verzi, P. Agarwal, C. Brown, D. J. McCulley, J. J. Schwarz, and B. L. Black. The transcription factor MEF2C is required for craniofacial development. *Developmental Cell*, 12(4):645–652, Apr. 2007.
- [281] I. D. Vilfan, C. C. Conwell, and N. V. Hud. Formation of Native-like Mammalian Sperm Cell Chromatin with Folded Bull Protamine. *Journal of Biological Chemistry*, 279(19):20088–20095, Apr. 2004.
- [282] T. Vinardell, E. J. Sheehy, C. T. Buckley, and D. J. Kelly. A Comparison of the Functionality and In Vivo Phenotypic Stability of Cartilaginous Tissues Engineered from Different Stem Cell Sources. *Tissue engineering. Part A*, 18(11-12):1161–1170, June 2012.
- [283] A. Vortkamp, K. Lee, B. Lanske, G. V. Segre, H. M. Kronenberg, and C. J. Tabin. Regulation of rate of cartilage differentiation by Indian hedgehog and PTH-related protein. *Science*, 273(5275):613–622, Aug. 1996.
- [284] G. Vunjak-Novakovic, B. Obradovic, I. Martin, P. M. Bursac, R. Langer, and L. E. Freed. Dynamic Cell Seeding of Polymer Scaffolds for Cartilage Tissue Engineering. *Biotechnology Process*, 14:193–202, Mar. 1998.
- [285] C.-Y. Wang, L.-L. Chen, P.-Y. Kuo, J.-L. Chang, Y.-J. Wang, and S.-C. Hung. Apoptosis in chondrogenesis of human mesenchymal stem cells: effect of serum and medium supplements. *Apoptosis*, 15(4):439–449, Dec. 2009.
- [286] W. Wang and T. Kirsch. Annexin V/beta5 Integrin Interactions Regulate Apoptosis of Growth Plate Chondrocytes. *Journal of Biological Chemistry*, 281(41):30848–30856, Oct. 2006.
- [287] Y. Wang, D. J. Blasioli, H.-J. Kim, H. S. Kim, and D. L. Kaplan. Cartilage tissue engineering with silk scaffolds and human articular chondrocytes. *Biomaterials*, 27(25):4434–4442, Sept. 2006.
- [288] F. Wei, J. Zhou, X. Wei, J. Zhang, B. C. Fleming, R. Terek, M. Pei, Q. Chen, T. Liu, and L. Wei. Activation of Indian hedgehog promotes chondrocyte hypertrophy and upregulation of MMP-13 in human osteoarthritic cartilage. *Osteoarthritis and Cartilage*, 20(7):755–763, July 2012.
- [289] S. Weiss, T. Hennig, R. Bock, E. Steck, and W. Richter. Impact of growth factors and PTHrP

- on early and late chondrogenic differentiation of human mesenchymal stem cells. *Journal of cellular physiology*, 223(1):84–93, Apr. 2010.
- [290] S. Werth, B. Urban-Klein, L. Dai, S. Höbel, M. Grzelinski, U. Bakowsky, F. Czubyko, and A. Aigner. A low molecular weight fraction of polyethylenimine (PEI) displays increased transfection efficiency of DNA and siRNA in fresh or lyophilized complexes. *Journal of Controlled Release*, 112(2):257–270, May 2006.
- [291] E. Wienholds and R. H. Plasterk. MicroRNA function in animal development. *Febs Letters*, 579(26):5911–5922, Oct. 2005.
- [292] M. Wolcott, S. Traub, and C. Efird. High tibial osteotomies in the young active patient. *International orthopaedics*, 34(2):161–166, Jan. 2010.
- [293] M. Wong and J. Medrano. Real-time PCR for mRNA quantitation. *BioTechniques*, 39(1):75–85, July 2005.
- [294] L. Wu, C. Bluguermann, L. Kyupelyan, B. Latour, S. Gonzalez, S. Shah, Z. Galic, S. Ge, Y. Zhu, F. A. Petrigliano, A. Nsair, S. G. Miriuka, X. Li, K. M. Lyons, G. M. Crooks, D. R. McAllister, B. Van Handel, J. S. Adams, and D. Evseenko. Human Developmental Chondrogenesis as a Basis for Engineering Chondrocytes from Pluripotent Stem Cells. *Stem Cell Reports*, 1(6):575–589, 2013.
- [295] J. J. Wysolmerski. Parathyroid hormone-related protein: an update. *The Journal of clinical endocrinology and metabolism*, 97(9):2947–2956, Sept. 2012.
- [296] J. J. Wysolmerski and A. F. Stewart. The physiology of parathyroid hormone-related protein: an emerging role as a developmental factor. *Annual review of physiology*, 60(1):431–460, 1998.
- [297] T. Xia, M. Kovichich, M. Liong, H. Meng, S. Kabehie, S. George, J. I. Zink, and A. E. Nel. Polyethyleneimine Coating Enhances the Cellular Uptake of Mesoporous Silica Nanoparticles and Allows Safe Delivery of siRNA and DNA Constructs. *ACS Nano*, 3(10):3273–3286, Oct. 2009.
- [298] F. Yamashita, K. Sakakida, F. Suzu, and S. Takai. The transplantation of an autogeneic osteochondral fragment for osteochondritis dissecans of the knee. *Clinical orthopaedics and related research*, (201):43–50, Dec. 1985.
- [299] S. Yamashita, M. Andoh, H. Ueno-Kudoh, T. Sato, S. Miyaki, and H. Asahara. Sox9 directly promotes Bapx1 gene expression to repress Runx2 in chondrocytes. *Experimental Cell Research*, 315(13):2231–2240, Aug. 2009.
- [300] X. Yang, L. Chen, X. L. Xu, C. L. Li, C. F. Huang, and C. X. Deng. TGF-beta/Smad3 signals repress chondrocyte hypertrophic differentiation and are required for maintaining articular cartilage. *Journal of Cell Biology*, 153(1):35–46, Apr. 2001.
- [301] J. U. Yoo, T. S. Barthel, K. Nishimura, and L. Solchaga. The Chondrogenic Potential of Human Bone-Marrow-Derived Mesenchymal Progenitor Cells. *The Journal of bone and joint surgery. American volume*, 80:1745–1757, 1998.

- [302] B. S. Yoon, R. Pogue, D. A. Ovchinnikov, I. Yoshii, Y. Mishina, R. R. Behringer, and K. M. Lyons. BMPs regulate multiple aspects of growth-plate chondrogenesis through opposing actions on FGF pathways. *Development*, 133(23):4667–4678, Dec. 2006.
- [303] C. A. Yoshida, H. Yamamoto, T. Fujita, T. Furuichi, K. Ito, K.-i. Inoue, K. Yamana, A. Zanma, K. Takada, Y. Ito, and T. Komori. Runx2 and Runx3 are essential for chondrocyte maturation, and Runx2 regulates limb growth through induction of Indian hedgehog. *Genes & Development*, 18(8):952–963, Apr. 2004.
- [304] D. Yu, Y. Zhang, X. Zhou, Z. Mao, and C. Gao. Influence of surface coating of PLGA particles on the internalization and functions of human endothelial cells. *Biomacromolecules*, 13(10):3272–3282, Oct. 2012.
- [305] L. Zak, C. Albrecht, B. Wondrasch, H. Widhalm, G. Vekszler, S. Trattnig, S. Marlovits, and S. Aldrian. Results 2 Years After Matrix-Associated Autologous Chondrocyte Transplantation Using the Novocart 3D Scaffold: An Analysis of Clinical and Radiological Data. *The American journal of sports medicine*, 42(7):1618–1627, May 2014.
- [306] J. L. Zakrzewski, M. R. M. van den Brink, and J. A. Hubbell. Overcoming immunological barriers in regenerative medicine. *Nature biotechnology*, 32(8):786–794, Aug. 2014.
- [307] J. Zhang, Z. Yang, C. Li, Y. Dou, Y. Li, T. Thote, D.-A. Wang, and Z. Ge. Cells Behave Distinctly Within Sponges and Hydrogels Due to Differences of Internal Structure. *Tissue engineering. Part A*, 19(19-20):2166–2175, Oct. 2013.
- [308] W. Zhang, R. W. Moskowitz, G. Nuki, S. Abramson, R. D. Altman, N. Arden, S. Bierma-Zeinstra, K. D. Brandt, P. Croft, M. Doherty, M. Dougados, M. Hochberg, D. J. Hunter, K. Kwok, L. S. Lohmander, and P. Tugwell. OARSI recommendations for the management of hip and knee osteoarthritis, Part II: OARSI evidence-based, expert consensus guidelines. *Osteoarthritis and Cartilage*, 16(2):137–162, Feb. 2008.
- [309] X. C. Zhen, L. Wei, Q. Q. Wu, Y. Zhang, and Q. Chen. Mitogen-activated protein kinase p38 mediates regulation of chondrocyte differentiation by parathyroid hormone. *Journal of Biological Chemistry*, 276(7):4879–4885, Feb. 2001.
- [310] M. Zheng, G. M. Pavan, M. Neeb, A. K. Schaper, A. Danani, G. Klebe, O. M. Merkel, and T. Kissel. Targeting the blind spot of polycationic nanocarrier-based siRNA delivery. *ACS Nano*, 6(11):9447–9454, Nov. 2012.
- [311] G. Zhou, Q. Zheng, F. Engin, E. Munivez, Y. Chen, E. Sebald, D. Krakow, and B. Lee. Dominance of SOX9 function over RUNX2 during skeletogenesis. *Proc Natl Acad Sci U S A*, 103(50):19004–19009, Dec. 2006.
- [312] P. Zimmermann, S. Boeuf, A. Dickhut, S. Boehmer, S. Olek, and W. Richter. Correlation of COL10A1 induction during chondrogenesis of mesenchymal stem cells with demethylation of two CpG sites in the COL10A1 promoter. *Arthritis and rheumatism*, 58(9):2743–2753, Sept. 2008.
- [313] T. S. Zimmermann, A. C. H. Lee, A. Akinc, B. Bramlage, D. Bumcrot, M. N. Fedoruk, J. Harborth, J. A. Heyes, L. B. Jeffs, M. John, A. D. Judge, K. Lam, K. McClintock, L. V. Nechev,

L. R. Palmer, T. Racie, I. Röhl, S. Seiffert, S. Shanmugam, V. Sood, J. Soutschek, I. Toudjarska, A. J. Wheat, E. Yaworski, W. Zedalis, V. Koteliansky, M. Manoharan, H.-P. Vornlocher, and I. MacLachlan. RNAi-mediated gene silencing in non-human primates. *Nature*, 441(7089):111–114, May 2006.



# Appendices



## A Pellet culture compared to chondrogenesis induced in scaffolds

Clinically, the most applied cell-based system for the treatment of cartilage lesions is the combination of a scaffold with cells. The question arises whether pellet culture, the most commonly studied *in vitro* system, is a predictive model for *in vivo* use. To address this question, we compared MSC pellets with cell-laden collagen I/III scaffolds based on proliferation, matrix production and gene expression profiles. Pellets were formed using  $2 \times 10^5$  cells, and 2 mm punches of Optimaix scaffold were seeded with  $2.35 \times 10^5$  cells.

Generally, chondrogenic extracellular matrix was produced in both culture systems as evidenced by the increase in s-GAG/DNA as well as the alcian blue staining. In total amount of GAG/construct, scaffolds are superior. The most striking difference was observed in the DNA content after 21 days which decreased in pellets and slightly increased in scaffolds. The same DNA loss in pellet culture has been reported by Sekiya et al. [239] where only 40% of the initial DNA was left after 21 days. In the work of Wang et al. [285] the decrease in cellularity was associated with increased Annexin V expression as well as lysosomal integrity, both typical for apoptosis. This process is not only an *in vitro* phenomenon but also occurs in the growth plate where terminally differentiated chondrocytes undergo programmed cell death [107]. The slight increase in DNA content in scaffolds could indicate an absence of apoptosis, or possibly the measured proliferation compensates for cell death. On the other hand, the high cell density in centrifuged pellets might present a situation where proliferation is completely hindered, and differentiation progresses in a short time towards endochondral ossification, inducing apoptosis earlier in pellets than scaffolds. The real reasons behind this fundamental difference remains to be elucidated.

## A. Pellets versus Scaffolds

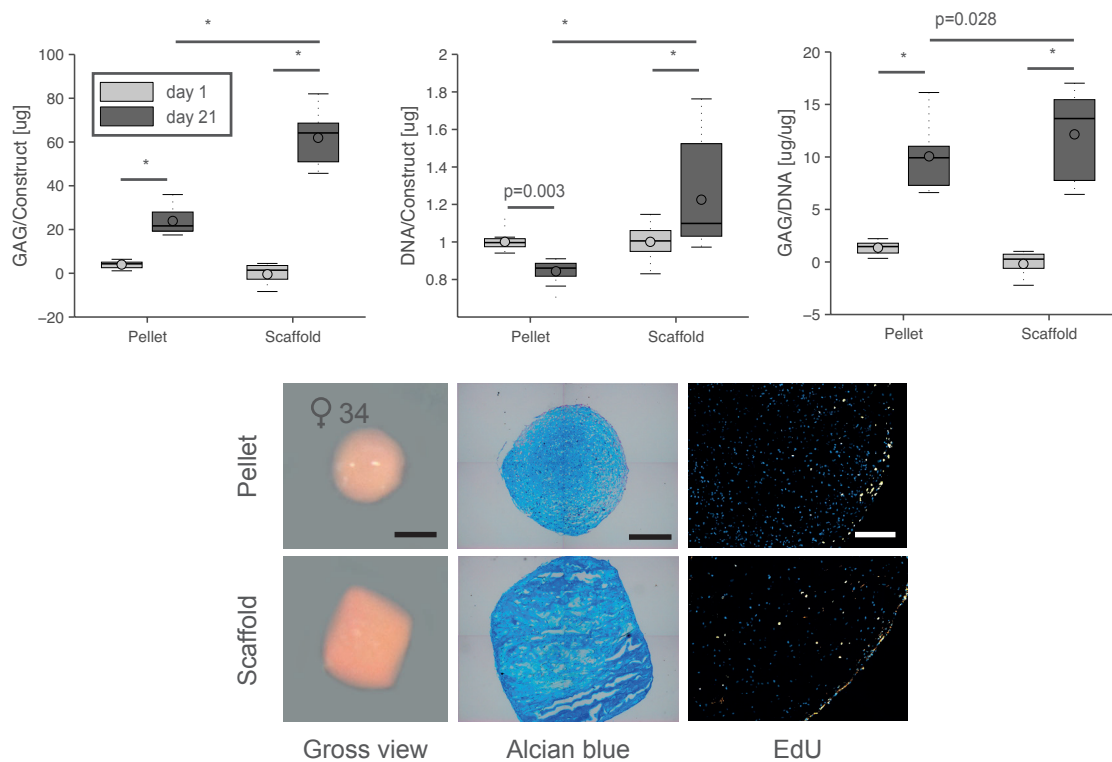


**Figure A.1.:** Pellets and Scaffolds of 3 MSC donors were analysed for GAG/scaffold, DNA normalised to day 1 and GAG/DNA. Further representative images of their gross appearance (scale bar 1mm), alcian blue (scale bar 500  $\mu$ m), and EdU staining (scale bar 200  $\mu$ m) are presented.

Except the difference in DNA content, both culture systems yield highly comparable mRNA levels of collagen 1 and 2, as well as the hypertrophic master gene, collagen 10. The same is observed for the immunostaining of the respective proteins. Overall, pellets are a good approximation for the more clinically-relevant scaffold system, a conclusion also drawn by Munir et al. [196] who compared adipo MSCs in pellets and collagen I/III scaffolds.

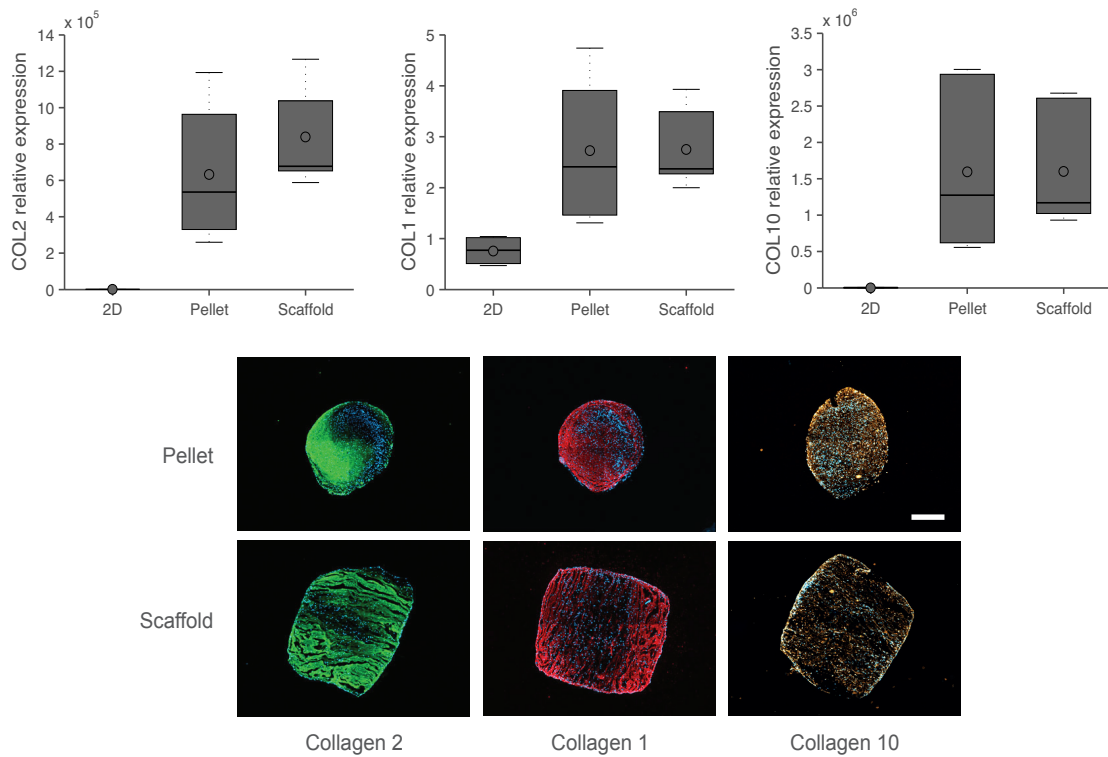


**Figure A.2.:** Gene expression analysis and immunostaining of collagen 1,2, and 10 in pellets and scaffolds after 21 days of chondrogenic induction. PCR data normalized to 2D. Scale bar 500 μm.



## B IGF-1 to replace TGF-beta for chondrogenic induction

TGF- $\beta$ -induced chondrogenesis has been extensively proven to induce hypertrophy in MSCs. Insulin-like growth factor 1 (IGF-1), on the other hand, is reported to stimulate collagen 2 production with minimal collagen 10 [197]. We thus tested the addition of 50 ng/ml IGF-1 alone and in combination with 10 ng/ml TGF- $\beta$ 3 on scaffold culture of MSCs and ECPs. The alcian blue staining revealed a low degree of matrix production in IGF-1 treated samples compared to TGF- $\beta$ . Interestingly, the combination of both growth factors only induced a strong chondrogenic response in MSCs whereas in ECPs, a partial inhibition was observed.

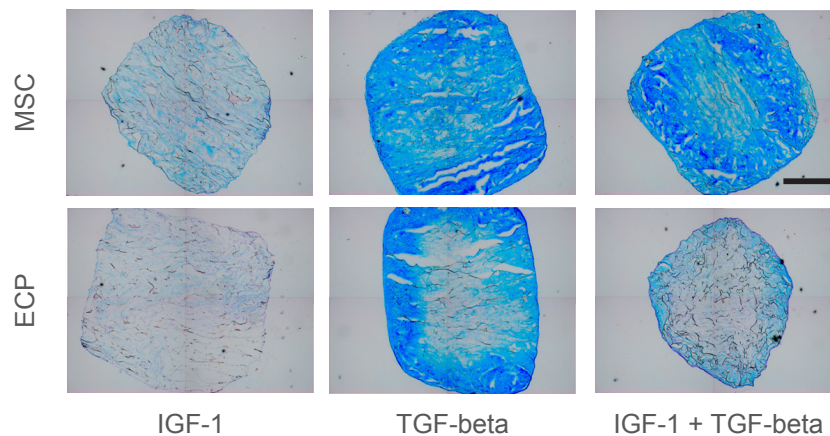


**Figure B.1.:** MSCs and ECP-loaded Optimaix scaffolds treated with 50 ng/ml IGF-1, 10 ng/ml TGF- $\beta$ , or the combination analysed with alcian blue staining at day 21 of culture. Scale bar 500  $\mu$ m.

Several publications support the absence of a chondrogenic induction using IGF-1 [125, 182, 289]. The discrepancy with other published results [170, 272] likely originates from the use of the serum replacement, ITS+ which contains insulin that binds to the same receptor as IGF-1 [170]. Mwale et al. [197] present an exception where

collagen 2 production upon IGF-1 delivery is observed, even in the presence of ITS+. The effect of IGF-1 in the absence of insulin remains to be tested, although a more recent publication by Longobardi et al. [169] also reports a strong induction of Ihh and collagen 10 with IGF-1 stimulation, calling its benefit over TGF- $\beta$  into question.



## C RPL13a as a reference gene for human bone marrow-derived mesenchymal stromal cells during expansion, adipo-, chondro- and osteogenesis

*Note: This chapter has been published in RPL13a as a Reference Gene for Human Bone Marrow-derived Mesenchymal Stromal Cells during Expansion, Adipo-, Chondro- and Osteogenesis, D. Studer et al., Tissue Engineering Part C Methods (2012), 18(10), 761-71.*

The growing field of research on mesenchymal stromal cells (MSCs) for tissue regeneration and tissue engineering [44, 130, 215, 270] highly depends on reliable, fast and sensitive methods to accurately detect small changes in gene expression during expansion, differentiation or re-differentiation. Real time quantitative reverse transcription polymerase chain reaction (termed qPCR according to MIQE guidelines [43]) is the most popular method due to its ease of use and high sensitivity so that it can be performed with a small number of cells. qPCR as a quantitative analysis method greatly depends on an appropriate internal data normalization [42, 119, 263, 293]. At the moment, so called reference genes (RGs) are the gold standard to correct for the amount of starting material, sample-to-sample variations, and amplification efficiencies [63, 119, 263]. Such RGs should show a constant expression in different tissues or cells under all experimental conditions. Candidate normalization genes are therefore constitutive genes, which are constantly expressed at abundant levels in cells under different conditions, generally involved in basic cellular functions. A vast number of possible RGs are used in current research however thorough validation of their presumed stability in mRNA expression is mostly lacking. Several studies have shown that the expression level of fre-

quently used control genes in MSCs studies, such as glyceraldehyde-3-phosphate dehydrogenase (GAPDH) and beta actin (ACTB) is notably unstable between different donors [278], differentiation [56, 222] and cell expansion conditions [56]. Although Quiroz et al. [222] conducted a study comparing GAPDH, ribosomal protein L13a (RPL13) and ACTB for normalization of osteogenic differentiation of MSCs, there are to our knowledge no comprehensive studies investigating the gene expression stability of a broad range of RG over all three mesodermal differentiation lineages: bone, cartilage and adipose tissue. In this study, we aim to establish one single RG for all three mesodermal differentiation line-ages in human bone marrow-derived MSCs (hBM-MSCs) as well as other human MSCs and bone progenitor cells. Seven commonly used RGs (18S ribosomal RNA,  $\beta$ 2-microglobulin B2M, eukaryotic translational elongation factor 1 alpha EF1 $\alpha$ , ACTB, GAPDH, RPL13a and tyrosine 3-monooxygenase/tryptophan 5-monooxygenase activation protein, zeta polypeptide YWHAZ) were analyzed based on different stability parameters.

## **Materials and methods**

### **Cells**

hBM-MSCs, human primary bone cells (HBCs) and human placenta-derived MSCs (hPD-MSCs) were freshly isolated (see protocols below) and expanded in MSC-proliferation medium composed of minimal essential medium (alpha-MEM; Invitrogen, 22561) supplemented with 10% fetal bovine serum (FBS; Lonza), 1% penicillin-streptomycin-neomycin antibiotic mixture (100X) (PSN; Gibco), 1 ng/ml human basic fibroblast growth factor (FGF-2; Sigma, F0291) in a humidified incubator at 37°C with 5% CO<sub>2</sub> and 95% air. Bone marrow-derived MSCs were also purchased from Lonza (Lonza MSCs, Lonza, PT-2501) and the MG-63 human osteosarcoma cell line from ATTC (CRL-1427). Lonza MSCs were expanded according to manufacturer's protocol and MG-63 in the MG-63-proliferation medium composed of dulbecco's modified eagle's medium (DMEM; Gibco, 41965) supplemented with 10% FBS, 1% PSN, 1% L-glutamine (Gibco, 25030, 100x), and 1% sodium pyruvate (Gibco, 11360, 100x). Cell passaging (split ratio 1 to 5) was performed using trypsin-EDTA (Sigma, T3924, 1x).

---

## Isolation of human primary cells

### *Isolation of human bone marrow-derived mesenchymal stromal cells*

The mesenchymal stromal cells (MSCs) were isolated from femur-derived bone marrow samples that were obtained during surgical hip replacement of otherwise healthy patients (two female and one male, aged between 44 and 79 years) after having received informed consent. The protocol was approved by the ethical board of the Kantonspital St.Gallen, Switzerland (ethical committee approval number EKSG08/014/1B). The bone marrow samples were incubated in 20 ml isolation medium (25 mM HEPES (Fluka, #54459), 128.5 mM NaCl (Fluka, #71380), 5.4 mM KCl (Fluka, #60130), 5.5 mM D(+)-glucose (Sigma, #G7528), 51.8 mM D(+)-saccharose (Sigma, #84097), 0.1% BSA (Sigma, #A6003)) overnight at 4°C. Afterwards, the sample was centrifuged at 110×g for 15 minutes at 4°C to remove fat tissue. The remaining pieces of trabecular bone were rinsed several times with isolation medium that was collected and filtered through a 200 µm filter. The filtered cell solution was centrifuged, the resulting cell pellet resuspended in MSC-proliferation medium for cell counting (Casy 1 DT, Roche Innovatis AG) and seeded at a density of  $1 \times 10^7$  cells in a T75 culture flask containing proliferation medium.

### *Isolation of human bone cells*

Primary human bone cells (HBCs) were isolated from the same samples as hBM-MSCs (see above). After the hBM-MSCs were collected, the pieces of trabecular bone were further cleaned from remaining tissue and cells under microscopic observation using forceps. Five to ten pieces of bone (~ 25 mg) were placed in a T75 flask together with 20 ml MSC-proliferation medium, which was changed for the first time after one week and later biweekly. The bone pieces were left in the culture flask until the outgrowing cells reached 70% confluency.

### *Isolation of human placenta-derived mesenchymal stromal cells*

The isolation of human placenta-derived mesenchymal stromal cells was performed according to Semenov et al. [241] following the protocol approved by the ethical committee of the district of Zurich (study Stv22/2006). Placentas were collected from two donors immediately after elective caesarean section and the isolated cells suspended in a T75 flask containing 15 ml MSC-proliferation medium.

## Multilineage differentiation assay

### *Adipogenic differentiation*

For adipogenic induction, MSCs were seeded at an initial density of 26'000 cells/cm<sup>2</sup> and were first cultivated in adipo-maintenance medium consisting of  $\alpha$ -MEM supplemented with 10% FBS, 1% PSN and 10  $\mu$ g/ml insulin (dissolved in 0.01 M HCl (pH 2-3); Sigma, #I-6634) for 1 day followed by cultivation in adipo-induction medium consisting of  $\alpha$ -MEM supplemented with 10% FBS, 1% PSN, 1  $\mu$ M dexamethasone (Sigma, #D-4902), 10  $\mu$ g/ml insulin, 0.5 mM isobutyl-1-methylxanthine (Sigma, #I-5879) and 200  $\mu$ M indomethacin (Sigma, #I-7378) for 3 days. The alteration of those two media was repeated over the whole cultivation period of 22 days. Control cultures were performed in MSC-proliferation medium (see above).

### *Chondrogenic differentiation*

Chondrogenic differentiation of MSCs was induced by pellet culture for which 250'000 cells were placed in a 15-ml polypropylene tube and centrifuged at 250 $\times$ g for 5 minutes. The pellet was cultured at 37°C with 5% CO<sub>2</sub> in 500  $\mu$ l of chondrogenic medium that consisted of high-glucose dulbecco's modified eagle's medium (DMEM; Gibco, #41965) supplemented with 100 ng/ml bone morphogenetic protein 2 (BMP-2; kind gift from F.Weber, University Hospital Zürich, Switzerland), 10 ng/ml transforming growth factor  $\beta$ 3 (TGF- $\beta$ 3, Peprotech, #100-36E), 100 nM dexamethasone, 50  $\mu$ g/ml ascorbate-2-phosphate (Sigma, #A8960), 40  $\mu$ g/ml proline (Fluka, #81709), 100  $\mu$ g/ml sodium pyruvate (Fluka, #15990), and 1% ITS+ Premix (6.25  $\mu$ g/mL insulin, 6.25  $\mu$ g/mL transferrin, 6.25 ng/mL selenious acid, 1.25 mg/mL serum albumin, and 5.35  $\mu$ g/mL linoleic acid; BD Biosciences, #354352). The medium was replaced every 3-4 days for 22 days. As a control, pellets were cultivated in chondrogenic medium lacking dexamethasone, BMP-2 and TGF- $\beta$ 3.

### *Osteogenic differentiation*

To induce osteogenic differentiation of MSCs and HBCs, the cells were seeded at an initial density of 2'000 cells/cm<sup>2</sup> and cultivated in  $\alpha$ -MEM supplemented with 10% FBS, 1% PSN, 10 nM dexamethasone, 50 mM ascorbate-2-phosphate, 2 mM  $\beta$ -glycerophosphate (Sigma, #G-9891) and 10 nM 1,25-dihydroxyvitamin D<sub>3</sub> (Sigma, #D-1530). MG-63 cells were osteogenically induced in MG-63-proliferation medium (composition see above) further supplemented with 50 nM 1,25-dihydroxyvitamin

---

D3, 50 µg/ml ascorbate-2-phosphate, 10 nM β-glycerolphosphate and 10 nM dexamethasone. The differentiation media was replaced every 3-4 days for up to 22 days (for MSCs) or for 7 days (HBCs and MG-63). As a control, cells were cultured in MSC- respectively MG-63-proliferation medium (composition see above).

### **RNA isolation and quantification**

Cells grown in monolayer were detached using trypsin-EDTA (Sigma, #T3924, 1×) and centrifuged at 250×g for 5 minutes to form a cell pellet. Cartilage pellets were digested with 3 mg/ml collagenase II (Sigma, #C6885) for 2 hours to break down the abundant negatively charged extracellular matrix and thereby increasing the RNA yield using affinity column-based extraction. Afterwards, the pellet was washed in PBS, and total RNA was prepared using the RNeasy<sup>®</sup> Micro Kit (Qiagen, Hombrechtikon, CH, #74004) according to the manufacturer's protocol. All samples were DNase I (Qiagen, #79254, 1500 Kunitz units) treated. The RNA concentration was determined using a Nanodrop<sup>™</sup> ND-1000 Spectrophotometer (Nanodrop, Wilmington, DE). Only RNA with an OD 260/280 ratio between 1.9-2.1 was used for PCR analysis. RNA was stored at -80°C until further use.

### **Quantitative reverse transcription real time PCR (qPCR)**

qPCR was performed on the CFX96<sup>™</sup> Real-Time PCR (Biorad Laboratories, #185-5096). Reverse transcription of 200 ng total RNA to cDNA was done with oligo(dT) and random primers using iScript<sup>™</sup> (Biorad Laboratories, #170-8891) in a total reaction volume of 20 µl. A temperature program of 5 minutes priming at 25°C followed by the reverse transcription at 42°C for 30 minutes and the reverse transcription inactivation at 85°C for 5 minutes was run. After a final cool-down to 4°C, the cDNA was stored at -80°C for subsequent use. The oligonucleotides (purchased from Microsynth AG, Balgach, Switzerland) displayed in Table C.1 were reconstituted at a concentration of 100 µM and stored at -20°C for further use. All primers are designed over exon-exon junctions using PrimerBlast and the Real Time PCR Design Tool from Integrated DNA Technologies to avoid the amplification of genomic DNA. Only primer pairs with efficiency between 90-110% were used in this study. A final concentration of 150 nM forward and reverse primer, respectively, was used for each qPCR reaction.

**Table C.1.:** Primer specifications

Function	Gene	Name	Accession n°	BP	Primer sequence (5'-3')
Reference	h18S	18S ribosomal	NR_003286	111	F - GGACAGGATTGACAGATTGAT R - AGTCTCGTTTCGTTATCGGAAT
	hACTB	Beta actin	NM_001101.3	83	F - CGAGAAGATGACCCAGATCA R - CGTACAGGGATAGCACAGC
	hB2M	beta-2-microglobulin	NM_004048.2	90	F - CGTGTGAACCATGTGACTTTG R - TGCGGCATCTTCAAACCTC
	hEF1 $\alpha$	Eukaryotic translational elongation factor 1 alpha	NM_001402	98	F - CCCCAGACAGTAGCATTG R - TGACTTTCCATCCCTTGAACC
	hGAPDH	Glyceraldehyde-3-phosphate dehydrogenase	NM_002046.3	98	F - AGTCAGCCGCATCTTCTTT R - CCAATACGACCAAATCCGTTG
	hRPL13a	Ribosomal protein L13a	NM_012423	100	F - AAGTACCAGGCAGTGACAG R - CCTGTTCCGTAGCCTCAIG
	YWHAZ	Tyrosine 3-monooxygenase /tryp.5 monoox. act. protein, zeta polypeptide	NM_145690.2	94	F - GGTCTGGCCCTTAACTTCTC R - TGGCTTCATCAAAGCTGTC
Adipo	haP2	Fatty acid binding protein 4	NM_001442	128	F - TGAGATTCCTTCATACTGGG R - TGGTTGATTTCCATCCCAIT
	hPPAR $\alpha$	Peroxisome proliferator-activated receptor gamma	NM_015869	124	F - TTGCTGTCATTATTCTCAGTGGAG R - GAGGACTCAGGGTGGTTCAGC
Chondro	hCollagen 2	Collagen, type II, alpha 1	NM_001844	92	F - GGAATTCGGTGTGGACATAGG R - ACTTGGGTCTTTGGGTTTG
	hAGG	Aggrecan	NM_001135	98	F - GAATGGGAACCCAGCCTATACC R - TCTGTACTTTCCTCTGTGTGCTG
Osteo	hCollagen I	Collagen, type I, alpha 1	NM_000088	83	F - CAGCCGCTTCACCTACAGC R - TTTTGTATTCAATCACTGTCCG
	hOsteocalcin	Bone gamma-carboxyglutamate protein	NM_199173	70	F - GAAGCCAGCGGTGCA R - CACTACCTCGCTGCCCTCC

The iQ SYBR<sup>®</sup> Green System (Biorad Laboratories, #170-8880) was used to perform the qPCR amplification from the cDNA in a final volume of 20  $\mu$ l with 5  $\mu$ l of 1:5 diluted cDNA. The cycling conditions were as follows: an initial 95°C for 3 minutes, followed by 40 cycles of 95°C for 10 sec, 60°C for 30 sec. Then, a melting curve was constructed by heating from 65°C to 95°C in temperature steps of 0.5°C. A multivariable, nonlinear regression method was used by the CFX Manager<sup>™</sup> Software (Version 2.0, Biorad Laboratories) to determine the quantification cycle values (termed Cq according to MIQE guidelines).

Results were exported to Microsoft Excel for analysis. Results are presented as mean values from triplicate measurements and variances are calculated according to the laws of uncertainty propagation [98].

---

## Expression of differentiation markers

All qPCR data differentiation markers were analyzed using the  $2^{-\Delta\Delta}$  Cq method [167] (assuming that the amplification efficiency equals 100%) and normalized against a reference gene. Day 2 of control culture was designated as the calibrator in each experiment. Each gene was evaluated in independent PCR runs including the complete set of samples of one donor and passage (i.e. donor 1, passage 1, day 2, 9, 16, 22 of control and differentiation culture).

## Immunofluorescent staining

For immunofluorescent staining, the cells were washed twice with phosphate-buffered saline without glucose (PBS w/o glucose, Gibco, #18912-014), treated with 4% paraformaldehyde (Sigma, #16005) plus 0.2% Triton-X for 8 minutes and then washed again twice with PBS w/o glucose. Non-specific binding of antibodies was blocked with PBS w/o glucose containing 5% goat serum (Sigma, #G6767) and 1% FCS for 30 minutes. The osteogenic characterisation was determined using the bone specific marker anti-collagen 1 (1:1000; Sigma, #C2456) and goat  $\alpha$ -mouse IgG Alexa Fluor 546 (1:400; Molecular Probes, #A11030). The antibody was diluted in 1.5% skim milk/PBS and incubated for 1 h at RT. The cell nuclei were stained with DAPI (4'-6-Diamidino-2-phenylindole, 10 mg/ml; Sigma, #D9542) together with the secondary antibody. Adipogenic differentiation was determined by Oil Red O staining. Briefly, cells were fixed with 4% paraformaldehyde (as described above), washed twice with distilled water, after one washing step with 60% isopropanol, the cells were incubated in 60% isopropanol for 5 minutes at RT. Further, the cells were incubated in Oil Red O working solution (2 mg/ml Oil Red O in isopropanol and double distilled water, ratio 3:2) for 10 minutes at RT. Before fluorescence microscope (Axio Imager.M1, Carl Zeiss AG, Switzerland) imaging was performed, the cells were washed with distilled water till optimal contrast of red-stained lipid droplets was achieved.

## Histology

Cell pellets were fixed with 4% formalin, embedded in paraffin, and sectioned at 2  $\mu$ m. Tissue sections were then deparaffinized using xylene followed by a graded alcohol series and stained with hematoxylin/eosin to identify histologic features and alcian blue/periodic acid schiff (PAS) for proteoglycan.

## Evaluation of reference genes

The expression stability of seven common RGs (18S, ACTB, B2M, EF1a, GAPDH, RPL13a, YWHAZ) was analyzed based on four different parameters:

- 1) Interquartile Range (IQR) representing the spreading of the Cq values. The IQR spans between the 75th and the 25th percentile of the boxplots delimiting with the whiskers the maximum and minimum values, with the horizontal line the median and the outliers with a point respectively.
- 2) Variation between differentiation culture and control culture (p-value) established by a unpaired one-way t-test at a 95% confidence level. The null hypothesis (differentiation equals control culture) is rejected if the p-value < 0.05 showed statistically significant difference between control and differentiation cultures.
- 3) Average fold changes (AFC) calculated by subtracting the mean Cq value for each time point in control or differentiation culture from the mean Cq value corresponding to the control culture at day 2.  $\Delta Cq$  is further transformed into fold differences with the formula  $2^{-\Delta Cq}$ . [62, 222]
- 4) Maximum fold change (MFC) calculated similarly to the AFC though considering the maximum/minimum instead of the mean Cq value. [60, 222]

1) & 2) were calculated of the entire dataset of Cq values of three different donors at two different passages in control as well as in differentiation culture. 3) & 4) were calculated at each time point, using day 2 of control culture as calibrator. The obtained values of all time points and conditions of the entire dataset are in the case of AFC averaged, and for MFC the highest one represented in Table C.2. The calculation of AFC and MFC assumes a primer efficiency of 100%. The perfect RG would show no variation in Cq value during the process of differentiation and would result in AFC and MFC values equal to one, p-value > 0.05, of 0% and IQR of zero. The statistical analysis was performed using the software R Project for Statistical Computing (<http://www.r-project.org/index.html>). In addition to the statistical evaluation of RG stability using the above described criteria, geNorm [278], Normfinder [13] and BestKeeper [214] algorithms were applied. Cq values were put into the data file of the Normfinder and BestKeeper software, whereas AFC values were used for geNorm analysis.



---

## Results

### Multilineage differentiation potential

The MSC multilineage differentiation potential of all donors was confirmed by qPCR (Figure C.1, Table C.2) as well as immunofluorescent and histochemical stainings (Figure C.2).

**Table C.2.: qPCR gene expression analysis of key differentiation markers.** Relative expression ( $2^{-\Delta\Delta Cq}$ ) of differentiation markers of all donors at passage one and four at day 22 of induction of adipogenesis (adipo), chondrogenesis (chondro) and osteogenesis (osteo). RPL13a used as normalizer and control culture day 2 as calibrator of all data

Donor	Passage	Adipo		Chondro		Osteo	
		aP2	PPAR $\gamma$	Coll II	Aggrecan	Coll I	Osteocalcin
1	1	635	7	1,452,393	228	6	3
	4	167	14	643,985	53	6	6
2	1	809	125	875,635	122	9	44
	4	6,237	558	374,170	80	4	20
3	1	17,783	48	139,187	12	8	7
	4	135,381	14	10,897	13	10	23

Adipogenic differentiation is marked by the appearance of oil droplets stained by Oil Red O on day 16 (Figure C.2A). The adipogenic markers fatty acid binding protein 4 (aP2) and peroxisome proliferator-activated receptor gamma (PPAR $\gamma$ ) were expressed significantly at day 22 in all donors and were at passage 4 sometimes even more abundant than at passage 1 (Table C.2). Chondrogenic differentiation was visualized using alcian blue/PAS staining, revealing a light blue colour upon the appearance of proteoglycans starting on day 16 (Figure C.2B). Aggrecan and collagen 2, the chondrogenic marker genes, are upregulated in all donors (Table C.2). In the osteogenically differentiated samples, collagen 1 staining increased during the entire 22 days culture period (Figure C.2C) which goes in line with the qPCR data (Figure C.1, Table C.2). Osteocalcin, a later marker of osteogenesis, was expressed around day 9 and steadily increased thereafter. The qPCR data shows that all three donors are exhibiting a multilineage differentiation potential (Figure C.1) with a certain interpatient variability typical for MSC studies (Table C.2). MSC-proliferation medium, containing FGF-2 to preserve the stem cell

character 21, was used as the control condition for adipo-, and osteogenesis, exhibiting no Oil Red O or collagen 1 staining on day 21, respectively. The appropriate control condition for chondrogenesis was confirmed by the absence of alcian blue staining in pellet cultures after 14 days.

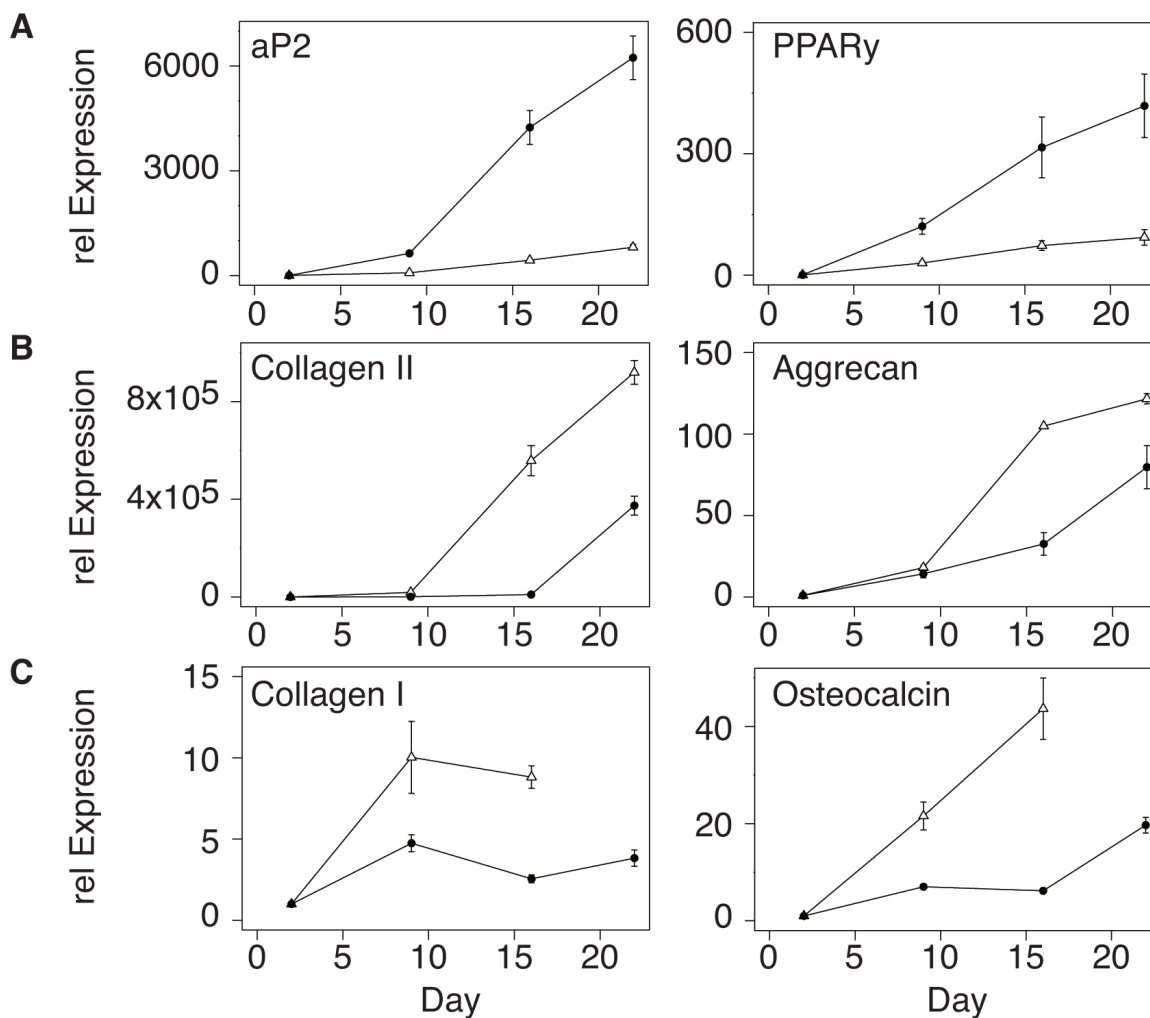


**Figure C.1.: Gene expression profile of key differentiation markers** Gene expression profile of donor 2 at passage 1 (triangle) and 4 (circle) during **A** adipogenic-, **B** chondrogenic- and **C** osteogenic differentiation over 22 days. RPL13a was used as normalizer and control culture day 2 as calibrator of all data.

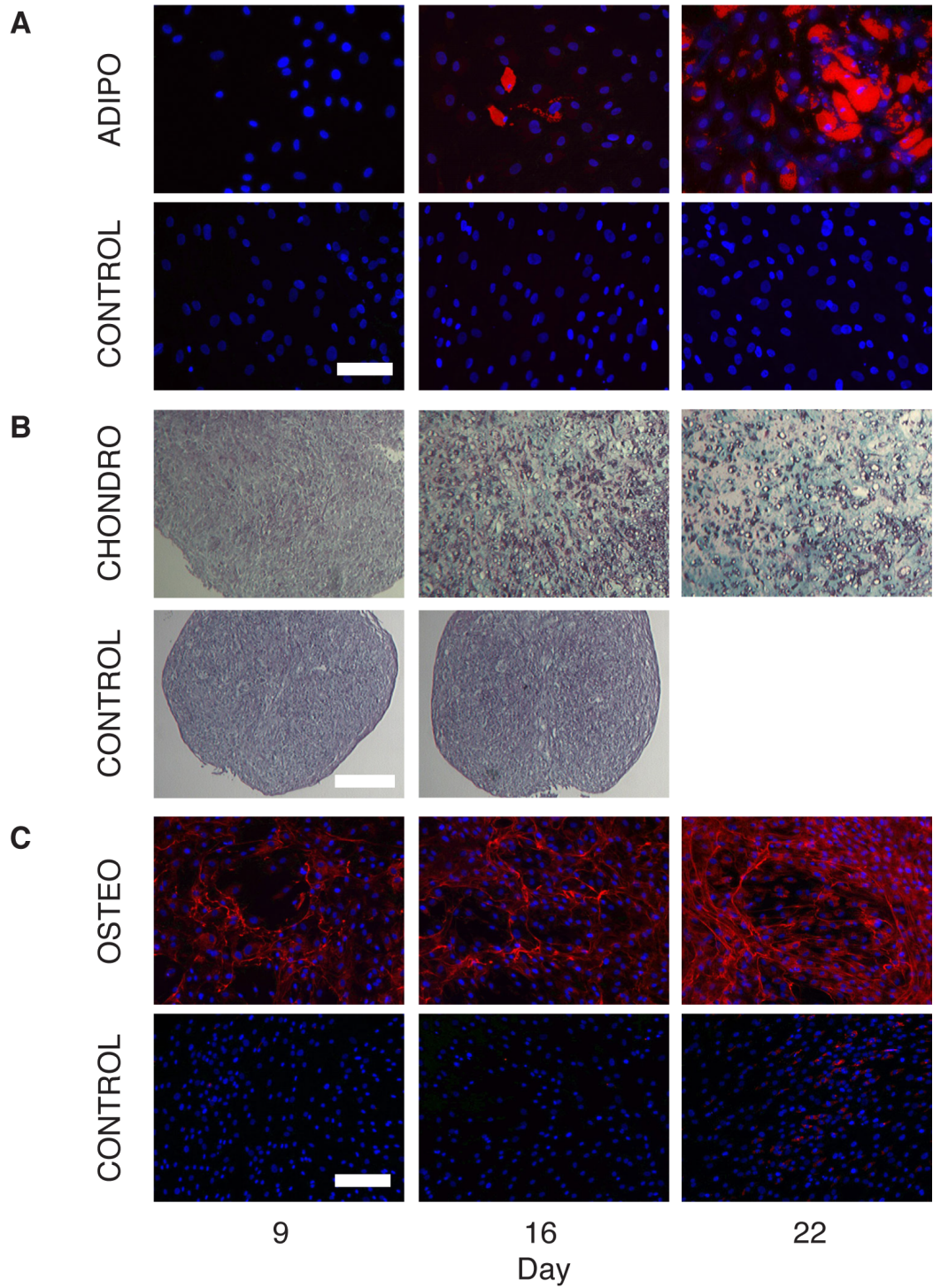


**Figure C.2.: Multilineage differentiation potential of MSCs** A Adipogenic (ADIPO) cultures stained with Oil Red O/DAPI. B Chondrogenic (CHONDRO) pellet culture stained with Alcian Blue/PAS. Control day 22 too small for analysis. C Osteogenic (OSTEO) cultures stained with collagen 1/DAPI at day 9, 16 and 22 of induction in differentiation or control medium. Scale bars 200 μm

## Evaluation of reference gene expression stability

### *Expansion and differentiation of hBM-MSCs*

To study the expression stability of the seven RGs selected during differentiation, we analyzed several parameters summarized in Table C.3. The distribution of the quantification cycle values (C<sub>q</sub>) of all donors was graphically depicted in boxplots (Figure C.3), which delimit the 25th and 75th percentile of the dataset also known as the interquartile range (IQR - Table C.3). Further, a t-test was performed to assess the change between control and differentiation cultures represented as side-by-side boxplots in Figure C.3 A-C right.

The resulting p-value (Table C.3) reflects the probability that the C<sub>q</sub> values for differentiated samples are statistically different than in control cultures. In addition, average and maximum fold changes (AFC and respectively MFC) [62, 222] were calculated (Figure C.4). The selection criteria applied in this work is: IQR < 0.7, p-value > 0.05, AFC < 2 (Figure C.4) and MFC < 2.2. On the basis of these criteria, 18S (IQR = 0.43, p-value = 0.35, AFC = 1.6, MFC = 1.92), EF1a (IQR = 0.67, p-value = 0.68, AFC = 1.39, MFC = 1.48) and RPL13a (IQR = 0.52, p-value = 0.07, AFC = 1.46, MFC = 1.57) are possible RGs to normalize adipogenic differentiation studies (Figure 3A and 4A). For chondrogenesis (Figure C.3B and C.4B), RPL13a (IQR = 0.35, p-value = 0.22, AFC = 1.9, MFC = 2.11) as well as YWHAZ (IQR = 0.43, p-value = 0.42, AFC = 1.53, MFC = 1.85) fulfilled the selection criteria whereas only RPL13a (IQR = 0.68, p-value = 0.06, AFC = 1.65, MFC = 1.83) was concluded to be a stably expressed RG during osteogenic differentiation (Figure C.3C and C.4C). On the other hand, the two most unstably expressed RGs were ACTB and GAPDH with MFC reaching up to 8.35 (ACTB during adipogenesis) and 20.05 (GAPDH during chondrogenesis). This instability was confirmed in the analysis of all differentiation lineages together resulting in the two highest IQRs for ACTB (1.21) and GAPDH (1.43) (Figure C.3D, Table C.3). Taken together, RPL13a shows the lowest variability across donors, passage numbers, as well as differentiation conditions with an IQR of 0.59, p-value of 0.56 and MFC smaller than 2. Based on these results, we ranked the genes according to their IQR (the lower, the more stable). This ranking represented in Table C.4 places RPL13a in the first place for chondrogenesis and osteogenesis and on the second place for adipogenesis. The algorithms of geNorm, NormFinder and Bestkeeper all support the first rank of RPL13a for the analysis of chondrogenic induction experiments whereas for adipogenesis and osteogenesis always two out of three show RPL13a in the first rank (Table C.4).

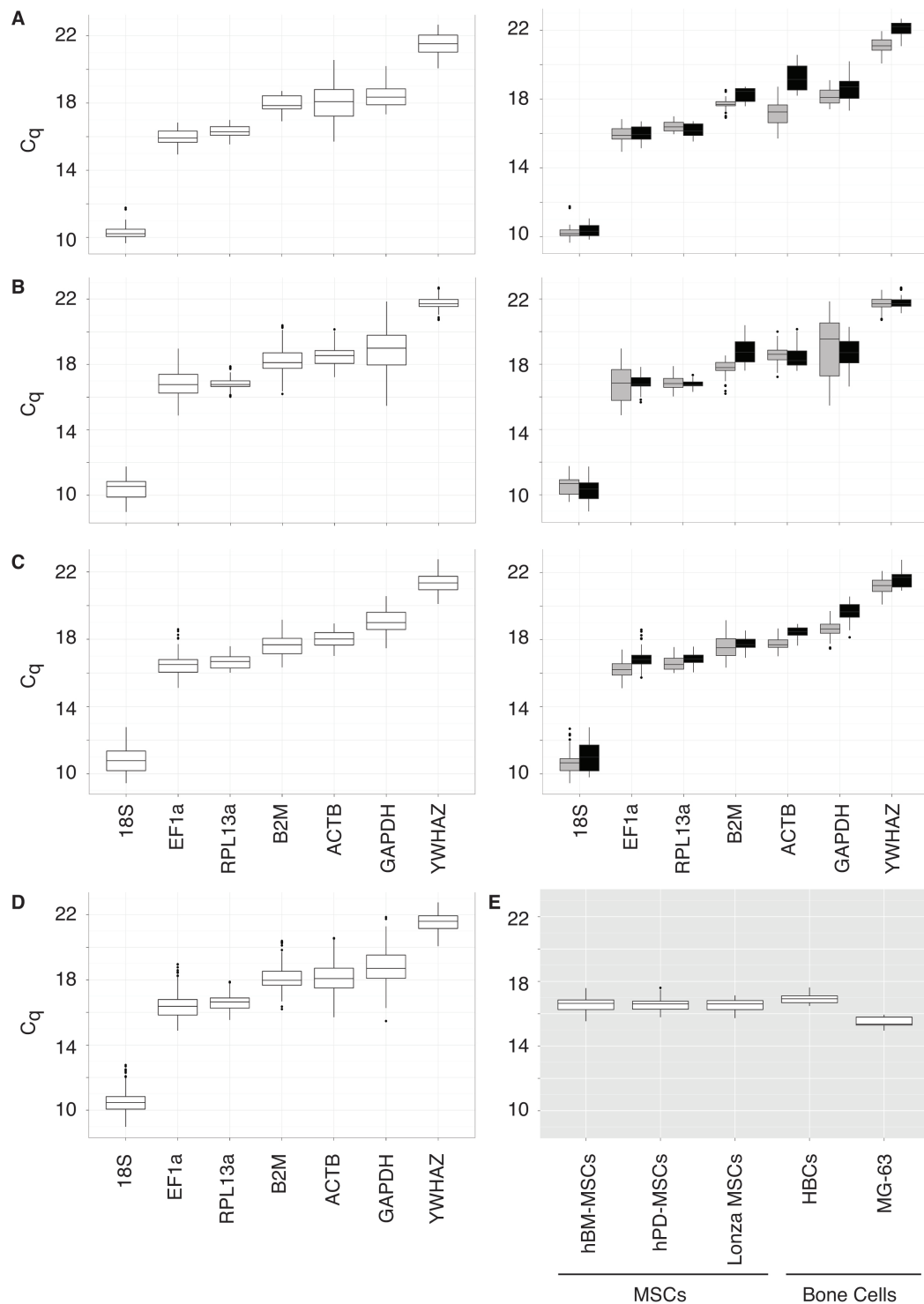


**Figure C.3.: Distribution of Cq values** **A** adipo-, **B** chondro- and **C** osteogenesis. Left, values of all donors /passages in control and differentiation culture. Right, data split up into control (grey) and differentiation (black) cultures. **D** all lineages together. **E** RPL13a values of freshly isolated (hBM-MSCs), commercial bone marrow- (Lonza MSCs) and placenta-derived MSCs (hPD-MSCs) as well as HBCs and MG-63.

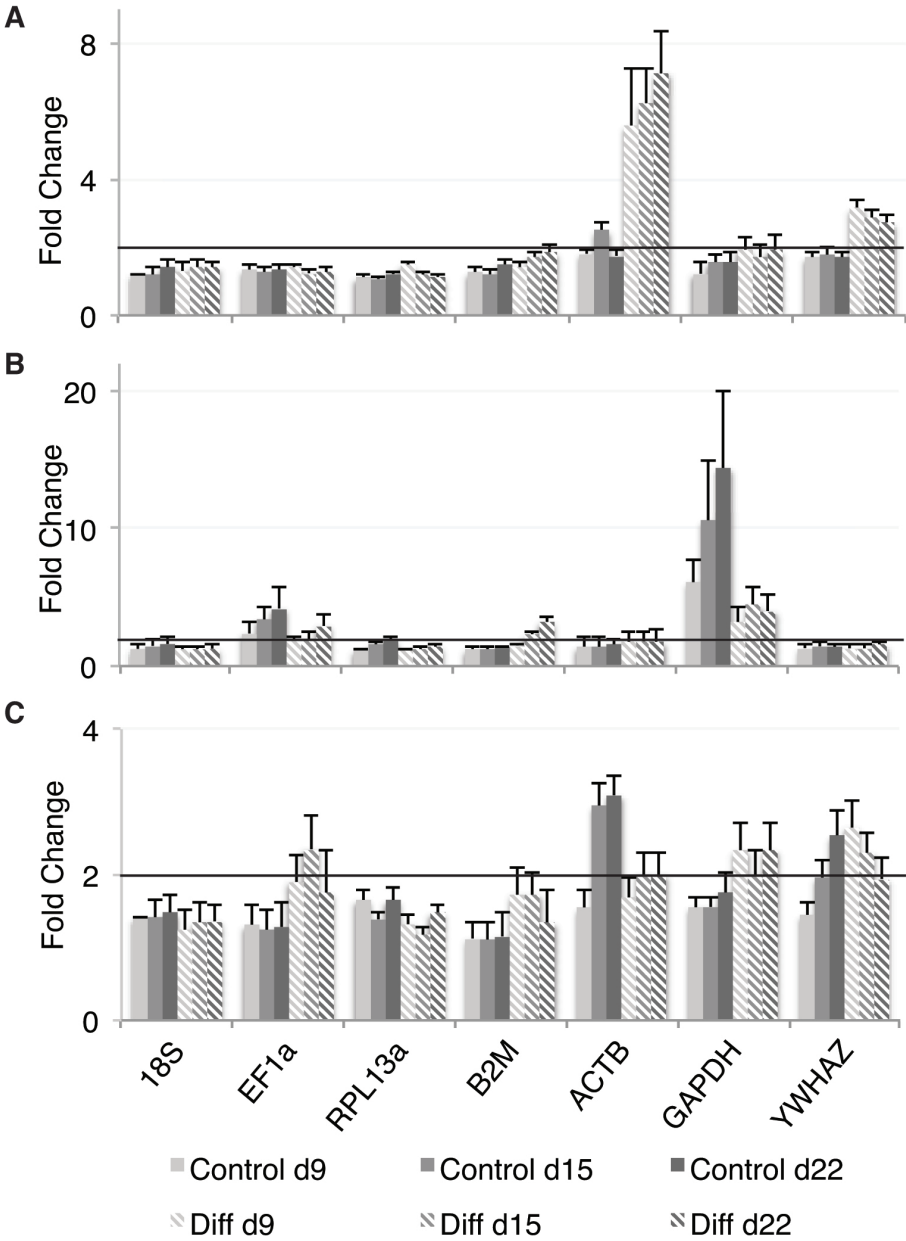


**Figure C.4.: Fold changes ( $2^{-\Delta Cq}$ ) in reference gene expression** Average (AFC, columns) and maximum fold change (MFC, error bars) of A adipo-, B chondro-, and C osteogenesis on day 9, 15, 22 in differentiation (diff) and control medium of all donors and passages. Control day 2 used as calibrator. Black line indicates the selection criteria of AFC < 2.

**Table C.3.: Summary of the stability parameters evaluated for all seven reference genes in chondro, adipo and osteogenic differentiation** Coefficient of variation (CV [%]) calculated by the standard deviation divided by the mean, p-value of the t-test showing the variation between the Ct values of control and differentiation cultures, inter quartile range (IQR), average (AFC) and maximum fold change (MFC). For AFC and MFC the highest value of the whole dataset is represented. The reference genes fulfilling the selection criteria (IQR < 0.7, p-value > 0.05, AFC < 2 and MFC < 2.2) during adipo-, chondro-, osteogenesis are highlighted in grey. The analysis of all Cq values of adipo-, chondro- and osteogenesis together (labeled as “all”) resulted in only RPL13a fulfilling the criteria.

Differentiation	Primer	IQR	p-value	AFC	MFC
adipogenesis	18S	0.43	3.5E-01	1.60	1.92
	EF1 $\alpha$	0.67	6.8E-01	1.39	1.48
	RPL13a	0.52	7.0E-02	1.46	1.57
	B2M	0.77	6.9E-15	1.85	2.08
	ACTB	1.59	2.2E-16	7.12	8.35
	GAPDH	0.95	3.9E-05	1.93	2.35
	YWHAZ	1.01	2.2E-16	3.14	3.43
chondrogenesis	18S	0.95	3.7E-02	1.61	1.90
	EF1 $\alpha$	1.15	7.5E-01	4.20	5.72
	RPL13a	0.35	2.2E-01	1.90	2.11
	B2M	0.95	1.3E-14	3.21	3.54
	ACTB	0.79	2.6E-01	1.8	2.61
	GAPDH	1.82	9.7E-02	14.43	20.05
	YWHAZ	0.43	4.2E-01	1.53	1.85
osteogenesis	18S	1.17	5.2E-02	1.47	1.71
	EF1 $\alpha$	0.75	2.1E-08	2.35	2.83
	RPL13a	0.68	6.0E-02	1.65	1.83
	B2M	0.74	4.6E-16	1.73	2.11
	ACTB	0.91	2.6E-01	3.09	3.36
	GAPDH	1.02	3.0E-16	2.33	2.72
	YWHAZ	0.80	1.2E-06	2.65	3.01
all	18S	0.77	8.5E-01	< 2	< 2.2
	EF1 $\alpha$	0.95	3.9E-03	> 2	> 2.2
	RPL13a	0.59	5.6E-01	< 2	< 2.2
	B2M	0.85	2.2E-16	> 2	> 2.2
	ACTB	1.21	9.5E-13	> 2	> 2.2
	GAPDH	1.43	3.6E-03	> 2	> 2.2
	YWHAZ	0.78	2.2E-16	> 2	> 2.2

**Table C.4.: Reference gene ranking based on geNorm, NormFinder and Bestkeeper algorithms and IQR rating** Rating based on different algorithms yielding expression stability values (shown in parenthesis). Algorithms used: geNorm (M value), NormFinder, BestKeeper (SD[±CP]), and IQR rating. Ranking of RPL13a highlighted in gray. SD[±CP], standard deviation of crossing point

Rank	GeNorm	NormFinder	BestKeeper	IQR rating
<i>Adipogenesis</i>				
1	EF1α(0.91)	GAPDH (0.40)	18S (0.25)	18S (0.43)
2	RPL13a (0.2)	B2M (0.48)	RPL13a (0.28)	RPL13a (0.52)
3	18S (0.21)	YWHAZ (0.5)	EF1α(0.37)	EF1α(0.67)
4	GAPDH (0.27)	EF1α(0.58)	B2M (0.38)	B2M (0.77)
5	B2M (0.3)	18S (0.58)	GAPDH (0.51)	GAPDH (0.95)
6	YWHAZ (0.36)	RPL13a (0.59)	YWHAZ (0.58)	YWHAZ (1.01)
7	ACTB (0.53)	ACTB (1.87)	ACTB (1.04)	ACTB (1.59)
<i>Chondrogenesis</i>				
1	RPL13a (0.14)	RPL13a (0.36)	RPL13a (0.28)	RPL13a (0.35)
2	18S (0.15)	18S (0.44)	YWHAZ (0.31)	YWHAZ (0.43)
3	YWHAZ (0.16)	EF1α(0.58)	ACTB (0.42)	ACTB (0.79)
4	ACTB (0.28)	YWHAZ (0.60)	18S (0.50)	B2M (0.95)
5	EF1α(0.37)	ACTB (1.00)	B2M (0.68)	18S (0.95)
6	B2M (0.51)	B2M (1.24)	EF1α(0.68)	EF1α(1.15)
7	GAPDH (0.7)	GAPDH (2.54)	GAPDH (1.09)	GAPDH (1.82)
<i>Osteogenesis</i>				
1	B2M (0.18)	RPL13a (0.23)	RPL13a (0.35)	RPL13a (0.68)
2	EF1α(0.2)	18S (0.25)	B2M (0.36)	B2M (0.74)
3	GAPDH (0.20)	B2M (0.26)	EF1α(0.43)	EF1α(0.75)
4	18S (0.24)	EF1α(0.35)	YWHAZ (0.46)	YWHAZ (0.80)
5	RPL13a (0.27)	YWHAZ (0.35)	ACTB (0.53)	ACTB (0.91)
6	YWHAZ (0.32)	GAPDH (0.39)	18S (0.59)	GAPDH (1.02)
7	ACTB (0.38)	ACTB (0.45)	GAPDH (0.6)	18S (1.17)



---

### *MSCs of different sources and bone cells*

Once RPL13a was selected as the RG of choice for bone marrow-derived MSCs (hBM-MSCs), we further tested its expression stability on commercially available hBM-MSCs (Lonza MSCs) as well as placenta-derived MSCs (hPD-MSCs) during adipo-, chondro- and osteogenesis. The differentiation experiments using Lonza MSCs were performed with purchased cells from one donor and the hPD-MSCs cells from two donors. RPL13a showed a similar distribution for these two MSCs (Figure C.3E) as it does for the freshly isolated hBM-MSCs and is therefore considered stably expressed throughout mesodermal differentiation of MSCs. In a subsequent step, we analyzed the RPL13a stability in gene expression during osteogenic differentiation of bone cells. Primary bone cells (HBCs) as well as the MG-63 (human osteosarcoma cell line) were therefore induced over 7 days (time points analyzed: day 1, 4, 7) in induction medium. The HBCs show a comparable Cq distribution to that of MSCs (Figure C.3E) whereas MG-63, the only non-primary cells, are expressing RPL13a at a higher level. Although exhibiting a lower Cq mean, the distribution is narrow, indicating a high expression stability of RPL13a during osteogenic differentiation.

### *Effect of reference gene expression stability on marker gene expression*

The effect of the RG variance on the expression pattern of the adipo-, chondro-, and osteo markers was analyzed (Figure C.5). For clarity, only the relative expression of the marker genes from donor 2 at passage 1 are shown using GAPDH, RPL13a and ACTB as RGs. The instability of ACTB during adipogenesis leads to an increase of 281% of the relative expression of aP2 at day 22 compared to RPL13a. GAPDH, being less variable, only shows an error of 28% (Figure C.5A). The expression of collagen 2 during the chondrogenic differentiation process is affected by a smaller degree by ACTB (40%) but more pronounced by GAPDH (222%) (Figure C.5B). This increase would be even higher when relating to the control cultures of the chondrogenic lineage (Figure C.4B). The normalization of the osteogenic-specific genes shows a resulting error in collagen 1 expression of 186% for ACTB and 55% for GAPDH (Figure C.5C).

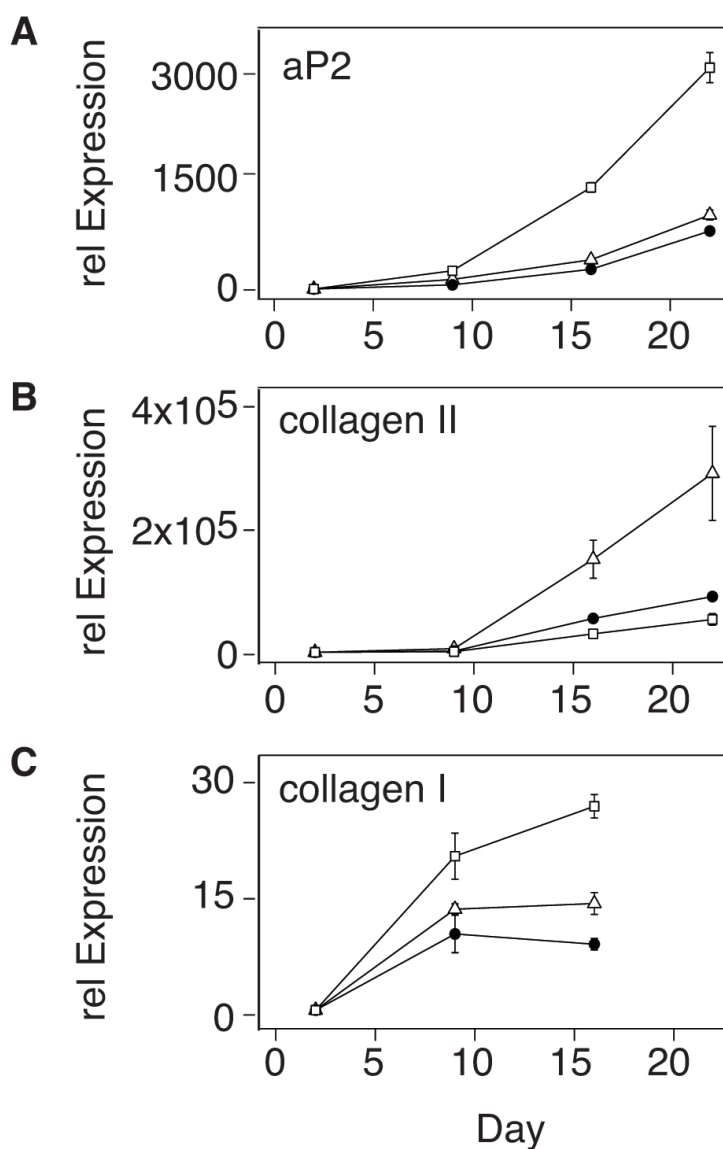


**Figure C.5.: Effect of reference gene stability on marker gene expression** Relative gene expression of **A** aP2 during adipogenic, **B** collagen 2 during chondrogenic, and **C** collagen 1 during osteogenic differentiation normalized by GAPDH (white triangle), RPL13a (black circle) and ACTB (white square). Data of donor 2 passage 1 represented. Control culture day 2 was used as calibrator.

---

## Discussion

In the present study we have established RPL13a, a member of the L13 ribosomal protein family and a structural component of the large 60S ribosomal subunit, as the RG of choice for mesenchymal stromal cell studies. Among the seven RGs GAPDH, RPL13a, ACTB, YWHAZ, EF1a and B2M, RPL13a showed the lowest expression variability throughout adipogenic, chondrogenic, osteogenic differentiation of MSCs. We have studied the stability in gene expression of the RGs of three different donors at passage one and four, proving that RPL13a expression is not only stable during differentiation but also during expansion to higher passages. This result is confirmed by at least two out of three algorithms (geNorm, NormFinder, BestKeeper) known for gene expression stability analysis. The discrepancy in the resulting stability ranking shows the difficulty of reference gene stability analysis, which are based on different arbitrarily chosen parameters. The majority of three out of four analysis methods supporting RPL13a as the reference gene of choice is a striking evidence for its stability. Next to freshly isolated hBM-MSCs, we applied RPL13a to studies with commercially available and placenta-derived MSCs, where its suitability for comparison studies between different MSCs was confirmed. These findings are in agreement with several studies on qPCR normalization. DeJonge et al. [60] performed a meta-analysis on 13'629 human gene array samples (including stem cells) and identified RPL13a as one of the top 15 candidate RGs. The ranking based on the CV, placed ACTB on position 57 and GAPDH on 139. Vandesompele et al. [278] studied different human tissues and cells (including bone marrow) and concluded that RPL13a together with Ubiquitin C are the RGs with the smallest variation in bone marrow samples. These two publications, studying the stability of RGs in a wide variety of tissues, are lacking the analysis of their variance during differentiation events. The work of Curtis et al. [56] focused on endothelial differentiation of bone marrow-derived MSCs as well as their expansion under different conditions. They have shown EF1a and RPL13a expression to be stable under all studied experimental conditions, however missing the differentiation into the common mesodermal lineages. Quiroz et al. [217, 222] demonstrated the stability of RPL13a expression for osteogenic differentiation of bone marrow-derived MSCs, applying the selection criteria of AFC and MFC < 2. Their study was performed using cells from one donor at passage five, thereby neglecting interpatient variability. We decided, in the present work, to use cells from three patients, to address this variability. Our results show that the gene expression stability of RPL13a in the osteogenically induced cultures fulfills the criteria proposed by Quiroz et al., including not only one but three donors at different pas-

sages. Osteogenesis though showed to be the mesodermal differentiation lineage the least affected by changes that result in RG expression instability. Taking adipogenesis and chondrogenesis in consideration as well, the selection criteria had to be slightly alleviated to  $AFC < 2$  and  $MFC < 2.2$ . Additionally, our data confirms the use of RPL13a as a RG in bone research, showing its stability not only under osteogenic differentiation of MSCs but also of MG-63 and primary bone cells. The higher abundance of RPL13a in the osteosarcoma cell line MG-63, most probably originates in the immortalization process, which is known to affect cellular processes [139,208]. GAPDH and ACTB, the two most widely used RGs in MSC studies [56,264], showed the highest expression variability of all seven RGs analyzed in bone marrow-derived MSCs. GAPDH has been shown to play a role in many cellular processes such as nuclear RNA export, DNA replication, DNA repair, exocytotic membrane fusion, cytoskeletal organisation and phosphotransferase activity [247] and therefore its mRNA level is prone to be affected by events such as differentiation. The expression level of ACTB, a structural protein associated with cell shape and motility, is expected to be altered during adipo-, chondro- and osteogenesis, three processes involving a major change in cell morphology [38,185,203,228]. The use of ribosomal RNA genes such as 18S, on the other hand, is not only problematic due to their proven instability [119,249,266] but also due to their high abundance and the different transcription mechanism which, compared to mRNA, is not carried out by RNA polymerase II but RNA polymerase I [223,249]. We therefore highly recommend abandoning the normalization based on these RGs in the field of human mesenchymal stromal cell research. The expression variability of RGs used in the MSC community hinders a conclusive comparison between different studies and therefore puts their value into question. Our work showing the instability in gene expression of commonly used RGs under expansion, adipo-, chondro- and osteogenic differentiation as well as between different MSCs further demonstrates the necessity of establishing a common RG to be used by all investigators working on mesenchymal stromal cells. We propose the use of RPL13a as a single RG instead of the multiple RG approach proposed by others [63] as the stability of RPL13a is sufficiently high.